Characterization and Functional Analysis of NET3C and VAP27-1 Interacting Proteins in Plants

ZANG, JINGZE

Characterization and Functional Analysis of NET3C and VAP27-1 Interacting Proteins in Plants

Jingze Zang

Submitted in accordance with the requirements for the degree of Doctor of Philosophy

Department of Biosciences

Durham University

January 2019

Abstract

In plants, the cortical ER network connects to the plasma membrane via the ER-PM contact sites (EPCS), whose structures are maintained by EPCS resident proteins (e. g. NET3C, VAP27-1 and SYT1) and the cytoskeleton. However, little is known about the mechanism of regulation of the cytoskeleton at the plant EPCS, and its biological functions remain poorly understood. From previous protein-protein interaction screens, hundreds of candidate proteins that potentially interact with NET3C or VAP27-1 were identified, and three proteins, KLCR1, AtBRO1 and SINE2 were selected for further study.

Firstly, microtubule binding proteins, KLCR1 and IQDs were identified to interact with NET3C and form an intermediate component of the plant EPCS. The NET3C-KLCR1-IQDs protein complex mediates links between actin filaments and microtubules, and their overexpression enhances their association. The expressions of NET3C and IQDs also have a direct influence to the ER morphology, with more ER polygonal and cisternal structures formed when their expression level is high. The loss of function of KLCR1 results in disorganization of both actin filaments and microtubules, which causes left handed helical growth of roots and defects in the shape of cotyledon pavement cells. AtBRO1 is another protein that has been confirmed to interact with NET3C. It localized to punctate structures and associated with the ER network and actin filaments in *N. benthamiana* leaf epidermal cells. Reverse-genetic analyses suggested the knockout AtBRO1 expression is lethal, and defective development was observed in about a quarter of seeds in siliques from heterozygous plants. Additionally, we also identified a protein complex which is comprised of VAP27-1, NET3A and SINE2. This protein complex links the nuclear envelope with the ER network and actin filaments and is likely to regulate the morphology of ER network and nuclear envelope during mitosis in plants.

In summary, our results revealed novel NET3C and VAP27-1 complexes that are important for the ER morphology, cytoskeleton structures and plant development.

Declaration

I confirm that this thesis is a presentation of my original research work with the exception of Figure 3.19, in which the ER morphology analysis was performed by Charlotte Pain (Oxford Brookes University). The fluorescence fusion constructs provided by others are listed in Table 2.2. The appropriate credit has been given where reference has been made to the work of others.

No material contained in this thesis has been submitted for the award of a higher degree elsewhere.

Acknowledgements

During my PhD, I would like to express my great gratitude to many people who have given me support, encouragement and guidance. Firstly, the most sincere thank goes to my supervisor, Professor Patrick Hussey. I would like to thank him for the opportunity to join his lab and participate in his research. Without his stimulating advice and invaluable feedback, it would be impossible for me to finish my research so smoothly.

I would like to thank Dr. Pengwei Wang, who mentored me during the whole period of my PhD. He provided exceptional technical guidance during my research and advice during the writing of my thesis. He has engaged my interest in plant cell science, and his serious research attitude and spirit of continuous learning made strong impression on me. I wish him all the best for the future as he develops his own research group at Huazhong Agriculture University in China. I also thank him for giving me the opportunity to further my research in his lab after my PhD.

I would like to thank Dr. Katharina Burstenbinder, Leibniz Institute of Plant Biochemistry for providing me the IQD fluorescence fusion constructs. I also want to thank Charlotte Pain, Oxford Brookes University for the ER morphology analysis.

I would like to thank all the other past and current members from the PMCB group for their cooperation during the course of my PhD. Dr Tim Hawkins, Dr Johan Kroon, Dr Greg Pridgeon, Dr Patrick Duckney and Teresa Braga, a visiting PhD candidate from University of Lisbon. They all provided a great working environment and offered me much useful suggestions throughout my PhD. Special thanks go to Dr. Patrick Duckney for proofreading my thesis.

Additionally, I would like to express my thanks to my parents, my relatives and my friends who support and encourage me during my study in the UK.

Table of Content

Chapter 1: Introduction

1.1. Overview of the Endomembrane System

The endomembrane system is one of the most important features of eukaryotes and is absent from prokaryotic cells (Gould *et al.,* 2016). It is an elaborate system with various organelles that play vital roles in the secretory, endocytic and degradative pathways of the cell (Lippincott-Schwartz and Phair, 2010). In cells from higher plants, the endomembrane system mainly consists of the endoplasmic reticulum (ER), the Golgi apparatus (GA), vacuoles, various secretory vesicles, endosomes, the nuclear envelope (NE) and also the plasma membrane (PM) (Harris, 1986, Lippincott-Schwartz and Phair, 2010). These functional compartments need to maintain a suitable environment for various kinds of intracellular functions such as sorting and trafficking of proteins, lipids as well as polysaccharides. During the past few years, many kinds of systems and techniques have been developed to study the plant endomembrane system. Different fluorescence proteins can be used as markers for visualizing organelles and the trafficking of cellular material. Arabidopsis, the model plant system, is usually used for functional and genetics studies of proteins which are localized to the endomembrane system (Jürgens, 2004).

1.1.1. Overview of the Endoplasmic Reticulum Functions and Dynamics

The ER network which is a continuous membrane enclosed network is considered to be one of the most architecturally complex organelles in most eukaryotic cells. It consists of the nuclear envelope as well as dynamic sheets and tubules. According to its function, the ER can be classified into two sub-groups: the rough ER (RER) which is attached with ribosomes and smooth ER (SER) that does not have ribosomes attached with it (Shibata *et al.,* 2006). The ER network is essential for protein production and secretion, lipid biosynthesis as well as calcium storage (Manford *et al.,*

2012). Additionally, it also plays some unique roles in plant cells. For example, it is a compartment that reserves receptors of some plant hormones such as auxin and ethylene (Chen *et al.*, 2002, Friml and Jones, 2010), and it also functions as a membrane source for lytic vacuole generation in meristematic cells of the root (Viotti *et al.*, 2013).

The delivery of proteins to their proper intracellular destination is important for the structure, organization and function of all eukaryotic cells (Saraogi and Shan, 2011). Nascent proteins need to be selectively recognized and targeted to the ER membrane through their N-terminal hydrophobic signal sequences. Next, soluble proteins and membrane proteins must translocate into the ER membrane completely or partially before initiating their secretory pathways. Co-translational translocation and post-translational translocation are two forms of targeting pathway in Eukaryotic cells. The co-translational pathway is the most common form, it requires the signal recognition particle (SPR) complex to deliver proteins that are being synthesized; while the post translational translocation pathway usually just occurs in simpler eukaryotes such as the yeast (Johnson *et al.*, 2013, Nyathi *et al.*, 2013, Walter and Johnson, 1994). After membrane translocation, signal sequences can be removed from pre-proteins by a membrane associated signal peptidase complex and proteins often attach with a carbohydrate complex (N-linked glycosylation) or the phospholipid glycosylphosphatidylinositol (GPI) before they enter the ER lumen or are integrated into its membrane (Martoglio and Dobberstein, 1998). In addition to translocation and modification, proper folding is also a critical process as misfolded proteins can be very harmful to cells (Hebert and Molinari, 2007). Protein folding is facilitated by molecular chaperones such as BiP and the lectin-mediated chaperoning system, which are two major forms of the ER quality control mechanism that is able to distinguish correctly folded proteins from unfolded or misfolded proteins and enable them to be re-folded or initiates their degradation (Ellgaard *et al.*, 1999, Gething, 1999).

In higher plants, the ER network is highly dynamic. Membrane tubules continuously grow, shrink and fuse with each other. The polygonal structure can be dynamically

changed by altering branching patterns of tubules, moving network junction as well as transiting between cisternae and tubules (Griffing, 2010, Sparkes *et al.*, 2011). The remodeling of the ER network is driven by actin motor protein Myosin (Sparkes *et al.*, 2009). The Myosin XI family has been reported to play a major role in the movement and remodeling of the ER network. The persistency of ER tubules and cisternae can be affected by Myosin XI-C, XI-E, XI-K and XI-1 overexpression. Myosin XI-1 increases cisternal number, while XI-2 reduces the reorganization of the ER (Griffing *et al.*, 2014). In addition, SYP73, one of the three members of the plant SYP7 family of SNARE proteins has proved to connect the ER network to actin filaments and coordinate the remodeling and streaming of the ER network. SYP73 is mainly localized to the ER network and contains an actin-binding domain. Overexpression and loss of function of this protein have dramatic effects on the ER morphology and dynamics (Cao *et al.*, 2016, Suwastika *et al.*, 2008). NET3B is another protein that is considered to be a linker between the ER network and actin filaments. It belongs to a specific actin-binding protein superfamily (Deeks *et al.*, 2012). The N-terminal domain of this protein binds to the actin cables and the C-terminal domain is associated with the ER. When NET3B is overexpressed, both the architecture of the ER network and diffusion of the ER membrane are affected (Wang and Hussey, 2017).

In mammalian cells, CLIMP-63/p63 was the first identified protein that acts as the linker between the ER membrane and the microtubules (MTs). It has a microtubule binding domain and is localized to the ER membrane. The ER structure can be rearranged when this protein is overexpressed (Sandoz and Van der Goot, 2015). Although proteins which anchor the plant ER to the microtubules are not yet known, microtubules are considered to be important to the rearrangement of the ER structure. MTs regulate the extension of the ER tubules with an almost 20-fold slower rate compared with the actin-based tubule extension, and the cortical microtubules also provide the branching points of the ER tubules which contribute to form the multi-way junctions (Hamada *et al.*, 2014).

In addition to the cytoskeleton, some ER proteins such as Arabidopsis RTNLB13 and RHD3 also participate in the shaping of the ER network. RTNLB13 is a member of the Arabidopsis reticulon family and it is localized to the ER tubules. Overexpression of this protein introduces constrictions in ER tubules and reduces diffusion of proteins in the ER lumen (Tolley *et al.*, 2010, Tolley *et al.*, 2008). As suggested by Breeze et al., (2016), the C-terminal amphipathic helix (APH) is considered to be very important to the function of RTN13. RTN13 without the APH region is still able to form oligomers, although its ability of constricting ER tubules is disrupted (Breeze *et al.*, 2016). RHD3 is another protein that regulates the ER membrane fusion. RHD3-like 1 and RHD3-like 2 are two RHD3 isoforms in Arabidopsis (Chen *et al.*, 2011, Lee *et al.*, 2013), and the two RHD like proteins are functionally redundant to RHD3 (Zhang *et al.*, 2013). According to Ueda et al. (2015), phosphorylation of the C-terminus of RHD3 promotes the fusion efficiency of the ER membrane and kinase treatment induces the oligomerization of RHD3, which regulates the ER-remodeling function of this protein (Ueda *et al.*, 2016).

During cell division, all organelles of the cell are significantly reorganized (Voeltz *et al.*, 2002). As for the ER network, it is divided between daughter cells by cytokinesis during the cell cycle instead of disassembling into vesicles (Voeltz *et al.*, 2002). In mammalian cells, during interphase, the ER displays the typical polygonal structure, with convolved cisternae associated with tubules localize mainly in the peripheral and bottom regions of the cells. However, from prometaphase to telophase, the cisternal ER extends, with a few tubular ER attached to spindle (Lu *et al.*, 2009).

1.1.2. The Golgi Apparatus and Endomembrane Trafficking

In eukaryotic cells, the Golgi apparatus (GA) is another important compartment of the secretory pathway in addition to the ER. In animal cells, it is stationary and near the nucleus and mainly comprises a stacks of flattened Golgi cisternae which can be sub-divided into trans-Golgi, medial-Golgi and cis-Golgi (Ladinsky *et al.*, 1999, Robinson *et al.*, 2015), but in higher plants, the GA is polydisperse and motile

(Robinson *et al.*, 2015). The main function of the GA is the modification and processing of newly synthesized lipids and proteins in various ways, such as adding *N*- or *O*-linked sugar chains, lipidation and phosphorylation (Capasso *et al.*, 1989, Gusarova *et al.*, 2007, Zhang and Wang, 2016). In addition, in plant cells, the GA also serves as polysaccharide factors and is involved in the biosynthesis of the cell wall polysaccharides (Pauly and Keegstra, 2016).

After modification, mature cargo proteins are ready to be sorted and transported to the final destinations including the extracellular space and the internal endomembrane compartments (Gomez-Navarro and Miller, 2016). Many intracellular organelles and intermediate compartments, such as the ER, ER exit sites (ERES), the ER-to-Golgi intermediate compartment (ERGIC), the GA and the trans-golgi network (TGN) are involved in the secretory pathway (Szul and Sztul, 2011). The first step of this pathway is ER-to-Golgi transport. Coat protein complex II (COPII) and coat protein complex I (COPI) are two cytoplasmic proteins used in this exocytic pathway. Secretory proteins which are correctly folded and assembled are captured into COPII coated vesicles and transported to the Golgi complex. Many soluble proteins are sorted by an appropriate receptor before being exported from the ER, but some of them can also simply diffuse into the forming vesicles by bulk flow without selection. Escaped ER proteins and some recycled essential vesicle components are retrieved to the ER by COPI coated vesicles (Barlowe and Miller, 2013, Gomez-Navarro and Miller, 2016).

Ras-related protein 1 (Sar1), Sec13/Sec31 and Sec23/Sec24 are the main components of COP II protein complex. Sec13 and Sec31 form the inner shell which functions in protein sorting, while Sec23 and Sec24 form the outer layer which contributes to the coat formation process (Lord *et al.*, 2013). These five proteins are highly conserved across eukaryotes and several COPII homologs have been identified for ER export in plants (Marti *et al.*, 2010). Recent studies have revealed some plant specific mechanisms and functions of the COPII mediated transport and the COPII machinery plays very important role in plant development and responses. For instance, loss of

function of Sec24A leads to lethality and in *sec16a* mutant seeds, the accumulation of storage protein precursors is abnormal. (De Craene *et al.*, 2014, Faso *et al.*, 2009, Takagi *et al.*, 2013, Zeng *et al.*, 2015). Although COPII proteins are considered to be very important in the early secretory pathway, there could also be a COPII vesicular-independent transport manner in several organisms, where the ER export is not affected in the absence of COPII coated vesicles (Ito *et al.*, 2018, Mironov, 2014, Viotti *et al.*, 2013). Unlike mammals and yeast, the plant ER-Golgi interface has unique structures (Chung *et al.*, 2016). In addition of the traditional vesicle budding transport manner, the plant ER can also link the Golgi apparatus directly through membrane-bound tubules which are used for the anterograde transport of proteins (Robinson *et al.*, 2015).

After protein and lipid cargos are transported from the ER to the cis-Golgi cisternae, they need to be properly modified as they pass through the cisternae of each stack of the GA and finally go to the trans-Golgi network (TGN) for further transportation (Jackson, 2009, Staehelin and Moore, 1995). There are three models for understanding the mechanisms of the transport through the Golgi apparatus, including the vesicle mediated anterograde transport model, the cisternal maturation model as well as the rapid-partitioning model which is developed recently and gives a new framework for the intra-Golgi trafficking (Figure 1.1) (Jackson, 2009).

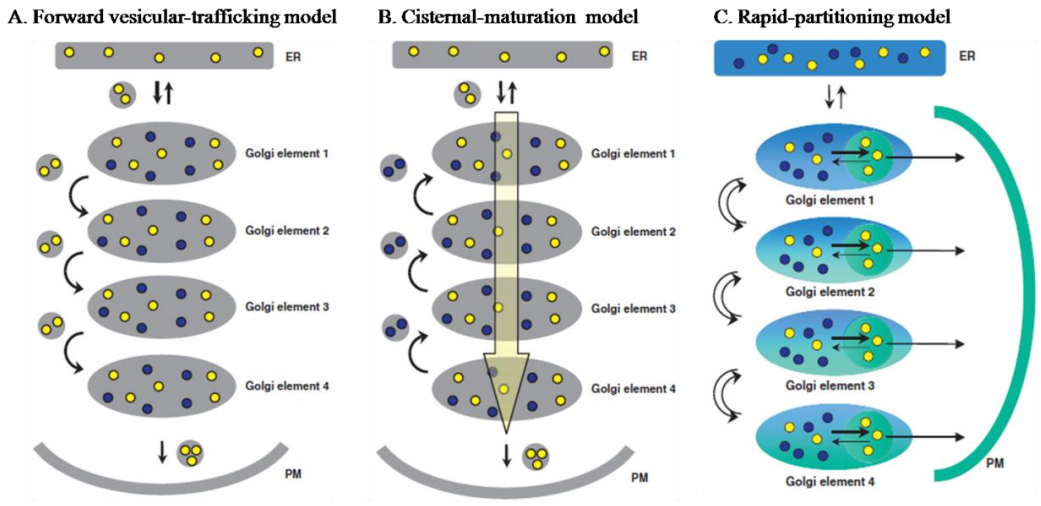

Figure 1.1 Models for intra-golgi trafficking. A. Forward vesicular-trafficking model. Vesicles carrying cargo bud from a donor compartment, and are then targeted to and fuse with the following compartment. B. Cisternal-maturation model. The cargo progresses as a result of maturation of an earlier compartment into a later one in the secretory pathway. Vesicles carrying Golgi processing enzymes bud from a later compartment, and then fuse with an earlier compartment. C. Rapid-partitioning model. Vesicles carrying cargo bud from the ER and are moved to the *cis*-Golgi. Cargo can move both in the *cis*-to-*trans* and *trans*-to-*cis* directions in the Golgi and can be delivered to the PM by transport carriers generated in the Golgi. Golgi processing enzymes synthesized in the ER are transported the Golgi via forward vesicular trafficking, and they can then move between the Golgi stacks in a bidirectional manner similar to the cargo. Cargo synthesized in the ER is shown in yellow; Golgi processing enzymes are shown in blue. Figure from Jackson (2009).

The trans-Golgi network plays a critical role in regulating a number of trafficking pathways, such as secretion to the PM and cell plate, traffic to the vacuole, and acting as the receptor of endocytic cargos (Gendre *et al.*, 2015). For many years, the morphology of the trans-Golgi network is not well described and is often considered to be released from the trans side of the Golgi (Hawes *et al.*, 2010, Suda and Nakano, 2012). However, more and more recent studies have revealed that the TGN is a functionally and morphologically independent organelle. It has a set of distinct protein residents which are locally regulated (Kang *et al.*, 2011, Uemura *et al.*, 2014, Viotti *et al.*, 2010). Although some of cargos can be secreted directly from the Golgi stack instead of passing through the TGN, a majority of the cell surface related cargos are secreted via the TGN platform (Gendre *et al.*, 2015). Secretory cargos are sorted and packaged into vesicles and released into the extracellular environment by

membrane fusion (Gendre *et al.*, 2015). In mammal cells, the interaction between cargo sorting motifs and specific vesicle coat components is essential for vesicle cargos selection at the TGN (Gu *et al.*, 2001). Recently, Ca^{2+} has also proved to be a main factor in cargo sorting process in mammal and yeast cells (Kienzle and von Blume, 2014). When the concentration of Ca^{2+} in the TGN is disrupted, the protein secretion can be reduced (von Blume *et al.*, 2012).

In addition to the membrane compartments, the cytoskeletons are also important in the secretory trafficking, where cargo vesicles are transported to the final destinations along microtubules and microfilaments (Gendre *et al.*, 2015). Polarized tip growth of plant cells needs additional cell wall material and membrane lipids that are transported by secretory vesicles to the cell surface, and this trafficking process is proved to be regulated by actin filaments (Nebenführ and Dixit, 2018). For example, after treatment with the actin polymerization inhibitor latrunculin B (Lat B), the pollen tube development was affected and the number of secretory vesicles in the pollen tubes significantly reduced (Chen *et al.*, 2006). According to Preuss et al (2004), RabA4b labeled secretory vesicles are specifically localized at the tips of root hair cells and the polar localization is disrupted after Lat B treatment (Preuss *et al.*, 2004b). Myosin motors are considered to be required for the transport of secretory vesicles to the growing tips as tip growth rates can be affected in myosin mutants (Madison *et al.*, 2015, Park and Nebenführ, 2013). Cellulose synthase complexes (CesAs) are essential for synthesizing cellulose microfibrils of the cell wall. The actin cytoskeleton is reported to be involved in the transport of the CesA to the PM as the delivery rate of the complexes reduces without actin filaments (Sampathkumar *et al.*, 2013). In addition to actin filaments, the microtubule cytoskeleton is also thought to mediate cellular vesicular delivery. Atkinesin-13A, one of the plant microtubule motor proteins is localized at Golgi stacks and loss of function of this protein leads to significant reduction of the size and number of secretory vesicles in root cap cells (Wei *et al.*, 2009). As suggested by Zhu et al (2015), The Arabidopsis kinesin-4 family member, Fragile Fiber1 (FRA1) participates in the delivery of vesicles

containing cell wall material along microtubules. The thickness of the cell wall and the growth rate of the stem are reduced in the *fra1* mutants (Zhu *et al.*, 2015). All of these examples demonstrate the indispensable function of actin in membrane trafficking.

Once secretory vesicles are transported to their final destination membranes, they need to be tethered, docked and fused specifically with the next compartment. Several proteins are required to accomplish these processes (Figure 1.2) (Behnia and Munro, 2005). The Ras-like GTPase (Rabs) and tethering proteins are major of proteins that regulate the accurate vesicle targeting before membrane fusion (Gendre *et al.*, 2015). Rab proteins can be activated by guanine-nucleotide exchange factors (GEFs) and then interact with various effector proteins which carry out their downstream functions such as cargo selection and vesicles transportation and fusion with the target membrane. After the correct targeting, the Rab bound GTP can be hydrolyzed to GDP and by GTPase activating proteins (GAPs) and the Rab becomes inactivated (Hervé and Bourmeyster, 2018, Müller and Goody, 2018). SNARE proteins (SNAP receptor) are integral membrane proteins that mediate docking and specific membrane fusion. They can be subdivided into vesicle localized v-SNAREs and target compartment localized t-SNAREs. The interaction between v-SNAREs and t-SNAREs leads to the formation of trans-SNARE complexes and the complexes pull the two membranes together and finally catalyze membrane fusion (Hong and Lev, 2014). Once the fusion process has occurred, N-ethylmaleimide-sensitive factor (NSF) and soluble NSP attachment protein (SNAP) are used to disassociate the SNARE complexes on the fused membrane (cis-SNARE complex) so that the SNAREs can be recycled for the new membrane fusion process (Jahn *et al.*, 2003, Sollner *et al.*, 1993).

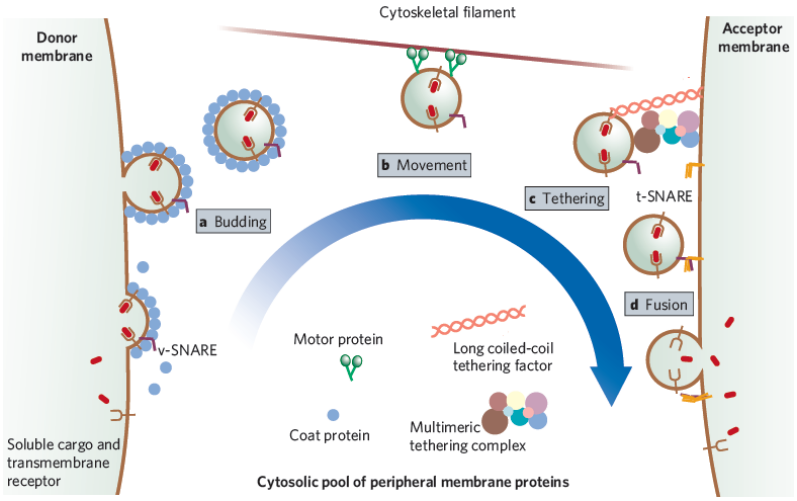

Figure 1.2 Steps of vesicle transport from donor membrane to acceptor membrane. a. Vesicles carrying cargo are coated with coat proteins and bud from the donor membrane. b. Uncoated vesicles travel along cytoskeleton through interacting with motor proteins. c. Vesicles are tethered to the acceptor membrane through long coiled-coil proteins or multimeric tethering complexes. d. The SNARE proteins drive membrane fusion and cargo is released. Figure form Behnia and Munro (2005).

1.1.3. The Nuclear Envelope

The nucleus which is considered as the home of the chromosomes is the most prominent compartment in eukaryotic cells. The delicate genetic information is separated from the periplasmic space and enclosed by a highly organized double membrane sheet, the nuclear envelop (NE) (Hetzer *et al.*, 2005). The NE is composed of two closely paralleled lipid membranes, the inner nuclear (INM) which encloses the nucleoplasm and the outer nuclear membrane (ONM) that is continuous with the ER. The INM and ONM are joined with each other at numerous specific sites to form membrane pores (De Magistris and Antonin, 2018). These aqueous pores are filled with large protein complexes termed nuclear pore complexes (NPCs) which serve as the main channels for the macromolecules trafficking between nucleoplasm and cytoplasma (Boruc *et al.*, 2012).

The ONM and INM contain their own specific integral membrane proteins that perform various kinds of cellular functions (Tamura *et al.*, 2015). In animals and yeast,

the nuclear envelope proteins have roles in nuclear morphology, cellular mechanotransduction, chromatin organization, gene regulation, cell cycle and cell migration (Gundersen and Worman, 2013, Isermann and Lammerding, 2013, Jevtic *et al.*, 2014, Wong *et al.*, 2014, Zuleger *et al.*, 2011). Although nuclear pore proteins are highly conserved among eukaryotes, the similarity of sequence between plants and opisthokonts (which include two large kingdoms with very different life styles: animals and fungi as well as their unicellular relatives) is very low (Devos *et al.*, 2014, Torruella *et al.*, 2011, Wilson and Dawson, 2011, Zhou and Meier, 2013).

The nuclear lamina (NL) is a meshwork of filaments situated beneath the INM. It plays a vital role in chromosome organization and gene expression by interacting with the genomic DNA (Amendola and van Steensel, 2014). In animal cells, the main component of the nuclear lamina structure is a set of long coiled-coil proteins termed lamins. Loss of function of lamins or the lamins binding partners leads to various human diseases called laminophathies (Tamura *et al.*, 2015). In plant cells, crowded nuclei (CRWN) proteins which are localized at the nuclear periphery or nucleoplasm are considered as protein candidates of the constituents of the lamina-like structure (Ciska and Moreno Diaz de la Espina, 2014, Sakamoto and Takagi, 2013, Wang *et al.*, 2013). Several functional studies revealed that the CRWNs are essential for the viability of cells and should be involved in the maintenance of the nuclear envelope morphology and the organization of chromosome (Dittmer *et al.*, 2007, Sakamoto and Takagi, 2013, Wang *et al.*, 2013). Recently, a novel protein KAKU4 has been identified as another component of plant lamina like structure. It is localized on the INM and interacts with CRWN1 and CRWN4. The functional study revealed that KAKU4 and CRWN1 work in the same pathway and this complex functions in the regulation of nuclear shape and size (Goto *et al.*, 2014).

LINC (linker of nucleoskeleton and cytoskeketon) complexes which link the nucleoskeleton to the cytoskeleton and motor proteins play an important role in various cellular functions, such as nuclear migration and chromosomal organization (Tamura *et al.*, 2015). In animals, the LINC complexes are made up of ONM

localized KASH (Klarsicht, ANC-1 and SYNE homology) domain proteins and INM localized SUN (Sad1 and UNC84) domain proteins (Zhou and Meier, 2013). SUN proteins interact with lamina structure and KASH proteins are directly or in directly associated with cytoskeleton system (Meier *et al.*, 2016). In Arabidopsis, there are five SUN proteins belonging to two subgroups. SUN1 and SUN2 are classical Cter-SUN proteins which have SUN domains at the C-terminus, while SUN3, SUN4 and SUN5 are mid-SUN proteins that have SUN domains between trans-membrane domains (Murphy *et al.*, 2010). SUN1 and SUN2 are localized on the INM and the localization of SUN3 and SUN4 are both the NE and ER (Evans *et al.*, 2014, Graumann *et al.*, 2014).

WPP domain-interacting proteins (WIPs) are the first identified KASH proteins in plants and all three Arabidopsis WIPs (AtWIP1, AtWIP2 and AtWIP3) interact with AtSUN1 and AtSUN2 and another ONM protein AtWIT1 (Zhao *et al.*, 2008, Zhou *et al.*, 2012). According to Zhou et al (2015), SUN, WIP and WIT form a complex at the pollen vegetative nucleus (VN) envelope. This complex functions in the migration of the VN and SUN, WIP and WIT are considered to be very important for the guidance and reception of pollen tubes (Zhou *et al.*, 2015c). In addition, because of the interaction of AtSUN with WIP, WIT2 and myosin XI-i, the nucleoskeleton links the cytoskeleton and plays a critical role in nuclear shape determination (Zhou *et al.*, 2015b). As suggested by Zhou et al. (2014), another five SINE proteins, SINE1, SINE2, SINE3, SINE4 and SINE5 have been confirmed to be plant KASH domain proteins by means of a computational method. They are localized on the NE and interact with SUN1 and SUN2 through their C-terminal tails. Some functional studies reveal that SINE1 is associated with actin filaments and involved in the nuclear positioning in Arabidopsis guard cells, while SINE2 is very important for plant immunity to the Arabidopsis downy mildew pathogen *Hyaloperonospora arabidopsidis* (*Hpa*) (Zhou *et al.*, 2014). In addition, AtTIK is another plant KASH protein which was identified by a membrane-based yeast-two-hybrid screen. It interacts with AtSUN1, AtSUN2 and AtSUN3 and participates in Arabidopsis root

development and nuclear size (Graumann *et al.*, 2014). NEAP proteins belong to a novel family of nuclear envelop-associated proteins in plant cells. They are able to form homo- and heteromers and localized on the inner nuclear membrane. They can be considered as part of the LINC complexes because of the interaction with AtSUN1 and AtSUN2. Loss of function of At NEAP1 and AtNEAP3 leads to the reduction of root growth and the nuclear morphology and chromatin organization are also affected (Pawar *et al.*, 2016). Functions of Arabidopsis SUN and KASH proteins are shown in Figure 1.3 (Zhou *et al.*, 2015a).

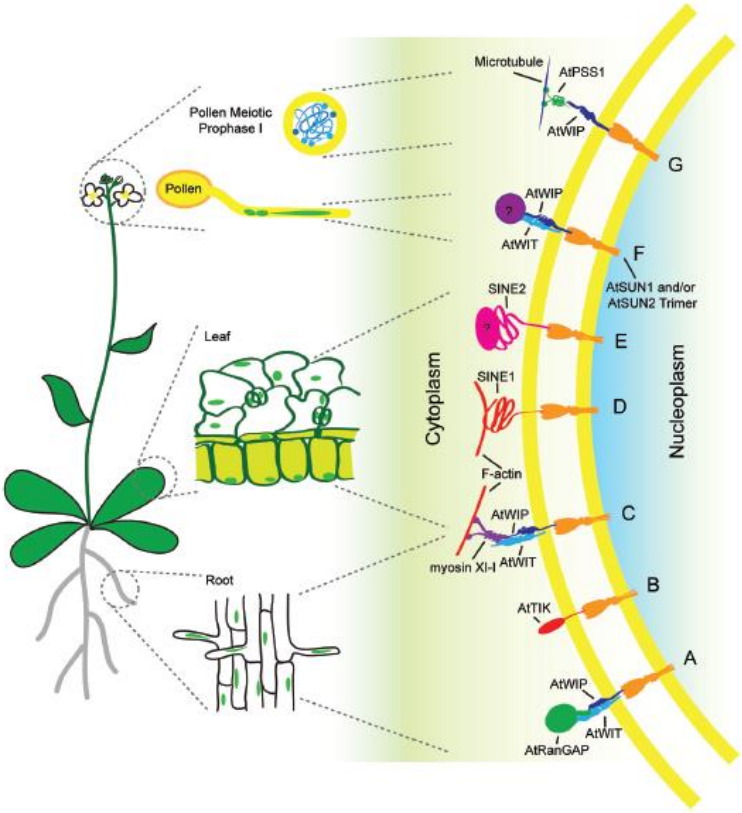

Figure 1.3 Functions of Arabidopsis SUN and KASH proteins have been studied. A. AtRanGAP is anchored at the NE by the AtSUN-AtWIP-AtWIT complex. B. The AtSUN-AtTIK complex functions in root development and nuclear size. C. The nucleoskeleton is associated with the cytoskeleton through the AtSUN-AtWIP-AtWIT-AtMyosin XI-i complex, regulating the nuclear shape and movement in roots. D. The AtSUN-SINE1 complex tethers nuclei to actin filaments in guard cells and regulates the nuclei position. E. The AtSUN-SINE2 complex is involved in plant immunity to the oomycete pathogen *Hpa*. F. The AtSUN-AtWIP-AtWIT complex mediates the migration of vegetative nucleus, guiding the growth of pollen tube. G. The AtSUN-AtWIP-AtPSS1 complex regulates the distribution of chromosome crossovers by transferring the forces generated by AtPSS1 to chromosomes. Figure from Zhou *et al*. (2015).

1.2. The Plant Cytoskeletons and Their Function in Cell Morphogenesis

The plant cytoskeleton is a highly dynamic filamentous system in plant cells. It is mainly comprised of two protein polymer networks, actin microfilaments and microtubules and forms an important part in various intracellular processes including cell division, cell expansion and differentiation, intracellular trafficking and stress tolerance (Kost and Chua, 2002, Petrasek and Schwarzerova, 2009, Wang *et al.*, 2011). Although the structure of plant cytoskeleton is not significantly different form animal and fungal, the unique architecture of plant cells requires this network to have plant-specific control mechanisms for the special strategies of cell development and responses of environmental signals (Kost and Chua, 2002). The development of the technology in cell research provides more opportunities to reveal the functions of the cytoskeleton in cell development processes (Wasteneys and Yang, 2004).

1.2.1. The Actin Cytoskeleton of Plants

Actin is a highly conserved protein which is expressed in all eukaryotic cells. It is considered to be very diverse and is comprised of different isoforms encoded by multiple actin genes. In animal cells, there are six genes encoding three isoforms of actin: α-actin, β-actin and γ-actin. Although all of these isoforms have remarkably similar amino acid sequences, they are present in different cell types and perform different functions. The α-actin is mainly expressed in muscle cells, while the other two isoforms, β-actin and γ-actin are present in nonmuscle cells (Perrin and Ervasti, 2010). In Eukaryotic cells, actin is found in two forms: globular actin monomers (G-actin) and filamentous actin (F-actin). Several proteins within cells are able to coordinate the transition between these two forms of actin by means of polymerization and depolymerization (Pollard and Borisy, 2003, Welch *et al.*, 1997).

The polymerization and depolymerization cycles of actin filaments is regulated by the

nucleotide binding activity of actin subunits, which are able to bind both ATP (adenosine triphosphate) and ADP (adenosine diphosphate) in a nucleotide binding site (Kabsch *et al.*, 1990). During polymerization, G-actin monomers being added to the elongating F-actin filaments are bound to ATP. After actin monomers are integrated into the filament, the ATP is subsequently hydrolyzed to ADP (Enrique *et al.*, 2000). F-actin subunits bound to ADP have reduced binding affinity for neighboring actin subunits, allowing disassociation of the filament more readily (Orlova and Egelman, 1992).

An actin filament is a right-handed double helical string of globular actin monomers. The head-to-tail organization of the subunits gives the filament a polar feature which is essential for cellular directional transportation and establishment of polarized cell shape. Based on the presence of the actin bound myosin, one end of the filament is called the barbed end (plus end) and the other one is the pointed end (minus end). The polarity is very important for actin polymerization and depolymerization. The plus end is favored for actin assembly, while depolymerization usually occurs on the minus end (Pollard and Borisy, 2003).

In plant cells, the dynamics and organization of actin filaments are regulated by a large number of actin binding proteins (ABPs) that are associated with actin monomers or actin filaments. These proteins enable actin to involve in various kinds of cellular processes, such as material transportation, actin polymerization and depolymerization, actin bundling, filament capping and so on (Hussey *et al.*, 2006).

1.2.2. The Microtubule Cytoskeleton in Plant Cells

The microtubule cytoskeleton is considered to be an “engine for cellular organization” (Ehrhardt and Shaw, 2006). In plant cells, it plays a vital role in various cellular processes such as cell division, directional cell expansion, cell wall formation and signal transduction (Mineyuki, 2007, Murata and Hasebe, 2007). Microtubules form a hollow tube about 25 nm in diameter and are assembled form protein tubulins.

Tubulin is a highly conserved heterodimeric protein which is comprised of one α-tubulin polypeptide and one β-tubulin polypeptide (Goddard *et al.*, 1994, Mineyuki, 2007). In Arabidopsis, there are six α-tubulin genes and nine β-tubulin genes. α-tubulin proteins are highly conserved, while the sequences of β-tubulin proteins vary at C-terminal regions which are correlated with different posttranslational modifications and potential binding proteins (Kopczak *et al.*, 1992, Parrotta *et al.*, 2014, Snustad *et al.*, 1992).

Each microtubule is a polar structure with two different ends because of the arrangement of subunits. A cap of β-tubulins is exposed at the plus end of the microtubule, while a ring of α-tubulins is exposed at the minus end (Zheng *et al.*, 1995). Microtubule assembly is a self-assembly process which depends on the high concentration of purified tubulin and GTP *in vitro* (Elliott and Shaw, 2018). In plant cells, an evolutionarily highly conserved protein γ-tubulin-containing ring complex (γ-TuRCs) is required for microtubule nucleation *in vivo*. This protein complex is localized to both the PM and the nuclear envelope and can be recruited to the sides of a preexisting microtubule or outer nuclear membranes to act as a template for new microtubules of defined geometry. (Erhardt *et al.*, 2002, Murata and Hasebe, 2007, Seltzer *et al.*, 2007, Zheng *et al.*, 1995).

The dynamic instability of microtubules is a unique polymerization mechanism which depends on the energy of GTP hydrolysis (Desai and Mitchison, 1997). They randomly switch between assembly and disassembly (Mitchison and Kirschner, 1984). The growth to shrinking transition is named catastrophe, while the transition from shrinking to growth is named rescue. GTP-bound tubulin dimer binds to the microtubule polymerizing end (plus end), the bound GTP is then hydrolyzed to GDP during or soon after polymerization and the microtubule lattice is mainly comprised of GDP-tubulin. Polymerizing microtubules infrequently transit to the depolymerization phase. Depolymerizaing is defined as the very rapid loss of GDP-tubulin subunits and oligomers from the microtubule end and depolymerizing microtubules can also infrequently transit back to the polymerization phase (Desai

and Mitchison, 1997).

The organization and dynamic instability of microtubules can be regulated by microtubule associated proteins (MAPs) which have direct or indirect interaction with microtubules (Struk and Dhonukshe, 2014). In plant cells, a large number of MAPs have been identified with various different functions. Arabidopsis MICTOTUBULE ORGNIZATION 1 (MOR1) is a member of the MAP215/DIS1 family (Whittington *et al.*, 2001). MOR1 is localized to cortical microtubules and to areas of overlapping microtubules in the phragmoplast, preprophase band and spindle. It is involved in stabilizing the growing ends of microtubules and is important for proper structure and function of preprophase bands and spindles (Kawamura *et al.*, 2006, Twell *et al.*, 2002). At restrictive temperatures, the loss of function of MOR1 causes shorter microtubules in all arrays, which results in aberrant chromosomal arrangements, misaligned or incomplete cell plates, and multinucleate cells (Kawamura *et al.*, 2006). The MAP65 family is a group of 60-65 kDa MAP proteins which are evolutionarily conserved (Chang-Jie and Sonobe, 1993). In plant cells, the MAP65 family stabilizes microtubules by forming cross-bridges between overlapping microtubules (Struk and Dhonukshe, 2014). The Arabidopsis genome contains nine MAP65 genes which encode proteins sharing identities between 28% (MAP65-4 and MAP65-8) and 78% (MAP65-1 and MAP65-2) (Smertenko *et al.*, 2008). During cell division, members of MAP65 family have diverse functions and localize to distinct microtubule arrays (Struk and Dhonukshe, 2014). Currently, MAP65-1 is the most studied member of the MAP65 family. It induces the formation of large microtubule bundles (Gaillard *et al.*, 2008). AtMAP65-1 is able to promote microtubule polymerization and nucleation, and reduce the cortical concentration for tubulin polymerization (Mao *et al.*, 2005). MAP65-2 is colocalized with MAP65-1 in almost all of the microtubule arrays during the cell cycle. Loss of function of both AtMAP65-1 and AtMAP65-2 genes results in significant growth retardation, indicating their important roles in axial cell growth (Lucas *et al.*, 2011). AtMAP65-3 is only localized to the preprophase band during cell division and cannot be observed at the interphase cortical microtubules. The

atmap65-3/pleiade mutants exhibit abnormal phragmoplast formation and defective root morphogenesis (Muller *et al.*, 2004).

Kinesins belong to a family of molecular motors that use the chemical energy of ATP hydrolysis to move along the surface microtubules (Verhey and Hammond, 2009). In Arabidopsis, 61 kinesin-like genes have been identified and they are important for various cellular processes (Reddy and Day, 2001, Zhu and Dixit, 2012). The kinesin 1 (ATK1) is involved in mitotic and meiotic spindle function. During cell division, loss of function of ATK1 results in abnormal spindle organization and chromosome segregation, thereby reducing male fertility (Ambrose *et al.*, 2005). ATK5 shares 83% amino acid sequence identity with ATK1 and also functions in spindle assembly and organization (Ambrose *et al.*, 2005). Armadillo repeat domain-containing kinesins ARK1 and ARK2 are likely to promote depolymerization of microtubules. ARK1 is involved in root hair morphogenesis and the loss of function of ARK2 leads to helical root growth (Sakai *et al.*, 2008).

1.2.3. The Regulation of Leaf Pavement Cell Shape

Cell polarity, considered as asymmetry within a cell, is an essential feature of cell function which is closely associated with developmental and environmental regulation. The cell polarity can be established through the regulation of the polar distribution of signaling molecules and maintained by the cytoskeleton and vesicular trafficking. In plant cells, polarity plays a vital role in development, growth as well as the cell shape formation (Yang, 2008). Various model systems including the pollen tube, trichome, the root hair and leaf pavement cells have been adopted for studying the establishment and maintenance of the polarity and morphogenesis (Yang, 2008).

Arabidopsis leaf pavement cells have an interlocking jigsaw puzzle appearance with lobes and indentations. The development of pavement cells relays on complicated and dynamic polarity formation (Lin *et al.*, 2015, Yang, 2008). The formation of the jigsaw-puzzle appearance can be separated into three stages and is associated with

both cortical actin filaments and microtubules. During the first stage, elongated polygons are formed from near-square pavement initial cells that preferentially expand along the leaf long axis. The stage I cells initiate multiple outgrowths or localized lateral expansion to generate alternating small bumps and indentations, producing stage II cells with multiple shallow lobes and indentations (also termed sinuses or necks). In the stage III, the formation of reiterative lobe and neck continues and highly lobed interlocking pavement cells with secondary lobes are generated (Figure 1.4) (Fu *et al.*, 2005, Smith, 2003). Development of the pavement cells is controlled by the cytoskeleton. Well-ordered cortical microtubules are associated with the neck regions and are thought to guide the deposition of cellulose microfibrils for the inhibition of cell expansion in the direction of their predominant orientation. Removal of cortical microtubules leads to isotropic cell expansion (Ehrhardt and Shaw, 2006, Wasteneys and Galway, 2003). In contrast, cortical fine actin filaments which are localized to the growing lobe tips lacking well ordered cortical microtubules are believed to regulate lobe initiation and outgrowth (Frank and Smith, 2002, Fu *et al.*, 2002).

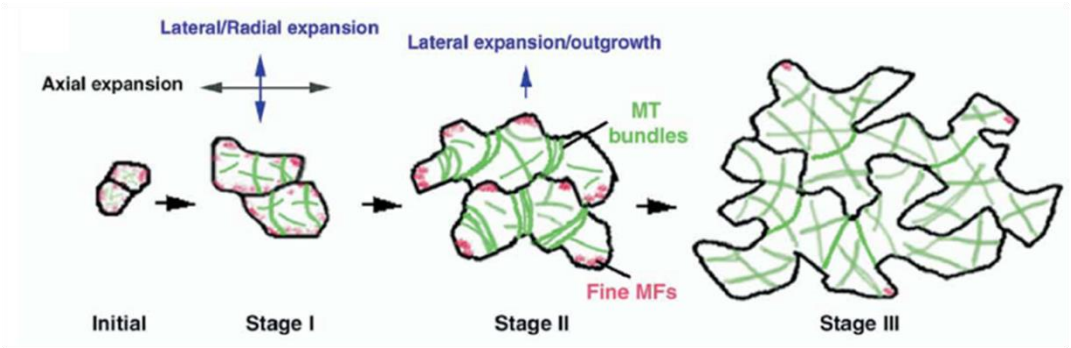

Figure 1.4 Model of development of Arabidopsis leaf pavement cell. Arrows represent directions of cell expansion. Figure from Fu *et al.* (2005).

Various proteins have been identified to regulate the organization and dynamics of actin filaments and microtubules and control the pavement cell expansion (Mathur, 2006). In eukaryotic cells, the Rho GTPase family is a conserved regulator of the cytoskeleton (Etienne-Manneville and Hall, 2002, Yang, 2008). In plant cells, a subfamily named ROP (Rho of Plants) has been found to be involved in

interdigitating cell growth. Members of ROP subfamily interact with ROP interactive CRIB motif-containing proteins (RIC) and function in cell growth by means of regulating cytoskeleton organization and membrane trafficking (Hussey *et al.*, 2006, Smith and Oppenheimer, 2005, Yalovsky *et al.*, 2008). To date, two ROP-based signaling pathways which regulate lobes outgrowth and necks expansion of pavement cells have been identified. It is an auxin-dependent, self-organizing system. In this mechanism, the auxin binding protein 1 (ABP1) forms an auxin sensing complex with the transmembrane Kinase 1 (TMK1) at the cell surface to sense the localized extracellular auxin and activate antagonistic ROP2 and ROP6 pathways, respectively, to regulate the pavement cell interdigitation. Lobe outgrowth is promoted by the ROP2-RIC4 pathway that regulates fine cortical actin filaments in the lobe tips, while the ROP6-RIC1-KTN1 (microtubule-severing protein, katanin) pathway promotes well-ordered cortical microtubules in the neck regions to inhibit indentation outgrowth. Localized extracellular auxin is generated by self-activation via the auxin-ROP2-PIN1-auxin feedback loop and is maintained via the antagonizing ROP6 pathway (Fu *et al.*, 2005, Fu *et al.*, 2002, Fu *et al.*, 2009, Lin *et al.*, 2013, Nakamura *et al.*, 2010, Xu *et al.*, 2014, Xu *et al.*, 2010). In addition to auxin, cytokinin signaling also functions as upstream of ROPs to regulate the pavement cell interdigitation pattern. Pavement cell interdigitation can be enhanced by reducing the cytokinin accumulation, while over production of cytokinin is able to delay or abolish pavement cell interdigitation (Li *et al.*, 2013).

ARP2/3 and SCAR/WAVE complex activity also functions in regulating the cytoskeleton organization and contributes to the normal pavement cell development (Qian *et al.*, 2009). Arp2/3 complex is able to cap the pointed end of the actin filaments and promote the barbed end actin assembly. It promotes actin nucleation from the flanks of existing actin filaments and actives the formation of branched F-actin (Hussey *et al.*, 2006). The development of puzzle piece-shaped epidermal cells can be affected in the *ARP2* or *ARP3* mutants. Loss of function of ARP2 or ARP3 leads to mislocalization of diffuse cortical actin filaments to the neck region

and suppresses lobe outgrowth (Li *et al.*, 2003). Arabidopsis WAVE complex is able to convert Rac/ROP small GTPase signals into an ARP2/3 activation response. The four SCAR subunits of the WAVE complex which bind to the ARP2/3 act as the primary activator of ARP2/3. The pavement cells of the *scar* quadruple mutant have a more simple shape compared with the wild type (Zhang *et al.*, 2008). According to Le et al. (2006), BRICK/HSPC330 is a critical subunit of WAVE complex that selectively stabilizes the ARP2/3 activator SCAR2 and loss of function of this protein causes abnormal pavement cell shape (Le *et al.*, 2006).

Additionally, some other proteins are also involved in modulating pavement cell development. For example, the receptor of *Irx1* (*rol1*) mutants of Arabidopsis display aberrant pavement cells and this is induced by the modified flavonol profile (Ringli *et al.*, 2008). Two *CONSTITUTIVE EXPRESSER OF PATHOGENESIS RELATED GENES1* (*CPR1*) alleles which are identified form ethyl methane sulfonate mutagenesis on Col-0 background are associated with pavement cell morphogenetic defects. In *cpr1*, the polar growth initiation and expansion of pavement cells are inhibited. The organization of microtubules is defective and the cortical fine actin filaments fail to aggregate to form actin cables (Han *et al.*, 2015). Plant formins (FH2 domain containing proteins) which is a large protein family of actin nucleators act as major regulators of actin bundling and dynamics (Blanchoin and Staiger, 2010). FH1, the class I formin, participates in pavement cell morphogenesis and macroscopic organ development through regulating actin bundling and microtubule dynamics (Rosero *et al.*, 2016). IQ67 DOMAIN (IQD) proteins are members of the largest class of CaM interacting protein family. They are microtubule localized and have many unknown molecular functions. A recent study reveals that loss of function of IQD5 leads to reduction interdigitation of leaf pavement cells. The reduced asymmetric expansion is associated with the reduced rates of cellulose deposition in anticlinal cell walls. As calmodulin calcium sensors can be recruited to cortical microtubules, calcium signaling can be associated with multi-polar growth in pavement cells (Liang *et al.*, 2018).

1.2.4. The Regulation of Organ Helical Growth

In plant cells, directional cell expansion plays a vital role in the formation of the final shape of the mature cells and organ architecture. Helical growth, in which the growth axis is continuously tilted ether to the right (right handed growth) or to the left (left handed growth) when the cell grows is an interesting mode of cell expansion. This kind of growth is usually found in climbing plants with twining tendrils and plants with spiral ordered leaves, petals and florets (Ishida *et al.*, 2007, Wada, 2012). In general, the polarity of cell expansion is mainly determined by the spatial distribution of cell wall microfibrils and the cortical microtubules have been proved to be a cytoplasmic template for microfibril orientation (Paredez *et al.*, 2006a).

The twisting mutants of Arabidopsis are considered to be an ideal system for studying the correlations between the alignment of cortical microtubules and the helical growth (Ishida *et al.*, 2007). Various Arabidopsis genes have been found to be essential for the microtubule organization and loss of function of these genes leads to twisting growth phenotypes in cells at the elongation zone such as roots, etiolated hypocotyls, petioles and petals (Ishida *et al.*, 2007). *Spiral* (*spr*) *spr1* and *spr2* mutants are the first identified twisting mutants. They are right handed mutants and their roots and hypocotyls tilt to the right on the hard agar. *Spr2* mutants also show right handed twisting in petioles and petals. The phenotype of the *spr1spr2* double mutants is synergistic, indicating that SPR1 and SPR2 function in different pathways in controlling directional cell elongation. It is a microtubule dependent process. The arrangement of cortical microtubules in elongating cells of *spr1* roots are left handed and the microtubule orientations of *spr1* hypocotyls are irregular (Furutani *et al.*, 2000). SPR1 is a plant specific microtubule localized protein and its conserved N- and C-terminal domains function in its microtubule localization and cell expansion control. SPR1 is mainly expressed in rapidly expanding cells. Plants overexpressing SPR1 have enhanced tolerance to microtubule drugs (Nakajima *et al.*, 2004). According to Shoji et al. (2006), loss of function of the PM Na^+/H^+ antiporter SOS1 and its

regulatory Kinase SOS2 is able to suppress both microtubule organization and twisting growth phenotype of *spr1* (Abe and Hashimoto, 2005).

WAVE-DAMPENED2 (*WVD2*) gene is another gene that regulates the anisotropic cell expansion. Loss of function of this gene results in suppressed root waving and leftward root slanting. In plants that overexpress *WVD2*, roots and etiolated hypocotyls exhibit right handed twisting, while the petioles of their rosette leaves show left-handed helical growth. In roots of *wvd2* mutants, the twisting phenotype is related with the left handed organizations of cortical microtubules in the elongating cells. WVD2 belongs to a plant specific hydrophilic protein family which contains a conserved KLEEL domain. Over-expression of another member of this protein family, *WVD2-LIKE1*, leads to similar twisting phenotype with *wvd2* (Yuen *et al.*, 2003).

Two semi-dominant left-handed twisting mutants termed *lefty1* and *lefty2* were identified as genetic suppressors of *spr1*. These *lefty* mutants exhibit left handed helical growth in roots, hypocotyls, petioles and petals. The right handed arrangement of cortical microtubules in *lefty* root epidermal cells contributes to the twisting phenotype. The *lefty1* and l*efty2* mutants are the dominant negative mutants of α-tubulins 4 and 6. Incorporation of the mutant tubulins leads to right-handed obliquely oriented cortical microtubule arrays (Thitamadee *et al.*, 2002). As suggested by Naoi et al. (2004), a novel *semidominant propyzamide-hypersensitivel-1* (*phs1-1*) mutant that shows left handed helical growth of seedling roots was identified. The *phs1-1* mutant exhibits hypersensitivity to at low dose of microtubule disrupting drugs, enhancement of the temperature-sensitive *mor1* phenotype, and less ordered and more fragmented cortical microtubule arrays. PHS1 is a phosphatase of the Arabidopsis mitogen activated protein kinase (MAPK) phosphatase subclass and the phosphatase activity is retained in PHS1 mutant. This study reveals that PHS1 phosphatase acts as a regulator of MAPKs which functions in the organization of cortical microtubules (Naoi and Hashimoto, 2004). According to Walia et al. (2009), Yeast two-hybrid assays showed that PHS1 interacts with two MAPKs, MPK12 and MPK18. Phospho-MPK18 can be dephosphorylated by recombinant PHS1. The *mpk18*

seedlings show defects in microtubule-related functions and have moderately stabilized microtubules. Loss of function of MPK18 results in enhanced stability of cortical microtubules. The root helical growth phenotype of *phs1-1* mutants can be partially complemented when MPK18 is knocked out in the *phs1-1* background. PHS1-1 and MPK18 can form a protein complex which functions in the phosphorylation-depended regulation of plant cortical microtubules (Walia *et al.*, 2009).

END-BINDING1 (EB1) proteins belong to a family of microtubule-associated proteins which are considered to be microtubule plus-end tracking proteins. T-DNA insertion homozygous mutants of each *EB1* gene have a root skewing phenotype on vertical or inclined plates and this phenotype is mainly because of delayed responses to gravity or touch signals. In the root growth of *EB1* mutants, microtubule integrity is not a major contributor (Bisgrove *et al.*, 2008). According to Galva et al. (2014), Roots of *eb1b* and *spr1* double mutants display right-looping growth and severe axial twisting phenotype which is more severe polar expansion defects than ether single mutant (Galva *et al.*, 2014). SPR1 has been proved to be concentrated at the growing ends of cortical microtubules and involved in microtubule polymerization dynamics (Sedbrook *et al.*, 2004). EB1b can interact with SPIRAL1 as they load onto microtubule plus ends and maintain proper polar cell expansion and organ growth in response to direction cues (Galva *et al.*, 2014).

Cellulose, which is a major component of plant cell wall is the most abundant biopolymer in Earth. It is synthesized by cellulose synthase (CesA) complexes (CSCs) at the PM of plant cells. The synthesis process can be guided by cortical microtubules via the protein CELLULOSE SYNTHASE INTERACTING (CSI)1/POM2. A family of microtubule-associated proteins, the cellulose synthase-microtubule uncouplings (CMUs) is essential to maintain microtubule stability to direct cellulose synthase movement, thus sustains anisotropic plant cell growth. Loss of functions of CMUs leads to lateral microtubule displacement and compromised microtubule based guidance of CSC movement. The cellulose deposition can be affected and the roots

and hypocotyls of mutant plants exhibit helical growth phenotype (Liu *et al.*, 2016).

1.3. Overview of the ER-PM Contact Sites

As described previously, secretory cargos are synthesized in the ER and then transported to different endomembrane destinations by means of the vesicle mediating trafficking pathway (Boevink *et al.*, 1998). In addition, the ER is able to connect with other cellular compartments including the Golgi, the endosome, the mitochondria, the PM as well as the plant chloroplast directly and involves in non-vesicular material transportation, cell signaling and organelle dynamics (Mehrshahi *et al.*, 2014, Salvador-Gallego *et al.*, 2017).

In eukaryotic cells, the ER-PM contact sites are regions where the two membranes are presented in very close contact (≤15nm) without fusion. These sites are usually organized by proteins that are able to bring the two membranes together and various kinds of proteins have been found to participate in the connection between the ER and the PM in various organisms (Carrasco and Meyer, 2011, McFarlane *et al.*, 2017, Wang *et al.*, 2014).

1.3.1. Functions of ER-PM Contact Sites in Animals and Yeast

ER-PM contact sites exist ubiquitously in eukaryotic organisms. In animals and yeast, various proteins have been identified to act as tethers between the ER and the PM and their functions have been well studied. For instance, in yeast, the ER-PM contact sites are essential for the synthesis of phosphatidylcholine and mediate the activity of Opi3 (the phosphatidylethanolamine *N-rethyltransferase* enzyme) (Tavassoli *et al.*, 2013). According to Stefan et al. (2010), the oxysterol-binding homology (Osh) protein, Osh3 which is localized to the ER-PM contact sites functions as a sensor of the PM PI4P (phosphatidylinositol 4-phosphate) levels and also activate the ER Sac1 phosphatase (Stefan *et al.*, 2011). In animal cells, protein STIM1 interacts with Orai1 at the ER-PM contact sites and this protein complex are able to regulate the Ca^{2+}

influx (Hogan *et al.*, 2010). As suggested by Sohn et al. (2018), the levels of the PM PI4P and PS (phosphatidylserine) can be regulated by PI(4,5)P_2 (Phospatidylinositol 4,5-bisphosphate) which is a regulatory lipid of the PM by means of recruiting the ER resident ORP5/ORP8 to the ER-PM contact sites (Sohn *et al.*, 2018). Besides, a recent study revealed that the ER-PM contact sites and Ca^{2+} release at these sites are needed for the endocytosis of EGFR (the epidermal growth factor receptor) (Bayer *et al.*, 2017).

1.3.2. Plant ER-PM Contact Sites

Although various proteins that are localized to the ER-PM contact sites have been identified in animals and yeast, plant ER-PM junctions have not been will studied. As described previously, in 2014, a protein complex which is made up of NET3C, VAP27-1, actin filaments and microtubule cytoskeleton has been identified to form the ER-PM contact sites in higher plants. At these sites, NET3C interacts with VAP27-1 and associates with actin filaments and microtubules (Wang *et al.*, 2014). When the expression of VAP27-1 and NET3C is limited under native conditions, only a small fraction of the ER can be attached to the PM via the interaction between VAP27-1 and PM associated NET3C. However, high level expression of VAP27-1 and NET3C is able to induce the formation of the ER derived membrane cisternae and the cisternae are closely associated with the PM (Wang *et al.*, 2016). In addition to VAP27-1, another protein of plant VAP27 family, VAP27-3 is also proved to interact with NET3C at the ER-PM contacts (Wang *et al.*, 2016). According to Siao et al. 2016, Arabidopsis synaptotagmin1 (SYT1) is another protein which is localized on the ER-PM contact sites. It is an ER membrane protein and belongs to a protein family with five members. It has an N-terminal transmembrane domain (TM), a synaptotagmin-like mitochondrial and lipid-binding protein (SMP) domain, and two C-terminal tandem C2 domains. VAP27-1 and SYT1 are localized on different ER-PM contact sites. SYT1 enriched ER-PM contact sites (S-EPCSs) are usually found closely surrounding the VAP27-1 enriched ER-PM contact sites (V-EPCSs).

SYT1 is important to stabilize the ER network and V-EPCSs because in the *SYT1* knock out mutant, The V-EPCSs can still be found, but the ER structure and the mobility of VAP27-1 can be affected (Figure 1.5) (Siao *et al.*, 2016). The Arabidopsis synaptotagmin SYTA is essential for endocytosis and regulating movement proteins (MPs)-mediated virus cell-to-cell transport by altering plasmodesmata (Levy *et al.*, 2015). A recent study revealed that SYTA is localized to ER-PM contact sites in Arabidopsis. It is able to interact with MPs and can be recruited to plasmodesmata for virus replication and cell-to-cell movement (Levy *et al.*, 2015).

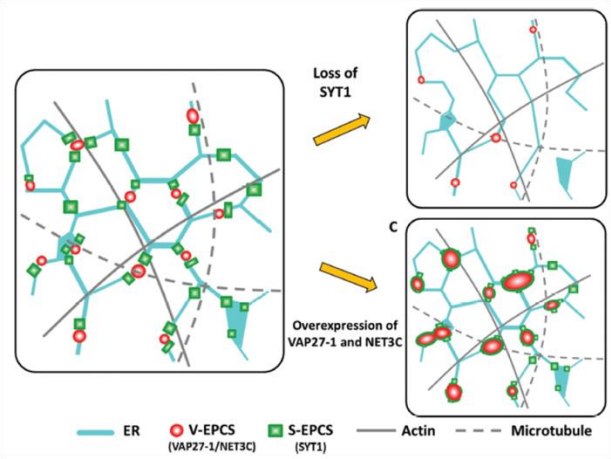

Figure 1.5 Model of the plant ER-PM contact sites.VAP27-1 is co-localized with NET3C and at the V-EPCSs, which are surrounded by the SYT1 enriched S-EPCSs. SYT1 stabilizes the ER network and the V-EPCSs by tethering the ER to the PM. SYT1 and NET3C are associated with actin filaments and VAP27-1 interacts with microtubules. Loss of SYT1 causes a less stable ER network and fewer V-EPCSs, and over-expression of VAP27-1 and NET3C enlarges the size of V-EPCSs. Figure form Siao *et al.* (2016).

1.4. The Role of VAP27 and NET3C

1.4.1. Plant VAP27 Proteins

The vesicle-associated membrane protein (VAMP) associated proteins (VAPs) are highly conserved integral ER membrane proteins cross eukaryotes (Lev *et al.*, 2008). VAPs are able to interact with various intracellular proteins and function in diverse cellular processes, such as mediating endomembrane trafficking, facilitating lipid

transport and homeostasis, promoting the unfolded protein response and maintaining the integrity of the microtubule (Kagiwada and Zen, 2003, Kanekura *et al.*, 2006, Kawano *et al.*, 2006, Pennetta *et al.*, 2002, Soussan *et al.*, 1999). The first VAP protein termed VAP-33 was identified in a search for proteins interacting with VAMP in a yeast two hybrid screen of *Aplysia californica*and the first VAP27 protein was observed in the year 2000 (Laurent *et al.*, 2000, Skehel *et al.*, 1995). Members of the VAP family are composed of a transmembrane domain at C-termini, a conserved major sperm domain at N-termini and a coiled-coil domain (Laurent *et al.*, 2000). In animals, VAPs bind to a wide range of SNAREs and fusion related proteins and are essential in SNARE-mediated vesicle trafficking (Amarilio *et al.*, 2005, Hamamoto *et al.*, 2005, Weir *et al.*, 2001, Wyles and Ridgway, 2004). According to Hua et al. (2017), two ER associated animal VAPs, VAPA and VAPB interact with the ACBD5 (peroxisomal membrane protein acyl-CoA binding domain containing 5). The VAP-ACBD5 complex enables the communication between these two organelles and is important to lipid homeostasis (Hua *et al.*, 2017). In addition, VAP proteins are able to interact with FFAT-motif containing proteins. For instance, the yeast VAP homologue Scs2p can interact with Opi1p, a transcriptional regulator of phospholipid synthesis in yeast and this interaction provides an important role for VAP homologues in mediating lipid transportation and metabolism (Loewen *et al.*, 2003).

In the Arabidopsis genome, ten VAP homologues (VAP27-1 to VAP27-10) have been identified and these VAP27 isoforms can be divided into three distinct clades. Proteins VAP27-1 to VAP27-6 belong to the subclade I, VAP27-8 to VAP27-10 belong to the subclade II and VAP27-2 and VAP27-4 belong to the subclade III. The isoforms from clade II do not have the transmembrane domain and their major sperm domain is localized at the center of the amino sequence rather than at the N-termini. According to the GENEVESTIGATOR analysis, most of the VAP27 isoforms express across a wide range of tissues except for VAP27-7 which can only be found in the leaf (Wang *et al.*, 2016).

In *N. benthamiana* leaf epidermal cells, the expression patterns of VAP27-3 of clade I

and VAP27-4 of clade III are similar with that of VAP27-1 which is localized at the ER network and also at the ER-PM contact sites (Wang *et al.*, 2014, Wang *et al.*, 2016). By contrast, VAP27-8 and VAP27-10 from clade II are localized to the PM instead of the ER. VAP27-8 also labels some immobile punctae which are associated with the PM (Wang *et al.*, 2016). In Arabidopsis, the subcellular localization of VAP27-1 is similar with that is observed in the *N. benthamiana*. The ER associated punctae can be found in various kinds of cells including the cotyledon, the shoot meristem, the root elongation and the mature trichome. However, no punctae can be seen in the early developmental stage of trichome cells. A number of VAP27-1 labeled ER-PM contact sites also associated with the plasmodesmata and the cell wall can stabilize the VAP27-1 punctae at these contact sites. The VAP27-1 labeled ER-PM contact sites are closely associated with the actin filaments and microtubules, but these contact sites are not maintained by the cytoskeleton (Wang *et al.*, 2016).

According to the functional studies, the VAP27-1 and VAP27-3 overexpressing lines exhibit pleiotropic phenotypes including defects in pollen, seeds and root development. The branched root hair is the most notable defect. The same phenotype can also be identified in VAP27-1 and VAP27-3 RNAi lines, the ER structure and actin organization are affected in the branched root hair. These results indicate that the expression level of VAP27 is very important to normal plant development (Wang *et al.*, 2016).

1.4.2. The Plant-Specific Networked Super-Family

In animal cells, a number of adaptor proteins are proved to be essential for actin-membrane interactions. Although these proteins are not found in plants, the interactions between microfilaments and endomembrane compartments play a critical role in coordinating the organization of cellular compartments, the intercellular communication as well as the membrane remodeling (Hussey *et al.*, 2006). Recently, a novel super-family of actin-binding proteins termed NETWORKED (NET) has been identified specifically in plant cells for actin-membrane interactions. In Arabidopsis,

these proteins have a highly conserved actin-binding (NAB) domain at the N termini and a variable C-terminal coiled-coil domain which is associated with different endomembrane compartments. According to the sequence of the NAB domain as well as the length and structure of the C termini, the NET superfamily can be subdivided into four distinct groups (NET1, NET2, NET3 and NET4) with thirteen members in total (NET1A-D, NET2A-D, NET3A-C and NET4A-B) (Figure 1.6) (Deeks *et al.*, 2012).

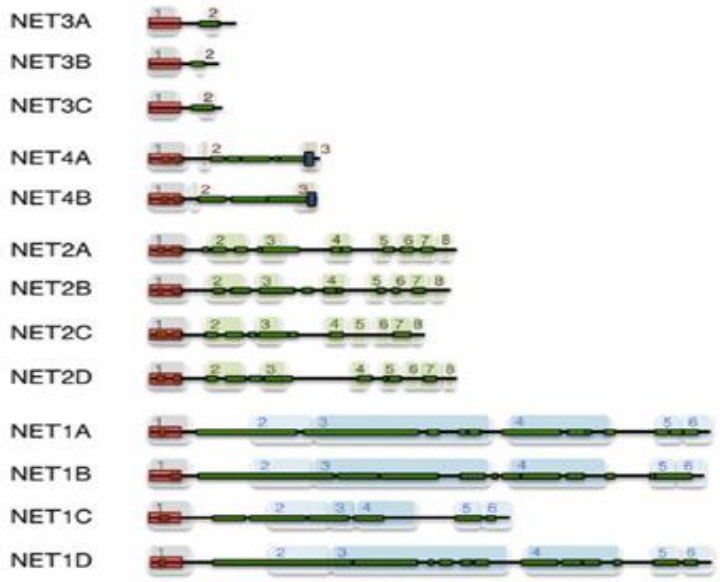

Figure 1.6 The Arabidopsis NET superfamily. Protein structures of the thirteen NET proteins. The NAB domain is shown in red and the predicted coiled-coil regions are shown in dark green. Figure form Deeks *et al.* (2012).

1.4.2.1. The NET1 Subfamily

The NET1A is the first NET superfamily protein that was identified by screening an Arabidopsis green fluorescence protein (GFP)-fusion cDNA library. Residues 1-94 of NET1A are found to be very essential for the interaction with actin filaments and this N-terminal region was then considered as the new plant specific actin-binding domain. In *N. benthamiana*, the full-length NET1A is associated with actin filaments and forms immobile punctae structure in a “beads on a string” pattern. In Arabidopsis, NET1A punctae are localized to the PM and plasmodesmata and also accumulate

along a small number of filaments. This indicates that NET1A is an adaptor protein between F-actin and the PM. The NET1 subfamily is very important for the development of the root. NET1A and its closest homolog NET1B are expressed in the root meristems and the double mutants of *NET1A* and *NET1B* show a significantly increased growth rate of primary roots (Deeks *et al.*, 2012).

1.4.2.2. The NET2 Subfamily

The NET2 proteins are phylogenetically closest with members of NET1 subfamily in accordance with the sequence comparison. NET2A is found to be expressed specifically in pollen. In Arabidopsis, NET2A forms distinct punctae and is localized at the PM in the shank region of growing pollen tubes. The punctae are arranged in a "beads on a string" manner which is similar to NET1A and closely associated with cortical longitudinal actin filaments of the pollen tube. NET2A has been proved to interact with PRK4 and PRK5, which are members of pollen receptor-like kinases (PRKs). These interactions facilitate the stable association between the actin cables and the PM in the growing pollen tube shank and might play an important role in extracellular signal response during fertilization (Deeks *et al.*, 2012, Duckney *et al.*, 2017).

1.4.2.3. The NET3 Subfamily

The NET3 subfamily is the smallest of the NET super-family. In BY-2 tissue culture cells, NET3A is mainly localized at the nuclear membrane and the filamentous structure in the cytoplasm is also labeled. Brighter punctae are found to be arranged in a "beads on a string" pattern on these filaments and nuclear membrane (Deeks *et al.*, 2012). NET3B is a new protein that is localized on the ER network and also associated with the actin cytoskeleton *in vivo*. It is expressed in various tissues such as pollen, embryos roots as well as the leaf vasculature and loss-of-function of this protein does not affect the growth and development of plants. As described previously,

NET3B is likely to be involved in remodeling processes together with some other ER associated actin motor proteins (Wang and Hussey, 2017). NET3C forms punctae structure and is associated with actin cytoskeleton at the Endoplasmic reticulum (ER)-plasma membrane (PM) contact sites (EPCS) in plant cells. These contact sites are shown to be organized by NET3C, VAP27-1 (a plant homolog of the yeast Scs2 protein) as well as cytoskeleton. Actin filaments and microtubules restrain the mobility of NET3C and VAP27-1 respectively. According to the functional study, proteins NET3B and NET3C are essential for the development of pollen grains. 25% of pollen grains from *NET3C RNAi/net3b* double mutants are abnormal. These defective pollen grains do not have any DNA and are unable to germinate (Wang *et al.*, 2014, Wang *et al.*, 2016).

1.4.2.4. The NET4 Subfamily

The NET4 proteins are the only NET subfamily which is common throughout the genomes of vascular plants. In Arabidopsis, NET4A is mainly expressed in roots and guard cells. It is associated with actin filaments surrounding the vacuole and is localized to the tonoplast in root cells (Deeks *et al.*, 2012). As F-actin plays a critical role in maintaining the morphology of vacuoles (Higaki *et al.*, 2006), NET4A is likely to act as a novel adaptor protein between F-actin and vacuoles for this purpose (Deeks *et al.*, 2012).

1.5. Characterization of NET3C and VAP27-1 Function: Strategic Approach

In this study, numerous different approaches were used to understand the roles of the EPCS resident proteins, NET3C and VAP27-1 in Arabidopsis. Previously, the identification of putative interacting partners of NET3C and VAP27-1 was performed using proteomic and yeast-two-hybrid screens (by Dr. Pengwei Wang), In order to investigate the cellular processes that NET3C and VAP27-1 may be involved in,

through interactions with other proteins. From the list of candidate proteins, two proteins that interact with NET3C (KLCR1 and AtBRO1), and one protein that interacts with VAP27-1 (SINE2) were selected for further study. The *in vivo* subcellular localization and reverse genetic analysis of different proteins was performed to investigate their potential roles and biological importance.

In chapter 3, bioinformatics analysis was used to predict the secondary structures of KLCR proteins and their potential functional domains. Publicly available gene expression data was then used in order to identify the gene tissue expression pattern. In order to study the subcellular localization of KLCR proteins, fluorescent fusion constructs were transiently expressed in *N. benthamiana* leaf epidermal cells. In addition, stable transgenetic Arabidopsis lines expressing KLCR1-GFP under the control of the endogenous *KLCR1* promoter were also generated and crossed with stable transgenic plants expressing the microtubule marker, tubulin-mCherry. Following this, co-localization analysis of NET3C with KLCR1 and IQD proteins was carried out in *N. benthamiana* leaf epidermal cells and the interactions between them were confirmed using fluorescence resonance energy transfer-fluorescence lifetime imaging microscopy (FRET-FLIM) analysis. Finally, changes in the ER morphology with overexpression of NET3C or IQD2 were studied microscopically.

In chapter 4, reverse genetic analysis was employed to investigate potential functions of KLCR proteins. During this investigation, T-DNA insertion mutant Arabidopsis lines in *KLCR1* and *KLCR2* were used to interrupt the expression of these genes. Genetic crosses were used for the phenotypic study.

In chapter 6 and chapter 7, subcellular localization of AtBRO1 and SINE2 was studied using both the transient *N. benthamiana* system and stable Arabidopsis transgene lines. AtBRO1 fluorescence fusion constructs were expressed in *N. benthamiana* leaf epidermal cells with the ER network marker, GFP-HDEL and the actin marker, Lifeact-GFP. AtBRO1-mCherry and SINE2-mCherry fusion proteins were also expressed in transgenic Arabidopsis plants under the control of the 35s

promoter. The interactions between NET3C and AtBRO1 and between VAP27-1 and SINE2 were then investigated using FRET-FLIM analysis or GFP-Trap assay. Reverse genetic analysis was performed to identify the potential functions of AtBRO1 in Arabidopsis.

1.6. Brief Introduction of Identifying Protein Candidates that Potentially Interact with NET3C and VAP27-1

In order to investigate the biological functions of the EPCS resident proteins, NET3C and VAP27-1, identification and characterization of potential interacting partners of NET3C and VAP27-1 was performed using yeast-two-hybrid screen and protein-protein interaction screen, TAP-MS (by Dr. Pengwei Wang).

1.6.1. An Introduction of the Yeast-two-Hybrid system

The yeast-two-hybrid system is a powerful method to investigate potential protein-protein interactions in *Saccharomyces cerevisiae* yeast cells. The occurrence of an interaction results in the formation of a functional transcription factor. The transcription factor activates downstream reporter genes which are necessary for yeast to survive and grow on selective media (Fields and Song, 1989).

In this study, the Clontech Matchmaker yeast-two-hybrid system was used. This system relies on the reconstruction of functional GAL4 transcription factor. In this system, the "GAL4 DNA binding domain" (BD) is fused to the bait protein (a protein of interest) and the "GAL4 activation domain" (AD) is fused to the prey protein (another protein of interest or a protein encoded by a cDNA library fragment). If the bait protein and prey protein interact, a functional GAL4 transcription factor is created. The transcription factor then binds to GAL4 promoter regions and activates transcription of the downstream reporter genes such as the *HIS3*, *ADE2* and *LacZ*. *HIS3* encodes a gene to produce histidine, *ADE2* encodes a gene to produce adenine, and LacZ encodes a gene to produce β-galactosidase (Clontech, 2013).

Two vectors, pGBKT7 and pGADT7, were used in the Clontech Matchmaker yeast-two-hybrid system. pGBKT7 was used to create DNA-binding domain fusion proteins and pGADT7 was used to create activation domain fusion proteins. pGBKT7 and pGADT7 vectors contain genes for the production of tryptophan and leucine respectively. Therefore, only the yeast transformed with these vectors are able to grow on media without either of these amino acids.

The bait and prey plasmids are transformed into two different yeast strains, AH109 and Y187. These yeast strains contain three reporter genes, *HIS3*, *ADE2* and *LacZ*, whose transcription can be activated by the GAL4 transcription factor. The two yeast strains are mated and diploids are then grown on media lacking tryptophan, leucine, histidine and adenine. If the bait and prey protein interact, the yeast are able to survive on media lacking these amino acids.

1.6.2. An Introduction of the TAP-MS system

Tandem affinity purification coupled to mass spectroscopy (TAP-MS) is one of the most powerful methods to identify potential binding partners of a certain protein of interest (known as the bait protein) in plants (Van Leene *et al.*, 2015). In this study, the TAP-MS system was used to identify potential interactors of NET3C and VAP27-1. In this system, the bait proteins (NET3C and VAP27-1 in this study) are fused to GS^{Rhino}, a double affinity tag, which combines a protein G Tag with a streptavidin-binding peptide (SBP) separated by a highly specific human rhinovirus 3C protease cleavage site (Van Leene *et al.*, 2015). Protein G tags enable protein purification on IgG beads and SBP fusions facilitate purification with streptavidin beads. In the first purification step, protein complexes which contain the bait construct are isolated through binding on an IgG resin. After washing of the isolated protein complex, its specific elution from the IgG resin is achieved through incubation with rhinovirus 3C protease, which will recognize its corresponding cleavage site. Next, the eluates bind to streptavidin-conjugated beads for a second purification step and the contaminating proteins are then washed away. Finally, SDS-PAGE gel

electrophoresis is used to separate proteins of isolated protein complexes and ultrasensitive mass spectrometry is used for protein identification (Van Leene *et al.*, 2015).

Chapter 2: Material and Methods

2.1. Materials

2.1.1. Plant Material

N. benthamiana plants were used for the transient expression of GFP fusion proteins in leaf epidermal cells for studying protein subcellular localization and fluorescence resonance energy transfer-fluorescence lifetime imaging microscopy (FRET-FLIM). Arabidopsis Columbia Col-0 ecotype (Lehle) was used as the background line for the generation of various stable transgenic plants.

The T-DNA insertional mutant lines of *atbro1*, *sine2*, *klcr1* and *klcr2* were obtained from NASC. The GABI_837H11 and GABI_780B02 lines were used for *AtBRO1*, the SAIL_335_B08 line was used for *KLCR1* and the SAIL_027301, SAIL_148296 and GABI_456B06 lines were used for *KLCR2*.

2.1.2. Bacterial Strains

The Agrobacterium strain, GV3101 was used for transient transformation of *N. benthamiana* leaf epidermal cells and stable transformation of Arabidopsis. The following *Escherichia coli* strain DH5α was used for cloning and the DB3.101 strain was used for amplifying empty Gateway vectors with the toxic cassette.

2.1.3. Vectors and Constructs

All vectors used are commercially available, except for pMDC83-mCherry which was created by Dr. Patrick Duckney (Durham University), facilitating constitutive expression of C-terminal mCherry fusion proteins under the *CaMV 35s*: promoter. All vectors used in this project are summarized in Table 2.1. The fluorescence fusion constructs provided by others are summarized in Table 2.2.

GFP-HDEL was used for labeling the ER network. The tetrapeptide HDEL (Histidine, aspartic acid, glutamic acid, leucine) is an ER targeting sequence which is identified at C-terminal end of many soluble proteins resident in the ER lumen and functions as an ER retention signal (Gomord *et al.*, 1997, Napier *et al.*, 1992). Microtubules were labeled with the kinesin motor domain fused to RFP (KMD-RFP) (Wang *et al.*, 2016). Actin filaments were labeled with Lifeact-GFP or YFP-Actin-Cb. Lifeact is a 17-amino-acid peptide which stains F-actin structures in eukaryotic cells and it does not interfere with actin dynamics *in vivo* and *in vitro*. It is the first 17 aa of protein Abp140, the only probe which can be used to label actin filaments in budding yeast (Riedl *et al.*, 2008). YFP-Actin-Cb is a modified version of the commercially available Actin-Chromobody (Actin-Cb) which can be used for labeling of the actin filaments and visualizing actin dynamics in tobacco leaf tissues. Chromobodies are nanobodies fused to fluorescent proteins, and therefore allowing antigen-binding and visualization by fluorescence (Rocchetti *et al.*, 2014). H2B-GFP was used to label the chromatin. H2B is one of the components of an octamer of histone proteins known as nucleosome. The nucleosome is the fundamental structural unit of chromatin (Howe *et al.*, 2012).

Table 2.1 Cloning and expression vectors used in this project

Vector name	Vector function	Vector size (bp)	Resistance	Supplier
pDONR207	Gateway entry vector	5585	Gentamicin (bacteria)	Invitrogen
pMDC43	Gateway expression vector for N-terminal GFP fusion under 2x35s promoter	12460	Kanamycin (bacteria) Hygromysin (Plants)	University of Zurich via ABRC
pMDC83	Gateway expression vector for C-terminal GFP fusion under 2x35s promoter	12513	Kanamycin (bacteria) Hygromysin (Plants)	University of Zurich via ABRC
pMDC83-mCherry	Gateway expression vector for C-terminal mCherry fusion under 2x35s promoter	12581	Kanamycin (bacteria) Hygromysin (Plants)	Durham University
pMDC107	Gateway expression vector for C-terminal GFP fusion under endogenous promoter	11738	Kanamycin (bacteria) Hygromysin (Plants)	University of Zurich via ABRC
pK7WGR2	Gateway expression vector for C-terminal GFP fusion under 35S promoter	11628	Spectinomycin (bacteria) Kanamycin (plants)	Ghent University Via ABRC

Table 2.2 Fluorescence fusion constructs provided by others

Construct	Supplier
RFP-NET3C	Dr. Pengwei Wang (Durham University)
GFP-NET3C	Dr. Pengwei Wang (Durham University)
YFP-NET3C	Dr. Pengwei Wang (Durham University)
NET3A-mCherry	Dr. Pengwei Wang (Durham University)
NET3A-GFP	Dr. Tim Hawkins (Durham University)
KLCR1-GFP	Dr. Pengwei Wang (Durham University)
KLCR1-RFP	Dr. Pengwei Wang (Durham University)
NET3B-GFP	Dr. Pengwei Wang (Durham University)
NET3B-RFP	Dr. Pengwei Wang (Durham University)
VAP27-1-YFP	Dr. Pengwei Wang (Durham University)
GFP-VAP27-1	Dr. Pengwei Wang (Durham University)
VAP27-1-RFP	Dr. Pengwei Wang (Durham University)
GFP-HDEL (ER marker)	Dr. Pengwei Wang (Durham University)
KMD-RFP (microtubule marker)	Dr. Pengwei Wang (Durham University)
Lifeact-GFP (actin marker)	Dr. Pengwei Wang (Durham University)
YFP-actin-Cb (actin marker)	Dr. Pengwei Wang (Durham University)
H2B-YFP (chromatin marker)	Dr. Pengwei Wang (Durham University)
GFP-IQD1	Dr. Katharina Burstenbinder (Leibniz Institute of plant biochemistry)
GFP-IQD2	Dr. Katharina Burstenbinder (Leibniz Institute of plant biochemistry)
GFP-IQD12	Dr. Katharina Burstenbinder (Leibniz Institute of plant biochemistry)
GFP-IQD22	Dr. Katharina Burstenbinder (Leibniz Institute of plant biochemistry)
GFP-IQD25	Dr. Katharina Burstenbinder (Leibniz Institute of plant biochemistry)

2.2. Molecular Biology Methods

2.2.1. Transformation of *E. coli* Using Electroporation

Glycerol stocks of DH5α or DB3.101 *E. coli* cells were streaked onto solid LB-media (20 g/l LB (Melford) and 10 g/l agar (Melford)) and grown overnight for about 16 hours at 37 ºC. A single colony was used to inoculate a liquid overnight culture of 5 ml LB medium (20 g/l LB), which was grown on a rotary shaker for about 16 hours at 37 ºC. 214 µl overnight culture was used to inoculate 10 ml LB media, which was grown on a rotary shaker for 3 hours at 37 ºC. 2-5 ml culture was centrifuged at 11,000 RPM for 30 seconds at 4 ºC, and the resultant pellet was suspended in 1 ml ice-cold sterile distilled water. The cells were centrifuged and resuspended for 2-4 times. The cells were then centrifuged and resuspended in 200 µl chilled sterile distilled water. 1 µl plasmid DNA (50-100 ng/µl) was added to the cells and then placed in a pre-chilled electroporation cuvette (2 mm gap electroporation cuvettes; VWR) for 2 hours on ice. The cells were electroporated at 2.5 kV using the BioRad MiroPulser and then recovered shaking at 37 ºC for 1 hour with 1ml liquid LB media. The cells were then spread on solid LB agar plates containing appropriate antibiotic selection (Table 2.1) and incubated at 37 ºC for about 16 hours.

2.2.2. Preparation of Chemically-Competent Agrobacterium GV3101 Strains

Glycerol stocks of GV3101 cells were streaked onto solid YEB media plates (Table 2.3) containing 10 µg/ml gentamicin (Melford) and 25µg/ml rifampicin (Melord) and grown at 30 ºC for 2 days. Single colonies were used to inoculate an overnight culture of 10 ml YEB liquid media containing 10 µg/ml gentamicin and 25 µg/ml rifampicin and grown on a on a rotary shaker for 16 hours at 30 ºC. 1ml of the overnight culture was used to inoculate 500 ml of YEB media without antibiotics, which was grown for about 4-5 hours until the cells reached a density (OD_{600}) of 0.6. The 500 ml of culture

was poured into two 250 ml oakridge tubes and the cells were centrifuged at 3000 RCF for 5 minutes at 4 ºC. The pellet faction was gently resuspended in 25 ml of ice-cold 0.15 M NaCl (BDH) before incubated for 15 minutes in ice. Another centrifugation at 3000 RCF was performed for 5 minutes at 4 ºC to spin down the pellet. Each pellet was gently resuspended in 5 ml of ice-cold 20 mM $CaCl_2$ (BDH), and cells were flash-frozen in liquid nitrogen in aliquots of 100-200 µl and stored at -80 ºC.

Table 2.3 YEB Media Recipe

Meat Extract (Merck)	5 g/l
Yeast Extract	1 g/l
Peptone	5 g/l
Sucrose (Melford)	5 g/l
$MgSO_4$. $7H_2O$ (BDH)	0.5 g/l
Agar (Melford)	10 g/l
Adjust pH to 7.0	

2.2.3. Transformation of Chemically-Competent Agrobacterium Strains Using the Heat Shock Method

About 100 ng plasmid DNA was added to each 50 µl of frozen Agrobacterium cells on ice. After incubating on ice for 12 minutes, the cells were quickly frozen in liquid nitrogen for 30 seconds and then incubated in a water bath at 37 ºC for 5 minutes. After incubating on ice for 1 minute, 1 ml LB liquid media was added to the cells and then they were recovered at 30 ºC for 2 hours. Cells were centrifuged at 5,000 RPM for 3 minutes and resuspended in 100 µl liquid LB media. The cells were then spread on LB agar plates containing 10 µg/ml gentamicin, 25 µg/ml rifampicin and appropriate antibiotics for the plasmid, and incubated at 30 ºC for 2 days.

2.2.4. Plasmid DNA Purification

Plasmid DNA was purified using the Promega Wizard Plus SV Miniprep DNA Purification System (Promega, UK). Single colonies were used to inoculate an overnight culture of 5 ml liquid media. Cells of overnight culture were then centrifuged at 3,500 RPM for 10 minutes to form a pellet. The resulting pellet was resuspended in 250 µl lysis solution to break the cells. A neutralizing solution was used to terminate the lysis and alkaline phosphatase was added to inactivate released bacterial proteins which may affect DNA purity. The lysate was cleared through centrifugation and transferred into a customized spin column containing a DNA binding matrix. The binding column was washed with washing buffer and the plasmid DNA was eluted in 100 µl nuclease-free water and stored at -20 ^{o}C.

2.2.5. DNA Restriction Digestion

Restriction digestion of the plasmid DNA was used to confirm the identities of purified plasmid DNA. The digestion reactions were performed using a mix which consists of 1 µl of the appropriate 10x reaction buffer, 0.5 µl restriction enzyme, 2 µl purified plasmid DNA (as described in 2.2.4), and 6.5 µl sterile distilled water. The reactions were incubated at 37 ^{o}C for 1 hour and resolved using agarose gel electrophoresis (2.2.6).

2.2.6. Agarose Gel Electrophoresis

Agarose gels were prepared by dissolving 1% (W/V) Agarose Low EEO (Melford) in 1x TAE buffer (40 mM Tris acetate (Fisher), 1 mM EDTA (Ethylenediaminetetraacetic acid (Sigma) pH 8.0) by heating in a microwave. Ethidium bromide (BDH) was added (3 µl/100ml) once the liquid gel was cooled to room temperature, and then the gel mixture was poured into trays to set. Before loading the DNA samples into the wells, the samples were mixed with DNA loading buffer blue (Bioline; 5x stock) in 5:1 ratio. Hyperladder I (Bioline) or 2-log DNA

Ladder (NEB) was used as molecular weight standards. Gel electrophoresis was performed at 150 volts in an electrophoresis tank containing 1x TAE buffer for 20-30 minutes and visualized using the Bio-Rad Gel-Doc 1000 system.

2.2.7. RNA Purification

Total mRNA was extracted from 15 day old Arabidopsis seedlings or whole Arabidopsis inflorescences using the Spectrum Plant Total RNA Kit (Sigma). 100-110 mg of tissue was quickly frozen in sterile Eppendorf tubes and ground using a liquid nitrogen cooled micropestle. The tissue samples were then lysed in 500µl lysis solution supplemented with 10 µl/ml β-mercaptopethanol (Sigma) and vortexed immediately and vigorously for 1 minute. After incubation at 56 ^{o}C for 5 minutes and centrifugation for 3 minutes, the lysate supernatant was transferred to a filtration column and centrifuged at top speed for 1 minute to remove debris. 750 µl of binding solution was added into the clarified lysate and mixed immediately. The mixture was then transferred into a RNA binding column and centrifuged at top speed for 1 minute to bind the RNA to the RNA binding matrix.

An on-column DNase digestion was performed for complete removal of traces of genomic DNA using the On-Column DNase I Digest Set (Sigma). The binding column was washed with wash solution and then 80 µl mixture of DNase I and DNase digestion buffer was applied to the RNA binding membrane. After incubation for 15 minutes at room temperature, the digested DNA was removed by washing the membrane with wash solution. RNA was eluted using 30 µl RNase-free water and stored at -80 ^{o}C.

2.2.8. cDNA Synthesis

cDNA was synthesized from Arabidopsis total RNA (as described in 2.2.7), using the SuperScript III Reverse Transcription System (Invitrogen) with oligo $(dT)_{15}$ primers and SuperScript reverse transcription enzyme. Heating steps were performed

using the G-Storm (GRI) PCR machine.

Firstly, the following components were mixed in a nuclease-free microcentrifuge tube: 1ul oligo $(dT)_{15}$ primer (0.5 µg/reaction), 2 µg total RNA, 1µl 10 mM dNTP mix, and sterile distilled water was added to a total volume of 13 µl. The mixtures were heated to 65 ^{o}C for 5 minutes and incubated on ice for at least 1 minute. After a brief centrifugation, 4µl 5x Fist-Strand Buffer, 1 µl 0.1 M DTT, 1µl recombinant RNase inhibitor, and 1µl of SuperScript III RT was added to the tube to a final volume of 20 µl. The subsequent mixture was incubated at 50 ^{o}C for 1 hour and then the reaction was inactivated by heating at 70 ^{o}C for 15 minutes. The cDNA was stored at -20 ^{o}C.

2.2.9. Genomic DNA Extraction using the Edwards Prep Method

Arabidopsis Genomic DNA was extracted from leaf tissue (Edwards *et al.*, 1991). About 10 mg of fresh tissue was ground in 400 µl extraction buffer (Table 2.4) using a pestle in an Eppendorf tube. The mixture was centrifuged at top speed for 5 minutes, and 200 µl of the supernatant was carefully collected and mixed with an equal volume of isopropanol (BDH) to precipitate the genomic DNA. After incubation at room temperature for 10 minutes, samples were centrifuged at top speed for 10 minutes and the supernatant was removed. The DNA pellet was left to dry at 37 ^{o}C for 15 minutes to remove any residual isopropanol. The DNA pellet was then resuspended in 30 µl of nuclease-free water and stored at -20 ^{o}C.

Table 2.4 DNA Extraction Buffer

NaCl	250 mM
Tris-HCl (Fisher) pH 7.5	200 mM
EDTA (Ethylenediaminetetraacetic acid) (Sigma)	25 mM
SDS (sodium dodecyl sulphate) (BDH)	0.5% (w/v)

2.2.10. Amplification of DNA Fragments Using the Polymerase Chain Reaction

DNA fragments of interest from genomic DNA, cDNA or purified plasmid DNA were amplified using the polymerase chain reaction (PCR). Q5 DNA polymerase (NEB) was used for high-fidelity PCR amplification, otherwise MyTaq Mix (Bioline) was used.

For reactions using the Q5 DNA polymerase, the following PCR reaction was set up for a 50 µl total reaction: 10 µl 5x Q5 reaction buffer, 1µl 10 mM dNTPs (made from 100 mM stocks of dATP, dGTP, dCTP and dTTP), 2 µl forward primer, 2 µl reverse primer (10 µM stock; Eurofins/IDT), 2 µl DNA template, 0.5 µl Q5 High-Fidelity DNA Polymerase, and 32.5 µl nuclease-free water. The routine PCR programme is summarized below:

Table 2.5 Standard Thermocycling Conditions using Q5 DNA Polymerase

Step	Temperature (°C)	Time	Cycles
Initial Denaturing	98	30 seconds	1
Denaturing	98	10 seconds	35
Annealing	55-72	30 seconds	
Extension	72	30-40 seconds/kb	
Final Extension	72	2 minutes	1

The annealing temperature was determined using the NEB T_m Calculator according to the primers used, and extension time was adjusted to suit the size of the fragment of interest.

When high-fidelity amplification was not needed, such as for RT-PCR and genotyping, MyTaq Mix was used. The following PCR reaction was set up for a 25 µl total reaction: 12.5 µl 2x MyTaq Mix, 1 µl forward primer, 1 µl reverse primer (10 µM stocks, Eurofins/IDT), 1ul template, and 9.5 µl nuclease-free water. The routine PCR

programme is summarized below:

Table 2.6 Standard Thermocycling Conditions using MyTaq Mix

Step	Temperature (°C)	Time	Cycles
Initial Denaturing	95	1 minute	1
Denaturing	95	15 seconds	35-40
Annealing	55-65	30 seconds	
Extension	72	10-30 seconds/kb	
Final Extension	72	10 minutes	1

The annealing temperature was set dependent upon the primer sequences and was usually 2-5 °C below the lower the predicted melting temperature of the pair. The extension time depends on the length of the amplicon and the complexity of the template. 10 seconds was enough for amplicons under 1kb or up to 5kb. For amplification of fragments over 1kb from high complexity template, the extension time can be increased to 30 seconds per kb.

2.2.11. Cloning using the Invitrogen Gateway Cloning System

The BP reaction was used to insert PCR amplified DNA fragments into the entry vector, pDONR207. The BP reaction was set up as follows: 50-100 fmol of PCR fragments with *attB* site, 50-100 fmol of pDONR207, 2 µl BP Clonase II enzyme mix, made up to total volume of 10 µl with 1x TE buffer (10 mM Tris-HCl pH 8.0, 1 mM EDTA pH 8.0). For each 100 fmol of plasmid or PCR, the amount of DNA used was calculated from the equation: ng=N x 0.066 (N is the number of base pairs). The reaction was incubated at 25 °C overnight and then was inhibited by adding 1 µl proteinase K.

The LR reaction was used to transfer genes of interest from the entry vector to the destination vector. The destination vectors used in this project were listed in table 2.1. The LR reaction was set up as follows: 25-50 fmol entry vector, 25-50 fmol

destination vector, 2 µl LR Clonase II enzyme mix, made up to total volume of 10 µl with 1x TE buffer (10 mM Tris-HCl pH 8.0, 1 mM EDTA pH 8.0). The reaction was incubated at 25 ^{o}C for 5 hours and then terminated by adding 1 µl proteinase K.

DH5α *E. coli* cells were transformed with the recombinant entry vector or destination vector using electroporation (as described in 2.2.1). The transformed cells were then streaked on to solid LB plates supplemented with appropriate selection as described in Table 2.1. The presence of the insert was confirmed by restriction digestion (as described in 2.2.5) followed by DNA sequencing (as described in 2.2.12).

2.2.12. DNA Sequencing

An Applied Biosystems 3730 DNA Analyser was used by Durham University Biological Sciences Genomics to perform all DNA sequencing reactions.

2.2.13. Agrobacterium-Mediated Transient Transformation of *N. benthamiana* Leaf Epidermal Cells

According to Sparkes et al. (2006), transformed Agrobacterium GV3101 cells (as described in 2.2.3) were used to set up a 5 ml overnight LB culture (supplemented with 10µg/ml gentamicin, 25 µg/ml rifampicin plus the appropriate plasmid selection). In order to suppress gene silencing in *N. benthamiana*, an overnight culture of GV3101 cells containing the p19 protein was also prepared. After being grown for 16 hours at 30 ^{o}C, bacteria cultures were centrifuged at 3500 RPM for 10 minutes to from pellets, which were then resuspended in 1ml infiltration medium (Table 2.7). Cells were washed twice in infiltration medium and resuspended in 1 ml infiltration medium. The optical density OD600 of bacteria cells was measured, and the original suspension was diluted with infiltration medium until desired OD was reached. The p19 construct was mixed with other constructs in a 1:1 ratio.

A needleless syringe was used for injection of the infiltration solution into the abaxial side of the leaf.

Table 2.7 Infiltration Medium Recipe

MES (2-(N-morpholino) ethanesulfonic acid) (Sigma)	50 mM
Na_3PO_4. $12H_2O$ (trisodium orthophosphate)	2 mM
D-glucose (Melford)	28 mM
acetosyringone (3',5'-Dimethoxy-4'-hyfroxyacetophone) (Fluka)	100 µM

2.2.14. Agrobacterium-Mediated Stable Transformation of Arabidopsis through Floral Dipping

According to Clough and Bent (1998), Arabidopsis plants at 6-8 weeks old were used for floral dipping. The stems of plants needed to be cut back to the rosette to promote the growth of more stems bearing more inflorescences a few weeks before floral dipping. Siliques and open flowers were removed prior to floral dipping to increase the efficiency of transformation.

Transformed Agrobacterium GV3101 cells were used to set up overnight LB cultures containing 10 µg/ml gentamicin, 25 µg/ml rifampicin and appropriate plasmid selection and left to grow at 30 ^{o}C for about 16 hours. This culture was used for inoculating 400 ml LB media containing the same selection and grown overnight on a shaker at 30 ^{o}C. A Beckman Coulter Avanti J-20 XP centrifuge was used for spinning down the bacterial culture and the pellet was resuspended with 500 ml 5% (w/v) sucrose solution (Melford) plus 0.02% (v/v) Silwett L-77 (Lehle Seeds).

The Arabidopsis plants were dipped into the pre-prepared bacterial solution with gentle stirring for about 15 seconds. The dipped plants were then placed into a plastic bag in a shaded environment to maintain humidity. The dipped plants were taken out of the plastic bag after 24 hours and then returned to normal growth conditions. The same dipping procedure could be repeated 5 days later to increase transformation

efficiency. The plants were left to mature for seeds collection.

2.2.15. Genotyping of the T-DNA Insertional Line Using PCR

MyTaq Mix (Bioline) PCR reactions (as described in 2.2.10) was used for genotyping of the T-DNA insertional lines. Genomic DNA was used as template for the PCR reaction. Two PCR reactions were used for genotyping one plant. The first PCR reaction used a gene specific primer and a T-DNA specific left border primer (LB1 for SAIL line, LBb1.3 for SALK lines and o8409 for GABI-Kat line). These two primers were used to confirm the presence of the T-DNA insert. The second PCR reaction used two gene specific primers which were designed at either side of the T-DNA insertion. These two primers were used to determine the T-DNA homozygocity (All primers are listed in Appendix 1.4). In wild type plants, only a band in the wild type allele would be amplified, in heterozygous plants, bands in both the wild type allele and the T-DNA insert allele would be amplified, and in homozygous plants, only the T-DNA insert allele would be amplified.

2.2.16. Reverse Transcription-PCR Analysis of the T-DNA Insertion Lines

Reverse transcription-PCR was used to analysis the disruption of the transcripts in the homozygous T-DNA insertion lines. Total RNA was purified as described in 2.2.7 and cDNA synthesis was performed as described in 2.2.8. Gene specific primers were used to amplify the full length gene as well as the upstream and downstream fragments of the T-DNA insertion for the mutant lines. All primers are listed in Appendix 1.5.DNA amplification was performed using the MyTaq Mix (Bioline) according to 2.2.10.

2.3. GFP-Trap Assay and Western Blotting

2.3.1. Protein Extraction

Transformed *N. benthamiana* leaves transiently expressing proteins of interest were cut and placed in microcentrifuge tubes with a few glass beads. The tubes were then placed in a polystyrene rack with liquid nitrogen and the fresh plant tissues were ground into a fine powder. 500 µl of lysis buffer (Table 2.8) was added to the leaf material and mixed well. The homogenate was then incubated on ice for 10 minutes. After centrifuge at top speed for 10 minutes, the supernatants were transformed to fresh microcentrifuge tubes and placed on ice.

2.8 Lysis Buffer

NaCl	150 mM
Tris-HCl (Fisher) pH 7.5	10 mM
EDTA pH 8.0	0.5 mM
Triton X-100	0.5% (v/v)
PMSF	1 mM
proteinase inhibiter	1%

2.3.2. Rinsing the GFP-Trap Agarose Beads and Protein Precipitation

GFP-Trap agarose beads (chromotek) were used to perform the co-immunoprecipitatin. Before use, the beads were rinsed and resuspended with ChIP dilution buffer (Table 2.9) to remove storage buffer from the beads. The end of a pipette tip was cut to assist in measuring out 25 µl beads. 500 µl of ChIP dilution buffer was added to the beads. Centrifuge at 5000 RPM for 1 minutes and remove the supernatant. This wash was repeated three times.

25 µl rinsed GFP-Trap agarose beads were added to the protein solution and the mixture was then incubated at 4 ^{o}C for 1 hour with agitation. After centrifugation at

13,000 RPM for 1 minute, the supernatant was transformed to a fresh tube and the pellet was washed three times with the ChIP dilution buffer. 2x SDS protein loading buffer (Table 2.10) was added to the supernatant and the pellet. Samples were then heated at 95 ^{o}C for 10 minutes and centrifuged at 13,000 RPM for 5 minutes. The supernatant was transformed to a fresh tube and stored at -20 ^{o}C.

Table 2.9 ChiP Dilution Buffer

EDTA	0.5 mM
Tris-HCl (Fisher) pH 7.5	10 mM
NaCl	150 mM

2.10 2x SDS Protein Loading Buffer

Tris-HCl (Fisher) pH 6.8	250 mM
SDS	4% (w/v)
glycerol	20% (v/v)
ß-mercaptoethanol	100 mM
Bromophenol blue (Sigma)	0.02% (w/v)

2.3.3. SDS-polyacrylamide Gel Electrophoresis (SDS-PAGE) and Western Blotting

Denatured proteins were separated on a polyacrylamide gel based on their molecular weight. The Bio-Rad Mini Protean II system was used to perform SDS-PAGE gel electrophoresis. The resolving gel (Table 2.11) was first cast and a layer of isopropanol was added on to the resolving gel to let it set. Isopropanol was removed once the resolving gel has set and then stacking gel (Table 2.11) was added on the top. Protein samples which were extracted as described above (2.2.1) were loaded. Electrophoresis was performed in a tank filled with 1x SDS running buffer (25 mM Tris, 192 mM glycine (Sigma), 0.1% SDS). Electrophoresis was first run at 100 V and when samples entered the stacking gel, the voltage was increased to 150-200 V.

After electrophoresis, protein samples which were separated using SDS-PAGE were transferred onto a nitrocellulose membrane (Whatman). The transfer was performed in a tank containing transfer buffer (Table 2.12) at 100 V for 1 hour or 20 V overnight. After transfer, the membrane was then washed in distilled water and stained using a 1: 100 dilution of Ponceau stain (0.1% Ponceau S (w/v: Sigma) in 5% acetic acid (v/v: Fisher)). After de-staining the membrane in distilled water for 5 minutes, the protein bands could be visualized.

The nitrocellulose membrane was first incubated in blocking solution 2x TBST (Table 2.12) containing 5% (w/v) dried skimmed milk powder (Tesco) for 30 minutes at room temperature to block non-specific binding. The membrane was then incubated with primary antibody diluted in blocking solution at 4 ^{o}C overnight. The membrane was then washed three times for 5 minutes with 2x TBST buffer before applying secondary antibody. After that, it was incubated with secondary antibody diluted 1:1500 in blocking buffer for 1 hour and washed again three times for 5 minutes in 2x TBST. The membrane was then detected using ECL Western Blotting Detection Reagent (Amersham Biosciences) in Fujifilm Intelligent Dark Box II system.

Table 2.11 SDS-PAGE Preparation

12.5% Resolving Gel (bottom)	
Acrylamide Solution (30%)	5 ml
SDS 10% (w/v)	120 µl
Tris-HCl (Fisher), 0.75 M, pH 8.8	6 ml
APS 10% (w/v) (Melford)	110 µl
Tetramethylethylenediamine (TEMED) (Fluka)	5 µl
dH_2O	0.8 ml
12 ml in total, enough for two mini gels	

5% Stacking Gel (Top)	
Acrylamide Solution (30%)	0.83 ml
SDS 10% (w/v)	50 µl
Tris-HCl (Fisher), 0.25 M, pH 8.8	2.5 ml
APS 10% (w/v) (Melford)	50 µl
Tetramethylethylenediamine (TEMED) (Fluka)	10 µl
dH_2O	1.6 ml
5 ml in total, enough for two mini gels	

Table 2.12 Buffer used in Western Blot

1x Transfer Buffer	**2x TBST**
Tris (Fisher) (48 mM)	Tris-HCl (Fisher) pH 7.4 (20 mM)
Glycine (39 mM)	NaCl (300 mM)
SDS (0.375% (w/v))	Tween 20 (Sigma) (0.1% (v/v))
Methanol (20% (v/v))	

2.4. Cell Biology

2.4.1. Live Cell Imaging

Confocal Laser Scanning Microscopy (CLSM) was used to visualize fluorophore fusion proteins expressed invarious plant tissues. Imaging of fusion proteins in *N. benthamiana* leaf epidermal cells was performed 2-4 days after infiltration. A small section of sample was cut from transformed tobacco leaves and mounted in sterile distilled water on a glass microscope slide with the abaxial surface facing up. The cover slip was placed on the top of the leaf sample and mineral oil was used for immersion objective lens. For imaging of fluorophore fusion proteins in Arabidopsis, seedlings were mounted in water on a glass slide under a cover slip.

Confocal imaging was carried out using a Leica SP5 confocal laser scanning microscope, with 40x or 63x oil immersion lenses. All images were taken at a resolution of 1024 x 1024 with 4x averaging and images were analysed using the Leica LAS AF software and the ImageJ 64 software.

For imaging GFP fusion proteins, the fluorophore was excited using the 488 nm 20 mW argon laser and the emission was detected at 505-550 nm. For imaging RFP fusion proteins, samples were excited using the 543 nm 12 mW HeNe laser and the emissions were detected at 590-650 nm. For mCherry imaging, a HeNe 594 laser was used with 600-650 nm emission detection. To image YFP fusion proteins, a 514 nm argon laser was used for excitation, and fluorescence emission was detected with a 530-550 nm filter. For the colocalization experiments, sequential scans were used. Some cells expressed only one of the fluorescent proteins needed to be observed, and were imaged under the same setting to make sure co-localization was not an artifact of bleed-through between channels. In order to reduce the likelihood of observing spectral bleed-through artifacts, for the GFP/YFP combinations, GFP was excited at 514 nm and the emission was detected at 470-510 nm, while YFP was excited at 514 nm and the emission was detected at 550-580 nm. For CFP/GFP combinations, CFP

was excited at 405 nm and detected at 450-490 nm, while GFP was excited at 488 nm and detected at 510-550 nm (Wang and Hussey, 2017). Depending on signal strength, the laser settings typically ranged between 20-100%. A smart gain of 800-1000 mV was used for PMT detectors, and for HyD detector, a smart gain of 70-100% was typically used.

2.4.2. FRET-FLIM

Protein interactions between GFP-fusion proteins (donors) and RFP-fusion proteins (acceptors) were assessed using FRET-FLIM. To perform this experiment, the fluorescence lifetimes of a donor GFP fusion protein expressed alone in *N. benthamiana* leaf epidermal cells were firstly measured as the negative control. The fluorescence lifetime measurements of the GFP donor fusion protein were taken in the presence of an RFP or mCherry fusion protein which acted as a FRET acceptor. After measurements, the comparison was made between the donor fluorescence lifetimes in the presence or absence of acceptors. An average significant reduction of GFP lifetime greater than 0.1 ns was regarded as a possible interaction. A Leica SP5 confocal laser scanning microscope with a PicoQuant FLIM LSM upgrade kit was used to perform this experiment. A 63x 1.2NA water immersion lens and the Leica SMD FLIM Wizard were used. The PicoQuant SymPhoTime 32 software was used for data acquisition and analysis. GFP was excited with a pulsed 470 nm laser and an internal spectral FLIM PMT detector with 500-560 nm emission detection was used to count photons. Image acquisition was performed with the above settings until 1000 photons had been detected in the brightest pixel. Tail fitting was used to calculate the average fluorescence lifetimes and the PicoQuant SymphoTime 32 software was used to perform data analysis and fluorescence lifetime calculation.

2.4.3. Cytoskeleton-Disrupting Drug Treatments on *N. benthamiana* leaves

Latrunculin B (Sigma) was used to depolymerise the actin cytoskeleton. It was dissolved in DMSO to make a 10 mM stock and leaf sections were incubated in 50 µM Latrunculin B solution for 30 minutes.

2.5. Plant Growth Conditions and Phenotypic Assays

2.5.1. *N. benthamiana* Growth Conditions

N. benthamiana plants were grown centrally by Durham University SBBS. Seeds were directly sown onto compost (seed and modular compost plus sand; F2+S (Levington)) and were covered with a plastic propagator lid to establish a seedling nursery. The seedlings were then transferred to individual pots and left to grow in the growth room under a 16/8 hour photoperiod, with temperatures of 24 ^{o}C and 21 ^{o}C during the day and night respectively.

2.5.2. Arabidopsis Growth Conditions

Seeds were surface sterilized in 10% sodium hypochlorite (BDH) for 15 minutes, and washed 3 times in sterile distilled water. The sterilized seeds were then stratified at 4 ^{o}C in darkness for two days and sown in Petri dishes onto 1/2 Murashige and Skoog (1/2 MS) basal salt mixture (Duchefa; pH 5.7 with KOH) and 0.7% plant agar (Duchefa). For root growth study, square Petri dishes were used to ensure uniform growth across the plates. Plates were sealed with micropore tape and kept in a temperature controlled Sanyo growth cabinet with a 16/8 hour photoperiod, and temperatures were set at 22 ^{o}C and 16 ^{o}C during the day and night respectively. Two weeks after germination, seedlings were transferred into plastic trays containing compost (seed and modular compost plus sand, F2+S (Levington)) which had been autoclaved to remove pests. Plants were grown in the Sanyo growth cabinet or a

growth room with the same growth environment described above. Trays were covered with a plastic propagator lid to maintain humidity until the plants were fully established.

2.5.3. Cross-Pollination of Arabidopsis Plants

Cross-pollination of Arabidopsis plants was used to generate the double T-DNA insertion mutant lines and the stable transgenic lines. Cross-pollination was performed under a dissecting microscope. Unopened flowers from one genetic line were dissected and all anthers were removed using forceps to prevent self-pollination. Anthers from another genetic line were taken and brushed against the papillae of the stigma to cover it in pollen. After successful pollination, the siliques would swell and grow. Mature siliques were transferred to a microcentrifuge tube and left to dry.

2.5.4. Arabidopsis Seeds Collection

The ARACON container system (Bethatech) was used for Arabidopsis seeds collection. Once floral bolting had occurred, the bases and tubes of ARACON were pleased over rosettes. Plants were left to grow to maturity in the growth room. When plants had become yellow, they were transferred to the seeds drying room and left to dry for two weeks before seeds collection. Collected seeds were kept in microcentrifuge tubes and stored at room temperature.

2.5.5. Screening for Positive Transformed Arabidopsis

Arabidopsis seeds collected for floral-dipped plants were fist sterilized and washed as described in 2.5.2. After keeping at 4 ^{o}C in the dark for two days, the seeds were sown on plates supplemented with 1/2 Murashige and Skoog (1/2 MS) basal salt medium (Duchefa, pH 5.7 with KOH) with 0.7% (w/v) plant agar (Duchefa) as well as appropriate selection (Table 2.1). These plates were then sealed with micropore tape and kept in a temperature-controlled Sanyo growth cabinet. After ten days, plants

which were successfully transformed survived. They were then transferred onto soil and left to grow in the growth room. Confocal imaging was performed to identify true positives of fluorescence protein fusion transformation. The positive plants identified at this stage were the F1 generation and Arabidopsis homozygous plants were then selected according to the Mendelian rules of genetic inheritance.

2.5.6. Phenotype Analysis of Seed Set

The number of seeds produced per silique was counted in each line to assess the fertility of Arabidopsis mutant lines. Siliques from plants of 6-8 weeks old were taken and the developing seeds were counted under an Olympus SZH10 Research Stereo Microscope. Images were taken using the QImaging QICAM digital camera and Improvision Openlab 5.5.0 software.

2.5.7. Root Growth Assay

The F3 generation *klcr1*, *klcr1/klcr2* and azygous plants were grown as described in 2.5.2 on 12 cm square 1/2 MS agar plates. Plants were grown vertically in a Sanyo growth chamber. The plates were scanned at day 7 using an Epson 1680 Pro flatbed scanner. The root slanting angles were measured using ImageJ software (Schindelin).

2.5.8. Pavement Cell Morphometric Analysis

The parameters of pavement cells were determined from 4 day after germination cotyledons stained with 7.8 µM FM4-64 for 30 minutes in the dark. Two images were taken from nonoverlapping regions in the apical side of the cotyledons using CLSM with 40x oil immersion lenses and 543 nm excitation. About 200 cells from 10 seedlings were selected for evaluation (about 20 cells per seedling). Parameters of pavement cell area, perimeter, circularity, lobe length and neck width were measured. Cell area and perimeter were measured using the ImageJ 64 software (http:// rsb.info.nih.gov/ij). The pavement cell circularity was calculated according to the

following equation: 4π x cell area / (cell perimeter)^2 (Le *et al.*, 2006). Lobe length and neck width were measured according to Lin et al. (2013) using the ImageJ 64 software (Figure 2.1) (Lin *et al.*, 2013).

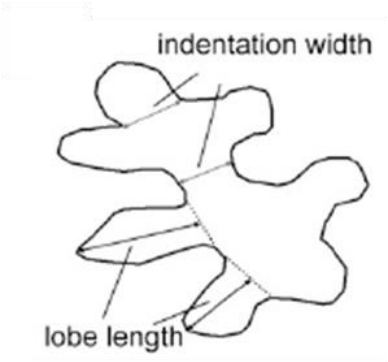

Figure 2.1 A carton illustrating how the neck width and the lobe length were measured. Figure form Lin *et al.* (2013).

2.5.9. Measuring Cytoskeletal Network on CLSM Stacks

The GFP-tagged cytoskeleton was visualized using CLSM as described in 2.4.1. Images were acquired as *xyz*-series with the 0.5 µm interval. About 7-10 wild type or mutant seedlings were selected for analyzing. For each seedling, 5-10 regions were evaluated. Skewness of fluorescence intensity distribution (correlated with microfilament bundling because bundles exhibit brighter fluorescence) was determined using the ImageJ 64 plugins and macros from Higaki's laboratory (Higaki *et al.*, 2010). The anisotrophy score was used to quantify the microtubule structure and the measurement was performed using the imageJ 64 plug-in, Fibriltool (Boudaoud *et al.*, 2014).

Chapter3: Investigation of NET3-KLCR-IQD Interactions

3.1. Protein-Protein Interaction Screens for Identifying Potential Interactors of NET3C and VAP27-1

In order to investigate the biological function of ER-PM contact sites using interactors of NET3C and VAP27-1, hundreds of candidate proteins that potentially interact with NET3C and VAP27-1 were obtained by protein-protein interaction screen, TAP-MS. In this study, the potential interactors of VAP27-1 and NET3C were named VAP27-1 interacting proteins (VIPs) and NET3C interacting proteins (NIPs) respectively. These proteins were then classified according to their functions and localizations in plant cells. 17 proteins that may have potential functions on endomembrane system and cytoskeleton were identified for further study, including 13 proteins that may interact with VAP27-1 (VIP1-VIP13) and 4 proteins which may interact with NET3C (NIP1-NIP4) (performed by Dr. Pengwei Wang). Among them, 7 genes were successfully cloned, including *NIP1*, *VIP2*, *VIP3*, *VIP6*, *VIP9*, *VIP10* and *VIP11*.

Co-localization and FRET-FLIM analyses were then performed to investigate the interactions between the selected potential interactors and NET3C/VAP27-1. FRET-FLIM was performed as described in section 2.4.2. GFP-VAP27-1 and GFP-NET3C were used as FRET-FLIM donor constructs, and NIP1-mCherry, VIP2-mCherry, VIP3-mCherry, VIP6-mCherry, VIP9-mCherry, VIP10-mCherry and mCherry-VIP11 were used as acceptor constructs. GFP-NET3C or GFP-VAP27-1 was expressed in *N. benthamiana* leaf tissues using agrobacterium-mediated transformation, alone, and with each FRET-FLIM acceptor construct. FRET-FLIM was also performed using GFP-RFP fusion protein as a positive control.

As shown in Figure 3.1A, the results indicate that GFP-VAP27-1 interacts with

VIP2-mCherry and mCherry-VIP11. GFP-VAP27-1 was not found to interact with VIP3-mCherry, VIP6-mCherry, VIP9-mCherry and VIP10-mCherry, none of which were able to reduce the average fluorescence lifetime of GFP-VAP27-1 by more than 0.06 ns. In contrast, VIP2-mCherry was able to induce a decrease in the average fluorescence lifetime of GFP-VAP27-1 from 2.58±0.04 ns to 2.37±0.02 ns (p= 1.497e-15). mCherry-VIP11 reduced the average fluorescence lifetime of GFP-VAP27-1 by 0.14 ns, to an average value of 2.44±0.04 ns (p=1.943e-10). GFP-NET3C was observed to interact with NIP1-mCherry, which induced a decrease in the average fluorescence lifetime of GFP-NET3C from 2.66±0.05 ns to 2.44±0.08 ns (p=2.2e-16). Taken together, these results indicate that GFP-VAP27-1 interacts with VIP2-mCherry and mCherry-VIP11 and GFP-NET3C interacts with NIP1-mCherry when co-expressed in *N. benthamiana* leaf epidermal cells. In addition, a yeast-two-hybrid screen was performed using NET3C as a bait against an Arabidopsis cDNA library, and KLCR1 was identified to be a potential interactor, whose interaction was further confirmed by a one-on-one yeast-two-hybrid test using full length genes (Figure 3.1B) (performed by Dr. Pengwei Wang). From these possible interactions, we selected three proteins (NIP1: AtBRO1, VIP11: SINE2 and KLCR1) for further study.

A

Constructs Expressed	Mean GFP Fluorescence Lifetime	Standard Deviation	n
GFP-VAP27-1	2.58	0.04	42
GFP-VAP27-1+VIP2-mCherry	2.37	0.02	22
GFP-VAP27-1+VIP3-mCherry	2.62	0.02	20
GFP-VAP27-1+VIP6-mCherry	2.60	0.02	21
GFP-VAP27-1+VIP9-mCherry	2.52	0.02	23
GFP-VAP27-1+VIP10-mCherry	2.57	0.02	20
GFP-VAP27-1+mCherry-VIP11	2.44	0.04	24
GFP-RFP	2.28	0.05	20
GFP-NET3C	2.66	0.05	18
GFP-NET3C+NIP1-mCherry	2.44	0.08	21
GFP-RFP	2.30	0.06	20

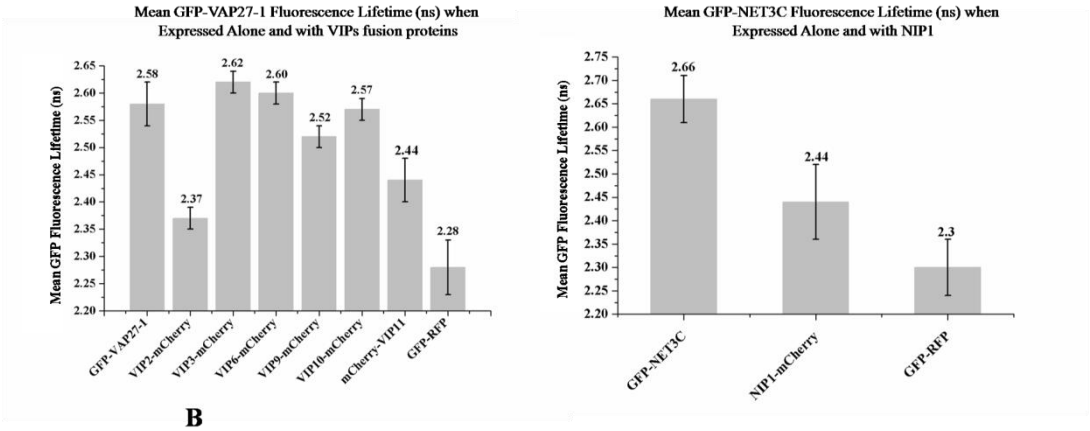

B

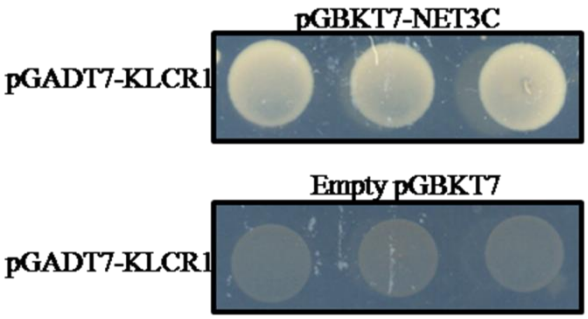

Figure 3.1 Identifying potential interactors of NET3C and VAP27-1. A. VIP2-mCherry and mCherry-VIP11 induce significant reductions in the fluorescence lifetime of GFP-VAP27-1 when co-expressed in *N. benthamiana* leaf tissues. NIP1-mCherry induces significant reduction in the fluorescence lifetime of GFP-NET3C when co-expressed in *N. benthamiana* leaf tissues. n=number of cells analysed. B. NET3C interacts with KLCR1 in a yeast-2-hybrid assay. Yeast were grown on selective media lacking tryptophan, leucine, histidine and adenine plus 2.5 mM 3AT (-WLHA+2.5 mM 3AT). Yeast containing pGADT7-KLCR1 and pGBKT7-NET3C was able to grow on selective media, indicating an interaction. Yeast containing pGADT7-KLCR1 and empty pGBKT7 was used as a negative control and was not able to grow on selective media.

3.2. Introduction of KLCR proteins

Kinesins belong to a large protein superfamily that is comprised of various motor

proteins that hydrolyze ATP and move unidirectionally along microtubules. It was first discovered in the giant axon of the squid about thirty years ago (Brady, 1985, Vale *et al.*, 1985). In eukaryotic cells, kinesin proteins play vital roles in the cellular transportation of vesicles, organelles, protein complexes and messenger RNAs, and are also involved in regulating microtubule dynamics (Hirokawa, 1998). In animals, the kinesin protein superfamily is commonly classified into 14 distinct classes depending on the position of their motor domains, the composition of the polypeptide chain and the directionality (Lawrence *et al.*, 2004). Among the members of kinesin superfamily, kinesin-1 is the most studied one. It is a tetrameric protein which is made up of two heavy chain subunits (KHCs) and two light chain subunits (KLCs). The KHCs (KIF5A, KIF5B and KIF5C) have the motor domain which moves along the microtubules and KLCs (KLC1 and KLC2) are essential for cargo binding (Hirokawa *et al.*, 2010, Rahman *et al.*, 1998).

In Arabidopsis, kinesin family is composed of 61 predicted members. However, the precise functions and biological roles of most of Arabidopsis kinesin proteins and their associated light chains are not well studied (Reddy and Day, 2001, Verhey *et al.*, 2011, Zhu and Dixit, 2012). According to Burstenbinder et al. (2012), Arabidopsis kinesin light chain-related protein-1 (KLCR1) and another two closely related tetratricopeptide repeat (TPR) domain-containing proteins, KLCR2 and KLCR3, are similar to mammalian kinesin light chain (KLC) subunit of kinesin motor proteins. A genetic yeast two-hybrid screen of an Arabidopsis flower cDNA library identified a novel microtubule binding protein, IQ67 domain 1 (IQD1) as the interactor of KLCR1. In tobacco leaf epidermal cells, KLCR1 and calmodulin 2 (CaM2) can be recruited to microtubules in the presence of IQD1, indicating that IQD1 may act as a recruiter of cargo to kinesin motors for directional transport along microtubular tracks in a Ca^{2+}/ calmodulin-dependent manner (Burstenbinder *et al.*, 2013).

The plant-specific IQ67 DOMAIN (IQD) protein family is considered to be the largest class of CaM-interacting proteins which link the Ca^{2+} signaling to the regulation of microtubule associated processes. IQD proteins are defined by their

characteristic IQ domain of 67 conserved amino acid residues, which harbors three different consensus CaM recruitment motifs in a unique and repetitive arrangement (Abel *et al.*, 2013). The IQD protein family has 33 members which can be divided into four major phylogenetic clades. They are localized to multiple subcellular sites, including microtubules, plasma membrane subdomains and nuclear compartments. The specific IQD localization patterns are closely related to the subcellular patterns of IQD-dependent CaM recruitment. Therefore, IQD proteins are considered as scaffold-like proteins that integrate CaM-dependent Ca^{2+} signaling at multiple subcellular sites to regulate cell function, shape and growth during plant development (Burstenbinder *et al.*, 2017).

As described before, NET3C is one of the members of the plant NET superfamily and it is proved to be one of the resident proteins of plant ER-PM contact sites (Deeks *et al.*, 2012, Wang *et al.*, 2014). However, the function of NET3C during plant development has not been well studied. In a previous study, KLCR1 was identified as a potential interactor of NET3C in a yeast-two-hybrid screen (by Dr. Pengwei Wang). In this chapter, several different bioinformatics approaches have been used to analyse the protein sequences of KLCR proteins and the interactions among NET3C, KLCR proteins and IQD proteins were studied.

3.3. Bioinformatics Analysis of KLCR Proteins

3.3.1. The Investigation of the Sequence of Arabidopsis Kinesin Light Chain-Related Proteins KLCR1, KLCR2 and KLCR3

Information regarding KLCR1, KLCR2 and KLCR3 was obtained from the Arabidopsis Information Resource (TAIR). According to the database, Arabidopsis KLCR1, KLCR2 and KLCR3 were encoded by the gene AT4g10840, AT3g27960 and AT1g27550 respectively. *KLCR1* had an open reading frame (ORF) of 2420 bp, consisting of 4 exons (1-686 bp, 794-1407 bp, 1794-2085 bp, and 2183-2420 bp),

which encoded a protein of 609 amino acids (aa) with a predicted molecular weight (MW) of 66.29 kDa. *KLCR2* consisted of an ORF of 2081 bp, with 2 exons situated at 1-1781 bp and 1871-2081 bp, encoding a 72.53 kDa protein of 663 residues. *KLCR3* had an ORF of 2026 bp, which contained 2 exons (1-1751 bp and 1825-2026 bp). This gene encoded a 650 aa protein with a predicted MW of 71.2 kDa (Figure 3.2).

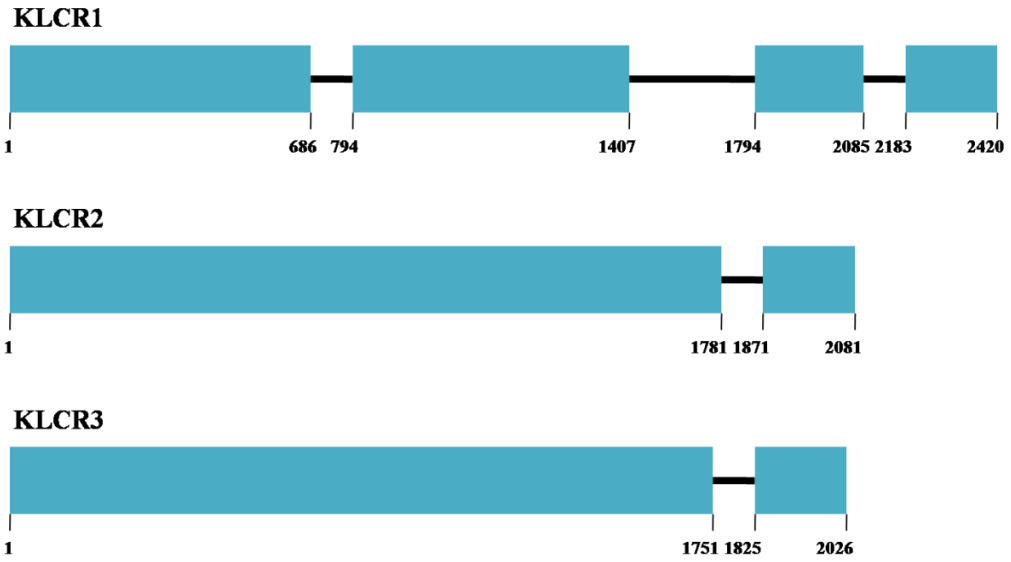

Figure 3.2 Schematic Diagrams of the gene structures of *KLCR1*, *KLCR2* and *KLCR3*. Exons are represented by light blue boxes and introns by black lines. Numbers below the diagrams represent the start and end positions (bp) of exons.

3.3.2. Predicted Protein Structure of KLCR1, KLCR2 and KLCR3

Next, the predicted domain structures of the KLCR proteins were analyzed by the Simple Modular Architecture Research Tool (SMART) programme (http://smart.embl-heidelberg.de/). The SMART programme is a web-based tool for detecting protein domains which match against sequences from the Database of Protein Families (Pfam) (Finn *et al.*, 2014).

Using the SMART program conserved Tetratricopeptide Repeat (TPR) domains were identified from the primary protein sequences of KLCR1, KLCR2 and KLCR3 (Figure 3.3, Table 3.1). TPR-containing proteins can be found in all species and have been shown to participate in various cellular functions such as cell division, RNA

metabolism, protein transport and neurogenesis. Typically, the three-dimensional structure of a TPR motif contains two antiparallel α-helices and these tandem arrays of TPR motif form a right-handed helical structure that serves as a platform to facilitate protein-protein interactions (Blatch and Lassle, 1999, Schottkowski *et al.*, 2009). The TPR regions were detected in-between amino acids 140-258 and 307-549 in KLCR1; amino acids 199-318 and 369-612 in KLCR2, and amino acids 235-310 and 363-602 within KLCR3. Regions of low complexity which represent simple sequence regions with significant biases in amino acid composition were identified at the N-termini of KLCR1 (aa 32-56), KLCR2 (aa 83-100) and KLCR3 (aa 66-78 and aa 117-129). For KLCR2, the region of low complexity was also detected between the two TPR regions (aa 320-330) (Wootton and Federhen, 1996).

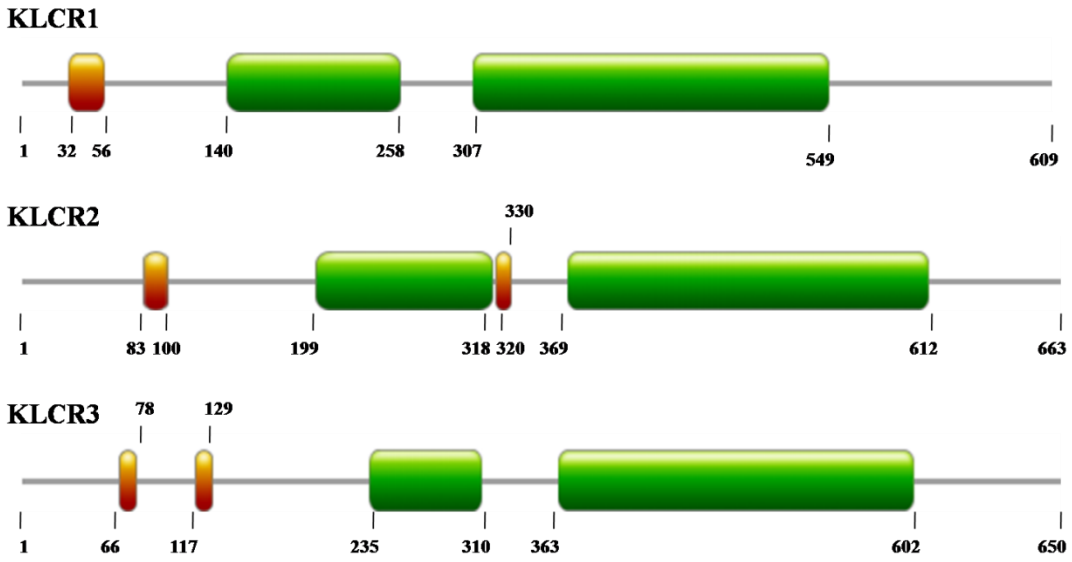

Figure 3.3 Predicted protein structures of KLCR proteins in Arabidopsis. The protein structures were predicted using the SMART programme. Green boxes indicate TPR regions, red boxes indicate regions of low complexity and gray lines represent non-domain containing protein regions. Numbers underneath the diagrams denote the start and end point (amino acids) of the labeled protein domain.

Protein	Predicted protein Domains	Positions (aa)
KLCR1	TPR Region 1	140-258
	TPR Region 2	307-549
	Region of low complexity	32-56
KLCR2	TPR Region 1	199-318
	TPR Region 2	369-612
	Region of low complexity	83-100 & 320-330
KLCR3	TPR Region 1	235-310
	TPR Region 2	363-602
	Region of low complexity	66-78 & 117-129

Table 3.1 List of protein domains possessed by KLCR1, KLCR2 and KLCR3 predicted using the SMART program.

3.3.3. Predicted Protein Sequence Similarity of KLCR1 with KLCR2 and KLCR3

Global sequence alignments were performed to analyze the protein sequence similarity between KLCR proteins using the European Molecular Biology Open Software Suite (EMBOSS) (Rice *et al.*, 2000). This programme uses the Needleman-Wunsch algorithm to create an optimal alignment along the entire length of two protein sequences. The alignments were created using the default settings for protein alignments (EBLOSUM62 protein weighting matrix, 10 gap opening penalty and 0.5 gap extension penalty).

As shown in Table 3.2, full length KLCR1 and KLCR2 held 46.4% identity and 61.3% similarity in amino acid composition. Within the TPR region 1, KLCR1 and KLCR2 displayed a high level of amino acid conservation, sharing 57.5% identity and 78.8% similarity identified between KLCR1 (a.a. 140-259) and KLCR2 (a.a. 199-318). A higher degree of conservation was observed between the TPR region 2 of KLCR1 and KLCR2, with 62.3% identity and 81.6% similarity within amino acids 307-549 of KLCR1 and amino acids 369-612 of KLCR2. It is clear that the protein sequence of KLCR1 and KLCR2 is highly conserved within the TPR regions.

Alignment	KLCR1 amino acid Location (aa)	KLCR2 amino acid Location (aa)	Length (aa)	% aa Identity	% aa Similarity	% Gaps	Score
Full length	1-609	1-663	701	46.4	61.3	18.5	1546
TPR region 1	140-258	199-318	120	57.5	78.8	0.8	367
TPR region 2	307-549	369-612	244	62.3	81.6	0.4	790

Table 3.2 Amino acids sequences alignment of KLCR1 and KLCR2 performed using the EMBOSS Needle tool. Alignments were performed between the sequences of full length proteins, TPR region 1 and TPR region 2.

The protein sequence similarity between KLCR1 and KLCR3 was then analyzed. As shown in Table 3.3, the two KLCR proteins share 45.9% identity and 60.6% similarity along the full peptide length. Within the TPR region 1 of KLCR1 and KLCR3, the degree of conservation is relatively low, sharing 38.7% amino acid identity and 51.2% amino acid similarity. There was relatively high similarity in the TPR region 2 of KLCR1 and KLCR3, with 59.4% identity and 78.3% similarity in amino acid composition. When compared to the protein sequence similarity between KLCR1 and KLCR2, the similarity between KLCR1 and KLCR3 was lower within the TPR region1. A diagram of the protein sequence alignments between the three KLCR proteins was generated using the ClustalX software (Larkin *et al.*, 2007) and visualized using Jalview (Figure 3.4) (Waterhouse *et al.*, 2009).

Alignment	KLCR1 amino acid Location (aa)	KLCR3 amino acid Location (aa)	Length (aa)	% aa identity	% aa Similarity	% Gaps	Score
Full length	1-609	1-650	687	45.9	60.6	16.7	1523.5
TPR region 1	140-258	235-310	119	38.7	52.1	36.1	255
TPR region 2	307-549	363-602	244	59.4	78.3	2.0	746

Table 3.3 Amino acids sequences alignment of KLCR1 and KLCR3 performed using the EMBOSS Needle tool. Alignments were performed between the sequences of full length proteins, TPR region 1 and TPR region 2.

A

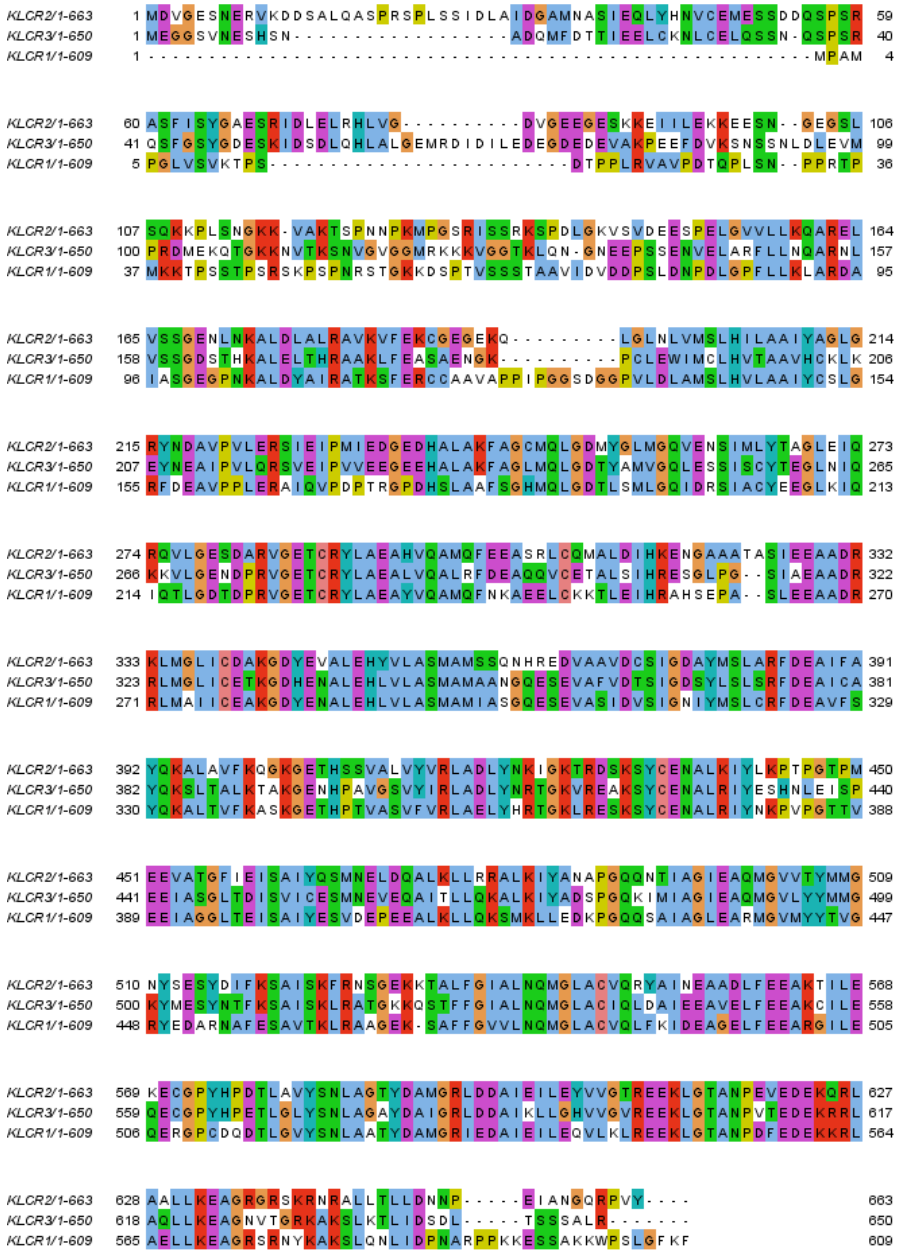

B

Color	Residue at Position	(Threshold, Residue Group)
Blue	A, I, L, M, F, W, V	(+60%, WLVIMAFCHP)
	C	(+60%, WLVIMAFCHP
Red	R, K	(+60%, KR) (80%, K, R, Q)
Green	N	(+50%, N) (+85%, N, Y)
	Q	(+60%, KR) (+50%, QE) (+85%, Q, E, K, R)
	S, T	(+60% WLVIMAFCHP) (+50%, TS) (+85%, S,T)
Pink	C	(100%, C)
Magenta	E	(+60%, K, R) (+50%, QE) (+85%, E, Q, D)
	D	(+60%, K, R) (+85%, K, R, Q) (+50%, ED)
orange	G	(+0%, G)
Cyan	H, Y	(+60%, WLVIMAFCHP) (+85%, W, Y, A, C, P, Q, F, H, I, L, M, V)
Yellow	p	(+0%, P)

Figure 3.4 Visual Projection of amino acid sequence alignment between KLCR proteins. A. Global pairwise alignment of full length sequences of KLCR proteins created using ClustalX and visualized using Jalview with the ClustalX default colors. B. ClustalX color scheme key in which amino acids are colored according to their characteristic and conservation. The color for the column is generated if the threshold value is met or exceeded. The amino acids needed to exceed the minimum threshold are indicated, with the minimum percentage needed to exceed the threshold value. If the residues are separated by commas such as "K, R", the color is applied when one individual amino acid meets or exceeds the threshold. If the amino acids are grouped together without commas such as "ED", the color is applied when any combination of these residues meets or exceeds the threshold value.

3.3.4. Gene Expression Analysis

The investigation of the gene expression pattern is able to provide information on gene expression localization within specific tissues. This information is considered to be essential for functional study of genes of interest. Computer programmes, Genevestigator and the Arabidopsis electronic Fluorescent Pictograph (eFP) Browser, were used for investigating the publicly available gene expression data for KLCR proteins (Hruz *et al.*, 2008, Winter *et al.*, 2007).

As shown in Figure 3.5, *KLCR1* has a high level of expression throughout the all plant developmental stages except for the senescence stage. The expression level of *KLCR2* is relatively high at the seed germination and seedling stages. However, *KLCR3* has the lowest expression level when compared with *KLCR1* and *KLCR2*, but the expression is slightly elevated during senescence.

As shown in Figure 3.6, the gene expression data from the Arabidopsis eFP browser revealed that *KLCR1* was expressed strongly in the first node and the second internode. The expression levels in root and stage 4, 6, and 7 seeds were slightly lower. Similar to *KLCR1*, *KLCR2* is most highly expressed in the first node and the second internode and high levels of expression were also found in root and stage 4 and 5 seeds. Expression for *KLCR3* was shown to be very low in various Arabidopsis tissues and this result largely corroborates with the expression information compiled from Genevestigator.

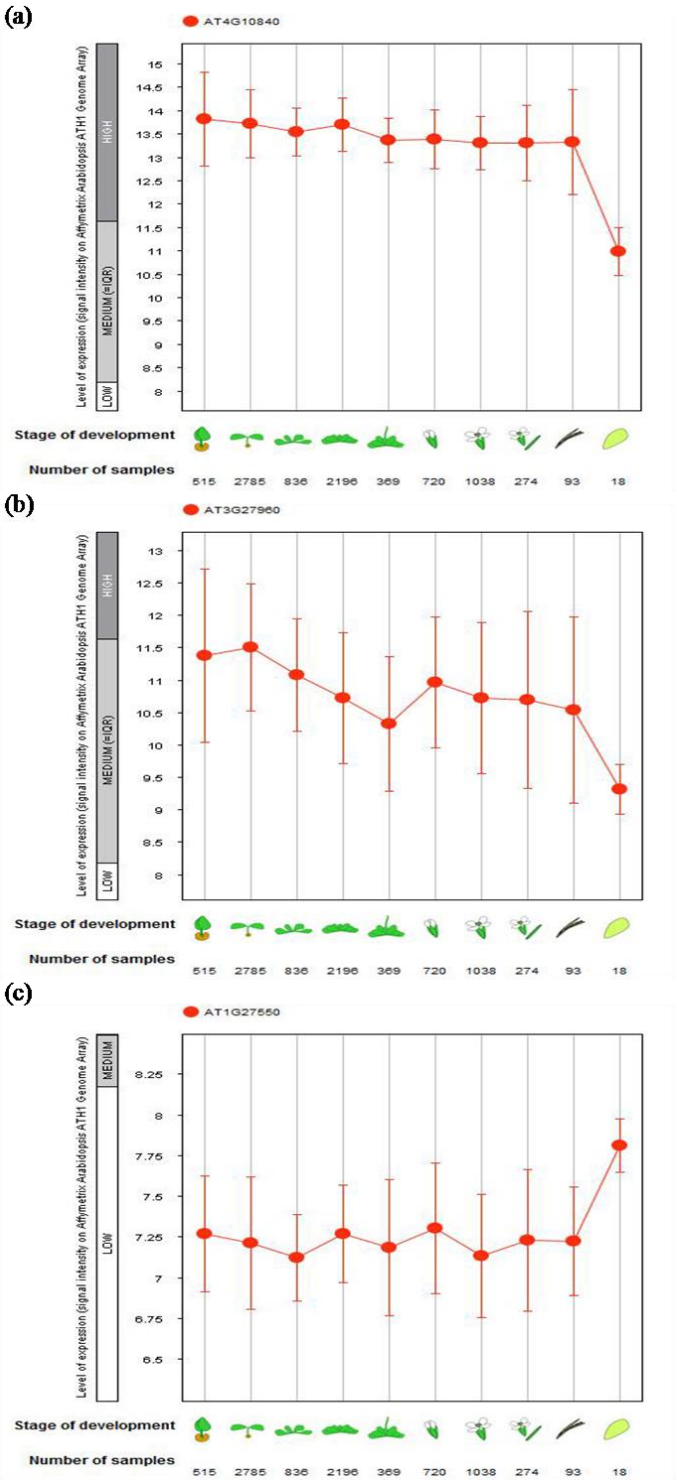

Figure 3.5 Expression of Arabidopsis *KLCR* genes across different stages of development (a) Genevestigator development map for Arabidopsis *KLCR1*. (b) Genevestigator development map for Arabidopsis *KLCR2*. (c) Genevestigator development map for Arabidopsis *KLCR3*. The level of expression is shown as the $\log_2$ value and the development stages are pictorially represented from left to right as follows: seed germination, seedling, early rosette growth, rosette growth complete, inflorescence emergence, young flower, developed flower, flowers and siliques, silique ripening and senescence.

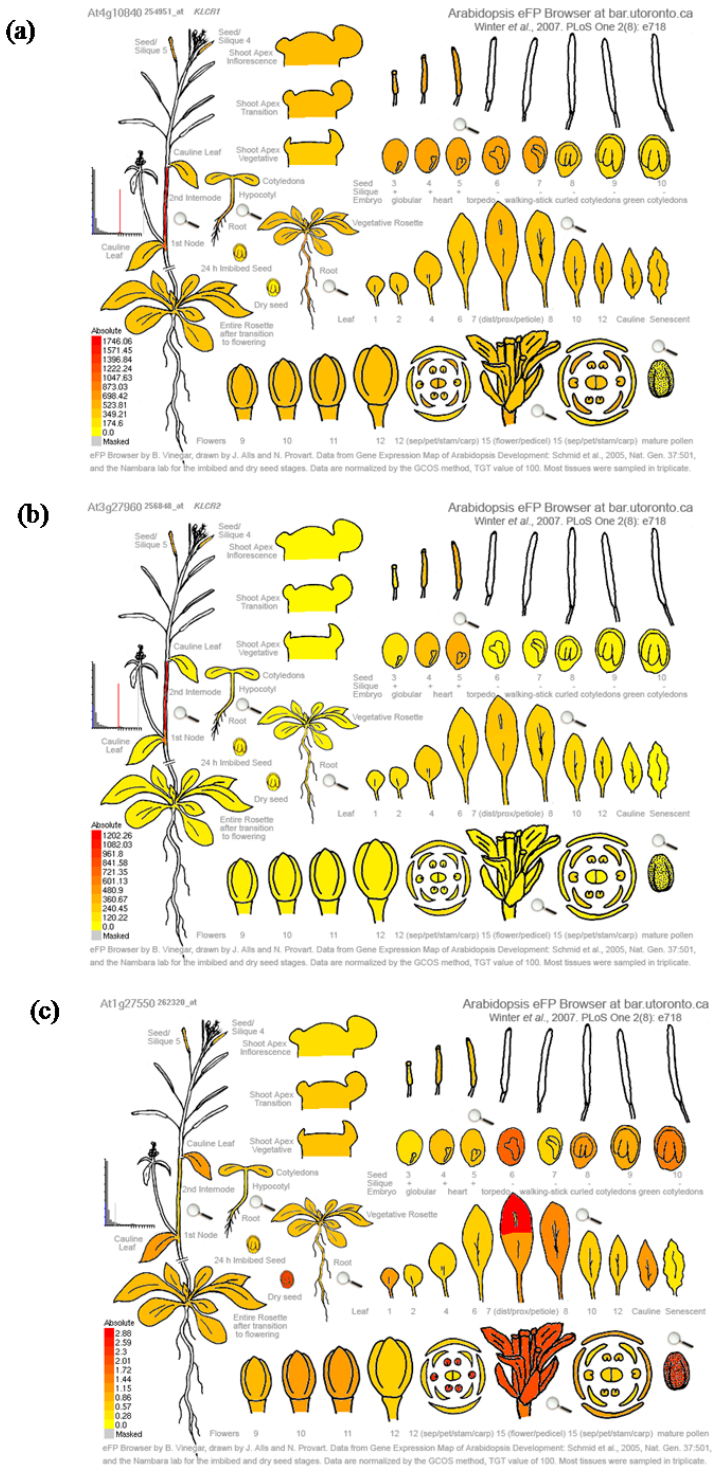

Figure 3.6 Tissue specific expression patterns of Arabidopsis *KLCR*. The range of absolute expression value with low levels in yellow and high levels in red is shown as a scale bar at the left bottom corner. (a) Tissue specific expression pattern of Arabidopsis *KLCR1*. The strongest *KLCR1* expressions are found in the first node and the second internode. High levels of expression are also found in root and seeds stages 4, 6 and 7. (b) Tissue specific expression pattern of Arabidopsis *KLCR2*. The highest expression levels are seen in the first node and the second internode. Strong expression can also be found in seeds stages 4 and 5, leaf 7 and root. (c) Tissue specific expression pattern of Arabidopsis *KLCR3*. *KLCR3* is expressed weakly in various plant tissues.

3.4. *In vivo* Study of KLCR Proteins

3.4.1 Cloning of the Full Length KLCR Proteins

In order to study the function and subcellular localization of KLCR proteins *in vivo*, full length genes were cloned into various expression vectors with different fluorescent proteins. To generate KLCR2-GFP and RFP-KLCR2 expression constructs, the coding sequence of KLCR2 was amplified by PCR from Arabidopsis cDNA and cloned into pDONR207 using gateway BP cloning. KLCR2 was then cloned into pMDC83-GFP and pK7WGR2 respectively to facilitate the expression of full length KLCR2-GFP and RFP-KLCR2 under the control of a 35s promoter. The entry clone of KLCR3 was obtained from Dr. Katharina Burstenbinder (Leibniz Institute of plant biochemistry). This gene was subsequently cloned into pMDC83-GFP and pK7WGR2 Gateway expression vectors to enable their expression under the expression of a 35s promoter. In order to generate *proKLCR1*:KLCR1-GFP Stable transgenic Arabidopsis lines, GFP-tagged KLCR1 driven by its endogenous promoter was created. KLCR1 with its promoter sequence (~2kb before its start codon) was amplified from Arabidopsis genomic DNA and cloned into pDONR207 by BP reaction. After conformation by sequencing, it was subsequently moved into pMDC107 by LR reaction. Gene specific primers for the different constructs are listed in Appendix 1.1 and 1.2. Schematics of expression constructs described above are listed in Figure 3.7.

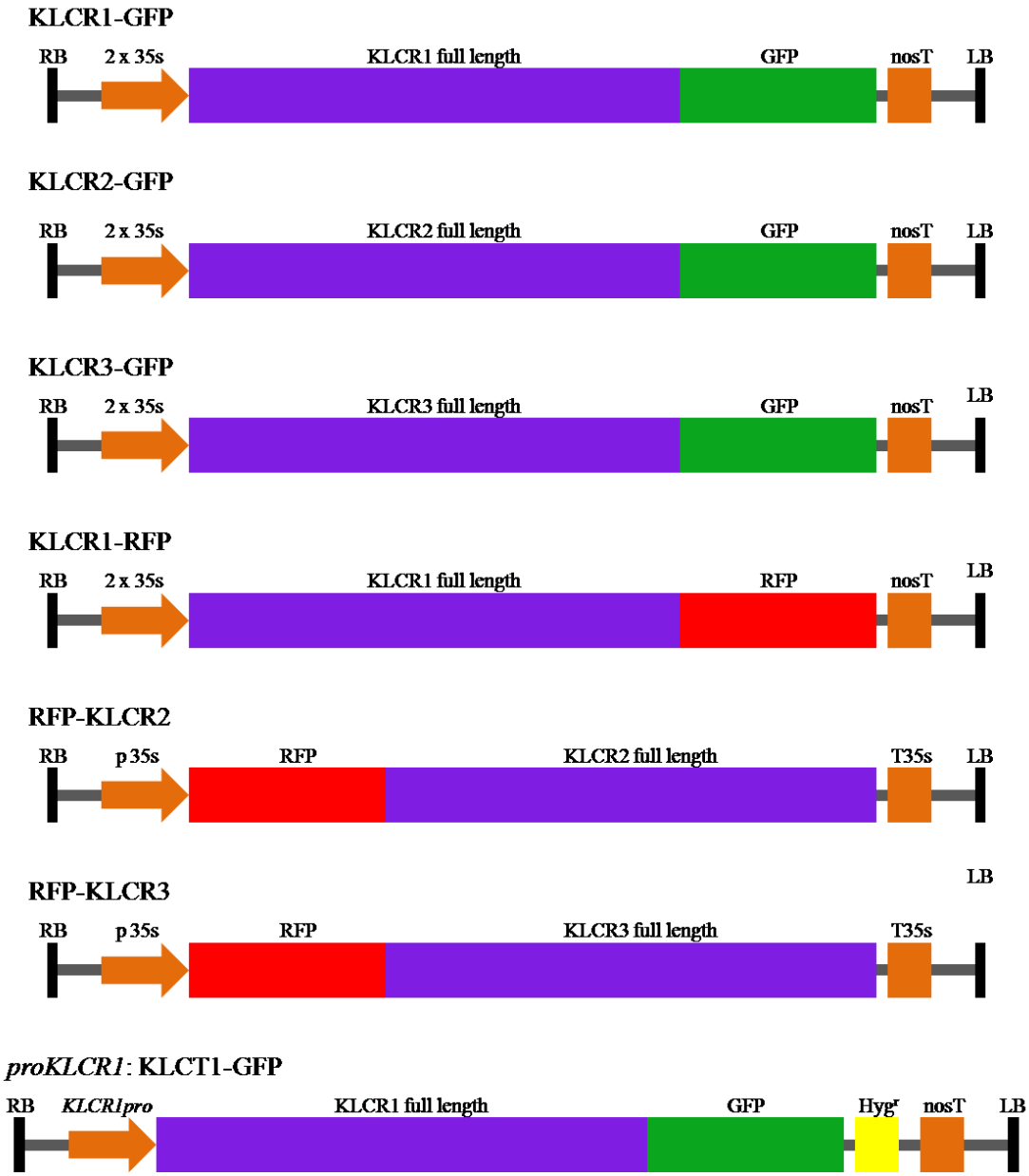

Figure 3.7 Schematics of expression constructs. KLCR1-GFP, KLCR2-GFP, KLCR3-GFP and KLCR1-RFP constructs were created using the pMDC83 vector. RFP-KLCR2 and RFP-KLCR3 contracts were generated using the pK7WGR2 vector. *ProKLCR1*:KLCR1-GFP contract was created using the pMDC107 vector.

3.4.2. Subcellular Localization of KLCR1, KLCR2 and KLCR3 in *N. benthamiana* Leaf Epidermal Cells

In order to study the subcellular localization of KLCR proteins *in vivo*, agrobacterium-mediated transient transformation was performed to facilitate their expression in *N. benthamiana* leaf epidermal cells.

Agrobacterium tumefaciens is a natural plant pathogen which is able to induce tumor formation during infection. It can be used to introduce the genetic expression constructs into plants by integrating transfer DNA (T-DNA) into the host genome. For commonly used binary vectors, the genes which are required for tumor formation have been removed from the T-DNA. The recombinant DNA constructs can be inserted, promoting their integration into host DNA (Zupan and Zambryski, 1995).

N. benthamiana leaf epidermal cells are commonly used for studying the subcellular localization of fluorescent protein-tagged fusion proteins. A solution of agrobacterium transformed with expression constructs of interest was infiltrated into the lower epidermal cells of *N. benthamiana* leaf, facilitating the expression of fluorescent fusion proteins (Kapila *et al.*, 1997).

KLCR1-GFP, KLCR2-GFP and KLCR3-GFP fusion proteins were transiently expressed in *N. benthamiana* leaf epidermal cells under the control of the 35s promoter, and their subcellular localizations were observed using CLSM. As shown in Figure 3.8, full length KLCR1-GFP was localized in the cytosol (a-c) and this expression pattern is similar with a previous study which revealed the localization of mRFP-KLCR1 (Burstenbinder *et al.*, 2017). The other two GFP tagged KLCR proteins KLCR2-GFP and KLCR3-GFP were also observed in the cytosol (d-f and g-i). The similar expression pattern in *N. benthamiana* leaf epidermal cells is likely to be because of the high protein sequence similarity of the three KLCR proteins. In addition, KLCR1-GFP was also transiently expressed *in N. benthamiana* leaf epidermal cells under the control of the endogenous promoter. Interestingly, some filamentous structure was observed (j-l). When *proKLCR1*:KLCR1-GFP was co-expressed with the microtubule marker, Tubulin-mCherry, the filaments were found to be co-localized with microtubules (m-o), indicating that KLCR1 was able to localize to microtubules by reducing its expression. The different expression of *35s*:KLCR1-GFP and *proKLCR1*:KLCR1-GFP is likely because the microtubule localization of KLCR1 relies on some other factors, such as IQD proteins and this will be discussed later.

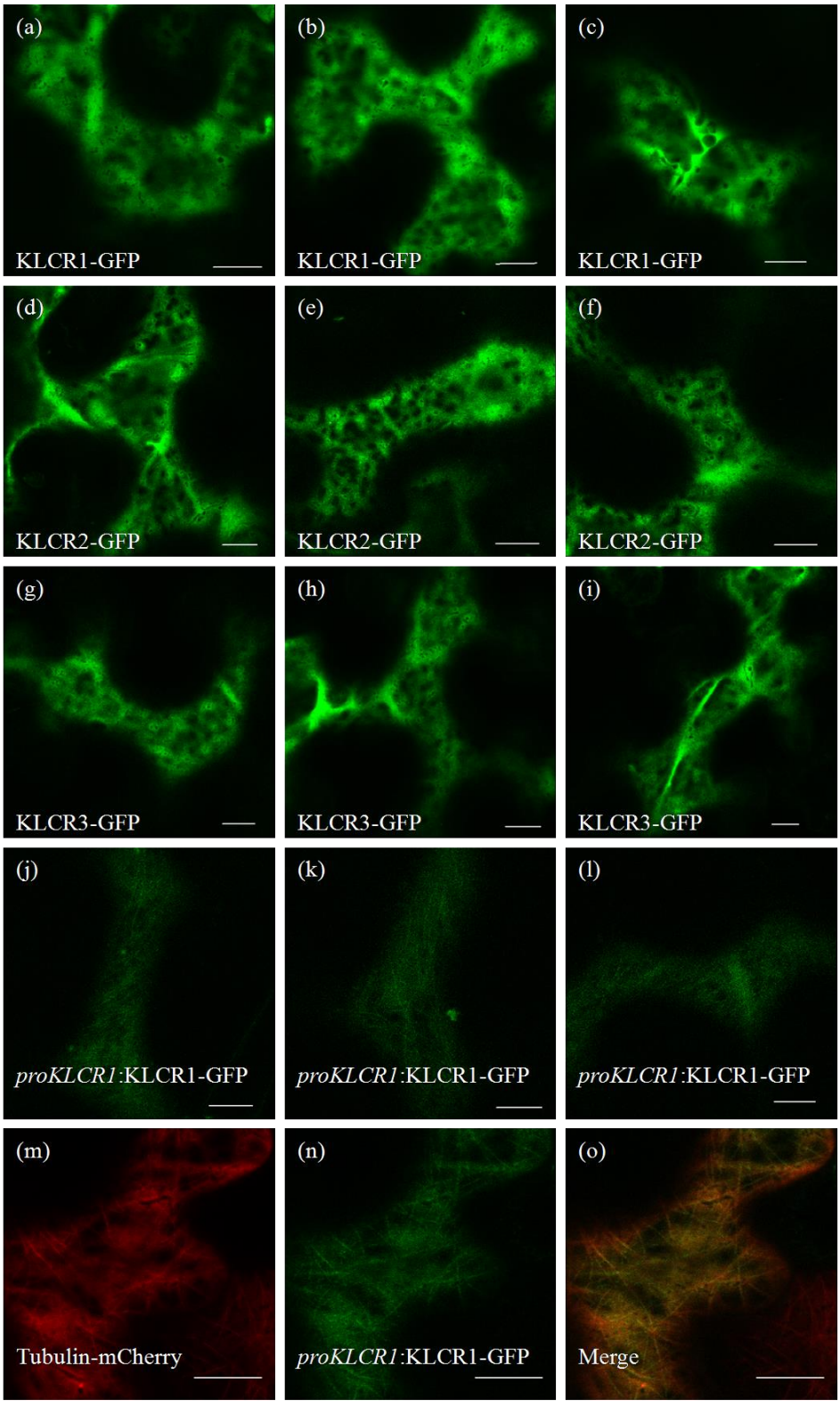

Figure 3.8 Subcellular localization of KLCR1, KLCR2, and KLCR3 in *N. benthamiana* leaf epidermal cells. (a)-(c): localization of KLCR1-GFP expressed under the control of 35s promoter. (d)-(f): localization of KLCR2-GFP expressed under the control of 35s promoter. (g)-(i): localization of KLCR3-GFP expressed under the control of 35s promoter. (j)-(o): localization of KLCR1-GFP expressed under the control of the endogenous promoter. (m)-(n): Scale bar: 10 μm.

3.4.3. Subcellular Localization of KLCR1-GFP in Arabidopsis Cotyledon Epidermal Cells.

Then, the subcellular localization of KLCR1 in stable Arabidopsis transgene lines was assessed. Arabidopsis transgenic lines stably expressing KLCR1-GFP under its native promoter were generated using the floral dipping method as described in chapter 2.2.14. Transformed plants were selected from the T1 generation seeds in 1/2 MS plates containing 40 µg/ml Hygromycin (Chapter 2.5.5). The selected plants were then manually screened for GFP fluorescence in leaf epidermal cells using confocal microscopy. The stable T3 generation was used for the subcellular localization study. Cotyledon epidermal cells of 5 days old seedlings were imaged and at least 3 independent transformed lines independent transformed were analyzed. Interestingly, in cells expressing *proKLCR1*:KLCR1-GFP, KLCR1 formed punctate structures which associated with microtubules (Figure 3.8, a-c). This pattern is different from the expression pattern in *N. benthamiana* leaf epidermal cells and this will be discussed later.

To assess whether KLCR1 was microtubule-localized, the microtubule marker, Tubulin-mCherry, was used to accomplish the co-visualization of KLCR1-GFP with microtubule. Stable Arabidopsis lines expressing Tubulin-mCherry were produced by Dr. Pengwei Wang (Durham University). Cross-pollination of *proKLCR1*:KLCR1-GFP and Tubulin-mCherry plants was performed to generate plants expressing both constructs. As shown in Figure 3.9, it is clear that the KLCR1 punctae aligned along the microtubules (d-f and g-i). In summary, the subcellular localization of KLCR1 in Arabidopsis is at the microtubule filaments.

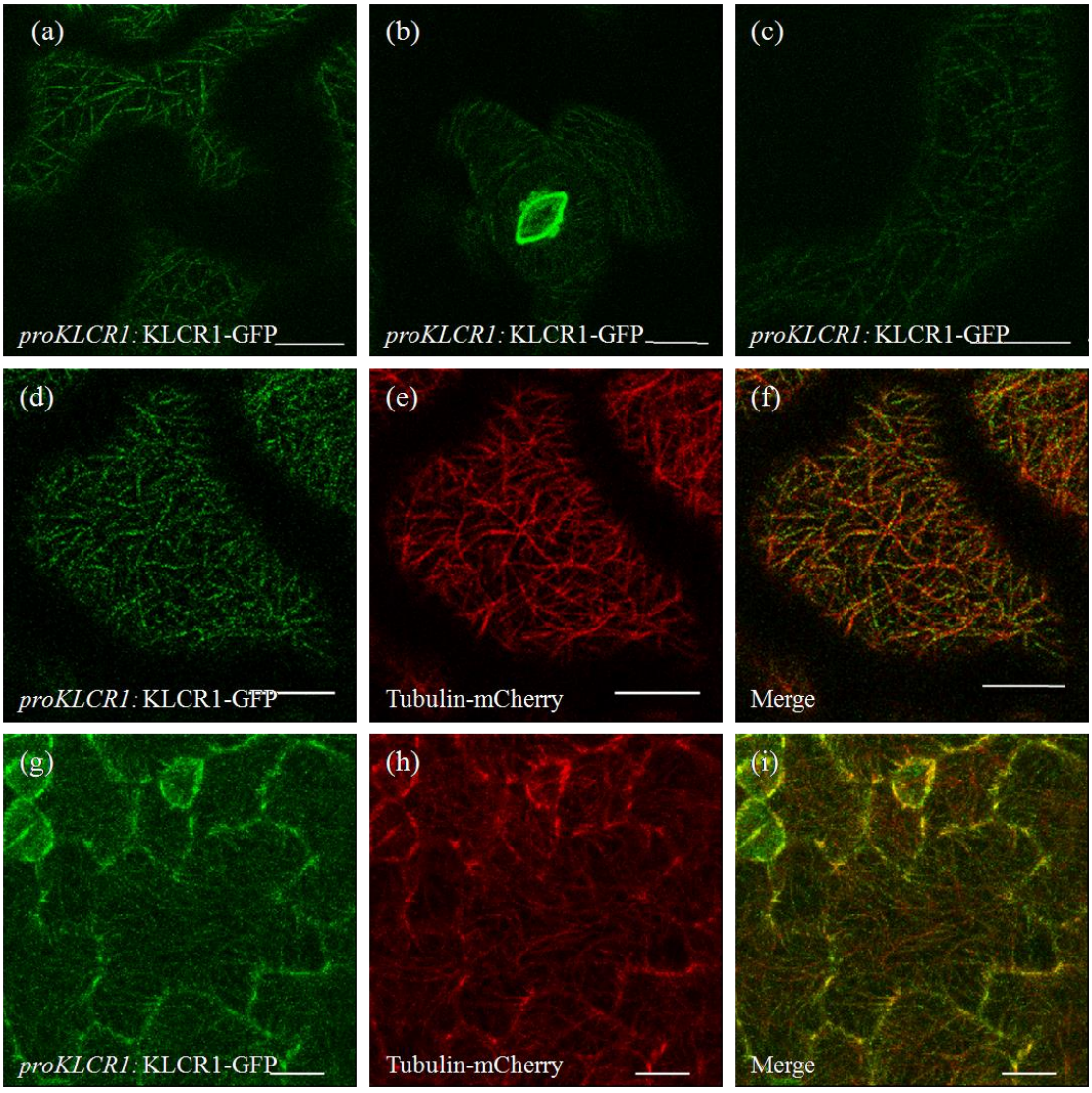

Figure 3.9 Subcellular localization of KLCR1-GFP in Arabidopsis cotyledon epidermal cells. (a)-(c): Arabidopsis expressing *proKLCR1*:KLCR1-GFP in cotyledon epidermal cells. KLCR1-GFP is localized in punctate structures in a striking filamentous network. (d)-(f): Co-localization of *proKLCR1*:KLCR1-GFP with Tubulin-mCherry in cotyledon epidermal cells. KLCR1-GFP punctae are localized to microtubules. (g)-(i): Z-projection. Scale bar: 10 µm.

3.4.4. *In vivo* Interaction Analysis between NET3C and KLCR Proteins

In a previous study, protein KLCR1 was identified to be a potential interactor of protein NET3C in a yeast-two-hybrid screen. As two proteins physically interact with each other, they are likely to co-localize at the same subcellular localization at a point in time. In order to confirm the interaction between KLCR1 and NET3C *in vivo*,

co-localization analysis between them was performed. Due to the high protein sequence similarity of KLCR1 with KLCR2 and KLCR3, the potential co-localization of RFP-NET3C with KLCR2-GFP and KLCR3-GFP was also analyzed. GFP and RFP fusion proteins were co-expressed in *N. benthamiana* leaf epidermal cells and could be visualized simultaneously because of their distinct spectral properties.

In cells that expressed both fluorescent fusion proteins, the cytosolic localized KLCR1-RFP was clearly observed to be recruited to the punctae which were co-localized with GFP-NET3C (Figure 3.10, a-c). KLCR2-GFP was weakly co-localized with RFP-NET3C at the punctate structure (Figure 3.10, a-f). However, this co-localization was not observed when co-expressed RFP-NET3C with GFP-KLCR3 (Figure 3.10, g-i). Therefore, NET3C seems to interact with KLCR1 and KLCR2.

In order to test this hypothesis, FRET-FLIM analysis was performed. Donor FRET-FLIM constructs GFP-NET3C and KLCR2-GFP were expressed alone, or co-expressed with the acceptor constructs KLCR1-RFP and RFP-NET3C respectively in *N. benthamiana* leaf epidermal cells. FRET-FLIM was also performed using GFP-RFP fusion protein as a positive control. As displayed in Figure 3.11, the average fluorescence lifetimes of GFP-NET3C and KLCR2-GFP when expressed alone were measured at 2.61±0.04 ns and 2.64±0.02 ns respectively, whereas the average fluorescence lifetime of GFP-NET3C was significantly reduced to 2.41±0.03 ns ($p<2.2E-16$) in the presence of KLCR1-RFP, an approximate 0.2 ns reduction was observed, indicating two proteins are in close association. In comparison, RFP-NET3C was only able to reduce the fluorescence lifetime of KLCR2-GFP by 0.07 ns, to an average value of 2.57±0.02 ns. This different in fluorescence lifetime is negligible, because the reduction of the fluorescence lifetime was less than 0.1 ns, accepted to indicate an interaction between donor and acceptor fluorescence fusion proteins. This is likely because the association between KLCR2 and NET3C was very weak (Figure 3.10, a-f). Moreover, the average fluorescence lifetime of the GFP-RFP fusion protein was measured at 2.33±0.03 ns. Therefore, the FRET-FLIM experiment

suggests that GFP-NET3C physically interacts with KLCR1-RFP *in vivo*, a result which is in agreement with the previous Y2H study that shows that NET3C interacts with KLCR1 in yeast. However, no interaction between KLCR2-GFP and RFP-NET3C could be detected using FRET-FLIM.

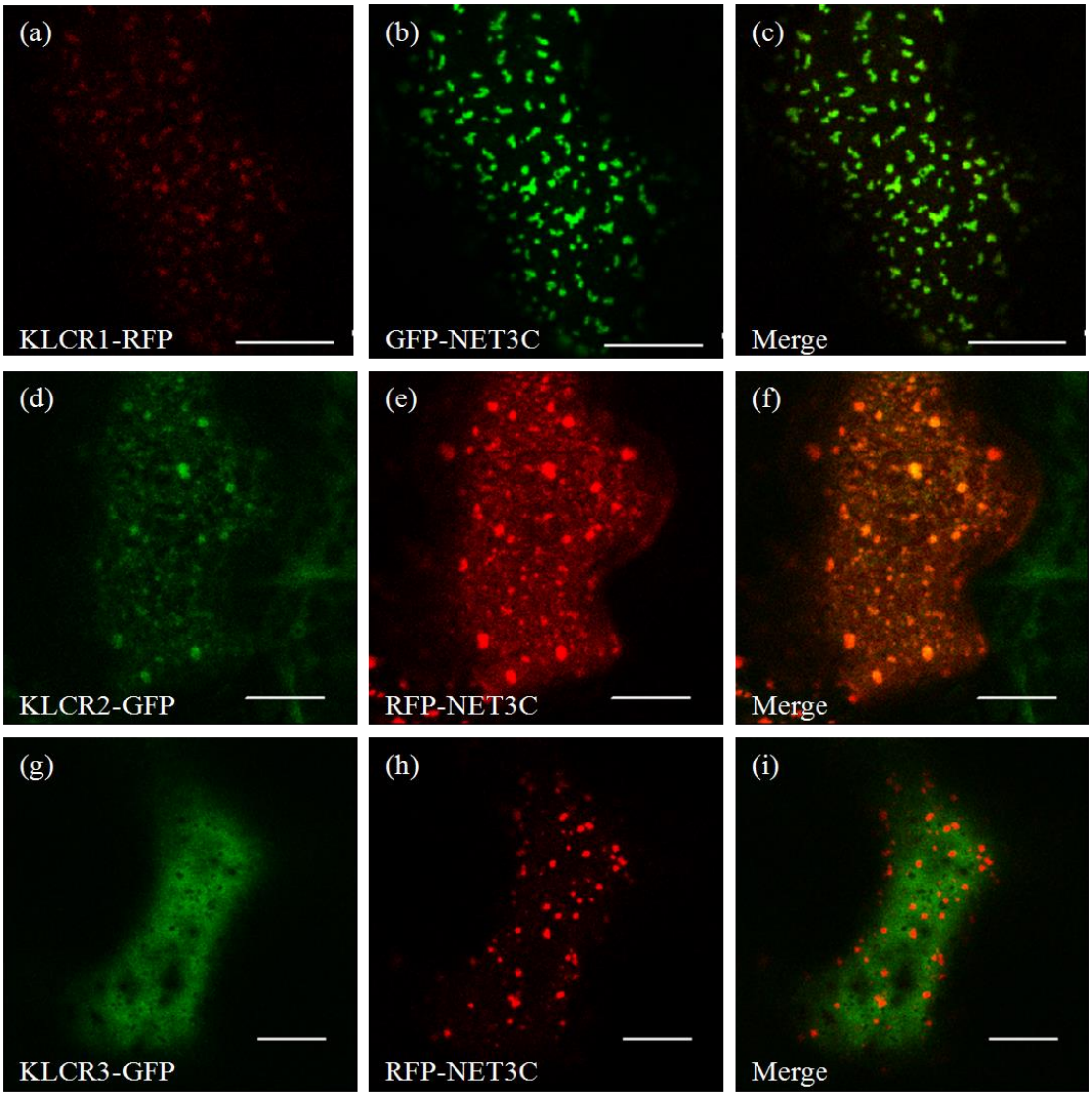

Figure 3.10 Co-localization of NET3C with KLCR proteins in vivo. *N. benthamiana* leaves were co-expressed with NET3C and KLCR proteins. (a)-(c): Co-expression of KLCR1-RFP with GFP-NET3C. The GFP-NET3C labels small punctate structures and KLCR1-RFP is co-localized with GFP-NET3C at these punctae. (d)-(f): Co-expression of KLCR2-GFP with RFP-NET3C. KLCR2-GFP is partially co-localized with RFP-NET3C at the punctate structure. (g)-(i): Co-expression of KLCR3-GFP with RFP-NET3C. KLCR3-GFP and RFP-NET3C are not co-localized with each other. Scale bar: 10 µm.

A

Constructs Expressed	Mean GFP Fluorescence Lifetime	Standard Deviation	n
GFP-NET3C	2.61 ns	0.04	10
GFP-NET3C+KLCR1-RFP	2.41 ns	0.03	10
KLCR2-GFP	2.64 ns	0.02	6
KLCR2-GFP+RFP-NET3C	2.57 ns	0.02	6
GFP-RFP	2.33 ns	0.03	10

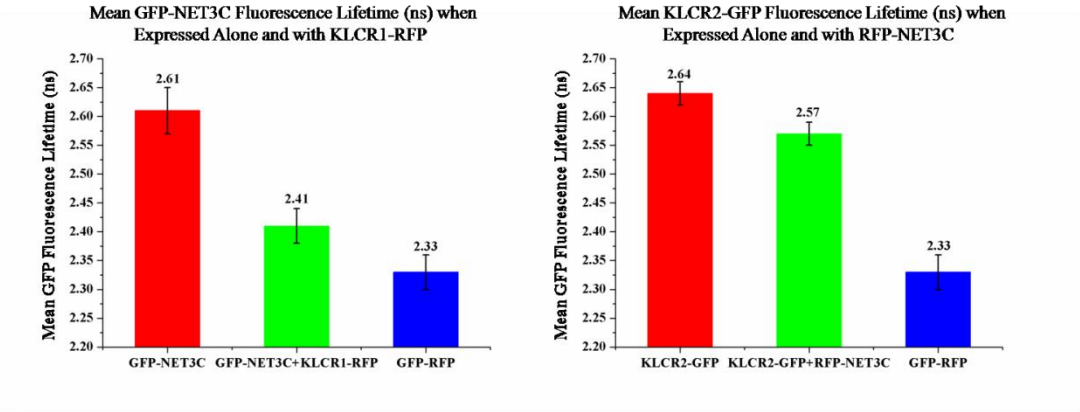

B

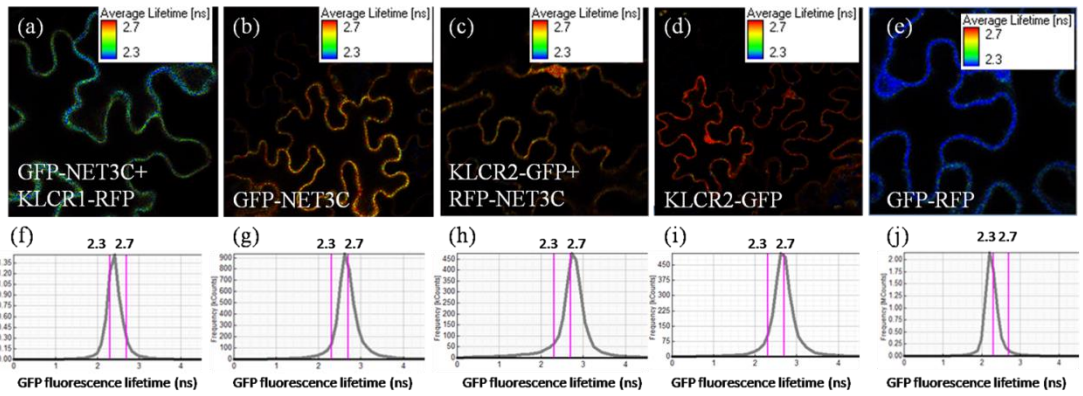

Figure 3.11 FRET-FLIM analysis of NET3C-KLCR1 and NET3C-KLCR2. A: Average fluorescence lifetime of GFP-NET3C significantly reduces when co-expressed with KLCR1-RFP. The reduction of fluorescence lifetime of KLCR2-GFP is negligible in the presence of RFP-NET3C. n = number of cells analyzed. B: Visualization of GFP-NET3C and KLCR2-GFP fluorescence lifetimes in *vivo* when expressed alone or expressed with KLCR1-RFP and RFP-NET3C respectively. (a)-(e): example images of GFP fluorescence detected in *N. benthamiana* leaf epidermal cells, pseudocoloured according to GFP fluorescence lifetime. (f)-(j): charts associated with images (a)-(e) respectively, show the frequency distributions of the fluorescence lifetimes (ns) of detected photons in each image. A leftward shift in peak GFP fluorescence lifetime indicates the reduction of average lifetime. (a) and (f): GFP-NET3C co-expressed with KLCR1-RFP. (b) and (g): GFP-NET3C expressed alone. (c) and (h): KLCR2-GFP co-expressed with RFP-NET3C. (d) and (i): KLCR2-GFP expressed alone. (e) and (j): GFP-RFP positive control.

3.4.5. Co-localization Analysis of KLCR1 with NET3A and NET3B *in vivo*

After co-localization analysis between NET3C and KLCR proteins, co-localization of KLCR1 with NET3A and NET3B was performed to investigate whether other members of the NET3 family may also interact with KLCR1 in plants.

NET3A-mCherry and NET3B-GFP were co-expressed with KLCR1-GFP and KLCR1-RFP respectively in *N. benthamiana* leaf epidermal cells using agrobacterium-mediated transformation. As a negative control, NET3A-mCherry and NET3B-GFP were also expressed on their own.

In the *N. benthamiana* leaf epidermal cells, actin filaments were decorated by NET3A-mCherry with brighter foci distributed on these filaments (Figure 3.11, a-c). This observation is similar with a previous study which reports the actin filaments labeling of NET3A-GFP in BY-2 tissue culture cells (Deeks *et al.*, 2012). In cells expressing both NET3A-mCherry and KLCR1-GFP, no co-localization was observed (Figure 3.12, d-f). On the other hand, NET3B is associated with both actin filaments and the ER network (Figure 3.12, g-i) (Wang and Hussey, 2017). When it is co-expressed with protein KLCR1, there is also no co-localization between these two proteins (Figure 3.12, j-l). Taken together, these results indicate that the interaction between NET3C and KLCR1 is specific among all NET3 family.

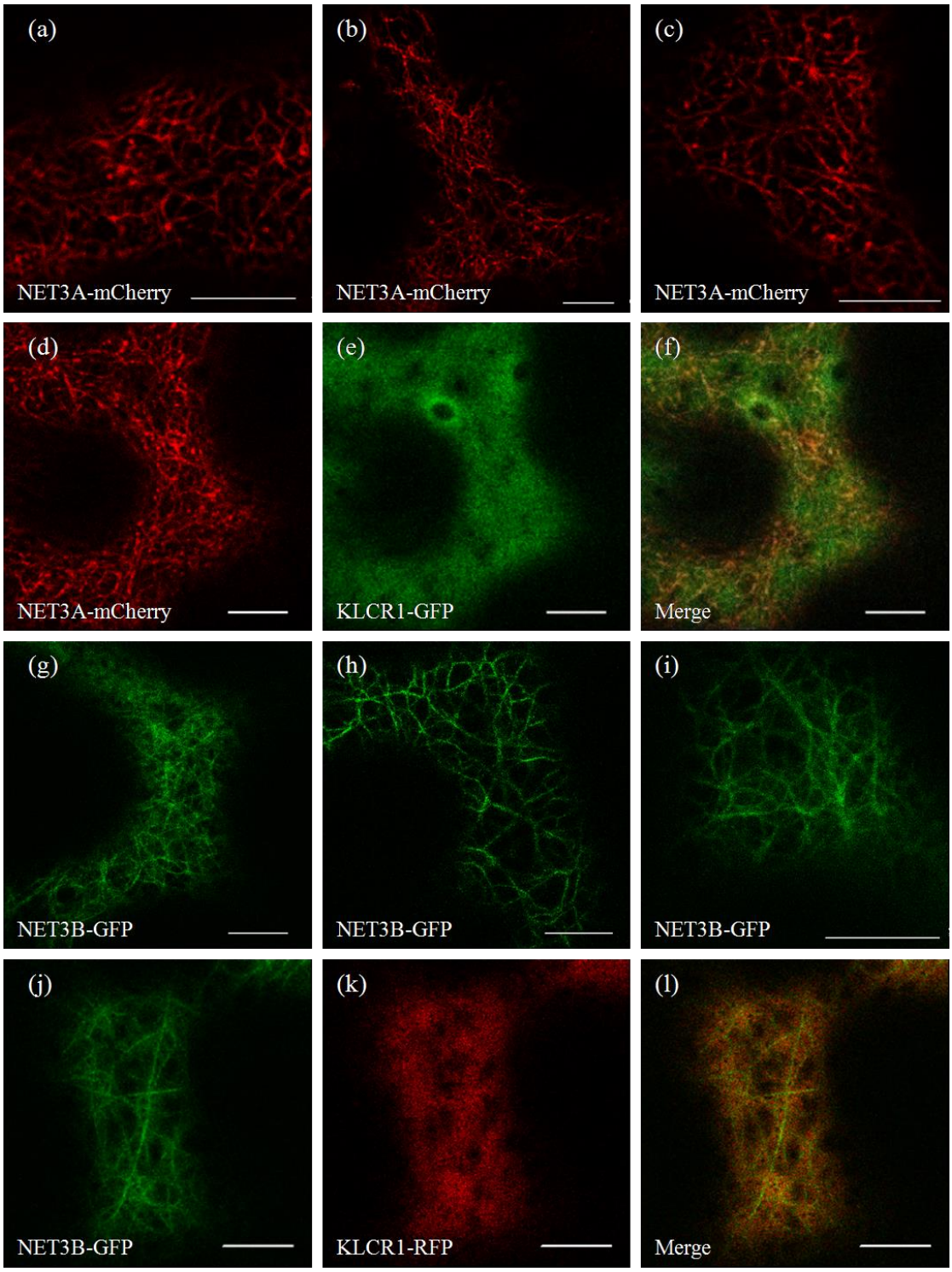

Figure 3.12 Co-localization analysis of KLCR1 with NET3A and NET3B *in vivo*. *N. benthamiana* leaves were transformed with the fluorescently-tagged proteins. (a)-(c): NET3A-mCherry expressed alone. NET3A-mCherry labels actin filaments with brighter foci on these filaments. (d)-(f): Co-expression of NET3A-mCherry with KLCR1-GFP. NET3A-mCherry is not co-localized with KLCR1-GFP. (g)-(i): NET3B-GFP expressed alone. NET3B-GFP labels both actin filaments and ER network. (j)-(l): Co-expression of NET3B-GFP with KLCR1-RFP. There is no co-localization between NET3B-GFP and KLCR1-RFP. Scale bar: 10 μm.

3.4.6. Co-localization Analysis of IQD1 with KLCR1, KLCR2 and KLCR3 *in vivo*

As described previously, KLCR1 has been identified as an IQD1 interactor from a genetic yeast two-hybrid screen of an Arabidopsis flower cDNA library and KLCR1 can be recruited to microtubules through the interaction with IQD1 in *N. benthamiana* leaf epidermal cells (Burstenbinder *et al.*, 2013). In addition, another two KLCR proteins, KLCR2 and KLCR3, also proved to interact with IQD1 in yeast two-hybrid assays (Burstenbinder Katharina, unpublished). In this section, co-localization of IQD1 with KLCR2 and KLCR3 was analyzed *in vivo* to see if IQD1 could also interact with KLCR2 and KLCR3.

Using agrobacterium-mediated transformation, KLCR1-RFP, RFP-KLCR2 and RFP-KLCR3 were expressed in *N. benthamiana* leaf epidermal cells either alone, or alongside GFP-IQD1. Their subcellular localizations were observed using the Leica SP5 CLSM.

In *N. benthamiana* leaf epidermal cells, the subcellular localizations of KLCR1-RFP, RFP-KLCR2 and RFP-KLCR3 were in cytosolic when expressed alone (Figure 3.13, a-c). However, they were recruited to the microtubules when co-expressed with GFP-IQD1, a microtubule binding protein (Figure 3.13, e-g, h-j and k-m). All three KLCR proteins were found to be co-localized with GFP-IQD1 at the microtubules. Therefore, protein IQD1 was likely to interact with KLCR proteins *in vivo*, which was similar with the previous Y2H assays (Burstenbinder Katharina, unpublished).

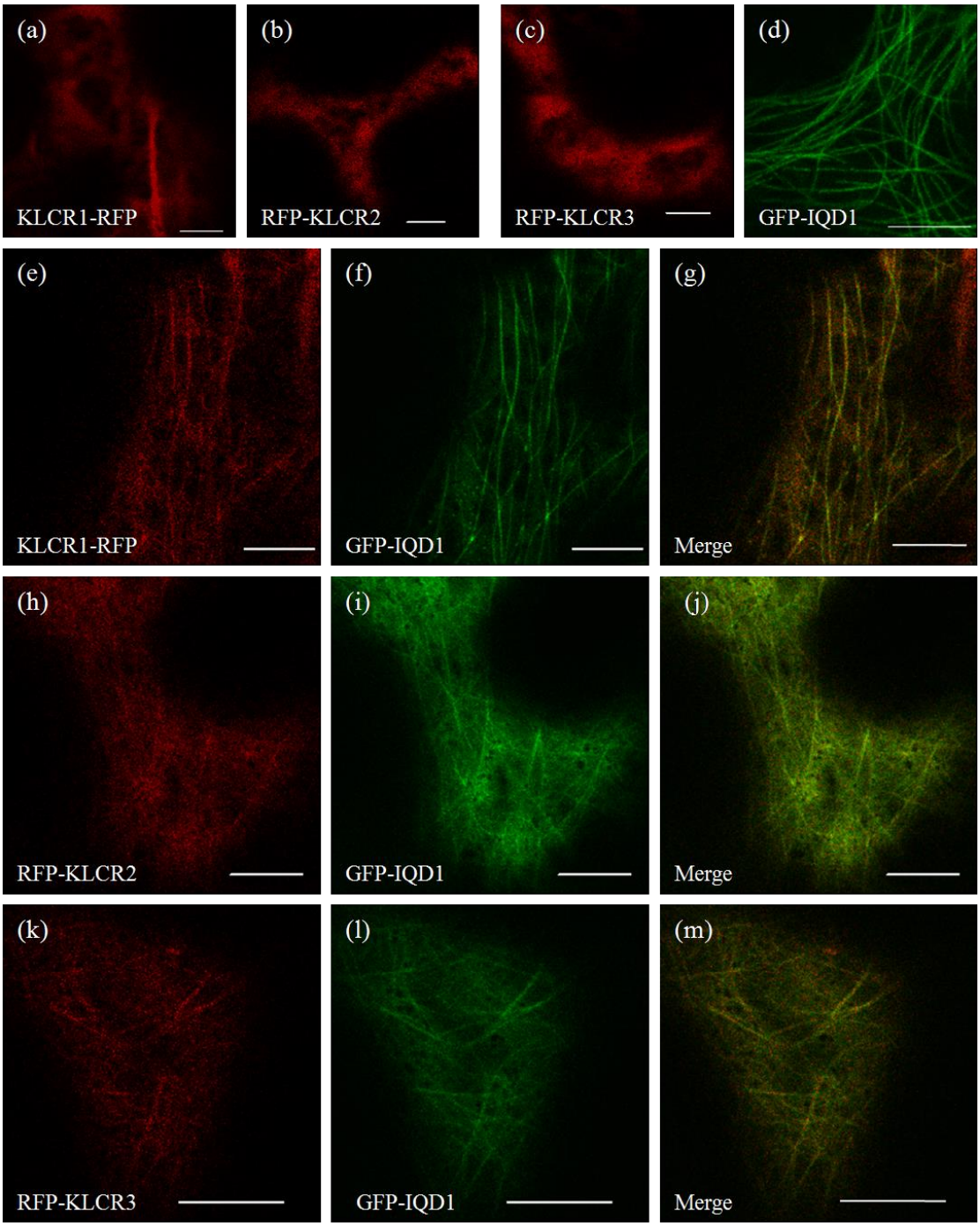

Figure 3.13 Co-localization analysis of IQD1 with KLCR proteins *in vivo*. *N. benthamiana* leaves expressing fluorescently-tagged KLCRs and IQD1. KLCR proteins need IQD1 to be recruited to the microtubules (a)-(c): KLCR proteins expressed alone. KLCR1-RFP, RFP-KLCR2 and RFP-KLCR3 are localized in cytosol. (d): GFP-IQD1 expressed alone. GFP-IQD1 labels microtubules. (e)-(g): Co-expression of KLCR1-RFP with GFP-IQD1. KLCR1-RFP and GFP-IQD1 are co-localized with each other on microtubules. (h)-(j): Co-expression of RFP-KLCR2 with GFP-IQD1. RFP-KLCR2 is recruited to microtubules by GFP-IQD1. (k)-(l): Co-expression of RFP-KLCR3 with GFP-IQD1. RFP-KLCR3 is recruited to microtubules when co-expressed with GFP-IQD1. Scale bar: 10 µm.

3.4.7 *In vivo* Interaction Analysis between NET3C and IQD Proteins

As described before, NET3C and IQD1 have been confirmed to be able to co-localize with KLCR1. It was then investigated whether NET3C may interact with IQD1 or some other members of IQD family in Arabidopsis. According to Burstenbinder et al. (2017), the IQD super family can be divided into five phylogenetic clades (Burstenbinder *et al.*, 2017). IQD1 and IQD2 from clade III, IQD12 from clade II and IQD22 and IQD25 from clade I were ether expressed alone, or co-expressed with NET3C in *N. benthamiana* leaf epidermal cells to perform the co-localization analysis. The subcellular localizations of these fusion proteins were observed using the Lecia SP5 CLSM.

The subcellular localizations of GFP-tagged IQD proteins and RFP-NET3C in *N. benthamiana* leaf epidermal cells are shown in Figure 3.14. The results are similar with the previous study (Burstenbinder *et al.*, 2017, Wang *et al.*, 2014). GFP-IQD1 and GFP-IQD2 decorate the microtubules (Figure 3.14, a and b). GFP-IQD12 and GFP-IQD22 label both microtubules and the PM (Figure 3.13, c and d). IQD25 decorates punctate structures that associated with the PM (Figure 3.14, e).

The results of the co-localization analysis are shown in Figure 3.15. It demonstrated that GFP-IQD1, GFP-IQD12 and GFP-IQD22 were found to be co-localized with RFP-NET3C at the punctate structure (Figure 3.15, a-c, g-i and j-l). In cells which expressed both GFP-IQD2 and RFP-NET3C, GFP-IQD2 induced drastic alterations in the subcellular localization of RFP-NET3C. The RFP-NET3C punctae were clearly observed to be recruited to microtubules (Figure 3.15, d-f). However, no co-localization was observed between RFP-NET3C and GFP-IQD25 Figure 3.15, m-o). These results revealed that GFP-IQD1, GFP-IQD2, GFP-IQD12 and GFP-IQD22, all of which localized to microtubules, are also likely to be associated with NET3C *in vivo*.

Next, FRET-FLIM was performed investigate whether NET3C was able to directly

interact with IQD proteins *in vivo*. In this project, we took IQD1 and IQD2 which have been confirmed to interact with KLCR proteins in a previous Y2H screen (Burstenbinder Katharina, unpublished) as examples to study. GFP-IQD1 and GFP-IQD2 were expressed alone, or co-expressed with RFP-NET3C in *N. benthamiana* leaf epidermal cells. FRET-FLIM also performed using GFP-RFP fusion protein as a positive control.

The results of the FRET-FLIM interaction assay between RFP-NET3C and GFP-IQD1 are displayed in Figure 3.16. The average fluorescence lifetime of GFP-IQD1 when expressed on its own was found to be 2.65±0.02 ns. In contrast, the average fluorescence lifetime of GFP-IQD1 in the presence of RFP-NET3C was 2.49±0.06 ns, indicating a reduction of 0.16 ns (p=6.658e-06). Therefore, an interaction between RFP-NET3C and GFP-IQD1 could be detected using the FRET-FLIM experiment. The average fluorescence lifetime of GFP-IQD2 was found to be 2.51±0.02 ns when co-expressed with RFP-NET3C, which was significantly reduced by 0.19 ns when compared to RFP-NET3C expressed alone (2.70±0.07 ns; p=2.145e-05). These results suggest a physical interaction between NET3C and IQD2. Moreover, the average fluorescence lifetime of GFP-RFP fusion protein was measured at 2.27±0.03 ns.

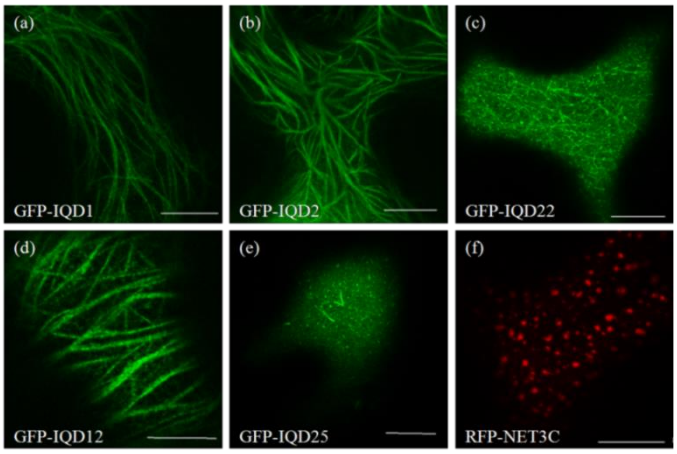

Figure 3.14 Subcellular localizations of RFP-NET3C and GFP-tagged IQD proteins in *N. benthamiana* leaf epidermal cells. (a): GFP-IQD1 localization. (b): GFP-IQD2 localization. (c): GFP-IQD22 localization. (d): GFP-IQD12 localization. (e): GFP-IQD25 localization. (f): RFP-NET3C localization. Scale bar: 10 µm.

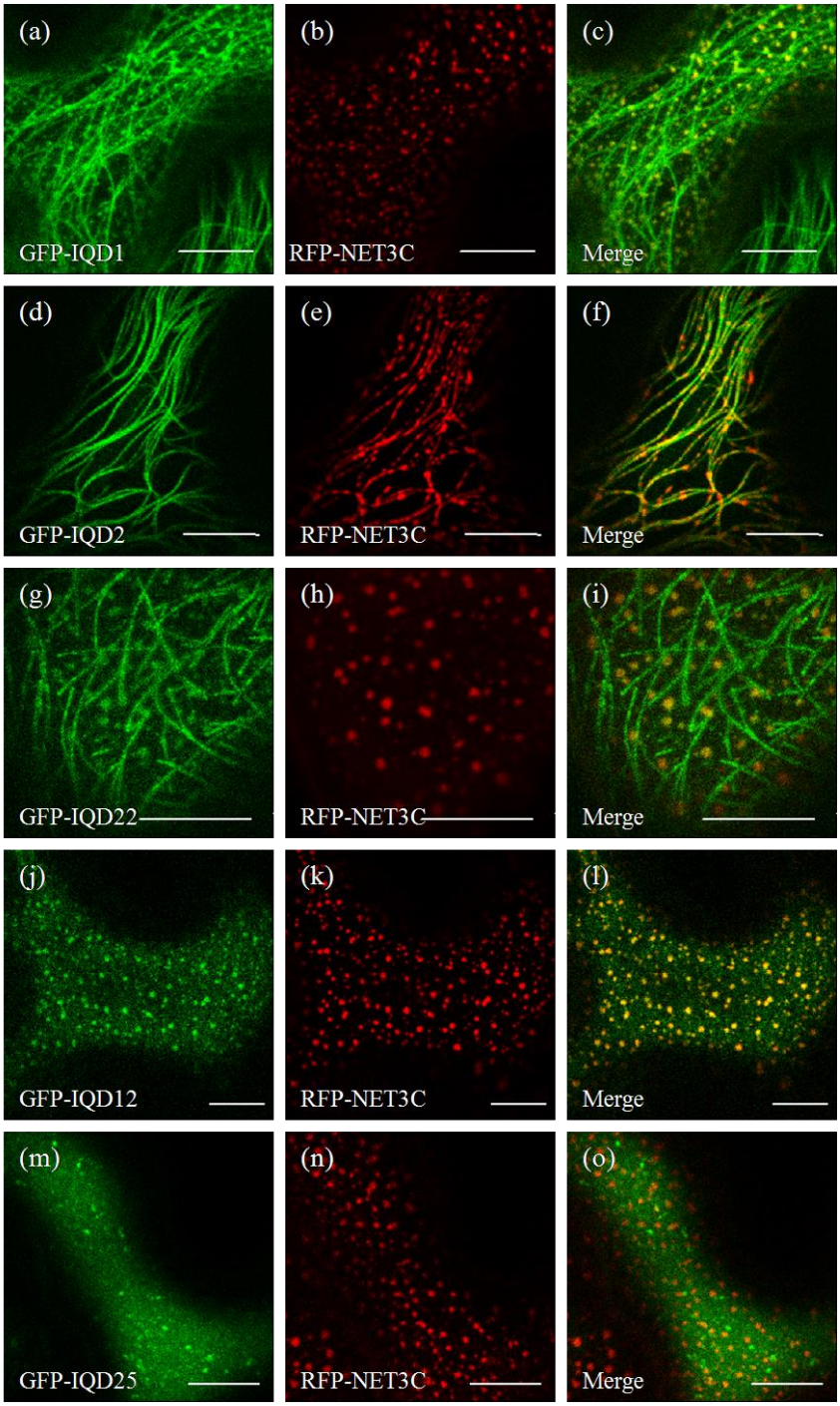

Figure 3.15 Co-localization analysis of NET3C with IQD proteins *in vivo*. *N. benthamiana* leaves were transformed with fluorescently-tagged NET3C and IQD proteins. (a)-(c): Co-expression of GFP-IQD1 with RFP-NET3C. GFP-IQD1 is co-localized with RFP-NET3C at the punctate structures. (d)-(f): Co-expression of GFP-IQD2 with RFP-NET3C. The RFP-NET3C punctae can be recruited to microtubules by GFP-IQD2. (g)-(i): Co-expression of GFP-IQD22 with RFP-NET3C. GFP-IQD22 is co-localized with RFP-NET3C at the punctate structures. (j)-(l): Co-expression of GFP-IQD12 with RFP-NET3C. GFP-IQD12 is co-localized with RFP-NET3C at the punctate structure. (m)-(n): Co-expression of GFP-IQD25 with RFP-NET3C. Scale bar: 10 μm.

A

Constructs Expressed	Mean GFP Fluorescence Lifetime	Standard Deviation	n
GFP-IQD1	2.65 ns	0.02	12
GFP-IQD1+RFP-NET3C	2.49 ns	0.06	10
GFP-IQD2	2.70 ns	0.07	10
GFP-IQD2+RFP-NET3C	2.51ns	0.02	10
GFP-RFP	2.27 ns	0.03	10

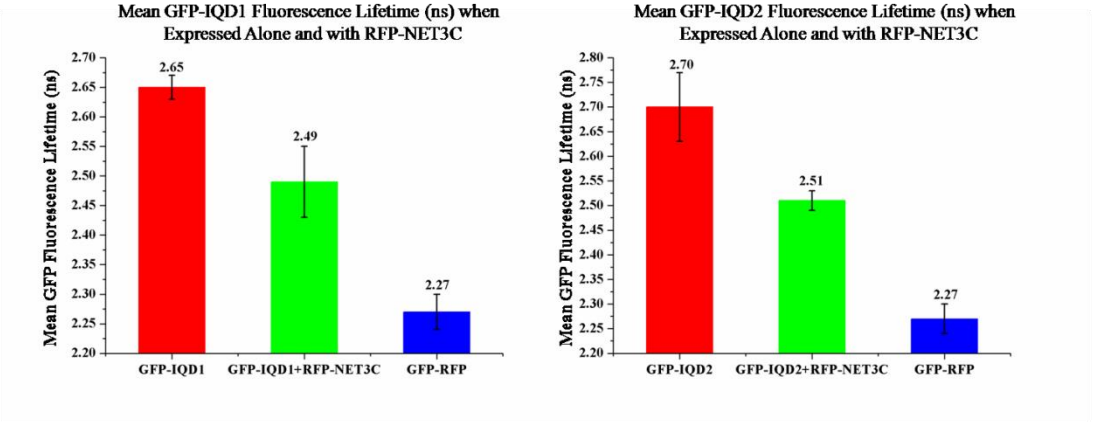

B

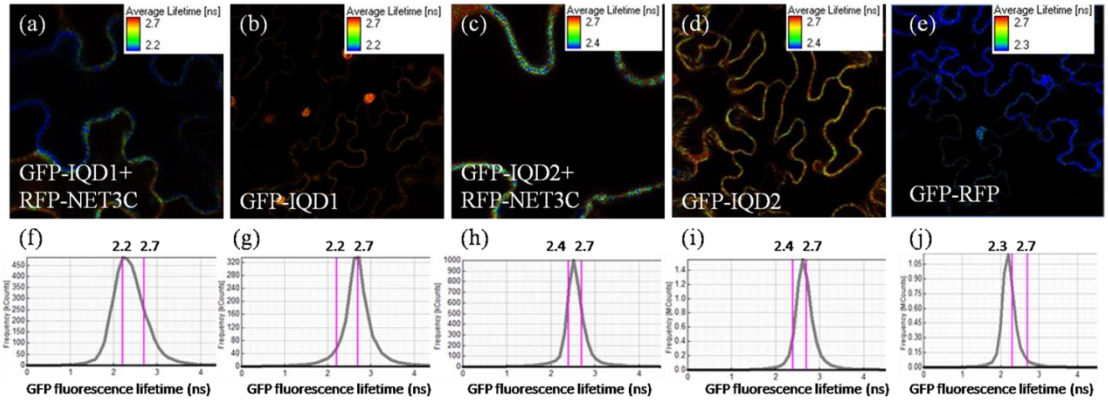

Figure 3.16 FRET-FLIM analysis of NET3C-IQD1 and NET3C-IQD2. A: Average fluorescence lifetimes of GFP-IQD1 and GFP-IQD2 significantly reduce when co-expressed with RFP-NET3C.n = number of cells analyzed. B: Visualization of GFP-IQD1and GFP-IQD2 fluorescence lifetimes in *vivo* when expressed alone or expressed with RFP-NET3C. (a)-(f): example images of GFP fluorescence detected in *N. benthamiana* leaf epidermal cells, pseudocoloured according to GFP fluorescence lifetime. (f)-(j): charts associated with images (a)-(e) respectively, show the frequency distributions of the fluorescence lifetimes (ns) of detected photons in each image. A leftward shift in peak GFP fluorescence lifetime indicates the reduction of average lifetime. (a) and (f): GFP-IQD1 co-expressed with RFP-NET3C. (b) and (g): GFP-IQD1 expressed alone. (c) and (h): GFP-IQD2 co-expressed with RFP-NET3C. (d) and (i): GFP-IQD2 expressed alone. (e) and (j): GFP-RFP positive control.

3.4.8. Co-localization Analysis of GFP-IQD1 and GFP-IQD2 with NET3A-mCherry and NET3B-RFP

Having confirmed the co-localization between NET3C and various IQD proteins, co-localization of IQD proteins with the other two members of NET3 subfamily, NET3A and NET3B was then performed. Using agrobacterium-mediated transformation, NET3A-mCherry and NET3B-RFP were co-expressed with GFP-IQD1 and GFP-IQD2 respectively in *N. benthamiana* leaf epidermal cells.

When NET3A-mCherry was co-expressed with GFP-IQD1 or GFP-IQD2, clear co-localizations were observed. NET3A-mCherry displayed the "beads on a string" arrangement and the beads were closely associated with microtubules (Figure 3.17, a-c and g-i). In cells which co-expressed NET3B-RFP with GFP-IQD1 or GFP-IQD2, NET3B-RFP was also found to be recruited to microtubules by GFP-IQD1 and GFP-IQD2 (Figure 3.17, d-f and j-l). Taken together, these results indicate that IQD proteins (at least the selected IQDs protein clade III) are likely to interact with every member of the NET3 subfamily and there may be potential functional redundancy between individual NET3 proteins.

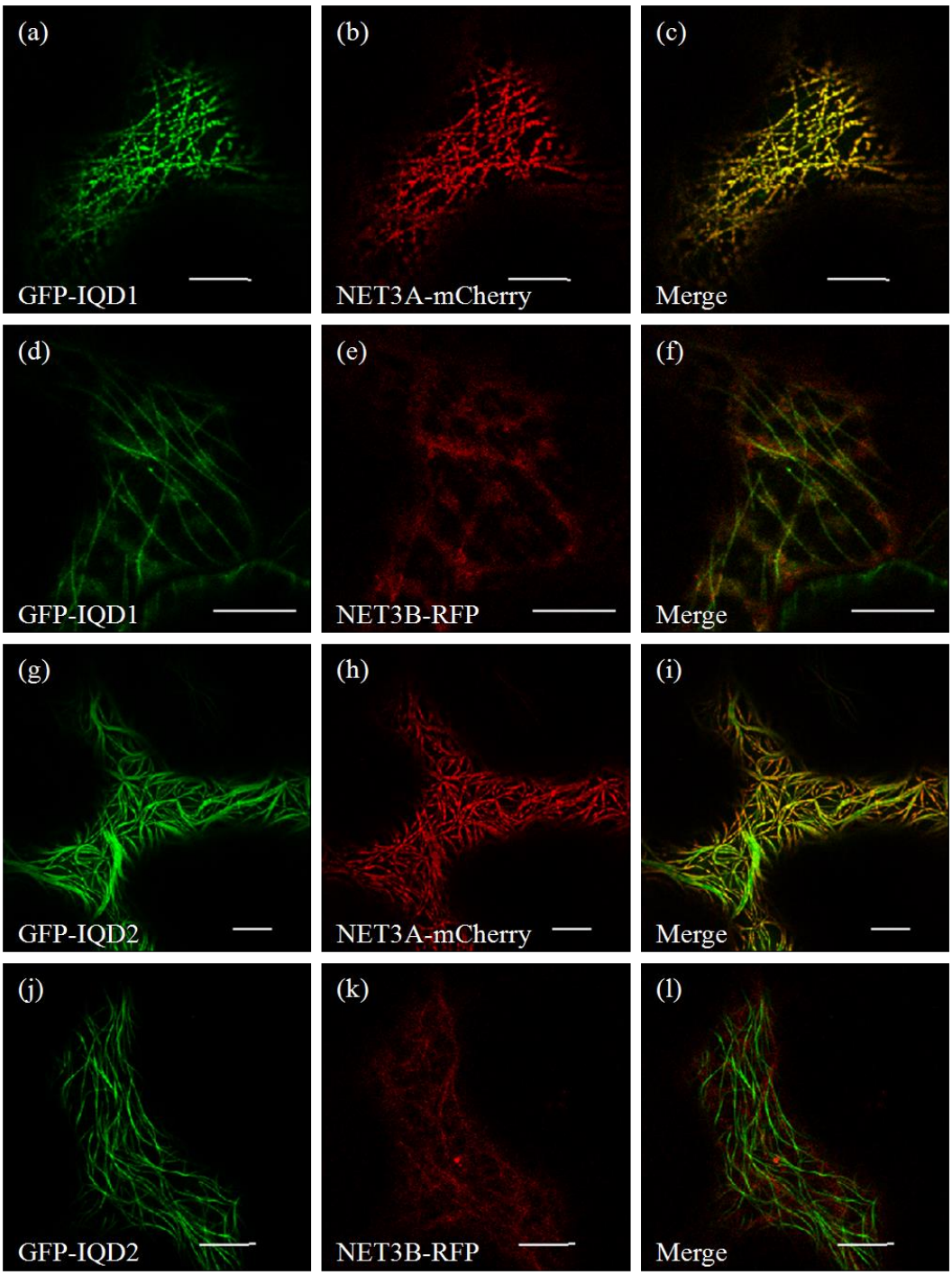

Figure 3.17 Co-localization analysis of NET3A-mCherry and NET3B-RFP with GFP-IQD1 or GFP-IQD2 *in vivo*. *N. benthamiana* leaf epidermal cells were transformed with fluorescently-tagged NET3A, NET3B and IQD proteins. (a)-(c): Co-expression of GFP-IQD1 with NET3A-mCherry. NET3A-mCherry was co-localized with GFP-IQD1 to microtubules. (d)-(f): Co-expression of GFP-IQD1 with NET3B-RFP. NET3B-RFP was recruited to microtubules by GFP-IQD1. (g)-(i): Co-expression of GFP-IQD2 with NET3B-RFP. NET3B-RFP was co-localized with GFP-IQD2 to microtubules. (j)-(l): Co-expression of GFP-IQD2 with NET3B-RFP. NET3C-RFP was recruited to microtubules by GFP-IQD2. Scale bar: 10 μm.

3.4.9. Co-localization Analysis of VAP27-1-YFP with KLCR1-GFP or GFP-IQD2

According to Wang et al. (2014), NET3C interacts with VAP27-1 at the ER-PM contact sites and as describe before, NET3C is able to physically interact with KLCR1, IQD1 and IQD2. To investigate whether KLCR1 and IQDs can form a protein complex with NET3C as well as VAP27-1 at the ER-PM contact sites, co-localization analysis ofVAP27-1 with KLCR1 or IQDs was performed in *N. benthamiana* leaf epidermal cells. Since the NET3C punctae were found to be recruited to microtubules by IQD2 (Figure 3.15, d-f), we took IQD2 as an example to investigate whether the subcellular localization of VAP27-1 can also be affected by IQD2, thereby affecting the ER morphology.

In *N. benthamiana* leaf epidermal cells, VAP27-1-YFP labeled the ER network and ER-PM contact sites when it was expressed alone (Figure 3.18, a). In cells expressing both VAP27-1-YFP and KLCR1-RFP, no co-localization between these two proteins was observed (Figure 3.18, e-g). The relationship between VAP27-1 and KLCR1 in the presence of NET3C was illustrated by the triple expression of VAP27-1-YFP, KLCR1-GFP and RFP-NET3C in cells. It demonstrates that VAP27-1-YFP and RFP-NET3C were co-localized with each other at the ER-PM contact sites, and KLCR1-GFP can also be recruited to these punctate structures (Figure 3.18, h-k), indicating that KLCR1-GFP was able to co-localize with VAP27-1-YFP in the presence of RFP-NET3C.When VAP27-1-YFP was co-expressed with GFP-IQD2 in cells, no co-localization between them was observed (Figure 3.18, l-n). However, in cells which expressed GFP-IQD2, RFP-NET3C and VAP27-1-YFP, clear co-localization between VAP27-1-YFP and GFP-IQD2 was found at the microtubules (Figure 3.18, o-r). Therefore, it is likely that the presence of NET3C may facilitate the association between IQD2 and VAP27-1. The ER morphology could be affected and this will be discussed later.

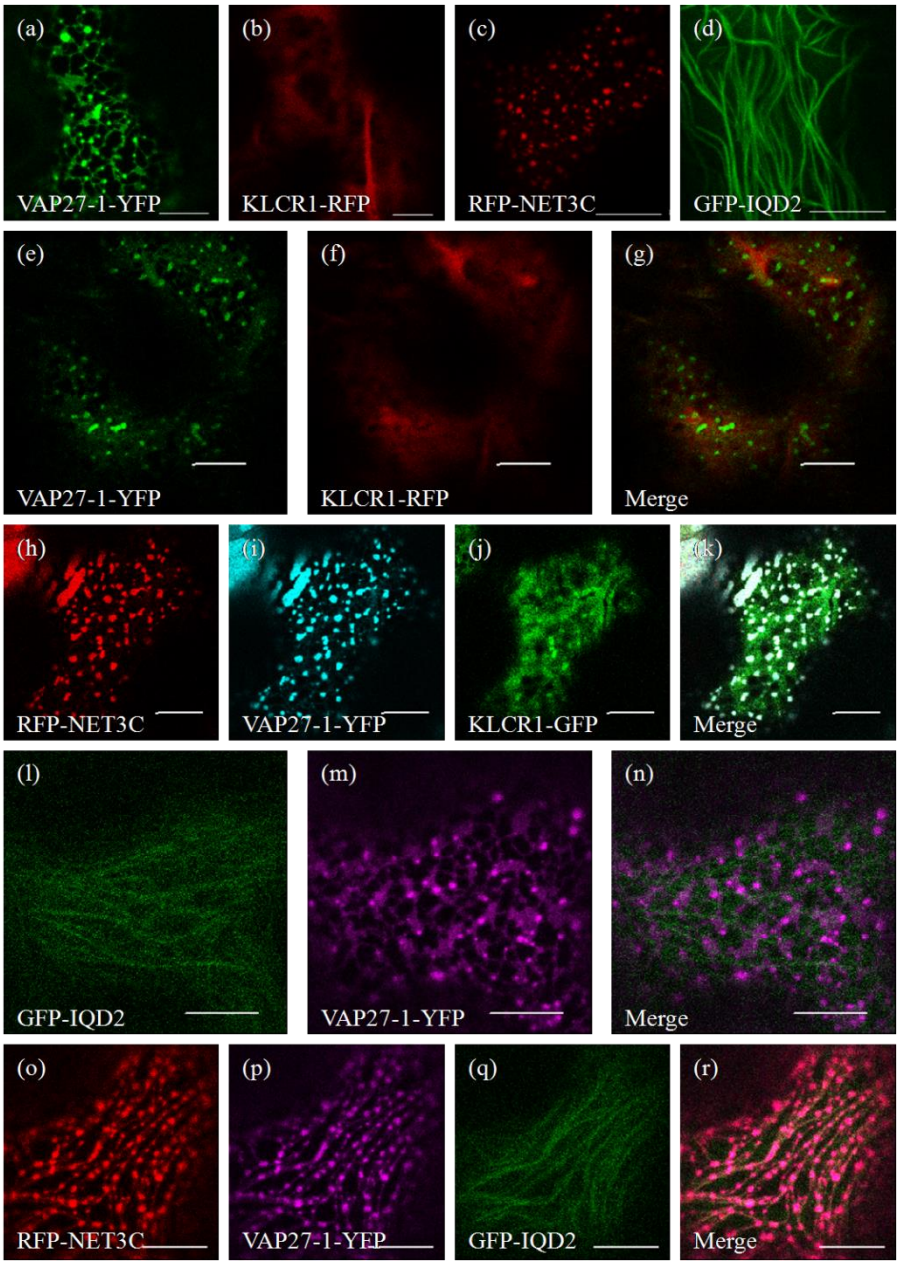

Figure 3.18 Co-localization analysis of VAP27-1-YFP with KLCR1-GFPand GFP-IQD2*in vivo.* *N. benthamiana* leaves were transformed with fluorescently-tagged VAP27-1, KLCR1, NET3C and IQD2. (a)-(d): Subcellular localizations of VAP27-1-YFP, KLCR1-RFP, RFP-NET3C and GFP-IQD2 expressed on their own. (e)-(g): co-localization of VAP27-1-YFP with KLCR1-RFP. VAP27-1-YFP is not co-localized with KLCR1-RFP. (h)-(k): co-localization of VAP27-1-YFP, KLCR1-GFP and RFP-NET3C. KLCR1 is able to be co-localized with VAP27-1 in the presence of NET3C. (l)-(n): Co-expression of GFP-IQD2 with VAP27-1-YFP. No co-localization between them was found. (o)-(r): Co-localization of GFP-IQD2, RFP-NET3C and VAP27-1-YFP. GFP-IQD2 was found to be co-localized with VAP27-1-YFP in the presence of RFP-NET3C. Scale bar: 10μm.

3.4.10. Overexpression of NET3C or IQD2 Affects the ER Morphology

It is known that VAP27-1 is localized to the ER network and interacts with NET3C at the immobile ER-PM contact sites (Wang *et al.*, 2014). Having confirmed that IQD2 is able to affect the localization of NET3C and VAP27-1, it was investigated as to whether over-expression of NET3C or IQD2 may also affect the ER morphology.

The ER marker GFP-HDEL and CFP-HDEL were co-expressed with RFP-NET3C and GFP-IQD2 respectively in *N. benthamiana* leaf epidermal cells. GFP-HDEL was also expressed alone as a control. The ER morphology analysis was performed by Charlotte Pain (Oxford Brookes University). 46 images in total were analyzed, including 17 control images, 17 images with the overexpression of RFP-NET3C and 12 images with the overexpression of GFP-IQD2.

The ER morphology in the presence of overexpressed NET3C or IQD2 was displayed in Figure 3.19 A. ANOVA analysis shows that the polygonal regions of the ER network are significantly smaller than the control in the presence of overexpressed IQD2 ($p=0.0018$). NET3C overexpression has a trend towards smaller polygonal regions, but this change is not significant ($p=0.0997$) (Figure 3.19 B). However, as shown in Figure 3.19 C, the ratio of the number of fully enclosed ER polygons to the total area of ER analyzed is significantly increased with the overexpression of NET3C ($p=9.1815e-04$). This result indicates that NET3C over expression results in an increased number of polygonal structures per area. Moreover, overexpression of IQD2 also significantly increases the mean size of ER *cisternae* ($p=0.0335$), but this effect cannot be seen after NET3C overexpression (Figure 3.18 D).

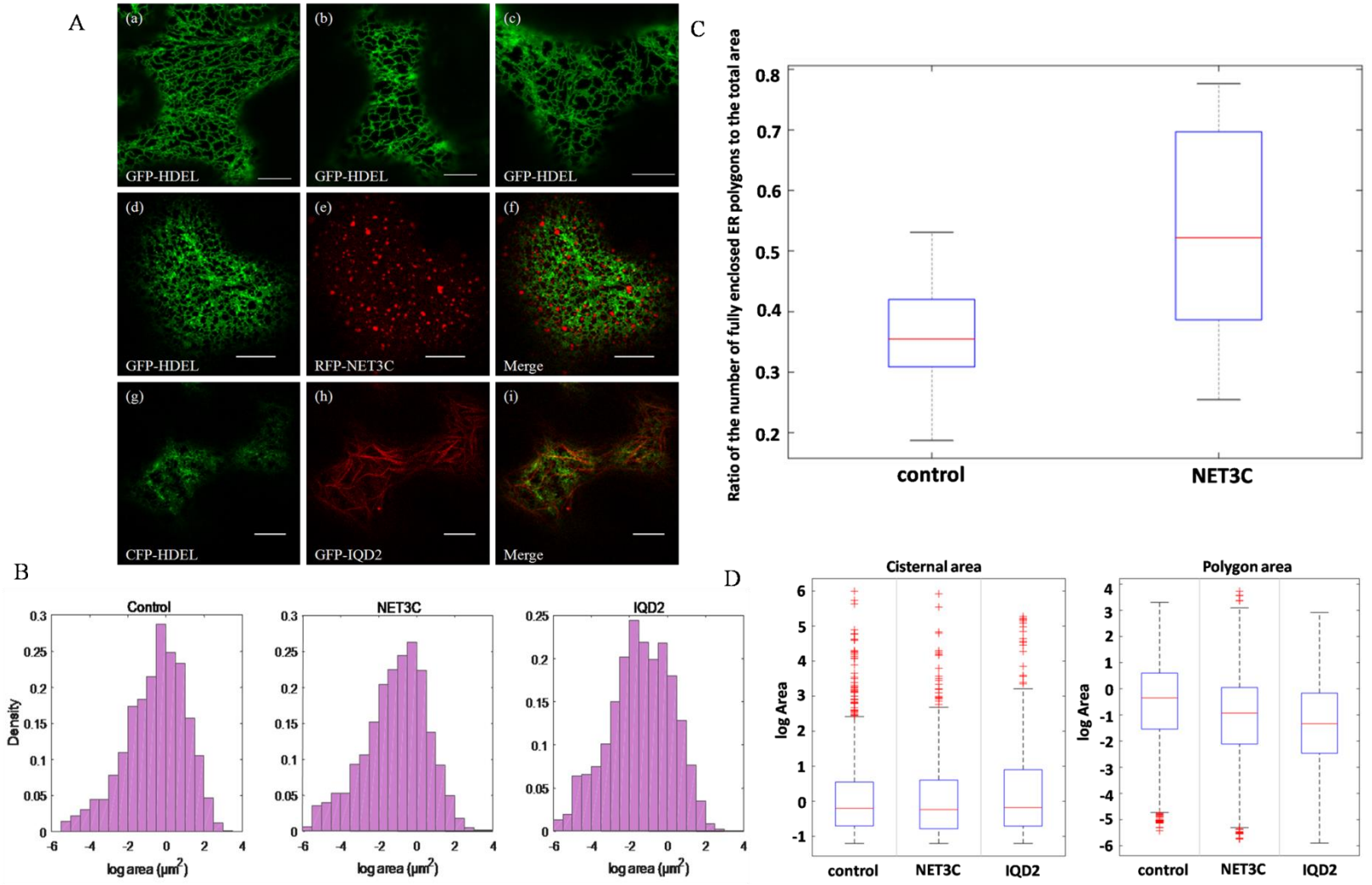
A
(a)
GFP-HDEL
(b)
GFP-HDEL
(c)
GFP-HDEL
(d)
GFP-HDEL
(e)
RFP-NET3C
(f)
Merge
(g)
CFP-HDEL
(h)
GFP-IQD2
(i)
Merge
C
Ratio of the number of fully enclosed ER polygons to the total area
control
NET3C
B
Control
NET3C
IQD2
Density
log area (μm²)
D
Cisternal area
Polygon area
log Area
control
NET3C
IQD2

Figure 3.19 ER morphology analysis with overexpression of RFP-NET3C or GFP-IQD2. A: (a)-(c): GFP-HDEL expressed alone. (d)-(f): Co-expression of GFP-HDEL with RFP-NET3C. Overexpression of NET3C increases the number of polygonal structures of the ER. (g)-(j): Co-expression of CFP-HDEL with GFP-IQD2. Overexpression of IQD2 increases the size of the ER cisternal area. B: Quantification of the size of the polygonal regions. C: Quantification of polygon numbers per area (essentially per micron). D: Quantification of cisternal area and polygonal area. Scale bar: 10μm.

3.4.11. Overexpression of Both NET3C and IQD2 Facilitates the Interaction between Actin Filaments and Microtubules

It has been reported that NET3C and IQD2 are associated with actin filaments and microtubules respectively (Burstenbinder *et al.*, 2017, Wang *et al.*, 2014). Because the localization of NET3C can be affected by IQD2 (Figure 3.15 d-f), it was investigated as to whether co-expression of NET3C and IQD2 may mediate the interaction between actin filaments and microtubules.

The actin marker (YFP-Actin-Cb) and microtubule marker (KMD-RFP) were co-expressed with both IQD2 and NET3C in *N. benthamiana* leaf tissues. YFP-Actin-Cb was also co-expressed with KMD-RFP as a negative control. As shown in Figure 3.20, GFP-IQD2 was co-localized with YFP-NET3C at KMD-RFP labeled microtubules, indicating that IQD2 was still associated with microtubules in the presence of NET3C (d-g). In cells expressing both YFP-Actin-Cb and KMD-RFP, no co-alignment between actin filaments and microtubules can be observed (a-c). However, in cells expressing both IQD2 and NET3C, YFP-Actin-Cb labeled actin filaments were clearly found to be co-aligned with IQD2 labeled microtubules (h-k). Taken together, these results suggest that overexpression of both IQD2 and NET3C facilitates the interaction between actin filaments and microtubules.

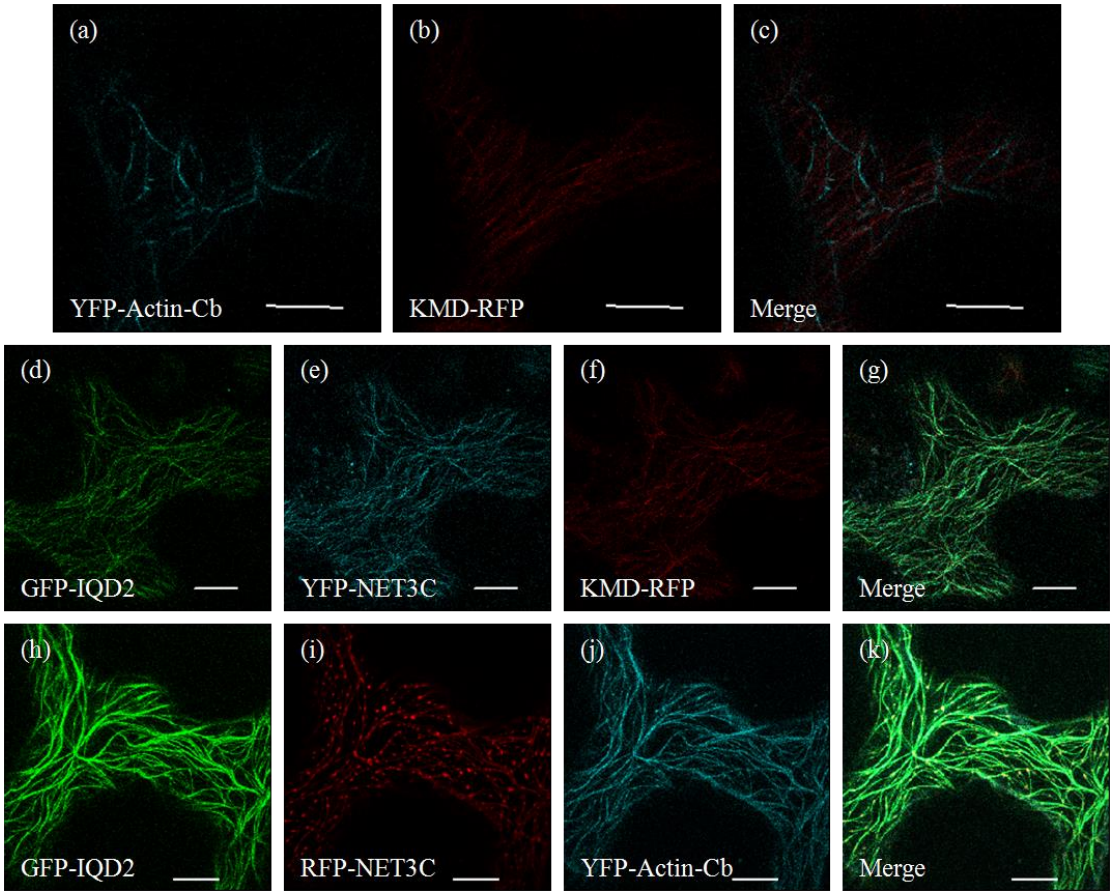

Figure 3.20 Co-expression of NET3C and IQD2 mediates the interaction between actin filaments and microtubules. (a)-(c): YFP-Actin-Cb was co-expressed with KMD-RFP. (d)-(g): Triple expression of GFP-IQD2, YFP-NET3C and KMD-RFP. IQD2 was still associated with microtubules in the presence of NET3C. (h)-(k): Triple expression of GFP-IQD2, RFP-NET3C and YFP-Actin-Cb. overexpression of both IQD2 and NET3C facilitates the interaction between actin filaments and microtubules . Scale bar: 10 µm.

3.5. *In vivo* Analysis of KLCR1 Domain Deletion Mutants

The results from the previous study have revealed that the full length KLCR1 protein can interact with NET3C and IQD2 *in vivo*. In order to demonstrate which domain of KLCR1 was responsible for the protein interaction, the N-terminal region (containing TRP1) and C-terminal region (containing TRP2) of KLCR1 fluorescence fusion proteins were generated and subsequently expressed in *N. benthamiana* leaf epidermal cells.

3.5.1. Cloning of the KLCR1 Domain Deletion Mutants

Two truncations of the KLCR1 gene were generated and subsequently fused to mCherry for transient expression in *N. benthamiana* leaves. These two domain deletion mutants were designed to cover the full length of the KLCR1 protein and were not overlapped with each other. Primers used for cloning are listed in Appendix 1.3. Schematics of the expression constructs were shown in Figure 3.21. The KLCR1ΔC-term-mCherry construct (aa 1-269) lacks the TPR region 2 and the KLCR1ΔN-term-mCherry construct (aa 270-609) lacks the TPR region 1. The different fragments were amplified using KLCR1 in the pMDC83 vector as DNA template, and were then cloned into the pDONR207 entry vector. The truncations were finally cloned into the pMDC83-mCherry expression vector using the gateway cloning system.

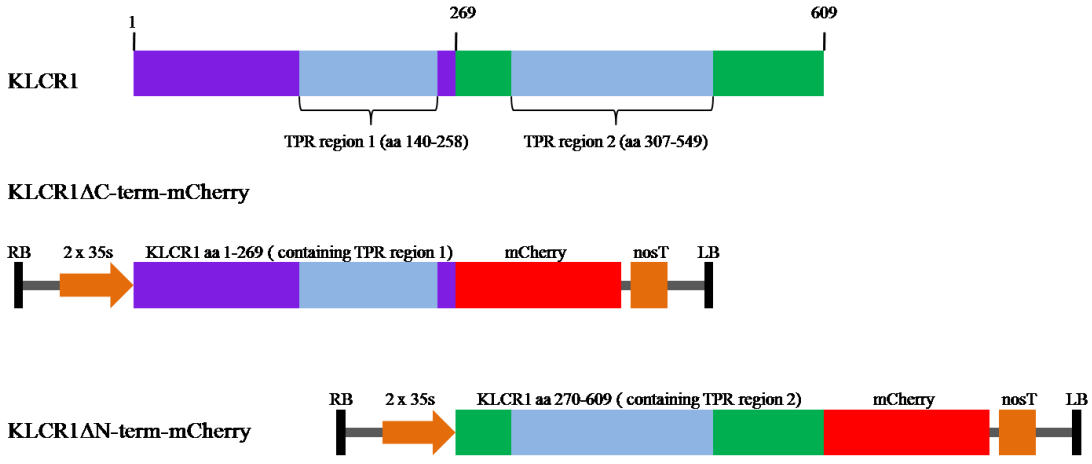

Figure 3.21: Schematics of KLCR1 domain deletion mutants. KLCR1ΔC-term-mCherry, KLCR1ΔN-term-mCherry constructs were created using the pMDC83 vector. The KLCR1ΔC-term-mCherry contains the TPR region 1 and the KLCR1ΔN-term-mCherry contains the TPR region 2.

3.5.2. Co-localization Analysis of KLCR1 Domain Mutants with NET3C or IQD2

KLCR1ΔC-mCherry and KLCR1ΔN-mCherry were expressed alone or co-expressed with GFP-NET3C and GFP-IQD2 respectively in *N. benthamiana* leaf epidermal cells.

Both KLCR1ΔC-mCherry and KLCR1ΔN-mCherry constructs showed a cytosolic localization (Figure 3.22, a and b), which was similar with the full length KLCR1. In cells co-expressing GFP-IQD2 with KLCR1ΔC-mCherry or KLCR1ΔN-mCherry, both N terminal region and C terminal region of KLCR1 can be recruited to microtubules by IQD2 (Figure 3.22, e-j), indicating that both halves of KLCR1 are capable of interacting with IQDs. In cells expressing both KLCR1ΔN-mCherry and GFP-NET3C, clear co-localization between the two proteins at the punctae was observed (Figure 3.22, n-p). However, when KLCR1ΔC-mCherry was co-expressed with GFP-NET3C, NET3C mainly localized to the cytosol and this localization appeared to be remarkably different to that observed with GFP-NET3C expressed alone (Figure 3.22, k-m). It is likely that defects of the function of KLCR1 results in the mislocalization of NET3C. Alternatively, the cytosolic localization of KLCR1 in *N. benthamiana* leaf epidermal cells is probably the result of strong overexpression and low amount of endogenous IQD proteins. In cells expressed IQDs, KLCR1ΔC-mCherry/KLCR1ΔN-mCherry and NET3C, IQDs are likely to recruit KLCR1ΔC-mCherry, KLCR1ΔN-mCherry and NET3C to microtubules. Taken together, it is possible that NET3C interacts with both the N terminal region and C terminal region of protein KLCR1. This should be confirmed using FRET-FLIM or GFP-Trap assay in the future.

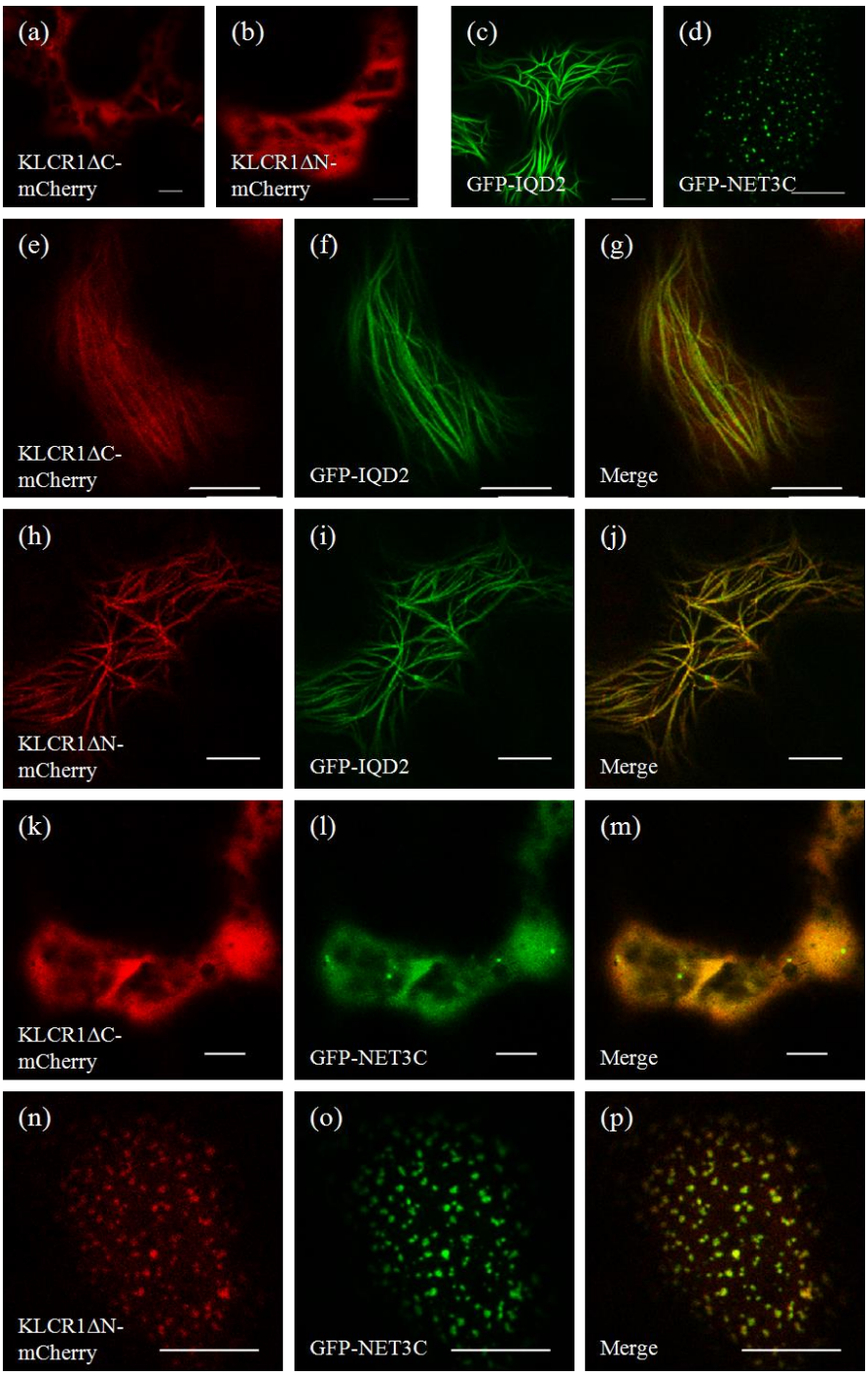

Figure 3.22 Co-expression analysis of KLCR1 domain mutants with KLCR1. (a)-(d): KLCR1ΔC-mCherry, KLCR1ΔN-mCherry, GFP-IQD2 and GFP-NET3C expressed alone. (e)-(g): Co-expression of KLCR1ΔC-mCherry with GFP-NET3C. GFP-NET3C was mainly localized to the cytosol. (h)-(j): C-localization of KLCR1ΔN-mCherry with GFP-NET3C. The C terminal region of KLCR1 was recruited to the punctate structure. (k)-(m): Co-localization of KLCR1ΔC-mCherry with GFP-IQD2. The N terminal region of KLCR1 was recruited to microtubules. (n)-(p): Co-localization of KLCR1ΔN-mCherry with GFP-IQD2. The C terminal region was co-localized with GFP-IQD2 at microtubules. Scale bar: 10 μm.

3.6. Conclusion

In this chapter, bioinformatics analysis was performed to study the gene sequence and protein structure of KLCR1, KLCR2 and KLCR3. The secondary structures of KLCR1, KLCR2 and KLCR3 showed that each protein contained two conserved TPR domains and the protein sequence of KLCR1 is highly conserved with KLCR2 or KLCR3, especially within the TPR regions. The gene expression analysis indicated that *KLCR1* was highly expressed during the whole developmental stages except for the senescence stage. *KLCR2* has a high level of expression in the seed germination and seedling stages. However, *KLCR3* expressed much lower in general throughout development. *In vivo* interaction analysis indicated that KLCR1 can form a protein complex with NET3C and IQDs at the ER-PM contact sites. The identification of novel protein complexes is highly important in understanding the mechanism of regulation of the cytoskeleton and ER structure at plant ER-PM contacts, and this could increase our current understanding of the biological function of plant ER-PM contact sites.

3.7. Discussion

3.7.1. The Association between KLCR Proteins with Microtubules May Depends Upon Other Intrinsic Arabidopsis Proteins or Expression Level

The subcellular localizations of KLCR proteins were studied using the transient *N. benthamiana* system and stable Arabidopsis transgene lines. KLCR1, KLCR2 and KLCR3 expressed under the control of 35s promoter showed cytosolic localization in *N. benthamiana* leaf epidermal cells and can be recruited to microtubules when co-expressed with protein IQD1. However, in Arabidopsis expressing *proKLCR1*:KLCR1-GFP, the protein was found to form stationary foci that co-aligned along the microtubules. In addition, KLCR2 and KLCR3 also showed microtubule

localization in Arabidopsis in a previous study (Liu *et al.*, 2016). Therefore, it is likely that the association of KLCR proteins with microtubules relies on some other factors, such as IQD proteins. Upon strong over-expression, such as 35s promoter driven expression in tobacco cells, KLCR proteins accumulate in the cytosol probably because the amount of endogenous IQD proteins (or other KLCR interacting proteins) is too low to recruit KLCR proteins onto microtubules. In fact, partial microtubule localization in *N. benthamiana* cells can be observed by reducing the expression of KLCR1 by use of the endogenous promoter (Figure 3.8, j-o). The data are very similar to the localization patterns observed for TON1 which also localize to the cytosol in tobacco cells and can be targeted to microtubules in the presence of TRM proteins. However, in Arabidopsis, TON1 was proved to be microtubule associated (Azimzadeh *et al.*, 2008, Drevensek *et al.*, 2012).

In addition, the different expression system in *N. benthamiana* and Arabidopsis may also result in the different results. Images taken in *N. benthamiana* are from cells expressing an additional p19 protein of tomato bushy stunt virus. It is a multifunctional viral protein that prevents the onset of post-transcriptional gene silencing (PTGS) in host tissue and enables high level of transient expression (Voinnet *et al.*, 2003). Therefore, the mislocalization of KLCR proteins in *N. benthamiana* leaf tissues may be because of the high expression level of p19. Additionally, in the transient expression experiments, recombinant bacterium *Agrobacterium tumefacients* with genes that have been inserted into the T-DNA region of the bacterial Ti plasmid was used (Voinnet *et al.*, 2003). The bacterium *Agrobacterium tumefacients* has its own set of effecter proteins to manipulate the infiltrated tissues, which may also lead to the different localization of KLCR proteins in *N. benthamiana* and Arabidopsis.

3.7.2. KLCR1 Forms a Protein Complex with NET3C and IQD Proteins, Possibly at the ER-PM Contact Sites

As described in a previous study, IQD proteins belong to a protein superfamily with 33 members. They can be divided into five major phylogenetic clades and most of IQD proteins are associated with microtubule arrays (Burstenbinder *et al.*, 2017). In this study, several IQD proteins from different phylogenetic clades were tested for co-localization analysis with NET3C as well as NET3A and NET3B. IQD1 and IQD2 from clade III, IQD12 from clade II and IQD22 from clade I were found to be co-localized with NET3C. It was also demonstrated that NET3A and NET3B were able to co-localize with IQD1 and IQD2. The interaction of NET3C with IQD1 and IQD2 was then confirmed using the FRET-FLIM analysis. It is surprising that the NET3C-IQDs interaction did not appear during any interaction screen performed previously, but the FRET-FLIM result was positive. It is reported that at high protein concentrations within a localized area, FRET can occur between adjacent, noninteracting fluorophores, which can give rise to false positive FRET signals (Broussard *et al.*, 2013). It is possible that close-proximity packing of NET3C and IQD proteins in a shared membrane results in FRET occurring. Therefore, some other methods should be used to confirm the interaction between NET3C and IQD proteins. In addition, a previous study demonstrated that KLCR1 interacts with various IQD proteins in the yeast-two-hybrid screen (Katharina Burstenbinder, unpublished) and co-localization and FRET-FLIM analysis of members from KLCR and NET3 family indicate the interaction between NET3C and KLCR1 is specific. It is surprising that the co-localization between KLCR2-GFP and RFP-NET3C is evident, but no interaction between them could be detected using FRET-FLIM. It is possible that KLCR2-GFP and RFP-NET3C proteins may physically interact in *N. benthamiana*, but no observable interaction was detected using FRET-FLIM. It is likely because the interaction between KLCR2 and NET3C proteins does not cause the positioning of the GFP and RFP probes within close enough for FRET to occur (Day and Davidson,

2012). Alternatively, unfavorable dipole-dipole alignment also prevent FRET occurring (Day and Davidson, 2012). The schematic diagram of interactions among IQDs, NET3s and KLCRs is shown in Figure 3.23.

It is known that the cortical ER network in plants contacts the PM at ER-PM contact sites, whose structure is maintained by the cytoskeleton as well as ER-PM contact sites resident proteins, such as VAP27-1, NET3C, SYT1 and some as yet unknown proteins (Wang *et al.*, 2014). In this study, VAP27-1 was also observed to be co-localized with KLCR1 and IQDs in the presence of NET3C. In order to investigate whether NET3C and VAP27-1 are still PM anchored in the presence of IQDs, GFP-IQD1/GFP-IQD2 was co-expressed with GFP-NET3C and VAP27-1-YFP in *N. benthamiana* leaf tissues. Because VAP27-1 can only be co-localized with IQDs in the presence of NET3C (Figure 3.18), cells that triple expressed IQD1/IQD2, NET3C and VAP27-1 were confirmed by the co-localization between IQDs and VAP27-1 (Figure 3.23, i-l and q-t). At the cell periphery, IQD1/IQD2 appeared to be co-localized with NET3C and VAP27-1 and closely attached to the PM (stained with FM4-64) (Figure 3.23, m-p and u-x). Therefore, it is likely that KLCR1 forms a protein complex with NET3C and IQD proteins at the plant ER-PM contact sites. This complex probably regulates the ER morphology and organization of the cytoskeleton, thereby regulating plant development. Since IQD proteins belong to a large protein superfamily, there may be functional redundancy between different family members.

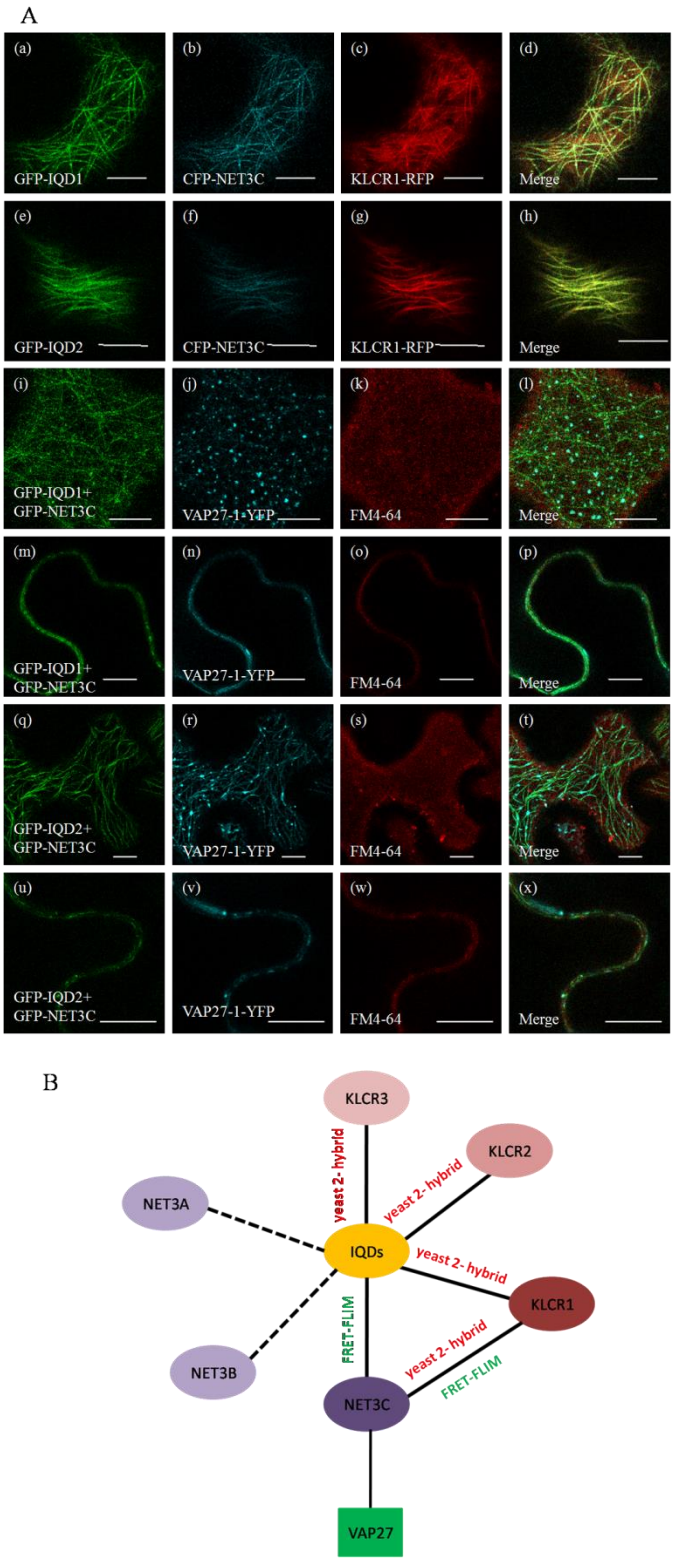

Figure 3.23 Schematic Diagram of interactions within IQDs, NET3s and KLCRs. A. KLCR1, NET3C and IQDs from a protein complex at the ER-PM contact sites. B. Black solid lines indicate physical interactions which were confirmed using FRET-FLIM (marked green) or yeast-two-hybrid (marked red). Dotted lines indicate a co-localization between two proteins whose interactions need to be further confirmed. Scale bar: 10 μm.

3.7.3. NET3C-KLCR1-IQDs Protein Complex is Likely to Mediate the Interaction between Actin Filaments and Microtubules

In eukaryote cells, the possible cross-talk between actin filaments and microtubules has been observed from light and electron microscopy studies (Collings, 2008, Mineyuki, 1999). Although numbers of studies have investigated the actin and microtubule cytoskeletons perform fundamental cellular functions in plant cells, little is known about how they work together to regulate a specific subcellular activity (Collings, 2008). Various candidate proteins have been identified to mediate the interaction between actin filaments and microtubules in plant cells, such as microtubule-binding kinesins, actin regulator formins and actin related protein-2/3 (ARP2/3) (Collings, 2008, Deeks *et al.*, 2010, Frey *et al.*, 2009, Havelkova *et al.*, 2015, Preuss *et al.*, 2004a, Rosero *et al.*, 2013, Saedler *et al.*, 2004, Xu *et al.*, 2009).

In this study, Co-alignment between actin filament and microtubules can be observed in cells which overexpress both NET3C and IQD2 (Figure 3.20). NET3C was localized to microtubules and associated with actin filaments (Wang *et al.*, 2014). KLCR1 and IQDs were demonstrated to be localized to microtubules. Therefore, a new molecular mechanism for actin-microtubule interaction mediated by the NET3C-KLCR1-IQDs complex was identified. When the expression of NET3C and IQDs is low in the native condition, NET3C is likely to be localized to the actin filaments with some co-occurrence at the cross-points between microtubules and microfilaments (Figure 3.24 A). When both NET3C and IQDs are overexpressed, more actin-microtubule co-alignments are induced, thereby enhancing their association (Figure 3.24 B).

It has been reported that disruption of microtubules results in hypersensitivity of cortical actin filaments to depolymerizing drugs treatment; whereas stabilization of microtubules enhances their association with actin filaments, indicating that the stability of actin filaments is dependent on cortical microtubules (Collings, 2008).

Based on observations of IQD1 and IQD2 in *N. benthamiana* leaf epidermal cells, it is likely that IQD1 and IQD2 have the ability to stabilize microtubules because IQD1 and IQD2 labeled microtubules appeared to be highly stable. Growth and shrinkage of microtubules could be seldom observed using the time-lapse imaging. The stabilization of microtubules induced by another IQD protein, IQD5, has been also reported recently (Liang *et al.*, 2018). Therefore, KLCR1 could also indirectly stabilize microfilaments and recruit them to microtubules by forming a protein complex with IQD proteins and NET3C.

It is also known that the nucleation of the actin filaments can occur at microtubule sites in Arabidopsis cells, and the polymerization of microtubules is also dependent on the actin cytoskeleton. Upon external stimuli, such as light exposure, the organization of microtubules is affected, thereby inducing changes in actin distribution (Sampathkumar *et al.*, 2011). Therefore, the NET3C-KLCR1-IQDs complex may regulate the re-organization of actin filaments by serving as a physical linker to microtubules. In addition, the emerging actin filaments may bind to microtubule filaments via this protein complex and travel along microtubules during assembly at the PM.

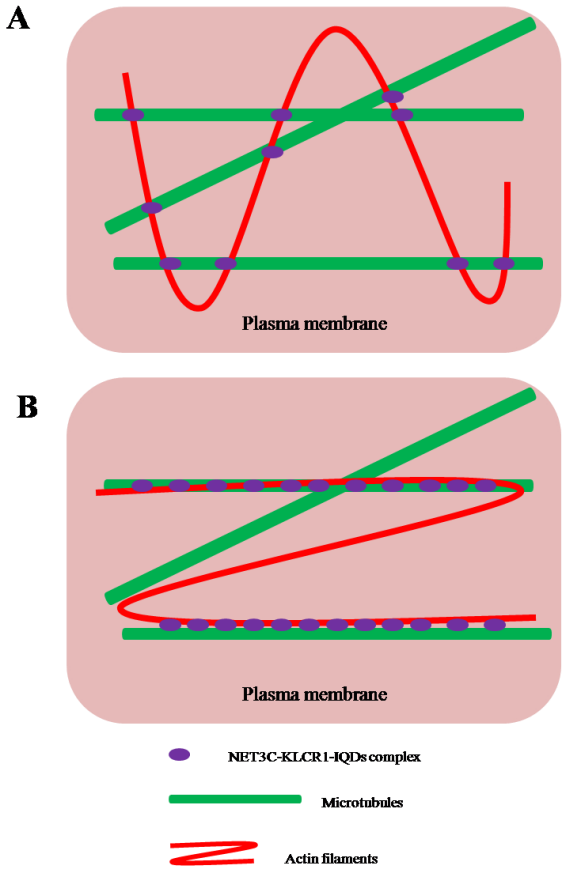

Figure 3.24 Possible model for NET3C-KLCR1-IQDs complex mediating the interaction between Actin filaments and microtubules. A. In the native condition, NET3C-KLCR1-IQDs complex is localized to cross-points of actin-microtubules. B. The association between actin filaments and microtubules was enhanced when NET3C and IQDs were highly expressed.

3.7.4. The NET3C-KLCR1-IQDs Protein Complex is Likely to Mediate the Connection between Microtubules and the ER Network, and Regulate the ER Structure

The ER morphology in the presence of overexpressed NET3C or IQD2 was analyzed in this study. Overexpression of NET3C induces more polygonal structures and a larger cisternal area was produced when IQD2 was over-expressed.

It is known that the ER network has stable contact sites which are associated with other cellular structures, such as the PM or cytoskeletal system. When an elongating ER tubule reaches an association point, a stable ER anchor is formed. New tubules

then grow outwards at these anchor sites. Hence, increasing the number of ER anchoring points produces fine ER meshwork with enclosed polygonal structures (Hamada *et al.*, 2014). Therefore, it could be hypothesized that NET3C overexpression results in the generation of additional ER-PM contact sites, thereby increasing the number of ER polygons (Figure 3.25).

The polygonal network of ER is composed of tubules and cisternal structures. The morphology of the ER network changes dynamically by the growth and shrinkage of tubules, cisternae expansion as well as lateral sliding of junctions (Griffing *et al.*, 2014). Lat B (a well-characterized G-actin agonist known to interfere with actin polymerization) treatment results in an increase in the number of persistent cisternae (Sparkes *et al.*, 2009). Therefore, it could be predicted that affecting the dynamics of actin filaments results in more cisternalization. As hypothesized above, overexpression of IQD2 may stabilize microtubules and indirectly stabilize actin filaments. Therefore, it is likely that the dynamics of actin filaments could be affected in cells overexpressed with IQD2, resulting in inhibition of ER dynamics and causing more cisternalization. In addition, the ER tubules can also grow along microtubules in plant cells and the elongation of ER tubules can be observed in both directions of microtubule polarity (Hamada *et al.*, 2014). Overexpression of IQD2 affects the dynamics of microtubules, thereby inhibiting the extension of ER tubules and leading to more surface area.

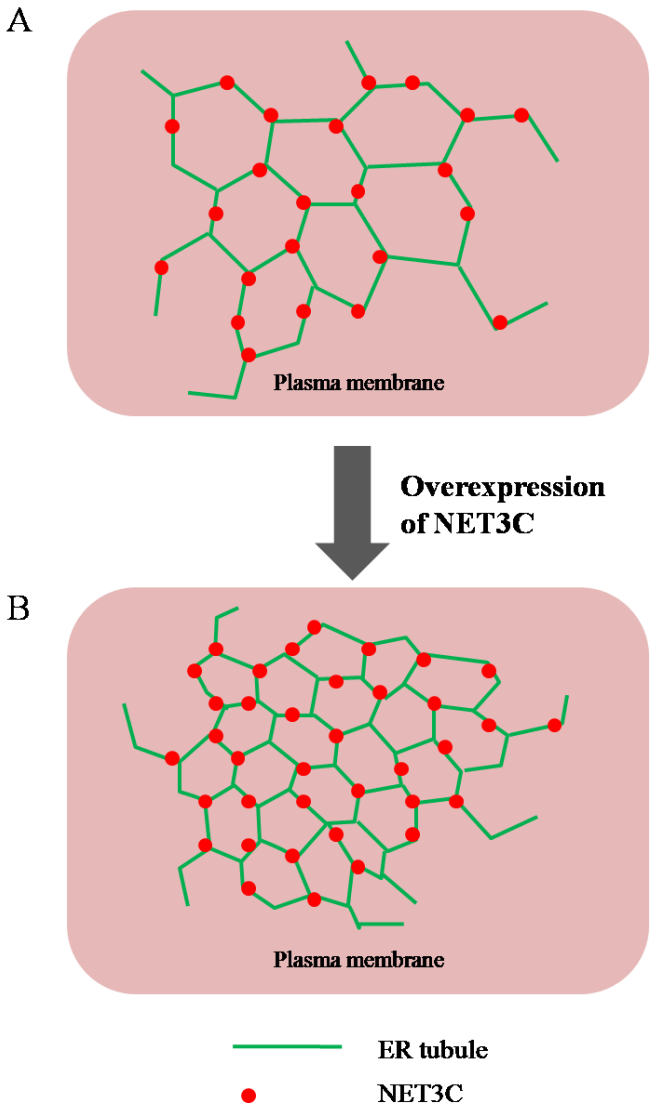

Figure 3.25 Schematic of NET3C on the cortical ER network. A. In the native condition, the expression level of NET3C is low and the ER meshwork appears to be normal. B. More ER polygonal rings are induced by overexpression of NET3C.

Interestingly, in cells overexpressing both NET3C and IQD2, ER membranes and microtubules are bundled (Figure 3.26). This rearrangement of the ER network along microtubules is likely due to an increased number of anchoring sites between the ER and microtubules. Overexpression of CLIMP-63, an ER-microtubule linker in animal cells was able to induce similar ER phenotypes (Vedrenne and Hauri, 2006). Therefore, it could be predicted that the NET3C-KLCR1-IQDs complex at the ER-PM contact sites may also function in ER-microtubule interaction in plant cells and as discussed above, the association between the ER network and microtubules

plays an important role in ER tubule growth. As hypothesized above, the NET3C-KLCR1-IQDs complex also could mediate the anchoring between actin filaments and microtubules. A novel ER-Actin-Microtubule contact sites is determined in this study and functions in the regulation of ER network and cytoskeleton.

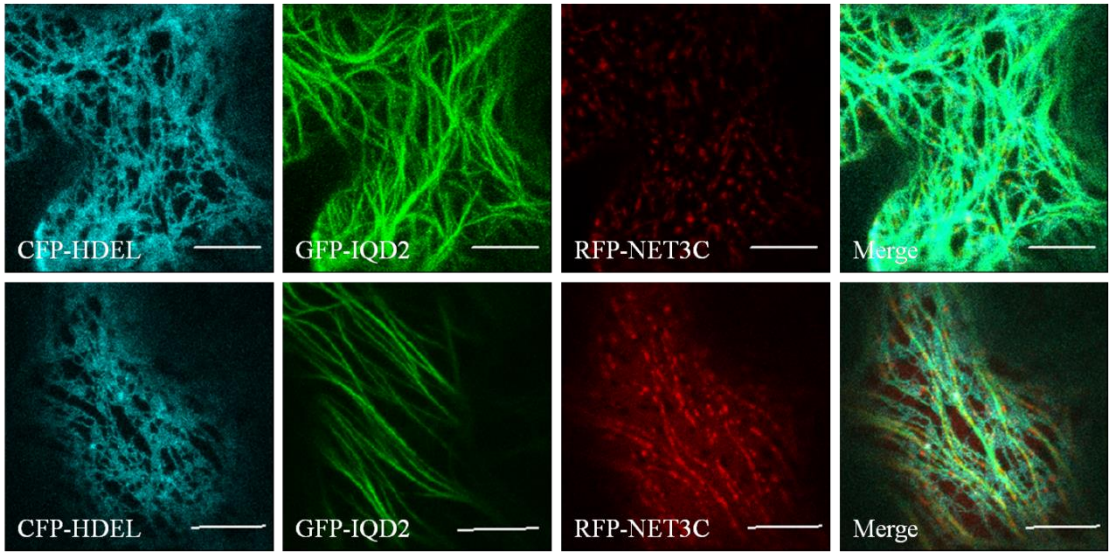

Figure 3.26 KLCR1, NET3C and IQD2 from a protein complex and facilitate the association between ER network and microtubules. *N. benthamiana* leaves were transformed with various fluorescence tagged proteins. Overexpression of both IQD2 and NET3C induces rearrangement of ER network along microtubules. Scale bar: 10 μm.

Chapter 4: Functional Analysis of Arabidopsis KLCR Proteins using Reverse Genetic Analysis

4.1. Introduction

The results from Chapter 3 have revealed the expression patterns, subcellular localization and interacting partners of KLCR proteins. In this chapter, reverse-genetic analysis of KLCR1 and KLCR2 was employed to elucidate their potential functions in Arabidopsis. Disrupting the expression of a specific gene and subsequently identifying the phenotypic effects arising from the mutants can help to investigate the possible role of this gene in specific cellular processes.

According to previous studies, overexpression of some IQD proteins such as IQD11, IQD14, IQD16 and IQD25 causes defects in Arabidopsis cotyledon epidermal cells. Loss of function of IQD5 results in reduced interdigitation of neighboring cells in the leaf epidermis. Histochemical analysis of cell wall composition of *iqd5* mutants further suggests reduced rates of cellulose deposition in anticlinal cell walls (Burstenbinder *et al.*, 2017, Liang *et al.*, 2018). Since KLCR1 is a microtubule-binding protein and it has been proved to be an interactor of many members from the IQD super-family in the Y2H assay (Katharina Unpublished), it may also participate in the development of leaf epidermal cells.

In this section, *klcr1* and *klcr2* T-DNA mutant lines were identified and validated. As there could be potential functional redundancy between KLCR proteins, *klcr1klcr2* double mutants were also generated through crossing.

4.2. Analysis of *klcr* Mutant Lines

4.2.1. An Introduction of T-DNA Insertion Lines

Insertional muatgenesis which is based on the insertion of foreign DNA into the gene of interest is a commonly used method to disrupt gene function. In Arabidopsis, this involves the use of either transposable elements or T-DNA.

T-DNA mutagenesis involves the insertion of transfer DNA (T-DNA) of 5 to 25 kb in length at random sites into plant genomic DNA through *Agrobacterium tumefaciens*-mediated transformation to generate an Arabidopsis T-DNA library(Krysan *et al.*, 1999). The Salk Institute Genomic Analysis Laboratory (SIGnAL) has created library of independent insertion events of T-DNA in the genome of Arabidopsis. More than 88,000 T-DNA insertions were generated and these insertions resulted in the mutation of 21,700 genes (Alonso *et al.*, 2003). A rich resource of SALK lines and other T-DNA insertion lines such as the Syngenta Arabidopsis Insertion Library (SAIL) lines and GABI-Kat lines are publicly available and can be obtained from the Nottingham Arabidopsis Stock Center (NASC).PCR genotyping is normally used to screen for individual plants that carry a particular T-DNA mutation of interest (Krysan *et al.*, 1999).

In this section, *klcr1* and *klcr2* T-DNA insertion mutant lines ordered from NASC were identified and their subsequent phenotypes were analyzed.

4.2.2. Analysis of the klcr1 and klcr2 T-DNA Insertion Lines

The SiGnAL T-DNA Express Arabidopsis Gene Mapping Tool (http://signal.salk.edu/) was used to identify T-DNA insertion positions in *KLCR1* and *KLCR2*. Only one T-DNA insertion line was identified for *KLCR1* (SAIL_335_B08), and three insertions were available for *KLCR2* (SALK_027301, SALK_148296 and GABI_456B06). The position of T-DNA insertions within the coding region may have

dramatic differences in disrupting gene expression. T-DNA insertions within the exons are likely to be effective in knocking out the target genes. However, T-DNA insertions that are located in introns could be removed during splicing and insertions within the promoter regions are likely to change the gene expression level instead of knocking out the gene expression (Wang, 2008). The T-DNA insertion site of *KLCR1* was predicted to be in the second intron and the three *KLCR2* T-DNA insertions were predicted to be located at 300 bp upstream of start codon, the first exon and the second exon respectively. Schematic maps of selected T-DNA alleles are shown in Figure 4.1.

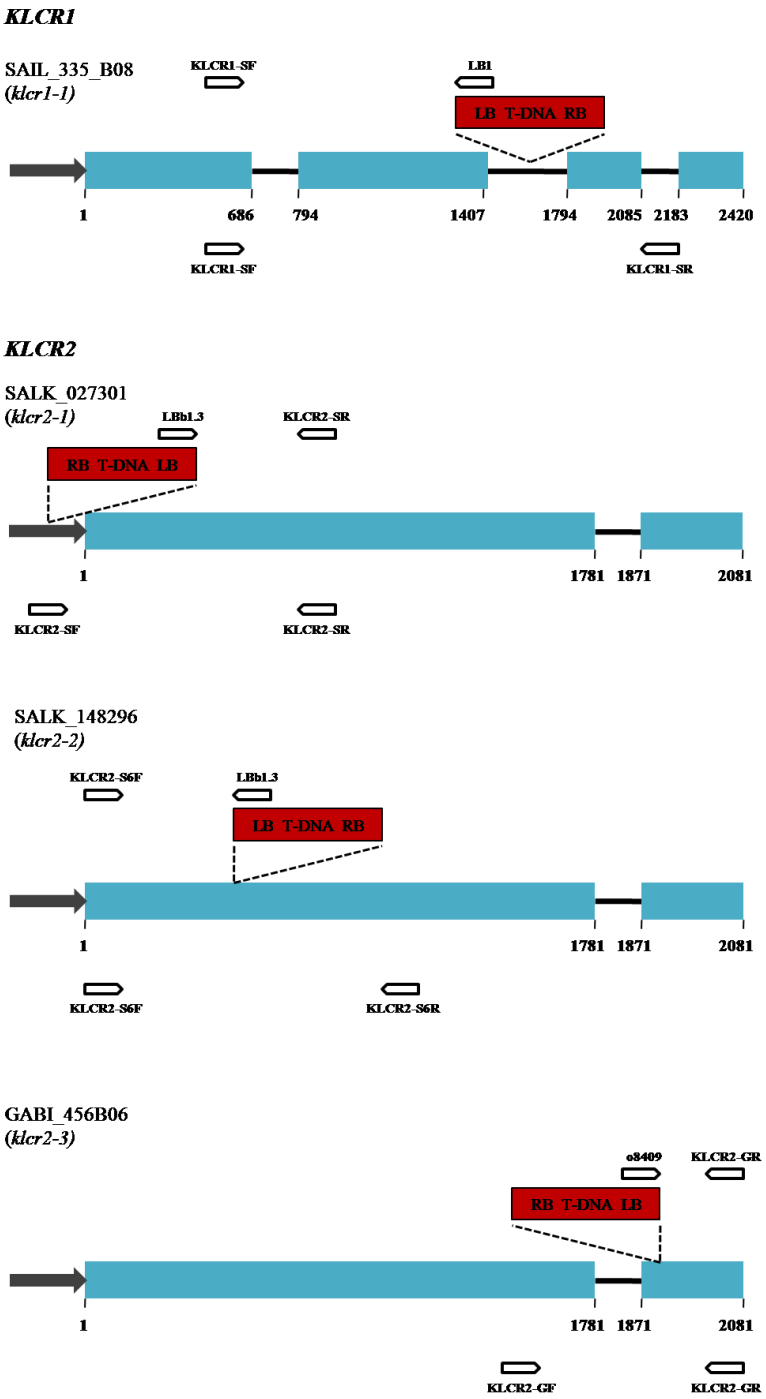

Figure 4.1 Predicted positions of the selected T-DNA insertion lines and the primers used for genotyping. Promoter regions are depicted in grey arrows. Exons are shown in blue and introns in black. The T-DNA insertions are represented by the red box and labeled with the left border (LB) and right border (RB). Primers used for genotyping are shown by the white arrows. Gene-specific primers below the gene were used to detect the wild-type allele and the insert-specific primers above the gene were used to detect the mutant allele.

4.2.3. Identification of the Homozygous *klcr1* and *klcr2* T-DNA Insertion Mutants

In order to identify the homozygous T-DNA mutant lines, two sets of PCR were performed using the genomic DNA extracted from mutant plants. The first PCR reaction (insert PCR) amplified a PCR fragment using the gene-specific primer and the T-DNA left border-specific primer. After agarose gel electrophoresis, the "insert band" of the predicted size can be detected if the T-DNA was present in the gene. The second PCR reaction (wild-type PCR) was performed to amplify a band using gene-specific primers. These primers were designed at either side of the T-DNA insertion site and the wild type band can only be observed if a plant carries the wild type allele of a gene of interest. The primers used for the insert PCR and wild type PCR were listed in Table 4.1.

Line	Predicted insertion site	Primers for WT PCR	WT PCR size (bp)	Primers for insert PCR	Insert PCR size (≈ bp)
KLCR1					
SAIL_335_B08	Intron 1	KLCR1-SF+ KLCR1-SR	1500	LB1+ KLCR1-SF	1100
KLCR2					
SALK_027301	300-UTR 5	KLCR2-SF+ KLCR2-SR	1340	LBb1.3+ KLCR2-SR	1000
SALK_148296	Exon 1	KLCR2-S6F+ KLCR2-S6R	1008	LBb1.3+ KLCR2-S6F	800
GABI_456B06	Exon 2	KLCR2-GF+ KLCR2-GR	1001	o8409+ KLCR2-GR	300

Table 4.1 Details of T-DNA insertion lines for *KLCR1* and *KLCR2*. Shown here are the insertion positions of each mutant line, the primers used for genotyping PCR and the predicted size of the PCR fragments.

Wild type plants would produce a band in the wild type PCR but not in the insert PCR. Both "insert band" and "wild type band" can be amplified from genomic DNA of heterozygous plants, whereas only "insert band" can be produced from genomic DNA of homozygous plants. Examples of insert PCR and wild type PCR reactions

performed on homozygotes of each T-DNA mutant line are shown in Figure 4.2.

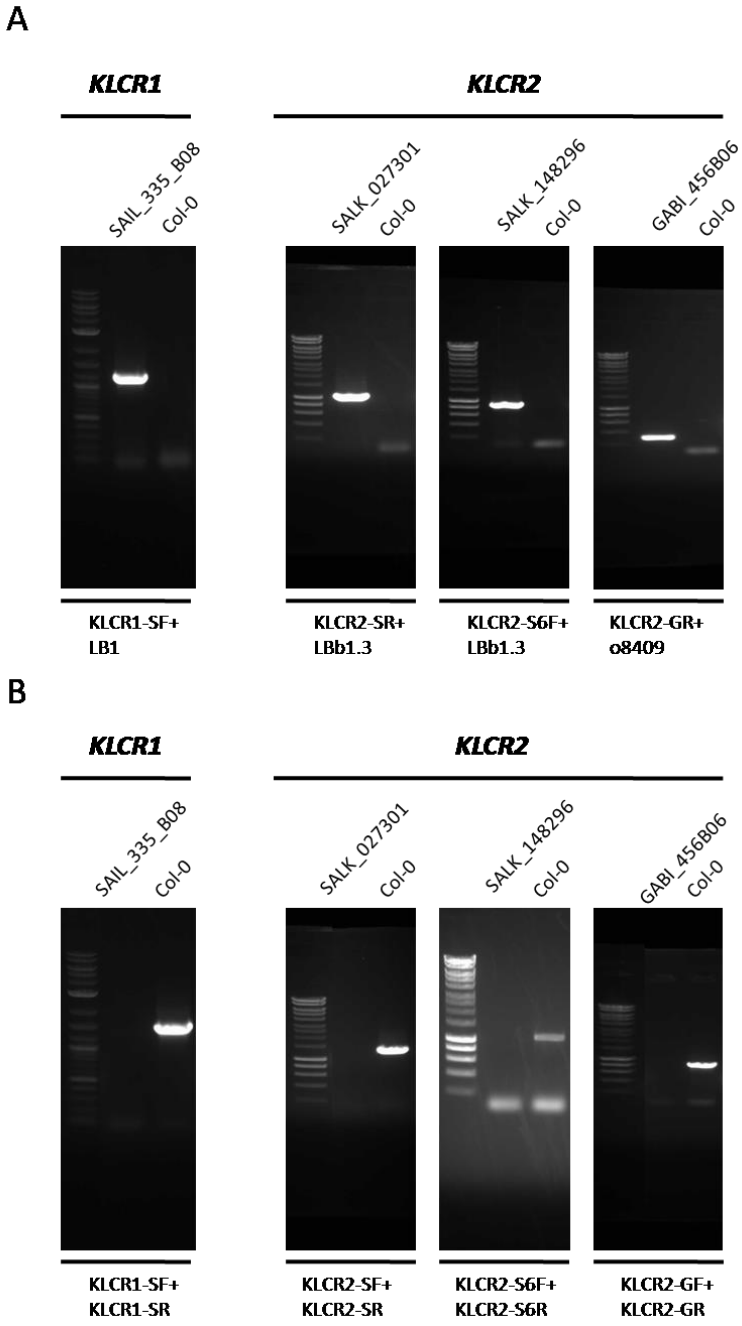

Figure 4.2 Examples of the PCR reactions used to genotype the T-DNA insertion mutants. A. Insert PCR reactions used to genotype *klcr1* and *klcr2* T-DNA insertion mutants. The insert-specific primers are shown below the gel. 2-Log DNA ladder or Hyperladder I was used as a molecular weight marker. B. Wild type PCR reactions used to genotype *klcr1* and *klcr2* T-DNA insertion mutants. The gene specific primers are shown below the gel. 2-Log DNA ladder or Hyperladder I was used as a molecular weight marker.

4.2.4. The Confirmation of the Disruption of the *KLCR1* and *KLCR2* Transcripts Using RT-PCR

Having confirmed that each of the selected T-DNA mutant lines were homozygous lines, RT-PCR was then performed to assess whether the transcripts of *KLCR1* and *KLCR2* were abolished.

RNA was extracted from 10-day old mutant and wild type Arabidopsis seedlings and used to generate template cDNA as described in chapter 2.2.7 and 2.2.8. Various different primer combinations shown in Table 4.2 and Figure 4.3 were used to amplify the coding sequence of each gene as well as fragments upstream and downstream of the T-DNA insertion sites. In these RT-PCR reactions, cDNA template from Col-0 was used as a positive control. As a negative control, deionised water was used instead. The housekeeping gene that is expressed at specific level, Actin, was used as an internal control to ensure the amount of the cDNA template used for each reaction was identical.

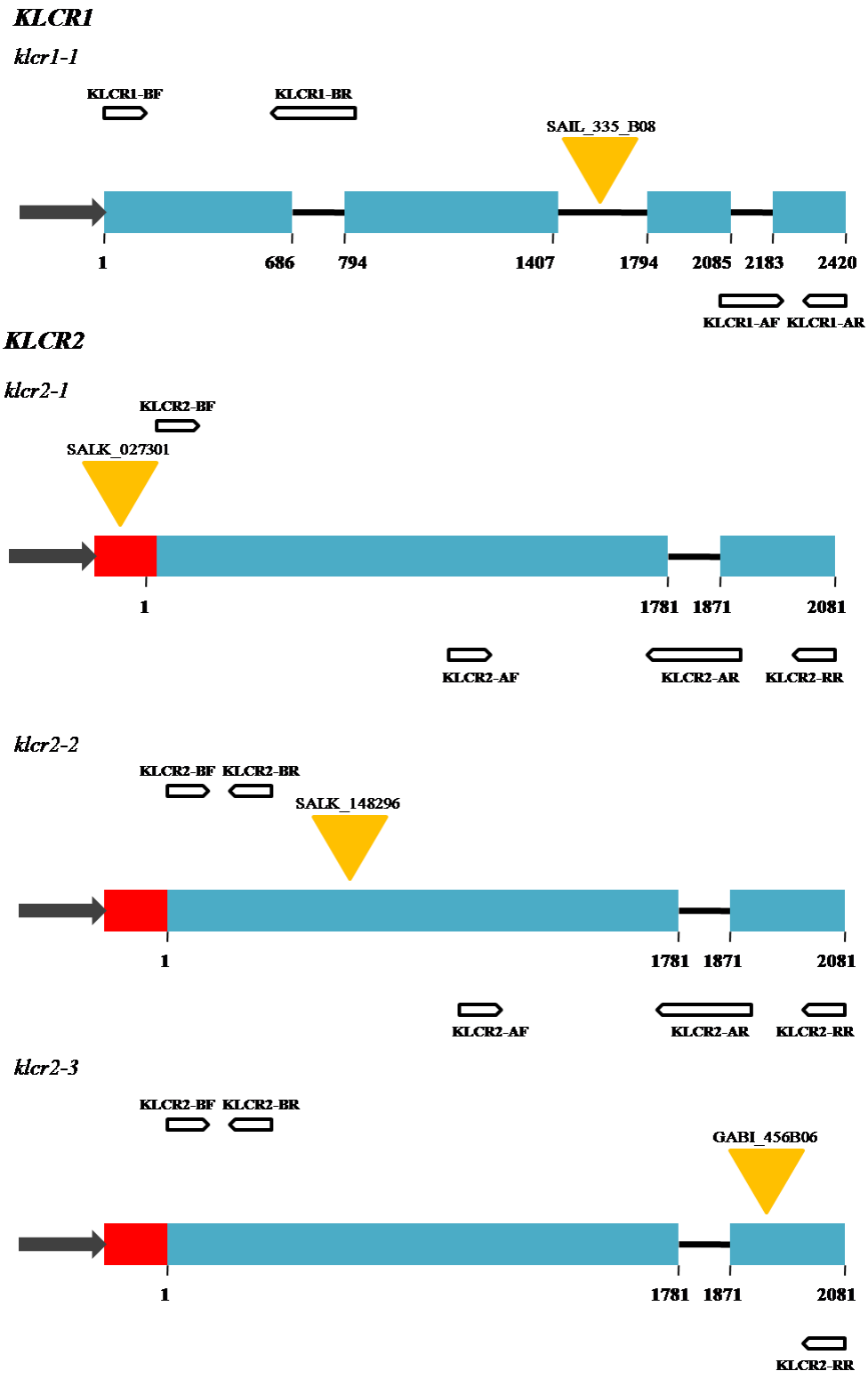

Figure 4.3 Primers used for RT-PCR to assess the disruption of the transcripts in the selected T-DNA insertion lines. Promoter regions are depicted in grey arrows. Exons are shown in blue, introns in black and the 5' UTR in red. The T-DNA insertions are represented by the yellow triangle. Primers used for RT-PCR are shown by the white arrows.

Gene	Mutant Line	Upstream primers	Upstream fragment size	Gene specific primers	Full length cDNA size	Downstream primers	Downstream fragment size
KLCR1	*klcr1-1*	KLCR1-BF+ KLCR1-BR	699 bp	KLCR1-BF+ KLCR1-AR	1830 bp	KLCR1-AF+ KLCR1-AR	249 bp
KLCR2	*klcr2-1*			KLCR2-BF+ KLCR2-RR	1992 bp	KLCR2-AF+ KLCR2-AR	693 bp
	klcr2-2	KLCR2-BF+ KLCR2-BR	324 bp	KLCR2-BF+ KLCR2-RR	1992 bp	KLCR2-AF+ KLCR2-AR	693 bp
	klcr2-3	KLCR2-BF+ KLCR2-BR	324 bp	KLCR2-BF+ KLCR2-RR	1992 bp		

Table 4.2 List of primers used for RT-PCR analysis. The fragments upstream and downstream of the T-DNA insertion are amplified by upstream primers and downstream primers respectively. Gene specific primers are used to amplify the full length coding sequence of KLCR1 and KLCR2. Shown here are the primer combinations and the predicted size of the PCR fragments.

The RT-PCR result of *klcr1-1*, *klcr2-1*, *klcr2-2* and *klcr2-3* T-DNA mutant alleles are shown in Figure 4.4. RT-PCR performed on Col-0 cDNA template indicated that the primer combinations listed in Table 4.2 were able to detect and amplify the target cDNA sequences. For the *klcr1-1* allele, the gene-specific primers were able to amplify the full length *KLCR1* from *klcr1-1* cDNA. However, the band appeared to be relatively weaker when compared to the Col-0 line, indicating that the transcript level of KLCR1 in *klcr1-1* line is reduced. Since the T-DNA insertion site is in the intron, the *klcr1-1* allele seems to be a "knock-down" mutant rather than a "knock-out" mutant. Both upstream and downstream transcripts could be detected using the upstream and downstream primer pairs, suggesting that the transcription of upstream and downstream of KLCR1 could occur. Although the up- and downstream sequence can be transcribed normally, protein translation could be interrupted by the T-DNA insert (Wang, 2008). RT-PCR was then performed in the *klcr2-1*, *klcr2-2* and *klcr2-3* mutant lines to investigate the transcriptional activity of *KLCR2*. As the klcr2-1 T-DNA insertion is in the 5'UTR region and the klcr2-3 T-DNA insertion is near the end of the gene sequence, upstream primers and downstream primers were not used respectively. In the *klcr2-2* mutant, both upstream band and downstream band could be amplified, indicating that the regions upstream and downstream of the SALK_148296 T-DNA insertion are still transcribed. For klcr2-1 and klcr2-3 mutants, the downstream and upstream primer pairs were also able to amplify the corresponding PCR fragments. However, no band could be produced by the gene specific primers in all three mutant lines, suggesting that they are all "knock-out" mutant lines.

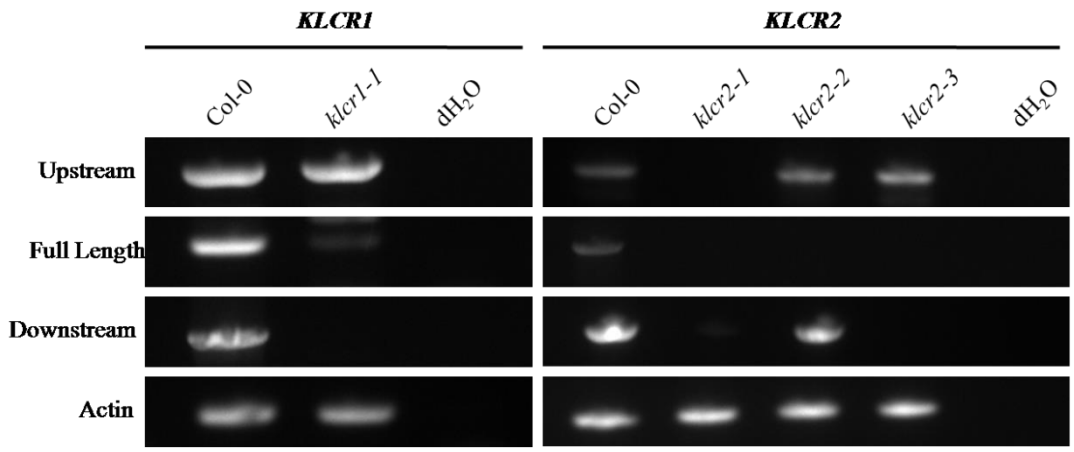

Figure 4.4 Analysis of the *KLCR1* and *KLCR2* transcripts in the mutant lines using RT-PCR. The top row represents the upstream bands. The second row represents the full length coding sequence bands. The third row represents the downstream bands. The bottom row represents the reference gene band. RT-PCR was performed on Col-0 cDNA, the *klcr1* and *klcr2* mutant cDNA and deionised water as a negative control.

4.2.5. Generation of *klcr1/klcr2* Double Mutant Lines

Next, *klcr1*/*klcr2* double mutants were created. It is known that functional redundancy is very likely between genes that share high homology. The disruption of one gene may be compensated by closely related genes from the same family. Therefore, a phenotype may be identified when two or more members of a gene family are disrupted. The *klcr1* and *klcr2* homozygous plants were grown up and crossed to generate *klcr1-1*/*klcr2-1*, *klcr1-1*/*klcr2-2* and *klcr1-1*/*klcr2-3* double mutant T-DNA insertion lines. After cross-pollination, the seeds were collected and germinated. Two genotyping PCR reactions were then performed to identify the F1 generation plants carrying two T-DNA alleles. The heterozygous plants were allowed to self-pollinate to produce the F2 generation. Seeds from F2 generation were grown and genotyping PCR was performed to identify homozygous plants for both *klcr1* and *klcr2* T-DNA alleles. Example genotyping PCRs of *klcr1/klcr2* homozygous lines are shown in Figure 4.5.

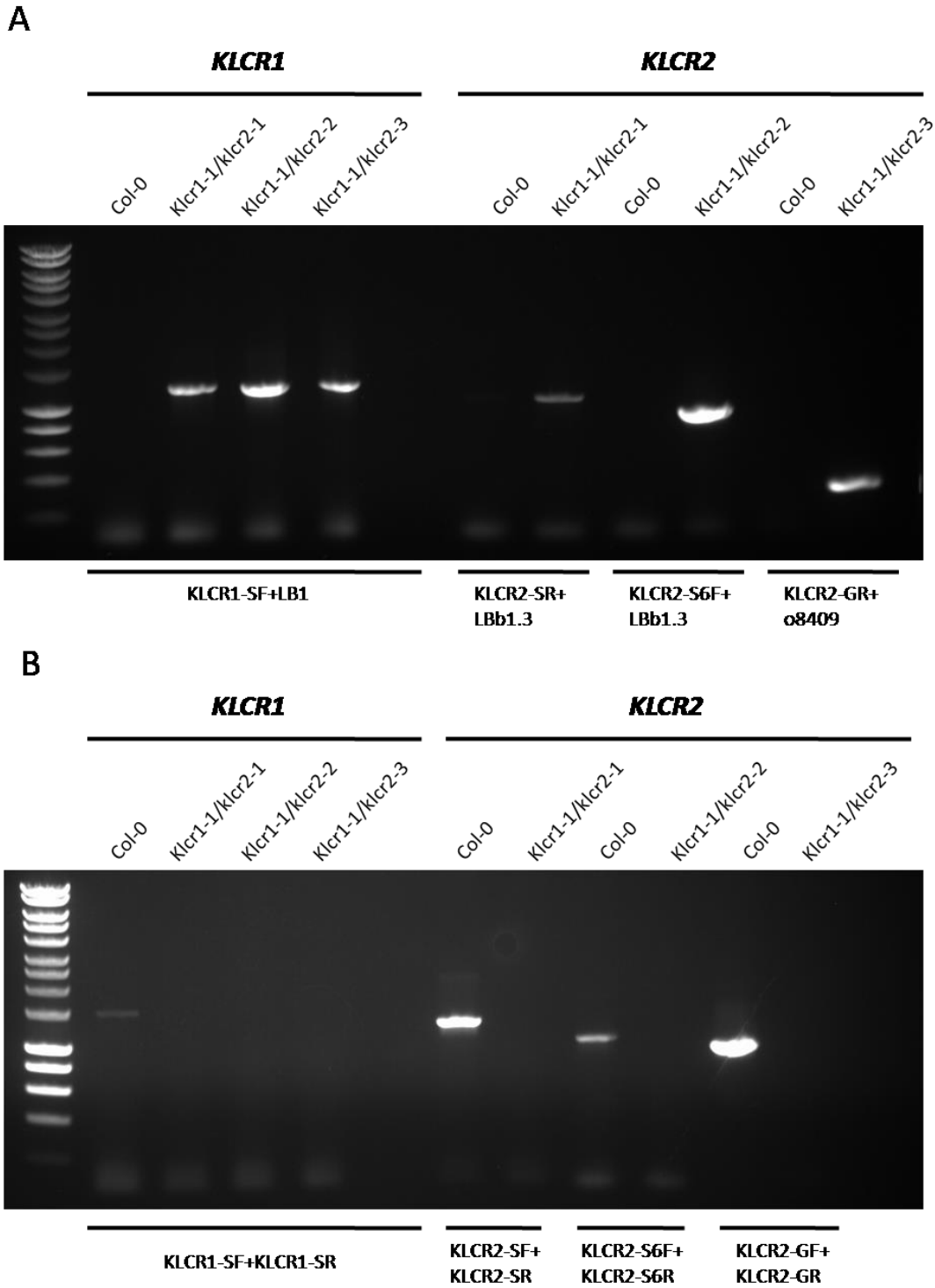

Figure 4.5 Examples of the PCR reactions used to genotype the *klcr1* and *klcr2* double mutants. A. Insert PCR reactions used to genotype *klcr1* and *klcr2* double mutant plants. The insert specific primers are shown below the gel. Hyperladder I was used as a molecular weight marker. B. Wild type PCR reactions used to genotype *klcr1* and *klcr2* double mutant plants. The gene specific primers are shown below the gel. Hyperladder I was used as a molecular weight marker.

4.3. Phenotypic Analysis of *klcr1* and *klcr2* Mutant Lines

After the identification *klrc1-1*, *klcr2-1*, *klcr2-2* and *klcr2-3* single mutants as well as *klcr1-1*/*klcr2-1*, *klcr1-1*/*klcr2-2* and *klcr1-1*/*klcr2-3* double mutant lines, phenotypic analysis was performed to investigate a potential role for the KLCR proteins in plant development.

4.3.1. KLCR1 Regulates Cell Morphology and Proper Direction Growth in Roots

In order to investigate plant development of *KLCR1* and *KLCR2* mutant lines, seedlings from the F3 generation *klcr1-1*, *klcr2-1*, *klcr2-2*, *klcr2-3*, *klcr1-1/klcr2-1*, *klcr1-1/klcr2-2*, *klcr1-1/klcr2-3* and Col-0 plants were grown vertically on 1/2 MS agar plates. After two days stratification, all the seeds were sown on the same day and were allowed to grow in a growth chamber for 7 days. As shown in Figure 4.6 and Table 4.3, the roots of all three *klcr2* alleles grew straight towards the direction of gravity, which were morphologically similar to wild type plants. In contrast, primary roots of homozygous *klcr1-1* mutant plants and *klcr1/klcr2* double mutant lines slanted towards the left side as viewed from above the plates. The average skewing angles of the *klcr1-1* allele and the three different *klcr1/klcr2* double mutant lines were 33.87^{o}, 31.95^{o}, 34.30^{o} and 33.84^{o} respectively and they were significantly greater than wild type plants (9.69^{o}, $p<0.01$). The root epidermal cells of *klcr1-1* showed left handed helical arrangement when compared to wild type, whose root epidermal cells exhibited parallel arrangement. Overall, KLCR1 is likely to be important in regulating cell expansion and growth during Arabidopsis root development, and this result is similar to a previous study (Liu *et al.*, 2016). In order to confirm the phenotype of *klcr1-1* mutant is directly related to the knock-down expression of KLCR1, genetic complementation was performed. Expression of *proKLCR1*:KLCR1-GFP in the *klcr1-1*mutant plants was able to rescue the twisting root growth phenotype. The roots of complemented lines skewed 10.32^{o}, which did

not show significant difference with wild type plants (p=0.6445), a result also indicates the C-terminal GFP fusion of KLCR1 is biologically functional. In addition, the root epidermal cell files of complemented plants exhibited similar morphology to control wild type plants.

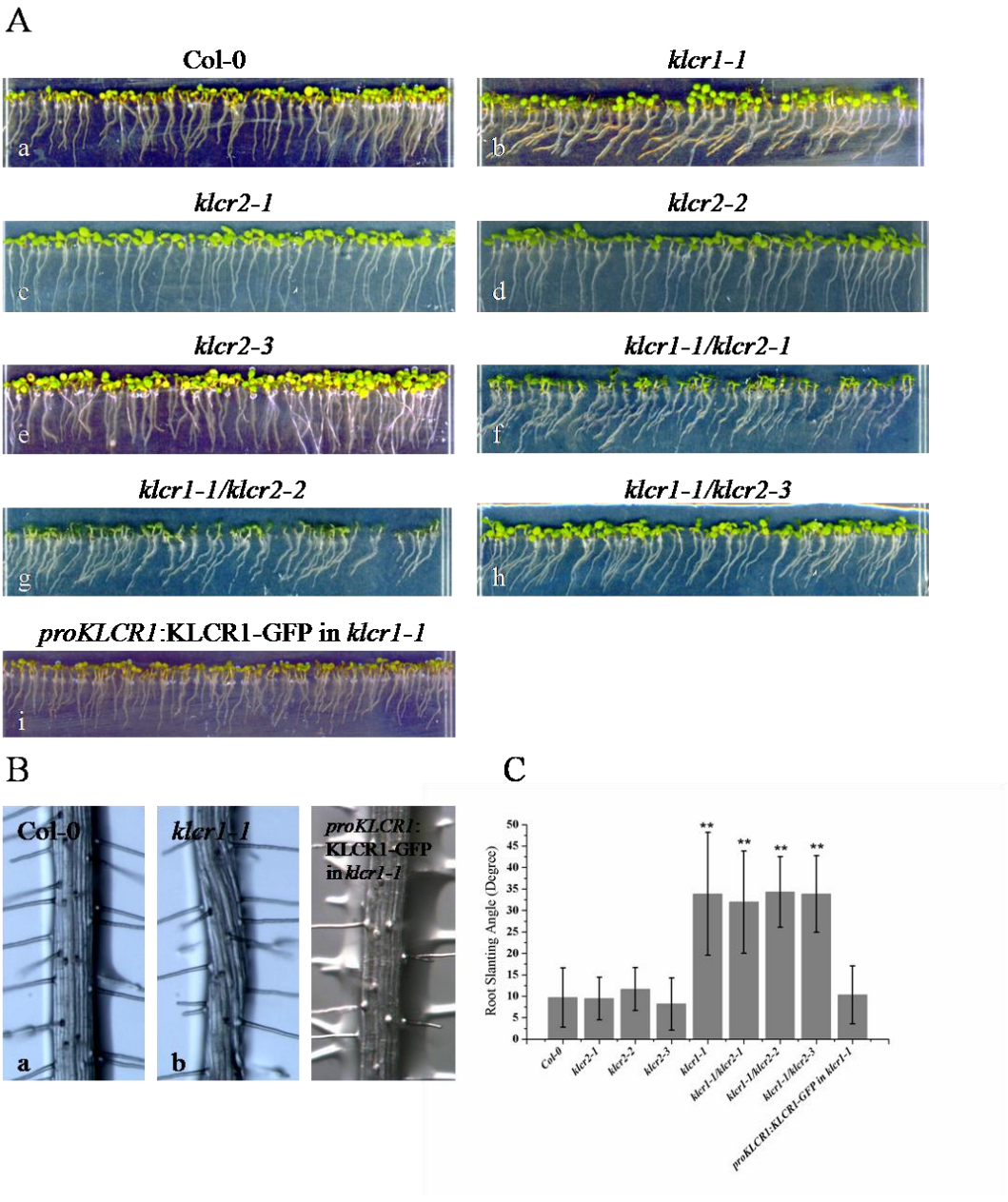

Figure 4.6 Morphology of *klcr1*, *klcr2* and *klcr1/klcr2* mutants. A. Phenotypes of 7 day old Arabidopsis seedlings. (a): Wild type plants (b): *klcr1* mutant plants (c)-(e): *klcr2* mutant plants (f)-(h): *klcr1/klcr2* double mutant plants (i): genetic complementation plants. B. The root epidermal cell files of wild type plants and *klcr1* mutant plants. C. Root slanting angles of 7 day old wild type and mutant seedlings grown vertically on agar plates. Asterisks indicate statistically significant differences from wild type ($p<0.01$).

Col-0 (n=42)	Average Root Slanting Angle (Degree)	9.69
	Standard Error	6.90
***klcr1-1* (n=54)**	Average Root Slanting Angle (Degree)	33.87
	Standard Error	14.32
	p value	<0.01
***klcr2-1* (n=34)**	Average Root Slanting Angle (Degree)	9.43
	Standard Error	4.97
	pvalue	0.8551
***klcr2-2* (n=40)**	Average Root Slanting Angle (Degree)	11.66
	Standard Error	5.03
	p value	0.1451
***klcr2-3* (n=57)**	Average Root Slanting Angle (Degree)	8.19
	Standard Error	6.06
	p value	0.2527
***klcr1-1/klcr2-1* (n=65)**	Average Root Slanting Angle (Degree)	31.95
	Standard Error	11.91
	p value	<0.01
***klcr1-1/klcr2-2* (n=44)**	Average Root Slanting Angle (Degree)	34.30
	Standard Error	8.25
	p value	<0.01
***klcr1-1/klcr2-3* (n=52)**	Average Root Slanting Angle (Degree)	33.84
	Standard Error	8.94
	p value	<0.01
***proKLCR1*:KLCR1-GFP in *klcr1-1* (n=62)**	Average Root Slanting Angle (Degree)	10.32
	Standard Error	6.74
	p value	0.6445

Table 4.3 Measurements of root slanting angles of wild type (Col-0), *klcr1* and *klcr2* mutant plants.

4.3.2. KLCR1 Regulates Cotyledon Pavement Cell Shape Formation

It is known that the organization of both cortical actin filaments and microtubules is essential for the formation of the jigsaw puzzle appearance of leaf pavement cells (Fu *et al.*, 2005, Smith, 2003). According to Burstenbinder et al. (2017), overexpression of several IQD proteins such as IQD11, IQD14, IQD16 and IQD25 altered the orientation of cellular microtubules and thus affected the cotyledon pavement cell shape (Burstenbinder *et al.*, 2017). IQD5 functions in stabilizing microtubules and loss of function of IQD5 results in reduction interdigitation of leaf pavement cells (Liang *et al.*, 2018). Since KLCR1 is a microtubule binding protein and interacts with several members of IQD protein family (Katharina Burstenbinder, unpublished), the biological function of KLCR1 in regulating the cell shape formation was studied.

To study the shape of cotyledon pavement cells, cotyledons from 4 day old Arabidopsis seedlings were stained with the PM dye FM4-64 and quantitative analysis of cell areas, cell circularities, lobes lengths and neck widths was performed. As shown in Figure 4.7 and Table 4.4, Wild type cotyledon pavement cells showed an interlocking jigsaw puzzle appearance with lobes and indentations. However, in *klcr1-1* mutant plants, the interdigitation pavement cell shape was dramatically altered. It was found that the average pavement cell area of *klcr1-1* was determined to be 2242.6±605.97 μm^2, which was significantly larger when compared with wild type plants. The average pavement cell circularity value of *klcr1-1* was observed to be 0.34 ±0.07 μm, whereas the average circularity value of wild type plants was remarkable smaller (0.32±0.08 μm). The circularity value is a dimensionless shape factor based on the perimeter, when the complexity of the shape increases, the circularity value decreases (Zhang *et al.*, 2011). In addition, the lobe lengths and neck widths were also measured as described in chapter 2.5.8. When compared with wild type plants, *klcr1-1* mutants showed wider necks and shorter lobes. Taken together, these results indicate that KLCR1 forms an important part in the formation of Arabidopsis pavement cells. It would be better to quantify the pavement cell shape of characterized mutants as a

control, such as mutants in the ROP pathways or one of the Arp2/3 or SCAR complex group. However, the mutant seeds are not available in this study.

A

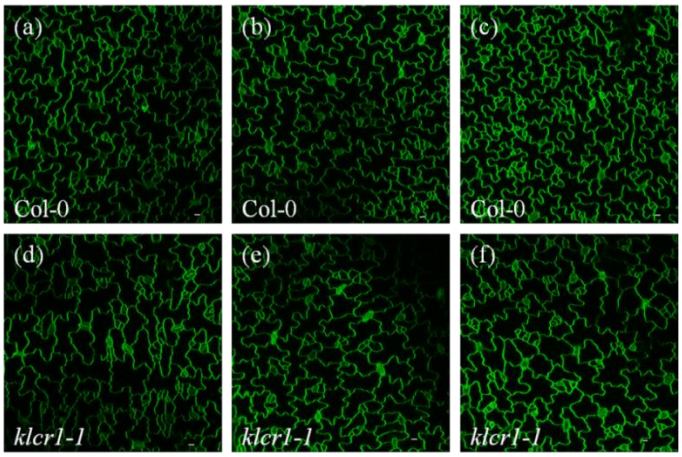

B

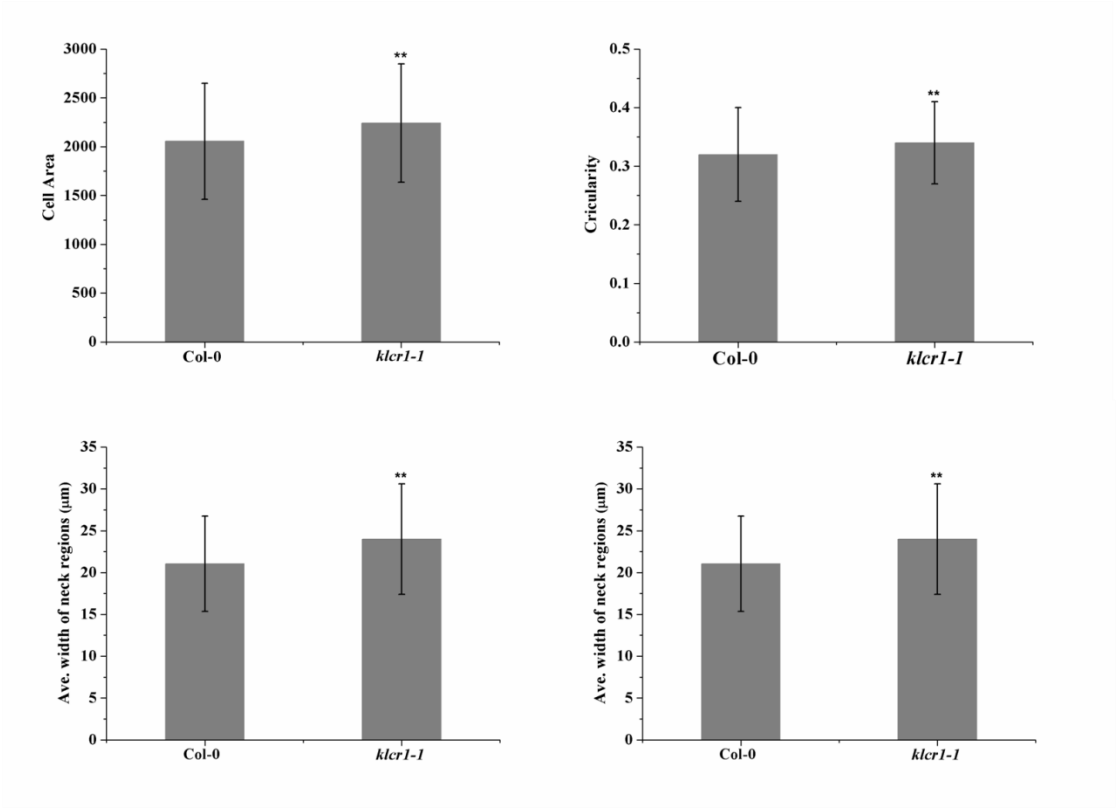

Figure 4.7 Pavement cell shape phenotype in the *klcr1-1* mutants. A. (a)-(c): Cotyledon pavement cell shape of wild type plants. (d)-(f): Cotyledon pavement cell shape of *klcr1-1* mutant plants. B. Quantitative analysis of *klcr1-1* pavement cell shape changes. The error bars show standard deviation (SD). Asterisks indicate statistically significant differences from wild type (Student's *t*-test, **p<0.01). Scale bar: 10 μm.

Cell Area (μm^2)		
Col-0 (n=222)	Average Cell Area	2056.43
	Standard Error	594.61
***klcr1-1* (n=232)**	Average Cell Area	2242.60
	Standard Error	605.97
	p value	<0.01
Circularity		
Col-0 (n=222)	Average Circularity	0.32
	Standard Error	0.08
***klcr1-1* (n=232)**	Average Circularity	0.34
	Standard Error	0.07
	p value	<0.01
Neck Width (μm)		
Col-0 (n=420)	Average Width of Neck Region	21.05
	Standard Error	5.69
***klcr1-1* (n=568)**	Average Width of Neck Region	24.01
	Standard Error	6.60
	p value	<0.01
Lobe length (μm)		
Col-0 (n=428)	Average Length of Lobes	16.19
	Standard Error	7.65
***klcr1-1* (n=595)**	Average Length of Lobes	11.96
	Standard Error	4.30
	P value	<0.01

Table 4.4 Quantitative analysis of the size of cotyledon pavement cells of *klcr1-1* mutants.

4.3.3. The Organization of Actin Filaments and Microtubules is influenced in *klcr1-1* Mutants

According to previous studies, the abnormal cell morphology is likely linked to the change of the cytoskeleton function (Liang *et al.*, 2018, Rosero *et al.*, 2016). Therefore, the structure of cytoskeleton in *klcr1-1* mutant was examined. Fluorescent protein tagged actin marker Lifeact-GFP was previously introduced by crossing into the *klcr1-1* genetic background. Compared with wild type plants, mutants carrying the actin marker appeared to have fewer weakly labeled thin bundles or single actin filaments and more thick bundling filaments (Figure 4.8 A, a-f). The skewness of fluorescence intensity distribution was used to investigate the level of actin filaments bundling. At least 60 cells from 6-10 seedlings per sample were assessed. The average skewness value of microfilaments in wild type plants was observed to be 2.03 ± 0.25, which was significantly smaller than the value in *klcr1-1* mutant plants (2.36 ± 0.29) (Figure 4.8 B). Therefore, our results suggested that KLCR1 is important in regulating the organization of actin filaments in Arabidopsis cotyledon pavement cells.

Next, the microtubule arrangement was assessed in *klcr1-1* mutants carrying the microtubule marker MAP4-GFP. The organization of microtubules was also affected in the *klcr1-1* mutants (Figure 4.8 A, g-l). According to Boudaoud et al. (2014), the microtubule structure was quantified using an imageJ plug-in, Fibriltool. The fibril array anisotrophy score was used to assess whether the fibrils are well ordered. The score is between 0 and 1, 0 for no order and 1 for perfectly ordered (Boudaoud *et al.*, 2014). At least 100 regions from 7-10 seedlings per sample were analyzed. The average anisotrophy score in wild type is observed to be 0.14 ± 0.05, which was significantly higher than that in *klcr1-1* mutants (0.11 ± 0.05) (Figure 4.8 C), indicating that the microtubule arrays in cotyledon pavement cells of *klcr1-1* were less ordered. Moreover, in *klcr1-1* mutants expressing *proKLCR1*:KLCR1-GFP, KLCR1-GFP labeled microtubules appeared to be well ordered (Figure 4.8 A, m-o), indicating that *proKLCR1*:KLCR1-GFP in *klcr1-1* mutant plants was able to rescue

the microtubule disorganization phenotype. Therefore, these data suggest that loss of function of KLCR1 results in the disorganization of microtubules.

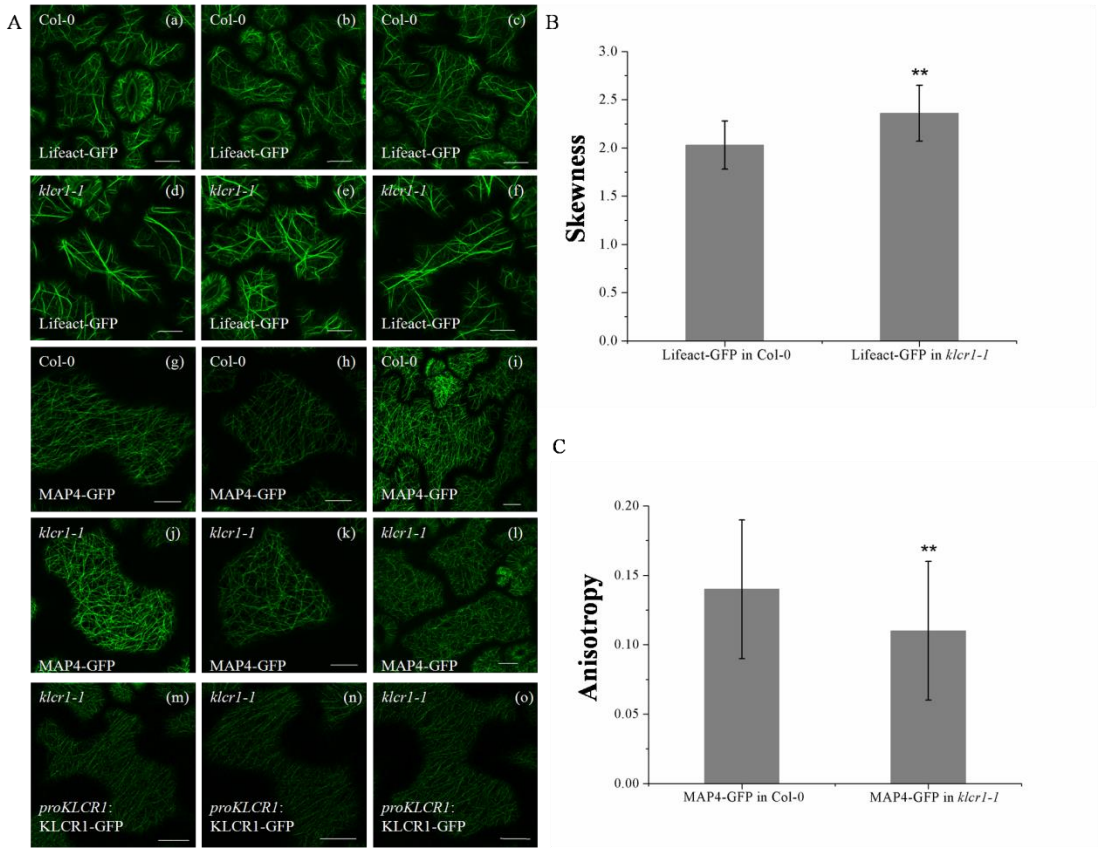

Figure 4.8 Organization of actin filaments and microtubules in cotyledon pavement cells of wild type and *klcr1-1* mutant seedlings at 4-day-old. A. (a)-(c): actin filaments labeled by Lifeact-GFP in cotyledon pavement cells of wild type seedlings. (d)-(f): actin filaments labeled by Lifeact-GFP in cotyledon pavement cells of *klcr1-1* seedlings. (j)-(i): microtubules labeled by MAP4-GFP in cotyledon pavement cells of wild type seedlings. (j)-(l): microtubules labeled by MAP4-GFP in cotyledon pavement cells of *klcr1-1* seedlings. (m)-(o): microtubules labeled by *proKLCR1*:KLCR1-GFP in cotyledon pavement cells of *klcr1-1* seedlings. B. Actin filaments bundling (skewness), Asterisks indicate statistically significant differences from wild type (Student's *t*-test, **p<0.01). C. Quantitative analysis of microtubule array anisotropy, Asterisks indicate statistically significant differences from wild type (Student's *t*-test, **p<0.01). Scale bar: 10μm.

4.4. Conclusion

In this chapter, phenotypic analysis was performed using T-DNA insertion lines to study functions for the KLCR proteins. One homozygous mutant line for *klcr1* and three homozygous lines for *klcr2* were identified. The *klcr1* mutant plants and *klcr2* mutant plants were then crossed together to generate double T-DNA insertional mutant lines.

Primary root growth was investigated in these mutant lines. Interestingly, primary roots of *klcr1* mutant plants and double mutant plants were shown to slant towards the left side and the root epidermal cell files showed left handed helical arrangement. The average skewing angle was significantly greater in comparison to wild type plants and this growth phenotype can be complemented after expression of *proKLCR1*:KLCR1-GFP. The function of KLCR1 in regulating the shape of cotyledon pavement cells was also investigated. In *klcr1* mutant lines, the interdigitation of pavement cell shape was dramatically altered. Cell areas, cell circularities, lobe lengths and neck widths of mutant plants were shown to be significantly different when compared with wild type plants. This phenotype is very likely due to the disorganization of the cytoskeletons. Taken together, our results indicate KLCR proteins are involved in cytoskeletal arrangement and cell morphogenesis during plant development.

4.5. Discussion

4.5.1. KLCR1 Regulates Pavement Cell Morphogenesis through Organizing Both Microtubules and Acin Filaments

It is known that well-organized cortical microtubules play a vital role in anisotropic growth in higher plants. Changes in microtubule dynamics by microtubule depolymerizing or stabilizing drugs are able to change cell polarity and growth

(Mathur, 2004). In this study, our results indicate that KLCR1 is essential for regulating the organization of microtubules. Genetic lesions in KLCR1 (*klcr1*) cause less ordered organization of cortical microtubule arrays in cotyledon pavement cells, thereby affecting the pavement cell morphogenesis. It has been reported that *klcr1* mutant plants appear to be more sensitive to the microtubule de-stabilizing drug oryzalin treatment when compared to wild type plants. Similarly, in *klcr1/klcr2* double mutants, the microtubule growth rate decreased while the shrinkage rate increased (Liu *et al.,* 2016). Therefore, it is likely that the loss of function of KLCR1 may affect microtubule stability. Several studies have reported that the organization of cortical microtubules can be affected by the alteration of microtubules dynamics (Liang *et al.*, 2018). Hence, changes in microtubule organization in *klcr1* mutant plants are likely attributed to the interference in microtubule dynamics. Moreover, the disorganization of microtubules could influence the deposition of cellulose microfibrils, thereby resulting in defects in cell expansion.

Several IQD proteins have also been reported to regulate the organization and dynamics of microtubules as well as the morphology of pavement cells. For example, overexpression of IQD11, IQD14, IQD16 and IQD25 affects the orientation of cortical microtubules in pavement cells, thereby altering the cell shape (Burstenbinder *et al.,* 2017). IQD5 functions in stabilizing microtubules and the loss of function of IQD5 leads to reduced interdigitation of pavement cells in cotyledons (Liang *et al.*, 2018). IQD15-18 can be regulated by auxin signaling and bind to calmodulins in a calcium-dependent manner, therefore integrating auxin and calcium signaling to modulate microtubule dynamics and cell shape formation (Wendrich *et al.,* 2018). As discussed before, the association of KLCR1 to microtubules is likely to depend on IQD proteins, suggesting that KLCR1 may regulate the microtubule cytoskeleton, presumably through its interaction with IQD proteins.

In addition to microtubules, cortical actin filaments also play a critical role in formation of the interdigitating pavement cell shape by controlling lobe initiation and outgrowth (Fu *et al.*, 2005). As discussed previously, KLCR1 may form a protein

complex with NET3C and IQDs, mediating interactions and cross-talk between microtubules and actin filaments. Any alterations in the stability and organization of microtubules may cause defects in actin organization. In this study, the structure of actin filaments was also assessed in the *klcr1* mutant. Interestingly, the results indicate that actin filaments in *klcr1* mutant cotyledon pavement cells appeared to be more bundled in comparison with wild type. Such abnormal actin filaments organization may also contribute to the defects of the mutant pavement cell shape. It has been reported that low concentrations Lat B, (a well-characterized G-actin agonist known to interfere with actin polymerization) could enhance actin bundling before the complete disappearance of F-actin in cotyledons (Mathur *et al.*, 2003). Therefore, inhibition of actin polymerization may induce the formation of actin bundling. Actin polymerization is likely to depend on microtubules (Sampathkumar *et al.*, 2011). Changes in microtubule dynamics and organization may influence the polymerization of actin filaments, thereby increasing actin bundling. Taken together, KLCR1 plays a critical role in plant cell morphogenesis by regulating the organization of both actin filaments and microtubules.

4.5.2. KLCR1 regulates root development through maintaining microtubule stability

In addition to the cotyledon pavement cell shape, the primary root of *klcr1* and *klcr1/klcr2* double mutant plants showed abnormal left handed helical growth. However, another independent study identified a similar phenotype while my study is ongoing.

In their study, KLCR proteins were named as cellulose-microtubule uncoupling (CMU) proteins and. The fluorescence recovery after photobleach (FRAP) experiments indicated that they were localized as static puncta that coincide with cortical microtubules. The mutant plants exhibited left-handed twisting of etiolated hypocotyls and increased sensitivity to microtubule de-stabilizing drug (oryzalin)

treatment. In *cmu1/cmu2* double mutant cells, arched microtubules that coincide with microtubule lateral displacement can be observed. After treating dual-labeled GFP-CMU1 mCh-TUA5 cells with the drug morlin (an inhibitor of microtubule dynamics and CesA movement), CMU1 fluorescence was absent at positions where microtubules arched. The microtubule lateral displacement is not due to the actomyosin-dependent cytoplasmic streaming because clear lateral microtubule displacement could still be observed in the mutant cells after treating with Lat B. In addition to the microtubule lateral displacement phenotype, pivoting microtubule ends in mutant cells could also be observed (Liu *et al.*, 2016).

During cellulose synthesis, cellulose synthase (CesA) complexes (CSCs) track along cortical microtubules (Paredez *et al.*, 2006b). However, in *cmu1/cmu2* double mutant plants, most of the CesA trajectories did not align with the cortical microtubules. Although the mean speeds of the CesA were similar in wild type plants and mutant plants, the traces of CesA particles in mutant plants sometimes deviated from straight lines. The microtubule displacement in the mutant plants was affected by the plasma membrane based CSC activity because after treating *cmu1/cmu2* mutant cells with isoxaben (the herbicide that depletes the plasma membrane of CesA particles), the level of microtubule lateral displacement was reduced. The CesAs are guided along cortical microtubules by interacting with the protein CSI1/POM2 which is considered to be a scaffold between the CSCs and the microtubules. The microtubule lateral displacement in mutant plants was caused by the SCI1/POM2 proteins because in *cmu1/cmu2/pom2* triple mutant cells, the level of the microtubule lateral displacement was reduced. Therefore, in *cmu1*/*cmu2* double mutant plants, the cellulose synthase complexes (CSC) drags microtubules during cellulose production, resulting in lateral instability of microtubules. CMU proteins are able to maintain microtubule stability to control the movement of the CSC, which is essential for directed plant cell growth (Liu *et al.*, 2016). The possible model in which the CMU proteins function in preventing microtubule lateral displacements caused by aberrant CSC movements at the cortex of growing plant cells is shown in Figure 4.9.

In our study, global sequence alignments demonstrated that the protein sequence similarity between KLCR1 and KLCR2 was high. However, in the phenotype analysis, the development of *klcr2* mutants was normal and both cotyledon pavement cell shape and primary root growth were not affected. Among the three members of KLCRs, only KLCR1 can form a protein complex with IQDs and NET3C. As described before, the KLCR1-IQDs-NET3C protein complex facilitates the cross talk between actin filaments and microtubules. Therefore, KLCR1 is essential for regulating the organization of the actin and microtubule cytoskeletons by forming protein complex with IQDs and NET3C, thereby affecting plant development.

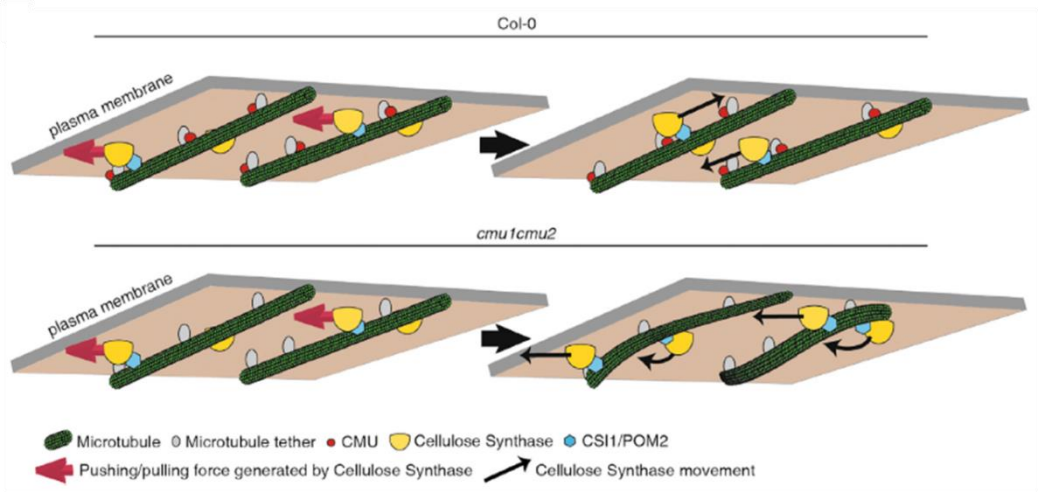

Figure 4.9 Schematic model showing that CUM proteins maintain lateral microtubule positions at cortex of growing plant cells. In wild type cells, CSI1/POM2 proteins interact with CSCs and associate with microtubules, which may redirect the movement of the CSCs so that the complexes move along the microtubules. In mutant cells that lack the CUMs, the microtubules are unable to withstand the forces generated by CSCs and a reorientation of the CSCs is therefore disabled. Figure from Liu *et al*. (2016).

4.5.3 NET3C-KLCR1-IQDs Protein Complex May Act as Cortical Microtubule-Plasma Membrane Nexus in Plant Cells

In plant cells, the cortical microtubule arrays play vital roles in cell wall development. Cortical microtubules are tightly anchored to the PM forming a highly ordered array, regulating the deposition pattern of cellulose microfibrils by guiding the movement of the cellulose synthase complex (Oda, 2018). Recent studies have identified various

proteins which facilitate the cortical microtubule-PM interaction, including Arabidopsis Phospholipase D (PLD) isoforms, plant-specific Rho/Rac GTPases and IQD13 (Andreeva *et al.*, 2009, Fu *et al.*, 2009, Gardiner *et al.*, 2001, Oda and Fukuda, 2012, Oda *et al.*, 2010, Sugiyama *et al.*, 2017, Wang and Wang, 2001, Yu *et al.*, 2010, Zhang *et al.*, 2012, Zhang *et al.*, 2017).

It has been reported that cellulose is synthesized by the PM-localized cellulose synthase complexes (CSCs) in plant cells. The CSCs move along the cortical microtubules by interacting with CSI1/POM2 which results in the lateral microtubule displacement during cellulose production (Bringmann *et al.*, 2012, Gu *et al.*, 2010, Li *et al.*, 2012). As discussed above, KLCRs are able to maintain cortical microtubule stability to direct the movement of CSCs. In growing cells, KLCR1 can only be observed at microtubules that are closely associated with the PM, but not at microtubules separated from the membrane (Liu *et al.*, 2016). Therefore, KLCR1 may be involved in a potential microtubule-PM tethering function.

Here, our study advanced the current understanding of how KLCR1 associates with the PM. The protein complex NET3C-KLCR1-IQDs may act as a linker between cortical microtubule and the PM. As shown in Figure 4.10, the PM-associated NET3C forms a platform with microtubule-binding IQDs at the microtubule-PM anchor sites. KLCR1 is recruited to these sites to stabilize the position of cortical microtubules and enable microtubules to withstand the propulsion generated by the motile CSCs during cellulose biosynthesis.

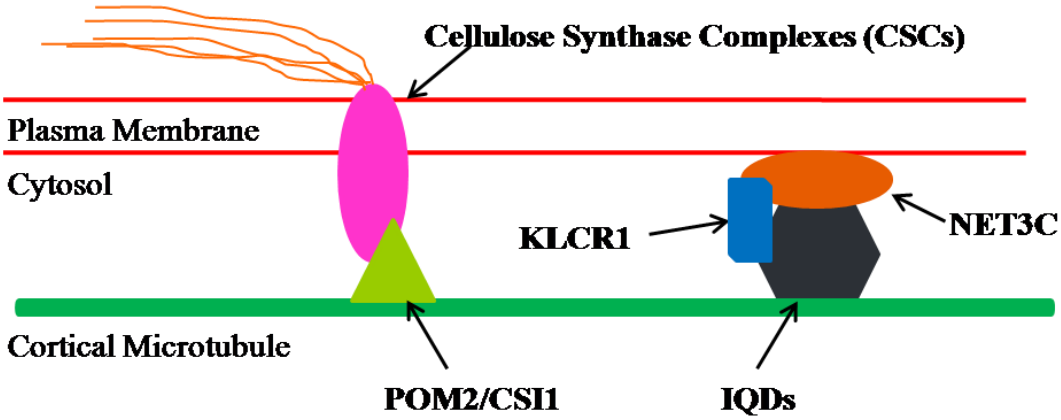

Figure 4.10 Possible model for the KLCR1-NET3C-IQDs complex involvement in microtubule-PM tethering function. NET3C directly interacts with IQD proteins and recruits KLCR1 to stabilize the localization of microtubules during CSCs movement.

Chapter 5: Investigation of NET3C-AtBRO1 Interaction and Reverse-Genetic Analysis of AtBRO1

5.1. Introduction

In a previous proteomics screen, Arabidopsis endosomal targeting BRO1-like domain containing protein (AtBRO1) was identified as a potential interactor of NET3C (Dr. Pengwei Wang, Unpublished). In eukaryotic cells, the BRO1 domain-containing proteins have been reported to be involved in the endosomal sorting complex required for transport (ESCRT) machinery. The ESCRT system is an evolutionarily conserved, multi-subunit membrane remodeling complex that plays essential roles in deforming membrane and severing membrane necks from the inside (Gao *et al.*, 2017).

The abundance and localization of integral PM proteins, such as signaling receptors, ion channels and nutrient transporters form an important part in the growth, differentiation and survival of eukaryotic cells (MacGurn *et al.*, 2012). Therefore, the selective vacuole/lysosome degradation of non-functional or misfolded membrane proteins plays a critical role in proper cell signaling and interactions with the environment (MacGurn *et al.*, 2012, Piper and Luzio, 2007). In the sorting process, membrane proteins are firstly tagged by ubiquitin (Ub) and then sorted into the intraluminal vesicles (ILVs) of multivesicular bodied (MVBs) or prevacuolar compartments (PVCs) through the ESCRT pathway. Finally, the membrane proteins are degraded in the lumen of the vacuole/lysosome through the fusion of the MVB/PVCs (Henne *et al.*, 2011, Schmidt and Teis, 2012). The ESCRT machinery is composed of several distinct complexes, including ESCRTs-0, -I, -II, -III and the Vps4 complex. Plant cells contain most members of the ESCRT machinery, except for ESCRT-0 and the ESCRT-I component Mvb12 (Gao *et al.*, 2014, Richardson *et al.*, 2011).

ALIX, the mammalian BRO1 domain containing protein is able to interact with

ESCRT-I and ESCRT-III directly and functions as a bridge between these two complexes (Odorizzi, 2006). Its yeast homolog Bro1p has been confirmed to bind the Snf7 subunit of ESCRT-III and functions in stabilizing the ESCRT-III complex by inhibiting Vps4-mediated disassembly in vivo and in vitro (Wemmer *et al.*, 2011). In Arabidopsis, AtBRO1 interacts with the ESCRT-III component SNF7 and functions in removing Ub from ubiquitinated proteins by recruiting the deubiquitinating enzyme (DUb) to late endosomes before sequestering the proteins into ILVs (Cardona-Lopez *et al.*, 2015, Kalinowska *et al.*, 2015).

Although numerous functions of ESCRTs in mammals and yeast have been reported in recent years, the characterization of ESCRT machinery in plants remains limited (Gao *et al.*, 2017). It is known that NET3C is localized to the ER-PM contact sites whose function remains largely unknown. Therefore, investigation of the interaction between NET3C and AtBRO1 was performed to determine if NET3C may play a role with the ESCRT machinery to mediate endosome budding at the PM.

5.2. The investigation of Nucleotide Sequences and Predicted Protein Structure of AtBRO1

Information regarding Arabidopsis BRO1 (AtBRO1) was obtained from the TAIR database. AtBRO1 was encoded by the gene AT1G15130 and had an open reading frame of 3632 bp which consists of 8 exons (1-666 bp, 815-1765 bp, 1979-2068 bp, 2163-2231 bp, 2330-2470 bp, 2657-2705 bp, 2895-2998 bp and 3162-3632 bp) as shown in Figure 5.1. This gene encoded a protein of 846 amino acid (aa) with a predicted molecular weight (MW) of 95.2 kDa.

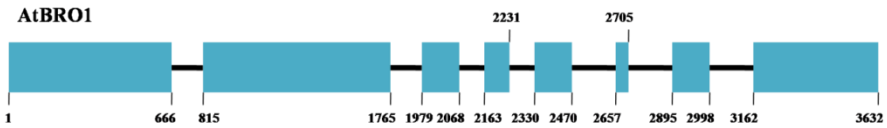

Figure 5.1 Schematic Diagram of AtBRO1 Gene Structure. Exons are represented by light blue boxes and introns by black lines. Numbers below the diagram indicate the start and end positions (bp) of exons.

Next, the SMART web resource was used to predict the secondary structure of the AtBRO1 protein and three main features were identified (Figure 5.2, Table 5.1). The BRO1 domain was detected at the N-termini from amino acid 9-393, which can be found in several late endosomal proteins, such as human ALIX and its yeast homolog Bro1p. The BRO1 domain of fungal and mammalian proteins is able to interact with multivesicular body components (ESCRT-III proteins) such as yeast Snf7 and mammalian CHMP4b, and recruits BRO1 domain containing proteins to late endosomes (Kim *et al.*, 2005). The Pfam ALIX_LYPAL_bnd domain was identified in AtBRO1 (aa 424-710). In Arabidopsis, this domain was confirmed to directly bind to monoubiquitin (Shen *et al.*, 2016). In addition, regions of low complexity which represent simple sequence regions with significant biases in amino acid composition were detected at the C-termini of AtBRO1 (aa 740-769, aa 755-815 and aa 816-844) . The C-terminal region of AtBRO1 is essential for its association with a unique plant ESCRT-I component named FREE1 and the interaction between these two proteins functions in recognizing and sorting ubiquitinated cargos into the ILVs of MVB/PVCs (Shen *et al.*, 2016).

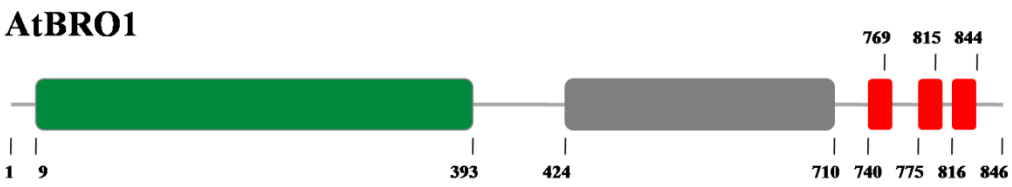

Figure 5.2 Predicted protein structure of AtBRO1 protein in Arabidopsis. The protein structure was predicted using the SMART programme. Green box indicates BRO1 domain, grey box indicates Pfam ALIX_LYPXL_bnd domain, red boxes indicate regions of low complexity and grey lines represent non-domain containing regions. Numbers underneath the diagrams denote the start and end point (amino acid) of the labeled protein domain.

Protein	Predicted protein Domains	Positions (aa)
AtBRO1	BRO1	9-393
	Pfam ALIX_LYPXL_bnd	424-710
	Region of low complexity	741-769, 775-815 &816-844

Table 5.1 List of Protein Domains Possessed by AtBRO1 Predicted using the SMART Program.

5.3. *In vivo* Analysis of Full Length AtBRO1 proteins

5.3.1. Subcellular Localization of AtBRO1

In order to investigate the subcellular localization of AtBRO1 *in vivo*, agrobacterium mediated transient expression assays were performed to express AtBRO1-GFP or AtBRO1-mCherry alone and co-expressed with ER and actin markers GFP-HDEL and Lifeact-GFP in *N. benthamiana* leaf epidermal cells.

The coding sequence of full length AtBRO1 was PCR amplified from Arabidopsis seedling cDNA using the primers listed in Appendix 1.1, and cloned into pDONR207 using gateway BP cloning. AtBRO1 was then subcloned into pMDC83-GFP and pMDC83-mCherry respectively to facilitate the expression of AtBRO1-GFP and AtBRO1-mCherry fusion proteins under the control of a 35s promoter (Figure 5.3 A).

In cells which expressed AtBRO1-GFP alone, AtBRO1-GFP was observed to be localized to punctae (Figure 5.3 B, a-c). To further investigate whether the AtBRO1 punctae may associate with the ER network or actin filaments *in vivo*, the AtBRO1-mCherry was transiently co-expressed with the ER marker, GFP-HDEL and actin marker, Lifeact-GFP. The AtBRO1-mCherry labeled punctae was observed to be closely associated with the ER and F-actin (Figure 5.3 B, d-i).

After investigating the subcellular localization of AtBRO1 in transient expression system, the subcellular localization of AtBRO1 in stable Arabidopsis transgene lines was analyzed. The floral dipping method as described in chapter 2.2.14 was used to

generate Arabidopsis transgene lines stablely expressing AtBRO1-mCherry under 35s promoter. After 40 µg/ml Hygromycin selection, confocal microscopy was used to check the mCherry fluorescence manually in leaf epidermal cells. The stable T3 generation was used for the subcellular localization study. Cotyledon pavement cells of 5 days old seedlings were imaged and at least 3 lines were assessed. *pro35s*:AtBRO1-mCherry appeared to be punctate dots in cotyledon pavement cells and this expression pattern is similar with AtBRO1-mCherry expressed in the *N. benthamiana* leaf epidermal cells (Figure 5.3 B, j-l). A large portion of these punctae was reported to be co-localized with the MVB marker (Shen *et al.*, 2016).

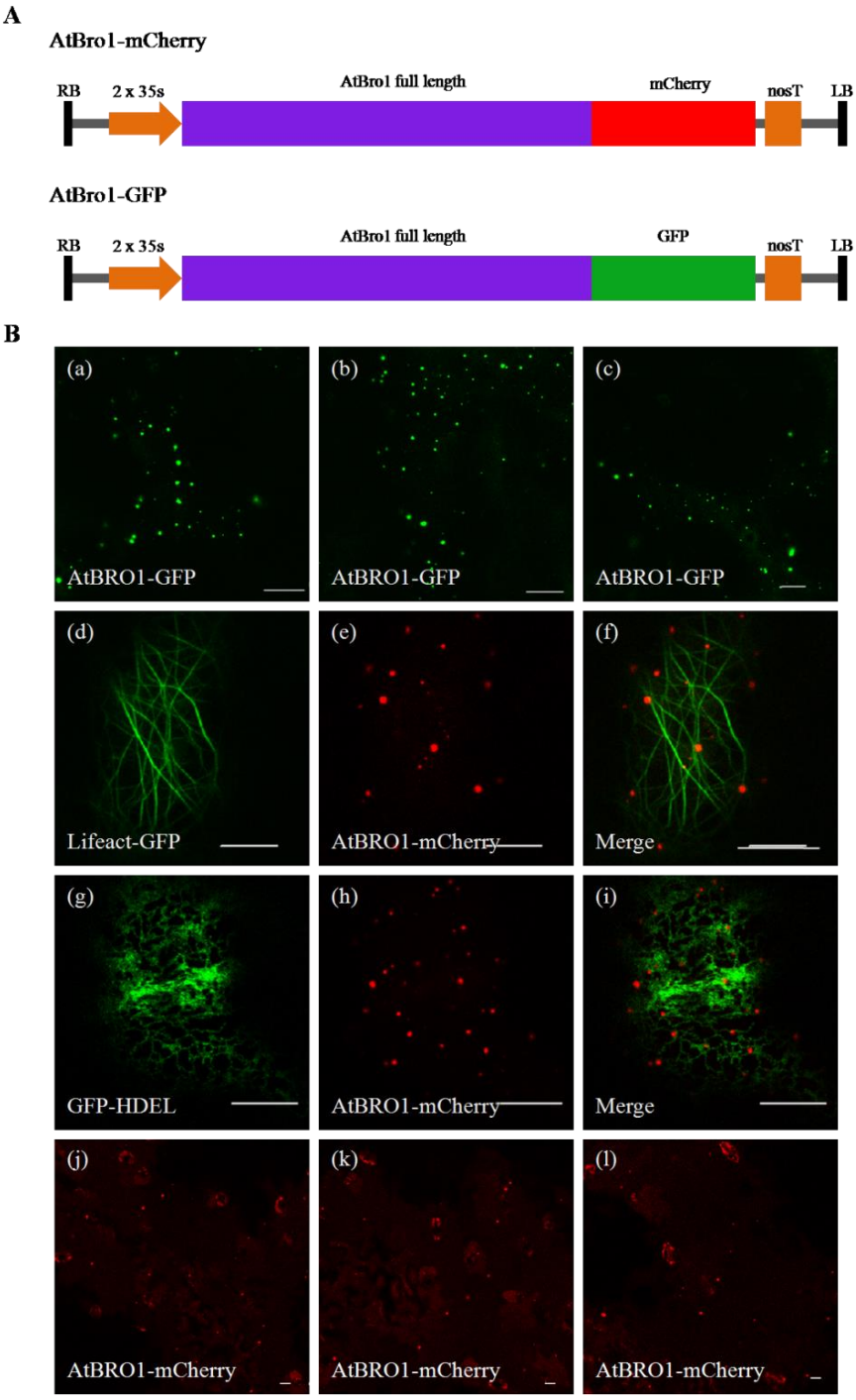

Figure 5.3 Schematics of expression constructs and the subcellular localization of AtBRO1. A. Schematics of expression constructs. AtBRO1-GFP and AtBRO1-mCherry were created using the pMDC83-GFP vector and pMDC83-mCherry vector respectively. B. Subcellular localization of AtBRO1. (a)-(c): AtBRO1-GFP localization in *N. benthamiana* leaf epidermal cells. (d)-(f): AtBRO1-mCherry is associated with actin filaments in *N. benthamiana* leaf epidermal cells. (g)-(i): AtBRO1-mCherry is associated with the ER network in *N. benthamiana* leaf epidermal cells. (j)-(l): Arabidopsis expressing *pro35s*:AtBRO1-mCherry in cotyledon epidermal cells. Scale bar: 10 µm.

5.3.2. *In vivo* Interaction Analysis between NET3C and AtBRO1

AtBRO1 was identified as a potential interactor of protein NET3C in a previous proteomics screen. To investigate whether these two proteins interact with each other *in vivo*, co-localization analysis between them was performed. AtBRO1-mCherry and GFP-NET3C were co-expressed in *N. benthamiana* leaf epidermal cells using agrobacterium mediated infiltration so that they can be visualized together. The subcellular localization of AtBRO1-mCherry and GFP-NET3C in *N. benthamiana* leaf epidermal cells was shown in Figure 5.4. AtBRO1-mCherry and GFP-NET3C punctae were clearly found to be co-localized *in vivo*.

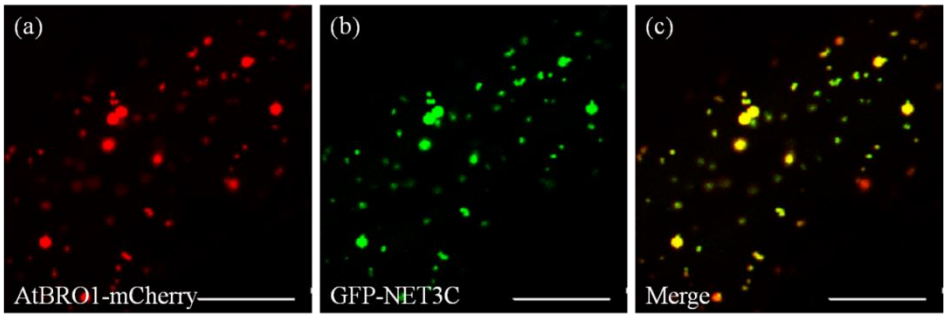

Figure 5.4 Co-localization analysis of AtBRO1-mCherry with GFP-NET3C *in vivo*. *N. benthamiana* leaves were expressed with the fluorescence tagged proteins. (a)-(c): Co-expression of AtBRO1-mCherry with GFP-NET3C. AtBRO1-mCherry punctae are co-localized with GFP-NET3C. Scale bar: 10 μm.

FRET-FLIM was then performed to determine whether AtBRO1 may directly interact with NET3C. GFP-NET3C was used as a FRET-FLIM donor construct and AtBRO1-mCherry was used as a FRET-FLIM acceptor construct. GFP-NET3C was transiently expressed in *N. benthamiana* leaf tissues either alone or with AtBRO1-mCherry using agrobacterium-mediated transformation. GFP-RFP fusion protein was also used as a positive control. As shown in Figure 5.5, the average fluorescence lifetime of the GFP-NET3C donor when expressed alone was measured at 2.66±0.05 ns. However, when co-expressed alongside the AtBRO1-mCHerry acceptor, the average fluorescence lifetime was significantly dropped by 0.22 ns (to 2.44 ± 0.08 ns; p=2.2E-16), suggesting a physical interaction. Moreover, the

fluorescence lifetime of GFP-RFP fusion protein was measured at 2.30±0.06 ns.

A

Constructs Expressed	Mean GFP Fluorescence Lifetime	Standard Deviation	n
GFP-NET3C	2.66 ns	0.05	18
GFP-NET3C+AtBRO1-mCherry	2.44 ns	0.08	21
GFP-RFP	2.30ns	0.06	20

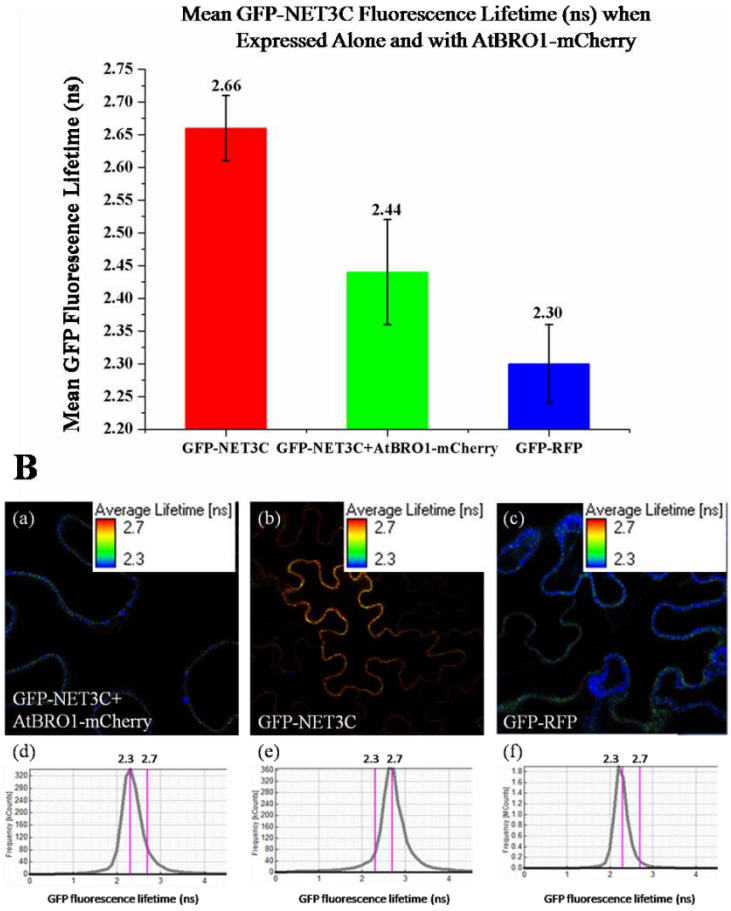

Figure 5.5 FRET-FLIM analysis of NET3C-AtBRO1 interactions. A: Average fluorescence lifetime of GFP-NET3C significantly reduced when co-expressed with AtBRO1-mCherry in *N. benthamiana* leaf epidermal cells. n=number of cells analyzed. B: Visualization of GFP-NET3C fluorescence lifetimes *in vivo* when co-expressed alone and with AtBRO1-mCherry. (a)-(c): example images of GFP fluorescence detected in *N. benthamiana* leaf epidermal cells, pseudocoloured according to GFP fluorescence lifetime. (d)-(f): charts associated with images (a)-(c) respectively, show the frequency distributions of the fluorescence lifetimes (ns) of detected photons in each image. A leftward shift in peak GFP fluorescence lifetime is indicative of reduced average lifetime. (a) and (d): GFP-NET3C expressed alone. (b) and (e): GFP-NET3C co-expressed with AtBRO1-mCherry. (c) and (f): GFP-RFP fusion protein positive control.

5.4. AtBRO1 is Essential for the Development of Arabidopsis Embryos

The T-DNA insertion positions in *atbro1* were identified using the SiGnAL T-DNA Express Arabidopsis Gene Mapping Tool. Two insertion lines were available in the catalogue for *AtBRO1* (GABI_837H11 and GABI_780B02) and they were ordered from the NASC. The insertion sites were predicted to be in the fifth exon and the last exon respectively. Schematic maps of selected T-DNA alleles are shown in Figure 5.6. Insert PCR and wild type PCR were performed to identify the homozygous T-DNA mutant lines. The primers used for these two types of PCR were listed in Table 5.2.

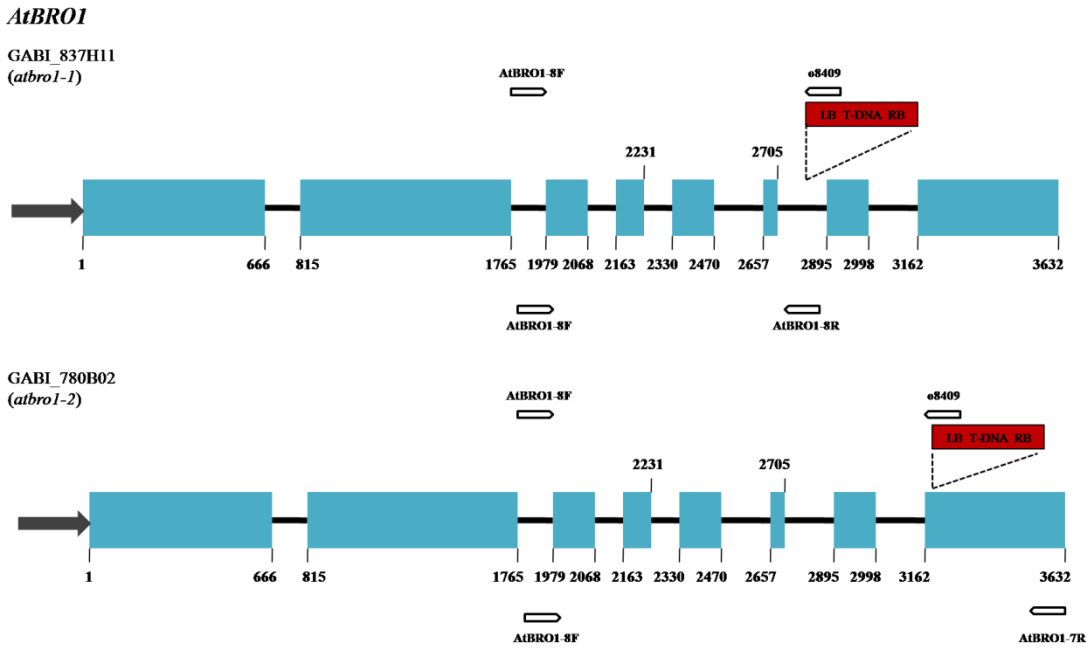

Figure 5.6 Predicted positions of the selected T-DNA insertion lines and the primers used for genotyping. Promoter regions are depicted in grey arrows. Exons are shown in blue and introns in black. The T-DNA insertions are represented by the red box and labeled with the left border (LB) and right border (RB). Primers used for genotyping are shown by the white arrows. Gene specific primers below the gene were used to detect the wild-type allele and the insert-specific primers above the gene were used to detect the mutant allele.

Line	Predicted insertion site	Primers for WT PCR	WT PCR size (bp)	Primers for insert PCR	Insert PCR size (≈ bp)
AtBro1					
GABI_837H11	Exon 5	AtBRO1-8F+ AtBRO1-8R	925	o8409+ AtBRO1-8F	900
GABI_780B02	Exon 8	AtBRO1-8F+ AtBRO1-7R	1810	o8409+ AtBRO1-8F	1400

Table 5.2 Details of T-DNA insertion lines for *AtBRO1*. Shown here are the insertion positions of each mutant line, the primers used for genotyping PCR and the predicted size of the PCR fragments.

Wild type plants only produce a band in the wild-type PCR and homozygous plants only produce a band in the insert PCR. However, both "insert band" and "wild type band" can be amplified from genomic DNA of heterozygous plants. According to the Mendelian rules of genetic inheritance, the ratio of homozygous plants should be a quarter in progenies derived from self-pollinated heterozygous lines, *atbro1-1 (+/-)* or *atbro1-2 (+/-)*. However, after genotyping analysis, no homozygous mutant plants were identified. As shown in Figure 5.7, 16 lines were used for *atbro1-1* and *atbro1-2* genotyping analysis respectively. For *atbro1-1*, 7 wild type plants and 9 heterozygous plants were identified and for *atbro1-2*, 9 wild type plants and 7 heterozygous were identified.

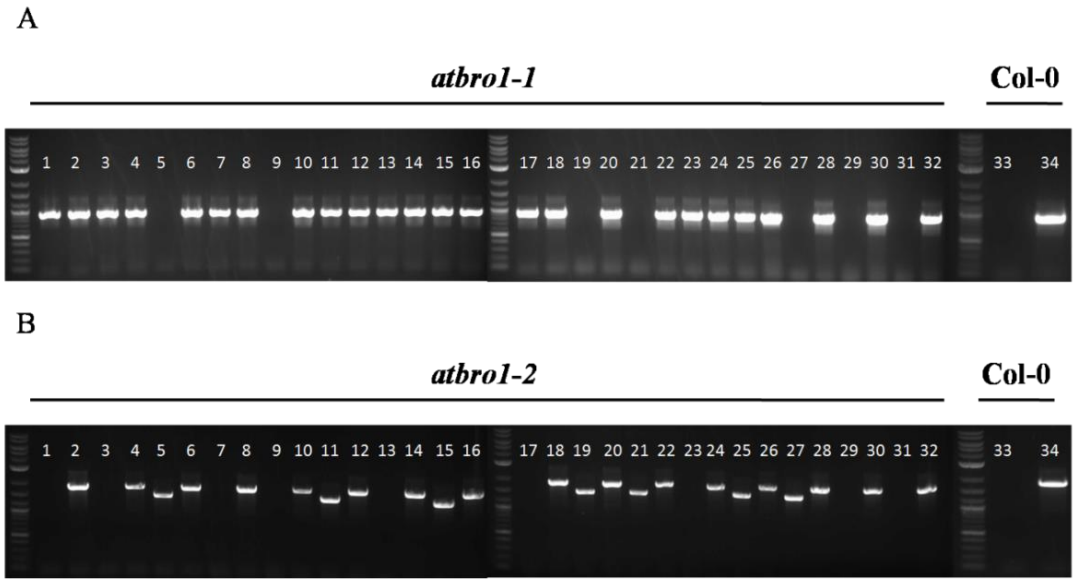

Figure 5.7 PCR reactions used to genotype the *atbro1* T-DNA insertion mutants. A.PCR reactions used to genotype *atbro1-1* T-DNA insertion mutants. Lane 1, 3, 5, 7, 9, 11, 13, 15, 17, 19, 21, 23, 25, 27, 29, 31 and 33 indicate the insert PCR reactions and lane 2, 4, 6, 8, 10, 12, 14, 16, 18, 20, 22, 24, 26, 28, 30, 32 and 34 indicate the wild type PCR reactions. 2-Log DNA ladder was used as a molecular marker. B. PCR reactions used to genotype *atbro1-2* T-DNA insertion mutants. Lane 1, 3, 5, 7, 9, 11, 13, 15, 17, 19, 21, 23, 25, 27, 29, 31 and 33 indicate the insert PCR reactions and lane 2, 4, 6, 8, 10, 12, 14, 16, 18, 20, 22, 24, 26, 28, 30, 32 and 34 indicate the wild type PCR reactions. 2-Log DNA ladder was used as a molecular marker.

As described above, no homozygous plants were identified in PCR genotype screens. It is possible that homozygote of *atbro1* leads to defects in embryo development and the missing homozygous mutants might be directly related to embryo lethality. During Arabidopsis seeds development, the colour of seeds changes from white to green and finally brown before maturation and release. All the seeds in a single silique develop in synchronization. Therefore, when compared with normal green developing seeds, abnormal seeds appear to be white or brown and shriveled (Meinke, 1994).

In order to determine if the mutant embryos were impaired in their development, the seed set of *atbro1-1* and *atbro1-2* heterozygous plants was analysed. Siliques removed from wild type plants and mutant plants were dissected to expose the seeds. In order to avoid the potential variation between different plants, 10 siliques from 3 individual plants were analysed for each mutant line. As shown in Figure 5.8 and Table 5.3, in siliques from *atbro1-1* and *atbro1-2* heterozygous mutant plants, paler

seeds could be clearly observed. The average frequency of abnormal seeds per silique for wild type plants was counted at 3.5%, which was significantly smaller than the average frequency for *atbro1-1* and *atbro1-2* heterozygous mutant plants, 22.1% and 29.6% respectively. The ratio of paler seeds within siliques from heterozygous mutant plants was approximately a quarter, which corresponds with Mendelian rules of genetic inheritance. Taken together, these results indicate that AtBRO1 plays a vital role in Arabidopsis embryo development.

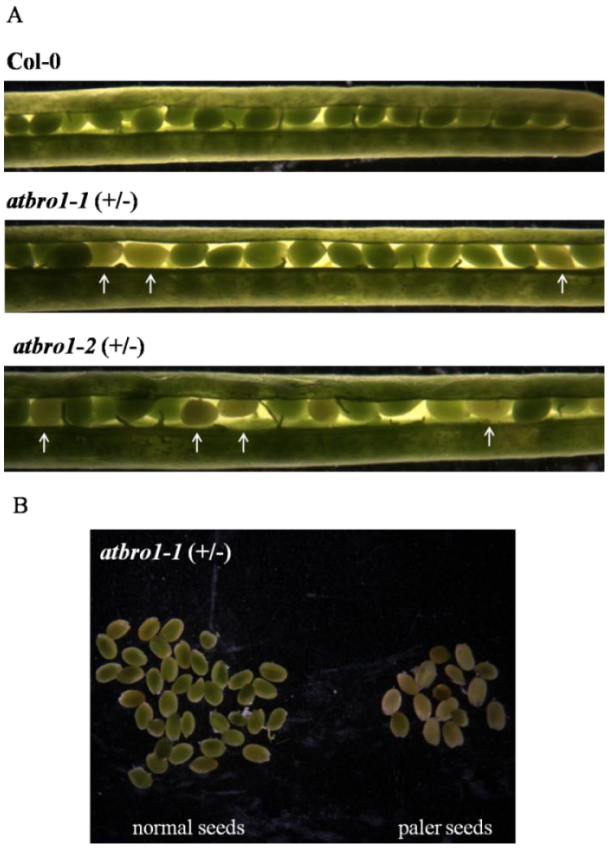

Figure 5.8 Seeds set of *atbro1* mutant plants. A. Example siliques collected from Col-0, *atbro1-1* and *atbro1-2* heterozygous plants. The paler seeds are indicated by white arrows. B. Normal seeds and paler seeds from one single mutant silique of *atbro1-1*(+/-).

	Normal seeds	**Paler seeds**	**Ratio**
Col-0	472	17	3.5%
***atbro1-1*(+/-)**	341	97	22.1%
***atbro1-2*(+/-)**	334	132	29.6%

Table 5.3 Statistical analysis of seed development *atbro1* mutant plants. For each line, 10 siliques from 3 individual plants were analyzed.

5.5. Conclusion

In this chapter, the gene sequence and protein structure of AtBRO1 were studied using bioinformatics analysis. The predicted secondary structure showed that AtBRO1 contained an N-terminal BRO1 domain, a C-terminal proline-rich domain and an ALIX domain between them. The subcellular localization of AtBRO1 was studied using both transient *N. benthamiana* system and stable Arabidopsis transgene lines. AtBRO1 expressed under the control of 35s promoter was shown to be localized at punctate dots and these punctae were associated with actin filaments and ER network. In vivo co-expression analysis indicated that AtBRO1 was co-localized with NET3C. FRET-FLIM analysis was used to confirm the interaction between them. Phenotypic analysis was then performed using T-DNA insertion lines to study functions of AtBRO1. However, no homozygous plants were identified in genotype screen. The seed set of heterozygous plants was then analyzed and there were about a quarter abnormal seeds within siliques from heterozygous plants. While my study was in progress, this phenotype was reported in another study in which AtBRO1 was proved to be engaged in ESCRT-I complex and regulate the sorting of ubiquitinated cargoes into the ILVs of MVBs (Shen *et al.*, 2016).

5.6. Discussion

5.6.1. NET3C Interacts with AtBRO1 and is Likely to be Engaged in the ESCRT Machinery, Regulating Endosomal Budding Processes

In recent years, research into the roles of the ESCRT machinery in the intracellular membrane budding and scission processes has undergone a significant revolution in yeast and mammals. However, the reported functions of ESCRT machinery in plants remain largely unknown (Gao *et al.*, 2017).

AtBRO1 is reported to be engaged in the ESCRT-I complex and associates with a

unique plant ESCRT-I component, FREE, whose mutant causes a defect in formation of vacuole and MVB for protein sorting and degradation (Gao *et al.*, 2014, Shen *et al.*, 2016). In siliques from *atbro1 (+/-)* plants, paler seeds can be observed and the ratio of abnormal seeds was approximately a quarter, which corresponds with mendelian rules of genetic inheritance, indicating that homozygous of *atbro1* causes defects in embryo development. The paler seeds were confirmed to be from *atbro1* homozygous mutant plants by Western blot analysis using Anti-AtBRO1 antibody and a complementation study using AtBRO1:YFP-AtBRO1. Knock down of AtBRO1 by DEX-inducible RNAi leads to a seedling lethal phenotype (Shen *et al.*, 2016). Similar with FREE1 mutant plants, the fragmented central lytic vacuoles can be observed in DEX- induced RNAi-*AtBRO1* plants and the number of intraluminal vesicles (ILVs) in MVBs was significantly reduced because of the reduced expression of AtBRO1. Therefore, AtBRO1 functions in the same pathway as FREE1 in the ESCRT-I complex and regulates the sorting of ubiquitinated cargoes into the ILVs of MVBs, thereby affecting the plant development (Shen *et al.*, 2016). In addition, AtBRO1 also functions in the ESCRT-III complex by interacting with the ESCRT-III component SNF7. AtBRO1 recruits the deubiquitinating enzyme AMSH3 to late endosomes to remove ubiquitin from ubiquitinated proteins before sequestering the proteins into ILVs (Cardona-Lopez *et al.*, 2015, Kalinowska *et al.*, 2015). The possible models for the ESCRT-I and ESCRT-III complexes are shown in Figure 5.9. Therefore, it could be predicted that NET3C is likely to be involved in the ESCRT machinery through its interaction with AtBRO1 and functions in sorting of ubiquitinated cargoes into the ILVs of MVBs. Additionally, it has been reported that VAP27-1 and VAP27-3 interact with clathrin and are involved in endocytosis and plant development (Stefano *et al.*, 2018). Thus, it could be speculated that plant ER-PM contact sites are involved in plant endocytosis. NET3C may recruit the ESCRT complexes to the PM and deform and sever membrane necks from the inside during endocytosis.

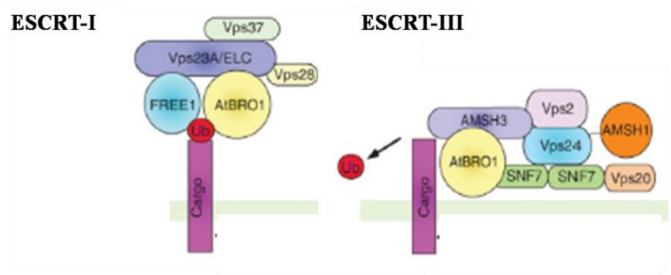

Figure 5.9 Possible models for the ESCRT-I and ESCRT-III complexes. Figure from Shen *et al.*, (2016).

5.6.2. AtBRO1 Interacts with NET3C and May Regulate the Structure of Actin Filaments

In this study, the subcellular localization of AtBRO1 was investigated using the transient *N. benthamiana* system and stable Arabidopsis transgenic lines. In both *N. benthamiana* leaf epidermal cells and Arabidopsis cotyledon pavement cells, AtBRO1 expressed under the control of 35s promoter was observed to be localized to punctae and was found to be closely associated with actin filaments, reminiscent of its human homolog, ALIX which also showed actin cytoskeleton association in cells from human lung fibroblasts (Pan *et al.*, 2006). The functions of ALIX in regulating actin cytoskeleton in human cell have been reported, but the role of AtBRO1 in actin filaments regulation remains largely unknown.

Human ALIX has been reported to be involved in the MVB pathway which mediates the transport between early endosomes and late endosomes/lysosomes (Haglund *et al.*, 2003). Depletion of ALIX results in a strong redistribution of early endosomes from a peripheral to a perinuclear location and an abnormal cortical actin organization. The abnormal actin structures contain both an actin polymerization factor (cortactin) and an endocytic compartment (clathrin), indicating that ALIX is involved in connecting the endocytic machinery to actin (Cabezas *et al.*, 2005). Therefore, it is possible that AtBRO1-NET3C interactions may be required for a proper organization of the cortical actin cytoskeleton in Arabidopsis, coordinating the interactions between the cortical actin cytoskeleton and the endocytic machinery.

Chapter 6: Investigation of VAP27-SINE2 Interactions

6.1. Introduction

In a previous proteomics screen, SUN-interacting nuclear envelope protein 2 (SINE2) was identified as a potential interactor of VAP27. SINE2 is one of the members of plant-specific KASH (Klarsicht, ANC-1, and SyneHomologe) proteins, which are situated at the inner nuclear membrane through interacting with the outer nuclear membrane protein AtSUN (Sad1 and Unc84) (Zhou *et al.*, 2015a).

Most of KASH proteins have a conserved C-terminal KASH domain which plays a vital role in their NE localization and varied plasmic N-terminal domains that may associate with the cytoskeleton and some motor proteins (Zhou *et al.*, 2015a). SUN proteins interact with KASH proteins and link between the nucleoskeleton and cytoskeleton. The SUN-KASH NE bridge is essential for various nuclear processed including nuclear shape maintenance as well as nuclear and chromosome movement (Crisp *et al.*, 2006, Zhou *et al.*, 2012).

WPP domain-interacting proteins (WIPs) are the first identified plant KASH proteins. All three Arabidopsis WIP proteins, AtWIP1, AtWIP2 and AtWIP3 interact with AtSUN1 and AtSUN2 (Zhou *et al.*, 2012). According to Zhou et al. (2014), another five putative KASH proteins, SINE1, SINE2, SINE3, SINE4 and SINE5 were identified. SINE1 and SINE2 are conserved across all land plants; SINE3 is specific to in eudicots; SINE4 only exists in *A. thaliana*, *A. lyrata* and *Capsellarunella* and SINE5 can only be found in *Medicagotruncatula* and *Medicago sativa* (Zhou *et al.*, 2014).

In higher eukaryotic cells, the nuclear envelope undergoes extensive rearrangement during mitosis (Ungricht and Kutay, 2017). The nuclear envelop proteins disperse into

the ER network during nuclear envelop breakdown (Yang *et al.*, 1997). Additionally, the ER is also the major source of membrane for the reformation of the nuclear envelope at the end of mitosis (Anderson and Hetzer, 2008b). Although various studies have reported the mechanism of nuclear envelope rearrangement in animal cells (Ungricht and Kutay, 2017), changes of nuclear envelope during plant mitosis process remains largely unknown. The interaction between SINE2 and VAP27-1 may link the plant ER network to the nuclear envelope, thereby regulating the rearrangement of the nuclear envelope during mitosis.

6.2. The investigation of Nucleotide and Protein Sequences of Arabidopsis KASH domain protein SINE2

SINE2 was encoded by the gene AT3G03970 and had an open reading frame of 1748 bp which is comprised of 2 exons (1-1155 bp and 1238-1748 bp) as shown in Figure 6.1. This gene encoded a protein of 554 amino acid (aa) with a predicted molecular weight (MW) of 61.4 kDa. According to Zhou et al, (2014), protein SINE2 is comprised of a C-terminal transmembrane KASH domain which is essential for SUN protein interaction and the armadillo (ARM) repeats in the N termini (Zhou *et al.*, 2014).

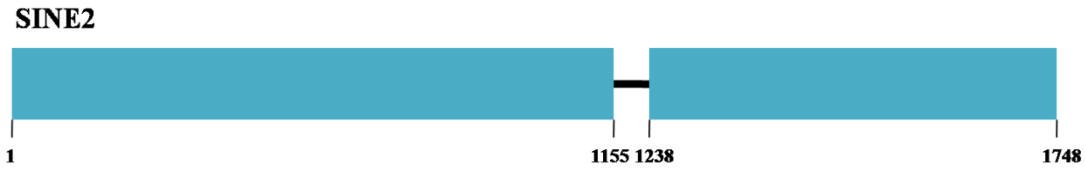

Figure 6.1 Schematic Diagram of the gene structure of *SINE2*. Exons are represented by light blue boxes and introns by black lines. Numbers below the diagrams indicate the start and end positions (bp) of exons.6.3. *In vivo* Analysis of Full Length SINE2 Protein

6.3. *In vivo* Analysis of Full Length SINE2 Protein

6.3.1. Cloning of the Full Length SINE2 Protein

In order to investigate the subcellular localization of SINE2 *in vivo*, various fluorescent fusion protein expression constructs were generated. The full length SINE2 coding sequence was PCR amplified from Arabidopsis seedling cDNA using primers listed in Appendix 1.1, and then cloned into pDONR207 using gateway BP cloning. After confirmation by sequencing, SINE2 was then cloned into different gateway expression vectors (pMDC83-mCherry, pMDC43-mCherry, pMDC43-GFP and pK7WGR2) by LR reaction to fuse this protein to various fluorescent tags and facilitate its expression under the control of the CaMV 35s promoter. Schematics of expression constructs described above are listed in Figure 6.2.

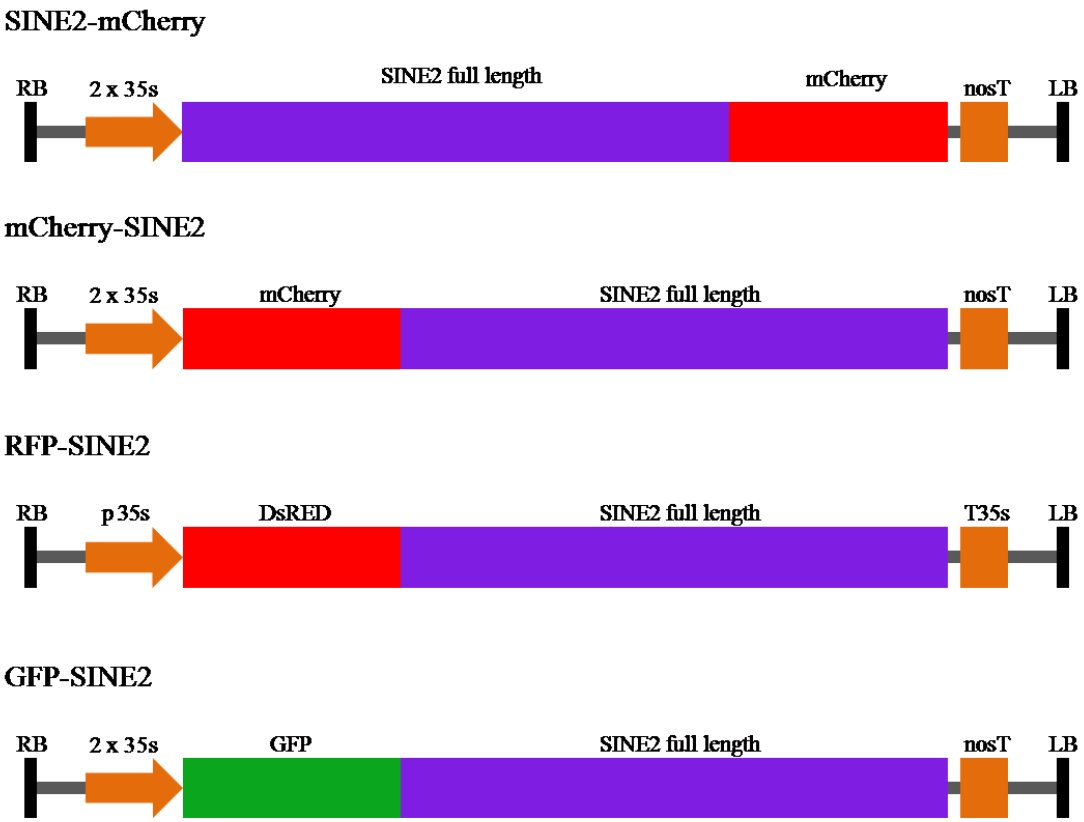

Figure 6.2 Schematics of expression constructs. SINE2-mCherry construct was generated using the pMDC83 vector. mCherry-SINE2 and GFP-SINE2 constructs were generated using the pMDC43 vector. RFP-SINE2 construct was created using the pK7WGR2 vector.

6.3.2. Subcellular Localization of SINE2

The subcellular localization of SINE2-mCherry and mCherry-SINE2 fusion proteins were studied in *N. benthamiana* leaf epidermal cells using agrobacterium-mediated transient expression assays. When SINE2-mCherry and mCherry-SINE2 were expressed alone, they were observed to decorate a mash-like network with some filament structure labeling within the cell, reminiscent of the ER network and actin filaments (Figure 6.3, a-b). In addition, SINE2-mCherry and mCherry-SINE2 also seemed to be localized to the nuclear envelope (Figure 6.3, c-d).

To further investigate the subcellular localization of SINE2, both SINE2-mCherry and mCherry-SINE2 fusion proteins were transiently co-expressed with the ER marker GFP-HDEL and the nuclear marker H2B-YFP in *N. benthamiana*. As shown in Figure 6.3, both SINE2-mCherry and mCherry-SINE2 were clearly co-localized with the ER network labeled by GFP-HDEL (e-j). In addition, the expression pattern of H2B-YFP and SINE2-mCherry/mCherry-SINE2 confirmed the nuclear envelope localization of SINE2 (k-p).

To determine whether the filamentous localization of SINE2 was dependent on the actin filament system, the actin-depolymerizing drug was used to disrupt the actin cytoskeleton. Leaf sections of *N. benthamiana* transient expressing mCherry-SINE2 were treated with anti-actin drug, Lat B, and this drug was also applied to leaf sections expressing Lifeact-GFP construct as a positive control for actin depolymerization. As shown in Figure 6.4, 30 minutes incubation with 50 µM Lat B was sufficient to breakdown the actin filaments labeled by the actin marker Lifeact-GFP (d-f). The filamentous network decorated by mCherry-SINE2 also disappeared and the normal ER network was restored (j-l). This result indicates that full length SINE2 is likely to associate with the actin cytoskeleton *in vivo*.

Next, the subcellular localization of SINE2 in stable Arabidopsis transgenic lines was studied. Arabidopsis transgenetic lines stably expression mCherry-SINE2 under the

control of 35s promoter were generated and the stable T3 generation was used for the sebcellular localization study. Cotyledon epidermal cells of 5 days old seedlings were imaged and at least 3 lines were analyzed. As shown in Figure 6.5, mCherry-SINE2 can only be found to localize to the nuclear membrane and no ER network or actin filament labeling can be observed. This expression pattern is similar to a previous study which reported that GFP-tagged SINE2 was associated with nuclear envelop in the Arabidopsis root tip cells (Zhou *et al.*, 2014). The different expression of SINE2 between Arabidopsis and *N. benthamiana* is probably because the nuclear envelope localization of SINE2 depends on the expression level of other intrinsic Arabidopsis proteins, such as inner nuclear membrane SUN proteins. In *N. benthamiana* cells, there are no specific interacting SUN proteins and not all SINE2 protein can be recruited to the nuclear membrane.

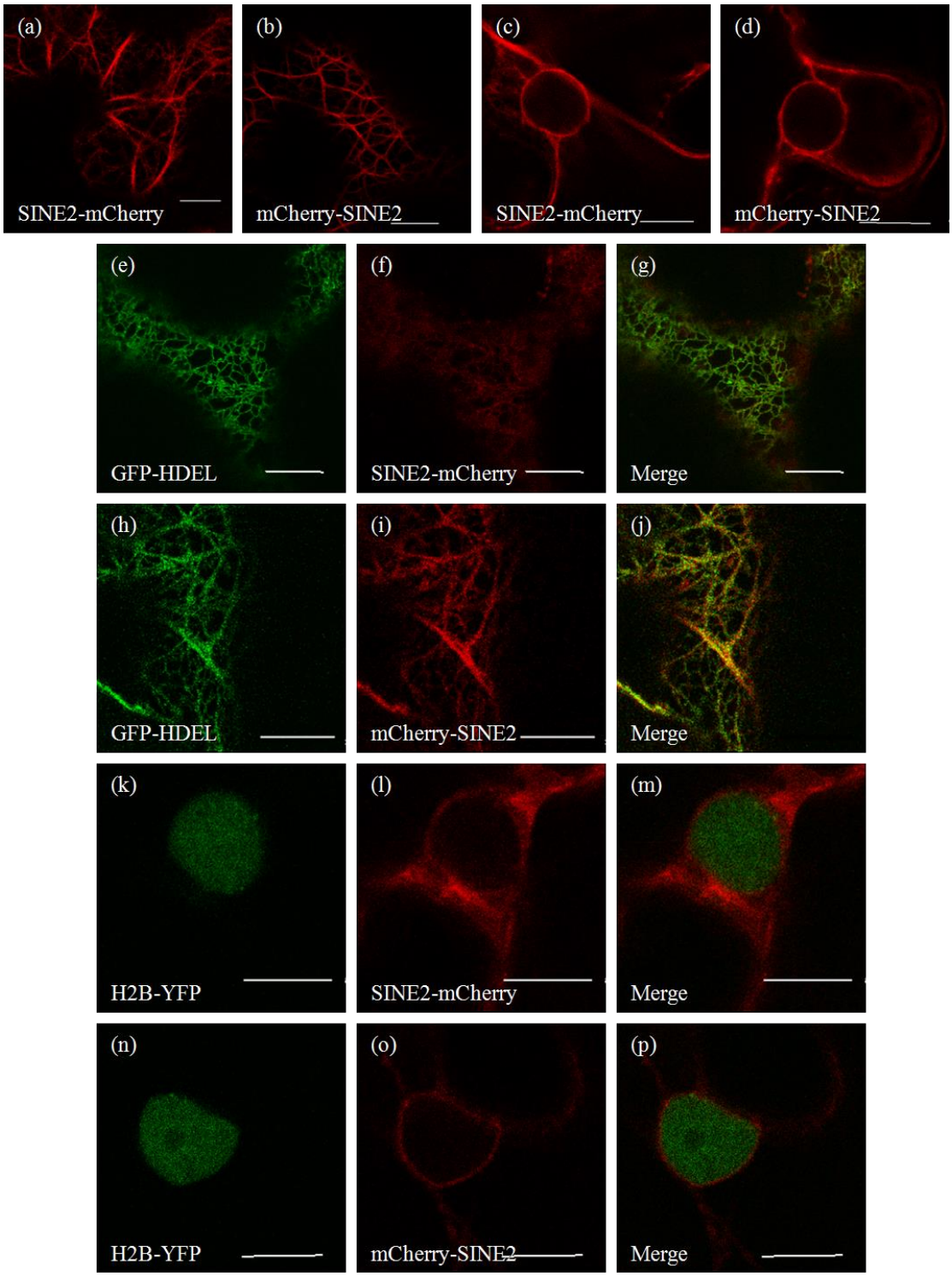

Figure 6.3 The subcellular localization of SINE2 in *N. benthamiana* leaf epidermal cells. (a)-(d): SINE2-mCherry or mCherry-SINE2 expressed alone. (e)-(j): Co-localization of SINE2-mCherry or mCherry-SINE2 with GFP-HDEL. (k)-(p): SINE2-mCherry or mCherry-SINE2 labeled nuclear envelope. Scale bar: 10 μm.

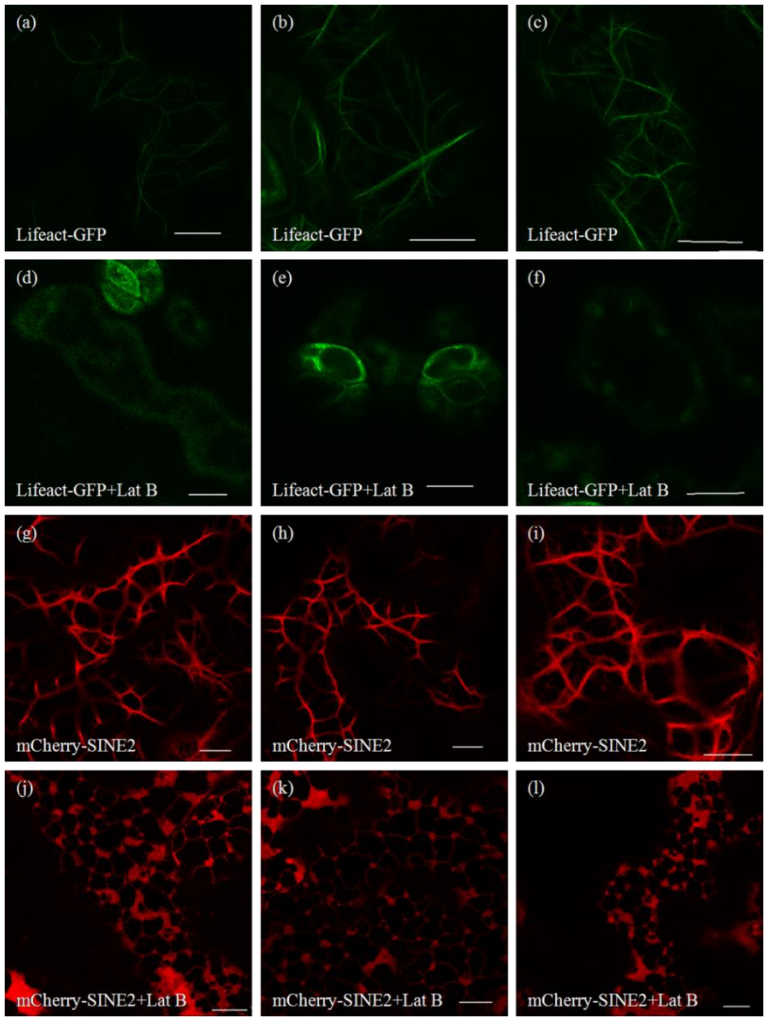

Figure 6.4 Effects of actin disrupting drug on Lifeact-GFP and mCherry-SINE2 decorated filaments. (a)-(c): *N. benthamiana* leaf sections expressing the actin marker Lifeact-GFP. (d)-(f): *N. benthamiana* leaf sections expressing the actin marker Lifeact-GFP were treated with 50 µM Latrunculin B for 30 minutes. (g)-(i): *N. benthamiana* leaf sections expressing mCherry-SINE2. (j)-(l): *N. benthamiana* leaf sections expressing mCherry-SINE2 were treated with 50 µM Lat B for 30 minutes. Scale bar: 10 µm.

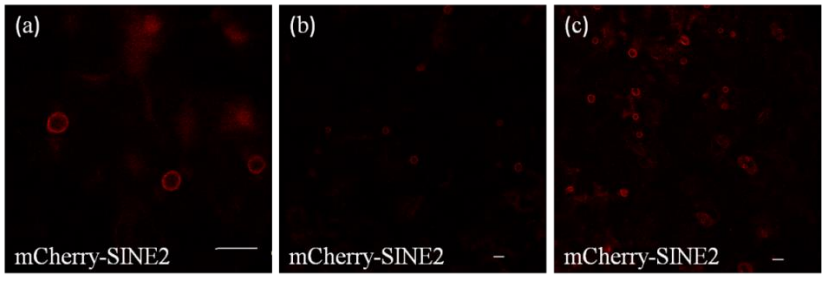

Figure 6.5 Subcellular localization of mCherry-SINE2 in Arabidopsis cotyledon epidermal cells. Arabidopsis expressing *35s*:mCherry-SINE2 in cotyledon epidermal cells. mCherry-SINE2 is localized on nuclear membrane. Scale bar: 10 µm.

6.3.3. *In vivo* Interaction Analysis between VAP27-1 and SINE2

SINE2 was identified to be a potential interactor of VAP27-1 in the proteomics screen. In order to study the interaction between these two proteins *in vivo*, the co-localization analysis between them was performed. VAP27-1-YFP and mCherry-SINE2 were co-expressed in *N. benthamiana* leaf epidermal cells using agrobacterium-mediated infiltration so that they could be visualized simultaneously. As a negative control, VAP27-1-YFP was also expressed on its own.

VAP27-1-YFP was localized to the ER network as well as the ER-PM contacts when it expressed alone (Figure 6.6, d). However, in cells expressing both VAP27-1-YFP and mCherry-SINE2, they were co-localized with each other to the ER network (Figure 6.6, a-c) and the nuclear envelope (Figure 6.6, e-g). In addition to this, the localization of VAP27-1-YFP was clearly affected.

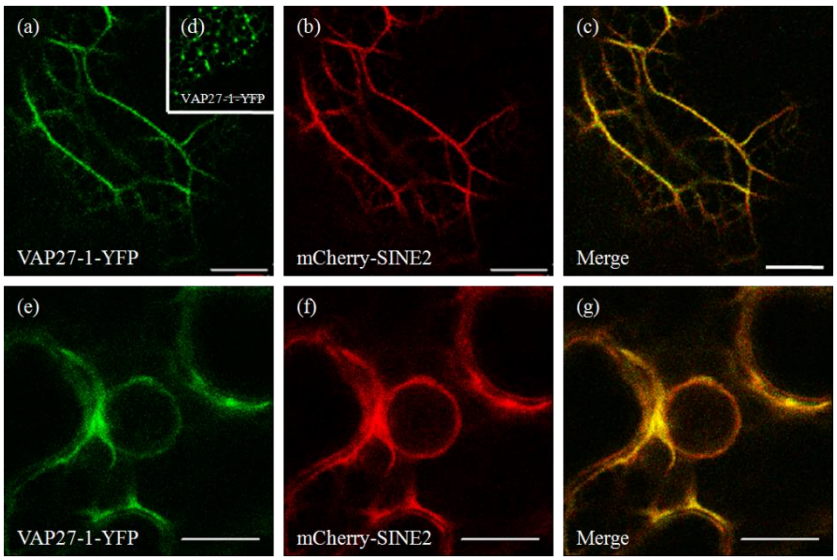

Figure 6.6 Co-localization analysis of VAP27-1 with SINE2 *in vivo*. *N. benthamiana* leaves were transformed with the fluorescently-tagged proteins. (a)-(c) and (e)-(g): Co-expression of VAP27-1-YFP with mCherry-SINE2. VAP27-1-YFP is co-localized with mCherry-SINE2 to the ER network, actin filaments as well as the nuclear envelope. (d): VAP27-1-YFP expressed alone. Scale bar: 10 µm.

FRET-FLIM and GFP-Trap assay were then performed to investigate a potential direct interaction between them. For FRET-FLIM analysis, donor FRET-FLIM

construct GFP-VAP27-1 was expressed alone, or co-expressed with the acceptor construct mCherry-SINE2 in *N. benthamiana* leaf epidermal cells. FRET-FLIM was also performed using GFP-RFP fusion protein as a positive control. As demonstrated in Figure 6.7, GFP-VAP27-1, when expressed on its own, exhibited an average fluorescence life time of 2.58±0.04 ns. However, the average fluorescence lifetime of GFP-VAP27-1 was measured at 2.44±0.04 ns in the presence of mCherry-SINE2, indicating a reduction of 0.14 ns (p=1.943e-10). Moreover, the fluorescence life time of GFP-RFP fusion protein was measured at 2.28±0.05 ns. Therefore, a physical interaction between VAP27-1 and mCherry-SINE2 could be detected using FRET-FLIM.

Next, GFP-Trap assay was performed to reconfirm the interaction. VAP27-1-RFP was co-expressed with GFP-SINE2 in *N. benthamiana* leaf epidermal cells and VAP27-1-RFP was also expressed alone as a negative control. After confirming the expression through the confocal laser scanning microscopy (CLSM), protein was extracted according to chapter 2. GFP-Trap agarose beads were used for protein precipitation as described in chapter 2. For western blotting, VAP27-1-RFP was detected with an anti-RFP antibody (1:1000, Invitrogen). As shown in figure 6.7, VAP27-1-RFP can be only observed in the pellet fraction in the presence of GFP-SINE2, suggesting an interaction between two proteins.

A

Constructs Expressed	Mean GFP Fluorescence Lifetime	Standard Deviation	n
GFP-VAP27-1	2.58 ns	0.04	42
GFP-VAP27-1+mCherry-SINE2	2.44 ns	0.04	24
GFP-RFP	2.28ns	0.05	20

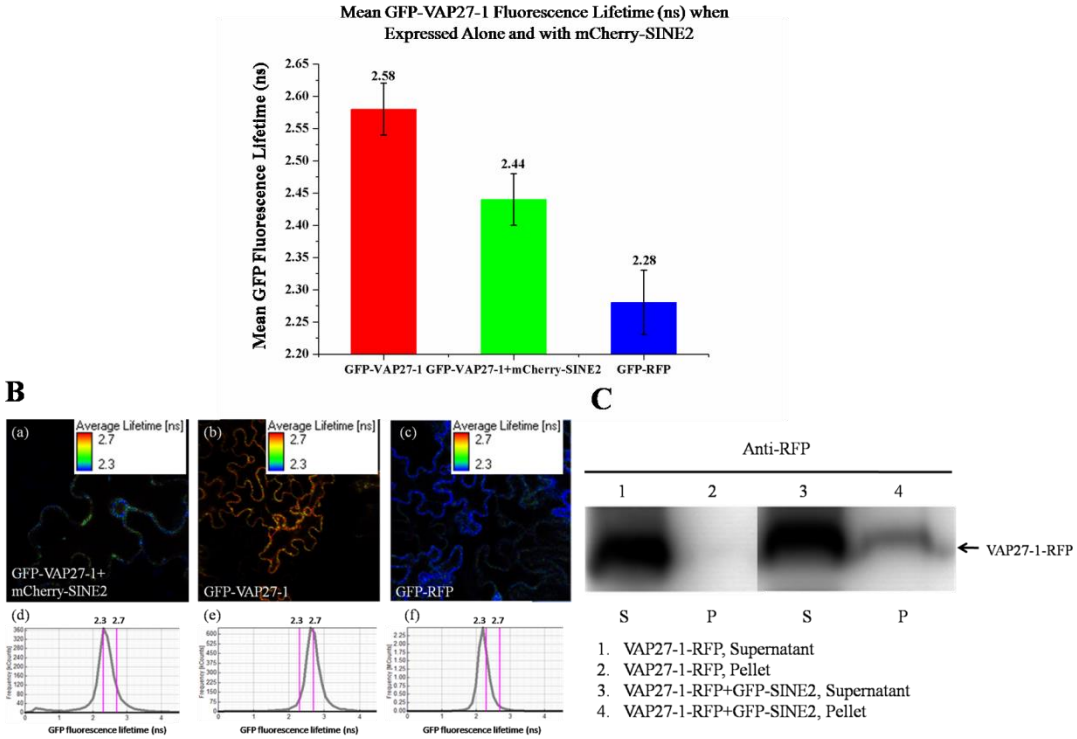

Figure 6.7 FRET-FLIM and GFP-Trap assay of SINE2-VAP27-1 interactions. A: Average fluorescence lifetime of GFP-VAP27-1 significantly reduced when co-expressed with mCherry-SINE2 in *N. benthamiana* leaf epidermal cells. n=number of cells analyzed. B: Visualization of GFP-VAP27-1 fluorescence lifetimes *in vivo* when co-expressed alone and with mCherry-SINE2. (a)-(c): example images of GFP fluorescence detected in *N. benthamiana* leaf epidermal cells, pseudocoloured according to GFP fluorescence lifetime. (d)-(f): charts associated with images (a)-(c) respectively, show the frequency distributions of the fluorescence lifetimes (ns) of detected photons in each image. A leftward shift in peak GFP fluorescence lifetime is indicative of reduced average lifetime. (a) and (d): GFP-VAP27-1 expressed alone. (b) and (e): GFP-VAP27-1 co-expressed with mCherry-SINE2. (c) and (f): GFP-RFP positive control. C: GFP-Trap assay of SINE2-VAP27-1 interaction. VAP27-1-RFP was detected with an anti-RFP antibody. GFP-Trap agarose beads do not pull down VAP27-1-RFP into pallet fraction (lanes 1 and 2), but pull down VAP27-1-RFP when co-expressed with GFP-SINE2 (lanes 3 and 4).

6.3.4. *In vivo* interaction analysis betweenNET3A with VAP27-1

According to Deeks et al. (2012), NET3A predominantly localizes at the nuclear membrane in BY2 tissue culture cells. It was investigated as to whether NET3A may interact with VAP27-1 and form a complex with SINE2 to link the nuclear envelope with the ER network and actin filaments. Using agrobacterium-mediated transformation, NET3A-GFP was transiently expressed alone or co-expressed with VAP27-1-RFP. As shown in Figure 6.8, in *N. benthamiana* leaf epidermal cells, VAP27-1-RFP labeled the ER network and NET3A-GFP appeared to be localized on the nuclear membrane and actin filaments with brighter foci distributed on them (a-c). When NET3A was co-expressed with VAP27-1, clear co-localization between them was observed.

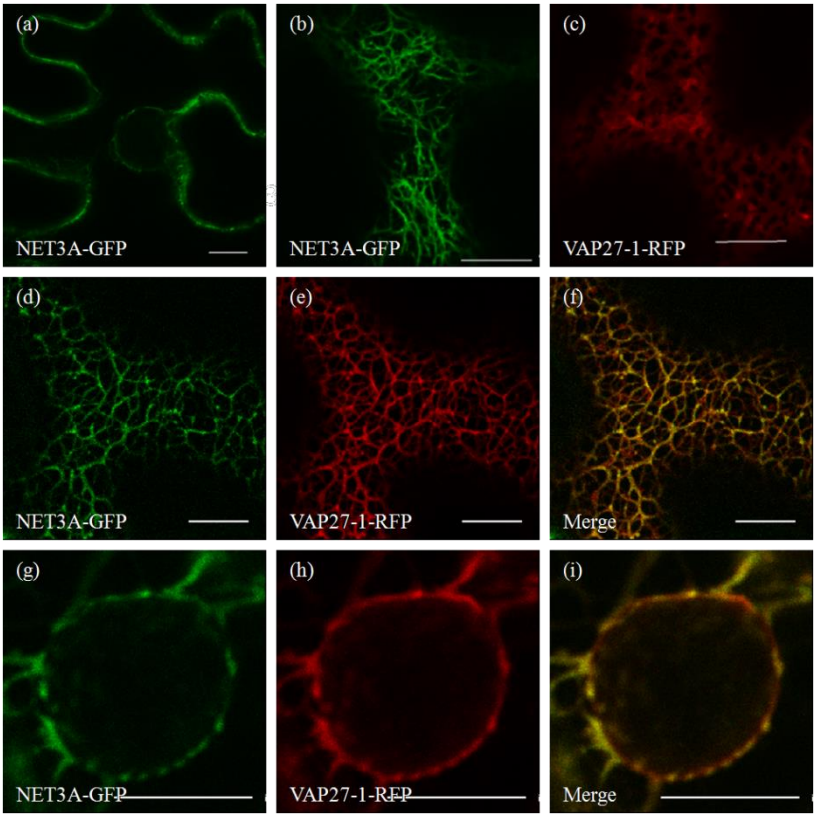

Figure 6.8 Co-localization analysis of NET3A with VAP27-1 *in vivo*. *N. benthamiana* leaves were transformed with the fluorescently-tagged proteins. (a)-(c): NET3A-GFP and VAP27-1-RFP expressed alone. (d)-(i): Co-expression of NET3A-GFP with VAP27-1-RFP. NET3A-GFP is co-localized with VAP27-1-RFP at actin filaments and nuclear envelope. Scale bar: 10 µm.

Next, FRET-FLIM was performed to investigate the direct interaction between them. Donor FRET-FLIM construct GFP-NET3A was expressed alone or co-expressed with the acceptor RFP-VAP27-1 in *N. benthamiana* leaf epidermal cells. FRET-FLIM was also performed using GFP-RFP fusion protein as a positive control. The results of the FRET-FLIM interaction assay between GFP-NET3A and RFP-VAP27-1 are shown in Figure 6.9. The average fluorescence lifetime of GFP-NET3A was found to be 2.45 ± 0.06 ns when co-expressed with RFP-VAP27-1, which was significantly reduced by 0.31 ns when compared to NET3A-GFP expressed on its own (2.76 ± 0.07 ns; p=7.25E-09), suggesting a physical interaction between these two proteins. Moreover, the fluorescence lifetime of GFP-RFP fusion protein was measured at 2.34±0.04 ns.

A

Constructs Expressed	Mean GFP Fluorescence Lifetime	Standard Deviation	n
NET3A-GFP	2.76 ns	0.07	10
NET3A-GFP+RFP-VAP27-1	2.45 ns	0.06	11
GFP-RFP	2.34ns	0.04	5

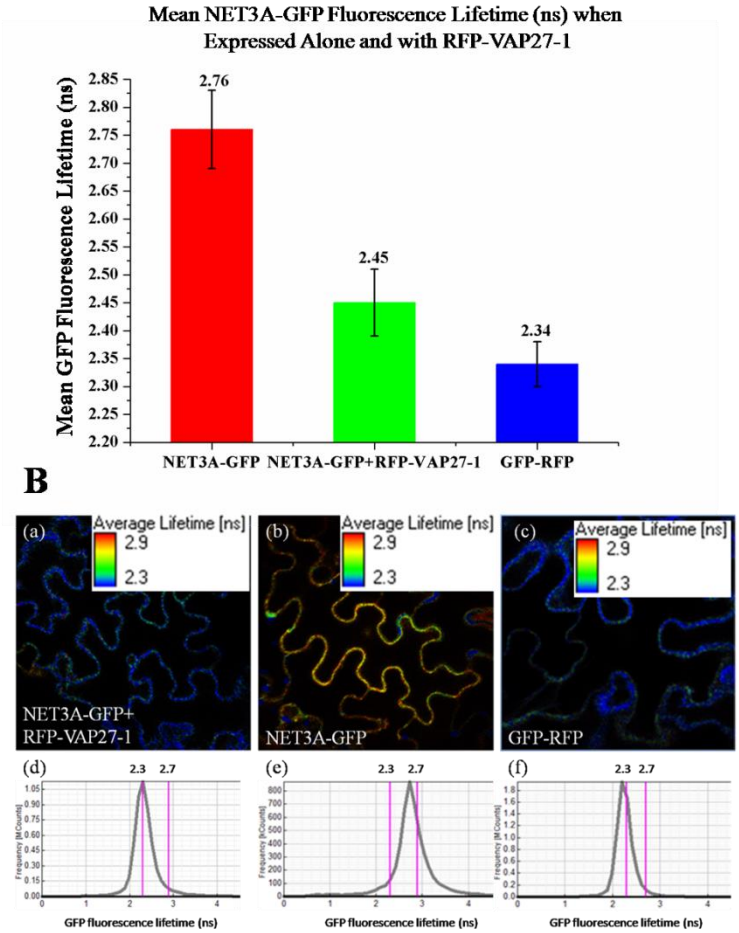

Figure 6.9 FRET-FLIM analysis of NET3A-VAP27-1 interactions. A: Average fluorescence lifetime of NET3A-GFP significantly reduced when co-expressed with RFP-VAP27-1 in *N. benthamiana* leaf epidermal cells. n=number of cells analyzed. B: Visualization of NET3A-GFP fluorescence lifetimes *in vivo* when co-expressed alone and with RFP-VAP27-1. (a)-(c): example images of GFP fluorescence detected in *N. benthamiana* leaf epidermal cells, pseudocoloured according to GFP fluorescence lifetime. (d)-(f): charts associated with images (a)-(c) respectively, show the frequency distributions of the fluorescence lifetimes (ns) of detected photons in each image. A leftward shift in peak GFP fluorescence lifetime is indicative of reduced average lifetime. (a) and (d): NET3A-GFP co-expressed with RFP-VAP27-1. (b) and (e): NET3A-GFP expressed alone. (c) and (f): GFP-RFP positive control.

6.3.5. RFP-SINE2 is Co-Localized with NET3A-GFP in the Presence of VAP27-1-YFP

As described above, VAP27-1 directly interacts with SINE2 and NET3A. Therefore, we investigated whether SINE2 may also interact with NET3A. Using agrobacterium-mediated transformation, mCherry-SINE2 was transiently co-expressed with NET3A-GFP. As shown in Figure 6.10, NET3A-GFP was not observed to be co-localized with mCherry-SINE2 (a-c). In cells expressing NET3A-GFP and mCherry-SINE2, mCherry-SINE2 was was absent from actin filaments (a-c). It is possible that the localization of SINE2 to the actin filaments may be relatively weak and its association with F-actin was disappeared in the presence of other actin-binding proteins.

Next, triple expression of VAP27-1-YFP, RFP-SINE2 and NET3A-GFP was performed in *N. benthamiana* leaf epidermal cells to investigate whether VAP27-1 is able to act as a linker between SINE2 and NET3A. As displayed in Figure 6.10, clear co-localization between SINE2 and NET3A was observed (d-g), indicating that VAP27-1 may facilitate the association between SINE2 and NET3A. Therefore, VAP27-1, SINE2, and NET3A are likely to form a protein complex to link the nuclear envelope with the ER network and actin filaments.

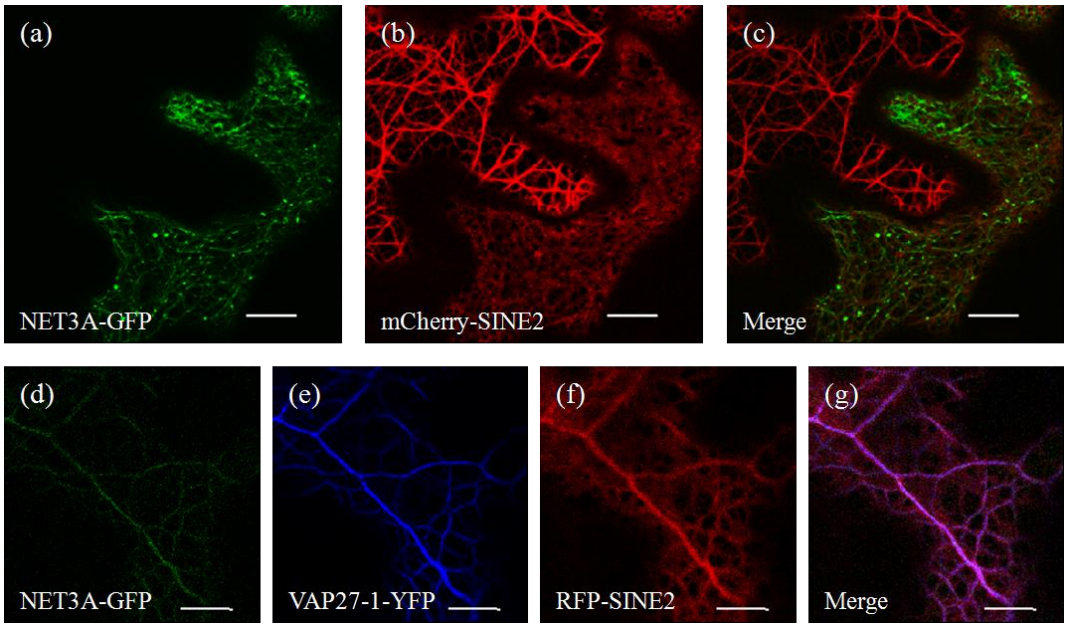

Figure 6.10 Co-localization analysis of NET3A-GFP with RFP-SINE2 in the presence of VAP27-YFP *in vivo*. *N. benthamiana* leaves were transformed with the fluorescently tagged proteins. (a)-(c): Co-expression of NET3A-GFP and mCherry-SINE2. No co-localization between them was observed (d)-(g): Co-localization of NET3A-GFP, VAP27-1-YFP and RFP-SINE2. RFP-SINE2 was found to be co-localized with NET3A-GFP in the presence of VAP27-1-YFP. Scale bar: 10 µm.

6.4. Conclusion

In this chapter, the subcellular localization of SINE2 was studied. SINE2 expressed under the control of 35s promoter was localized to the nuclear membrane, while in *N. benthamiana* leaf epidermal cells, the ER network and actin filaments were also labeled. The different expression pattern may be because the nuclear envelope localization of SINE2 depends on its interaction with AtSUN and this will be discussed later. The *in vivo* co-localization analysis of VAP27-1 with SINE2 was performed and the interaction between them was confirmed using FRET-FLIM and GFP-Trap assay. Additionally, NET3A was also confirmed to interact with VAP27-1. Therefore, VAP27-1 and NET3A are likely to form a protein complex with SINE2. This protein complex links the nuclear envelope to the ER network and actin filaments and the identification of this new protein complex may help us to understand the structural rearrangement of the ER network and nuclear envelope during mitosis in plant cells.

6.5. Discussion

6.5.1. The Localization of SINE2 is Dependent on AtSUN

In this study, mCherry-SINE2 was transiently expressed in *N. benthamiana* leaf epidermal cell and stably expressed in Arabidopsis under the control of 35s promoter. In *N. benthamiana* leaf epidermal cells, mCherry-SINE2 localized to the nuclear envelope, ER network and actin filaments. However, in Arabidopsis, only the nuclear envelope was labeled. It has been reported that in the *sun1-KO/sun2-KD* mutant Arabidopsis, GFP-tagged SINE2 was only weakly associated with the nuclear periphery and was abundantly found in the cytoplasm and associated with the PM and other components of the endomembrane system, indicating that the localization of SINE2 relies on its interaction with AtSUN (Zhou *et al.*, 2014). Upon strong expression of SINE2 under the control of the 35s promoter, the strong ER localization in tobacco cells may be because the absent of SINE2 interacting SUN proteins. Since the ER network is continuous with the nuclear envelope, the ER localization can be observed. In addition to the interaction with AtSUN, as discussed in section 3.6.1, the *N. benthamiana* transient expression system may also result in the difference in results from *N. benthamiana* and Arabidopsis.

6.5.2. VAP27 Acts as a Binding Adaptor for SINE2

VAP27-1 was observed to be co-localized with SINE2 at the nuclear envelope in *N. benthamiana* leaf epidermal cells and the interaction between these two proteins was confirmed by FRET-FLIM and GFP-Trap assay in this study. This interaction is likely to be involved in multiple biological processes.

It has been reported that the connection between nucleoskeleton and cytoskeleton is facilitated by the LINC (linker of nucleoskeleton and cytoskeleton) complex which are composed of the inner nuclear membrane localized SUN proteins and outer nuclear membrane localized KASH proteins (Zhou *et al.*, 2014). The first identified

plant-spicific KASH proteins, AtWIPs (Arabidopsis WPP domain-interacting proteins) interact with AtWITs (Arabidopsis WPP domain interacting tail anchored proteins) and synergistically recruit RanGAP1 (Ran GTPase-activating protein1) and Myosin XI-I to the nuclear envelope to regulate nuclear morphology and nuclear movement (Tamura *et al.*, 2013, Zhao *et al.*, 2008, Zhou *et al.*, 2012). Therefore, AtWITs probably function as adaptor proteins for AtWIPs.

In this study, the NET3A was confirmed to interact with VAP27. NET3A was also observed to be co-localized with SINE2 in the presence of VAP27-1. It is possible that VAP27-1 may also act as an adaptor of SINE2 and links to actin and actin associated proteins to the nuclear envelope. SINE1 has been reported to be exclusively expressed in guard cells and guard mother cells, where it associated with both the nuclear envelope fibers and actin filaments to maintain the nuclear position (Zhou *et al.*, 2014). Whereas, SINE2 is predominantly expressed in epidermal cells, mesophyll cells and trichomes (Zhou *et al.*, 2014), the SINE2-VAP27-1-NET3A complex may link actin to the nuclear envelope, regulating the morphology, position and movement of the nucleus in these cells. The structure of this complex was shown in Figure 6.11.

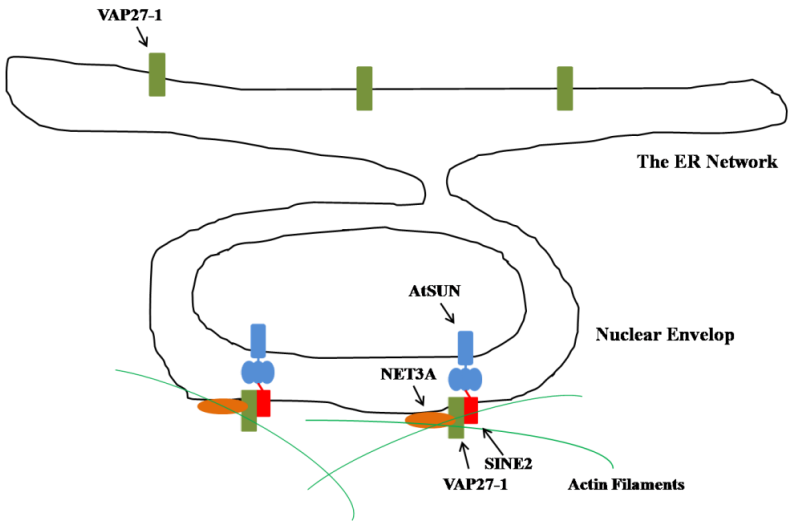

Figure 6.11 The structure of the AtSUN-SINE2-VAP27-1-NET3A complex. Diagrammatic representation of the protein complex that links the nuclear envelope to the actin filaments. AtSUN proteins localized to the inner nuclear membrane interact with the outer nuclear membrane protein, SINE2. VAP27-1 functions as a binding adaptor for SINE2, binding actin filaments to the nuclear envelope through its interaction with NET3A.

6.5.3. The Novel SINE2 Complex May Regulate the Rearrangement of the Nuclear Envelope during Mitosis

When higher eukaryotic cells enter mitosis, the nuclear envelope undergoes extensive rearrangement during nuclear envelope breakdown (NEBD) (Ungricht and Kutay, 2017). The nuclear envelope membrane proteins are disintegrated from nuclear binding partners and disperse into the ER network which is continuous with the nuclear envelope (Yang *et al.,* 1997). In vertebrate cells, the disassembly of nuclear membrane in prophase and the subsequent removal of NE/ER membrane from chromatin during prometaphase depend on a microtubule based tearing process (Ungricht and Kutay, 2017). The microtubule minus-end-directed motor, dynein generates pulling forces on the nuclear surface, facilitating the NE/ER membrane invaginations around centrosomes and promoting nuclear envelope fenestration (Beaudouin *et al.*, 2002, Muhlhausser and Kutay, 2007, Salina *et al.*, 2002).

It is also reported that the depletion of human SUN1 and SUN2 prevents the formation of the NE/ER membrane invaginations and delays the clearance of membranes from chromatin during NEBD. Inhibition of actin or microtubule polymerization was also observed to inhibit the removal of NE/ER membranes. These results indicate that the LINC protein complexes and cytoskeleton play an important role in NEBD process (Turgay *et al.*, 2014). Although a previous study reported that in cultured Arabidopsis cells, spindle microtubules penetrate and break the AtSUN1-labeled nuclear envelope at the beginning of NEBD, the changes of the nuclear envelope during the plant specific mitotic process remains poorly understood (Oda and Fukuda, 2011). Therefore, this newly identified protein complex is likely to facilitate the association of NE/ER network with actin filaments, and probably regulates the process of NEBD in coordination with microtubules during mitosis in plant cells. The possible mechanism of AtSUN-SINE2-VAP27-1-NET3A complex mediated nuclear envelope break down in plant cells is shown in Figure 6.12.

Lipid metabolism also contributes to the nuclear envelope dynamics. In metazoan cells, the unlimited PI levels led to ectopic ER sheets that encased the nuclear envelope with an extra ER membrane and interfered with nuclear envelope disassembly during cell division (Bahmanyar *et al.*, 2014). The yeast VAP proteins, Scs2/Scs22 were reported to be able to modulate PI levels at the yeast ER-PM contact sites (Stefan *et al.*, 2011). Therefore, it is likely that plant VAP27-1 also can regulate phospholipid metabolism in the vicinity of the nucleus to balance PI levels and interact with SINE2, thereby facilitating the NEBD process.

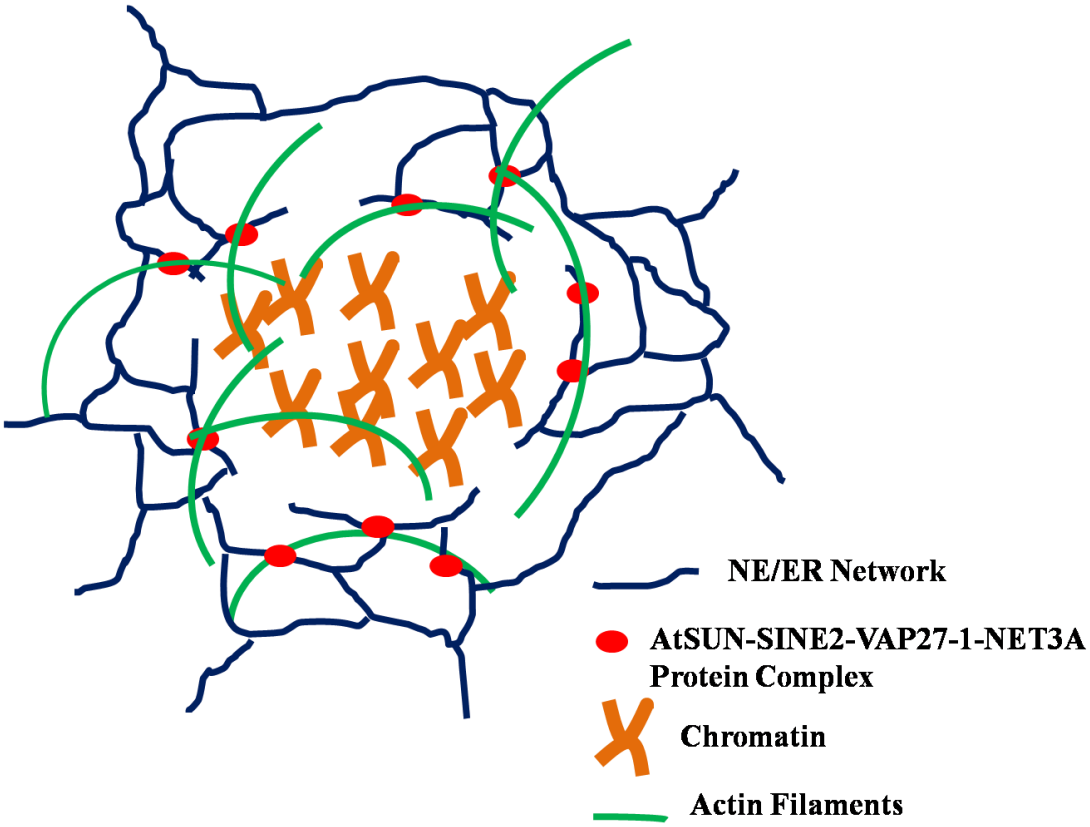

Figure 6.12 possible mechanism of nuclear envelope break down mediated by the AtSUN-SINE2-VAP27-1-NET3A complex in plant cells.

In addition to the rearrangement of the nuclear envelope, the architecture of the ER network also undergoes a major transformation during mitosis in animal cells. From prometaphase to telophase, the majority of the ER is organized as extended sheet-like structures due to the onset microtubule depolymerization during cell division (Lu *et al.*, 2009). However, the organization of the ER network during mitosis in plant cells

is not well studied. It is known that in plants, the organization and dynamics of the ER network are mainly regulated by actin filaments (Sparkes *et al.*, 2009). Therefore, it is possible that the AtSUN-SINE2-VAP27-1-NET3A protein complex which links the ER/NE network with actin filaments functions in the regulation of the ER structure during mitosis in plant cells.

At the end of mitosis, the nuclear envelope reforms around segregated chromosomes to generate the daughter nuclei. Recent data suggested that in animal cells, the ER is considered as the major source of membrane for the postmitotic reformation of the nuclear envelope and the nuclear envelope formation occurs by a massive reorganization of the tubular ER network on chromatin (Anderson and Hetzer, 2008b). The overexpression of ER tubule-forming proteins (such as reticulons) delay nuclear envelop formation and their knockdown accelerates the nuclear envelope assembly, indicating that the formation of the nuclear membrane is influenced by the transition from membrane tubules to sheets and the balance between tubules and sheets in the ER is essential for proper nuclear envelope formation (Anderson and Hetzer, 2008a). As described above, actin filaments play a critical role in the dynamics and organization of the ER network in plant cells. Therefore, it is likely that the assembly of nuclear envelope in plant cells is regulated by actin filaments and the AtSUN-SINE2-VAP27-1-NET3A protein complex may be involved in this process.

Chapter 7: Summary and Future Perspective

7.1. Summary

In plant cells, the cortical ER network contacts with the PM at the ER-PM contact sites (EPCS), whose structures are organized by the cytoskeleton as well as EPCS resident proteins, such as NET3C, VAP27-1 and STY1 (Siao *et al.*, 2016, Wang *et al.*, 2014). However, little is known about the mechanism of regulation of the cytoskeleton at plant EPCS, and its biological functions remain poorly understood. To identify potential functions of NET3C and VAP27-1 *in vivo*, protein-protein interaction screens were performed previously to obtain a list of proteins that potentially interact with NET3C or VAP27-1. According to their functions and localizations, three proteins, KLCR1, AtBRO1 and SINE2 were selected for further study. The aim of this project was to elucidate the functions for the interactions of these three proteins with NET3C or VAP27 in plant development, and understand how the different protein complexes may regulate the cytoskeleton, the morphology of the ER network and nuclear envelope.

In chapter 3, the subcellular localization of KLCR1 was studied in both *N. benthamiana* leaf epidermal cells and Arabidopsis cotyledon pavement cells and different expression patterns were observed in these two expression system. A new protein complex which is composed of NET3C, KLCR1 and IQD proteins was identified at the EPCS. This protein complex will be predicted to mediate the interaction of microtubules with actin filaments and ER network, regulating the organization of the cytoskeleton and ER structure at plant EPCSs. The identification of the NET3C-KLCR1-IQDs protein complex increases our knowledge on the mechanism of regulation of the cytoskeleton and ER structure at plant ER-PM contact sites. These were discussed in section 3.5.

In chapter 4, reverse-genetic analysis of KLCR1 and KLCR2 was performed.

Disrupting the expression of KLCR1 and KLCR2 and identification of the phenotypes arising from the mutant plants would help to investigate their possible functions in plant development. The results were discussed in section 4.5.

As described in chapter 5, AtBRO1 was observed to be associated with the actin filaments and ER network. The interaction between AtBRO1 and NET3C was also investigated. The potential role of NET3C in the ESCRT machinery through interaction with AtBRO1 was hypothesized in section 5.6.

In chapter 6, *in vivo* co-localization analysis indicated that VAP27-1, NET3A and NET3C form a protein complex with SINE2 and this protein complex is predicted to mediate the association of nuclear envelope with the ER network and actin filaments. The potential role of this complex in the structural rearrangement of the ER network and nuclear envelope during mitosis was discussed in section 6.5.

To better understand the role of protein complexes identified in this study, some further experiments would be required, as described below.

7.2. Further Characterization of the NET3C-KLCR1-IQDs Protein Complex

It has been reported that IQD5 is able to stabilize microtubules (Liang *et al.*, 2018). Therefore, it could be predicted that IQD1 and IQD2 may also have the ability to affect the dynamics of microtubules (discussed in section 4.5). Because KLCR1 can be recruited to microtubules by IQDs, therefore it is also likely to regulate microtubule dynamics. To test this hypothesis, the effects of these two proteins on cortical microtubules in Arabidopsis should be assessed. This analysis could be achieved using GFP-IQD and KLCR1-GFP overexpressing or knock out lines that carry the microtubule marker tubulin-mCherry. The growth and shrinkage rates of microtubules can be calculated by dividing the distance grown and shrunk by the total time spent in that event. The frequency of catastrophe and rescue can be calculated

from the inverse of the mean time spent in growth and shrinkage respectively. Microtubule dynamicity can be calculated by dividing the sum of the grown and shortened length by the total time (Abe and Hashimoto, 2005, Dhonukshe and Gadella, 2003). Alternatively, the direct effects of IQD1, IQD2 and KLCR1 on microtubules could also be investigated *in vitro*. Microtubule polymerization and nucleation activities can be quantified by microtubule turbidity assays (Mao *et al.*, 2005).

It has been reported that depolymerization of the cortical microtubules is essential for plants to withstand salt stress. Depolymerizing microtubules with microtubule-depolymerizing drugs was able to increase the survival rate of salt-stressed seedlings. In contrast, stabilization of microtubules using drugs that promote microtubule stability resulted in more seedling death under salt stress (Wang *et al.*, 2007). As discussed above, over-expression of IQD1, IQD2 and KLCR1 could enhance the microtubule stability. Therefore, for future study, it is necessary to investigate the survival of salt-stressed Arabidopsis seedlings overexpressing GFP-IQDs and KLCR1-GFP.

As discussed in section 4.5, the NET3C-KLCR1-IQDs complex is likely to mediate the association between actin filaments and microtubules. KLCR1 and IQDs may regulate the actin filaments through the interaction with NET3C. It has been reported that the organization and stability of actin filaments is dependent on cortical microtubules (Collings, 2008), which may be mediated by KLCR1 and IQDs. Therefore, for future study, pharmacological analysis could be performed by treating Arabidopsis seedlings overexpressing KLCR1-GFP and GFP-IQDs, or *klcr1* and *iqd* mutants with actin depolymerizing drugs, to determine their sensitivity to actin disruption.

The ER morphology in the presence of overexpressed IQD2 has been studied in the transient *N. benthamiana* system. Over-expression of IQD2 increased the area of ER cisternae and it is likely because over-expression of IQD2 affects the dynamics of

microtubules (discussed in section 4.5). Therefore, it could be speculated that the ER morphology could also be affected by KLCR1. Arabidopsis transgenic lines could be used for this analysis because over-expressed KLCR1 is mislocalized in *N. benthamiana*. Further investigation into the effects of IQDs on the ER morphology in stable Arabidopsis transgenic lines should also be considered. Co-visualization of the ER network with stably-expressed GFP-IQDs and KLCR1-GFP should be performed in stable transgenic Arabidopsis lines co-expressing both markers, which should be generated by cross-pollination of stable Arabidopsis lines described in this. Alternatively, the photostable ER-staining probe, ER-Tracker Red, could be used for visualizing the ER in live cells.

Reverse-genetic analysis of KLCR1 indicates that the loss of function of KLCR1 causes the disorganization of cortical microtubules and actin filaments, thereby resulting in root helical growth and defects in cotyledon pavement cell morphogenesis. For future studies, the light-sheet fluorescence microscopy (LSFM), a technique which can be used for long-term fluorescence imaging of growing plants (Ovecka *et al.*, 2015), could be used to investigate the changes in actin filaments and microtubules during the development of *klcr1* mutants and wild type plants. This analysis may be likely to reveal how KLCR1 regulates the organization of actin filaments and microtubules during plant development.

7.3. Further Perspectives of the role of the NET3A-VAP27-1-SINE2 Complex

During this study, VAP27-1 was determined to interact with SINE2 using FRET-FLIM and GFP-Trap assay in the transient *N. benthamiana* system. Therefore, it is interesting to investigate whether VAP27-1 is also able to interact with other members of plant KASH proteins to see if the role of SINE2 is functionally redundant to other KASH protein members. In addition, it is necessary to confirm the interaction between VAP27-1 and SINE2 in the stable Arabidopsis transgenic lines and see if the

localization of SINE2 can be affected because of its interaction with VAP27-1. Cross-pollination of mCherry-SINE2 and VAP27-YFP plants could be performed to create plants expressing both constructs.

As discussed in section 6.5, SINE2 forms a protein complex with VAP27-1 and NET3A. This protein complex links the nuclear envelope to the ER network and actin filaments and is likely to be involved in the rearrangement of the ER network and nuclear envelope throughout the plant cell cycle. In order to understand the dynamics of VAP27-1 and SINE2 during the cell division process, they can be observed simultaneously by transforming BY2 cells with VAP27-1-GFP and mCherry-SINE2. The real-time spinning disk confocal microscopy can be used to image live BY2 cells at different stages throughout the cell cycle (Lu *et al.*, 2009). In addition, reverse-genetic analysis of VAP27-1 is necessary to reveal the importance of the SINE2-VAP27-1-NET3C protein complex. In *vap27-1* mutants, the indirect interaction between SINE2 and NET3A is abolished, thereby affecting the association between the NE/ER membrane and actin filaments. As discussed in section 6.5, this association may be involved in the process of nuclear envelope break down (NEBD) and nuclear envelope reformation. Therefore, the loss of function of VAP27-1 is likely to result in defects of the nuclear morphology and reorganization of the nuclear envelope during plant cell mitosis.

7.4 Investigating NET3C-AtBRO1 interactions

NET3C was confirmed to directly interact with AtBRO1 in chapter 5. It is known that AtBRO1 is engaged in the ESCRT-I and ESCRT-III complexes which are involved in the biogenesis of the multivesicular body (MVB) and MVB-mediated membrane ubiquitinated protein sorting (Shen *et al.*, 2016). To understand the importance of NET3C in the ESCRT machinery in plant cells, some further experiments should be performed.

The interaction analysis should be performed between NET3C and some other

components of the ESCRT-1 and ESCRT-III complexes to investigate which complex NET3C performs a function in. Reverse-genetic analysis of NET3C is critical to investigate its role in protein sorting and endosomal budding processes at the PM. It has been reported that VAP27-1 and VAP27-3 interact with clathrin and function in endocytosis and plant growth (Stefano *et al.*, 2018). Therefore, it could be speculated that plant ER-PM contacts are involved in plant endocytosis. NET3C may function in the ESCRT complex to deform and sever membrane necks from the inside. FM4-64 (a PM dye) internalization assay can be used to trace the endocytic process (Bashline *et al.*, 2015). This analysis could be achieved by treating roots of mutants and wild type plants with FM4-64 which can be internalized into endosomes. The intracellular FM4-64 punctae can be visualized using the confocal imaging. The fluorescence intensity of the punctae can be used to quantify the FM4-64 internalization. Decreased fluorescence levels indicate a delay in endocytosis (Bashline *et al.*, 2015). In addition, Transmission electron microscopy (TEM) study of root tips of *net3c* should also be conducted to investigate the effects of NET3C on sorting proteins into the ILVs (intraluminal vesicles) of MVBs. Immunogold labeling with anti-VSR antibodies can be used to visualize the MVBs with numerous ILVs. If the loss of function of NET3C results in defects in the formation of ILVs in MVBs, the number of ILVs per MVB could be reduced.

Appendices

Appendix 1: Primers

1.1. Primers used to Amplify Full-Length Coding Sequences for Insertion into pDONR207

Primer name	Sequence	Tm (°C)	Target gene
KLCR2-F	GGGGACAAGTTTGTACAAAAAAGCAGGCTT CCCGCCAATGGACGTAGGAGAGAGCAATG	56	*KLCR2* (AT3G27960)
KLCR2-CR (C-terminal fusion)	GGGGACCACTTTGTACAAGAAAGCTGGGTCA TAAACCGGTCTCTGTCCATTTGC	56	
KLCR2-NR (N-terminal fusion)	GGGGACCACTTTGTACAAGAAAGCTGGGTCT CAATAAACCGGTCTCTGTCCATTT	56	
AtBRO1-F	GGGGACAAGTTTGTACAAAAAAGCAGGCTT CCCGCCAATGGCTTCTTCTTCGCTCTCT	56	*AtBRO1* (AT1G15130)
AtBRO1-CR(C-terminal fusion)	GGGGACCACTTTGTACAAGAAAGCTGGGTCT TGCCTGTAGTATCCTCCACCTTG	57	
SINE2-F	GGGGACAAGTTTGTACAAAAAAGCAGGCTT CCCGCCAATGGGAAGAAATCTTGGTTCGGC	56	*SINE2* (AT3G03970)
SINE2-CR (C-terminal fusion)	GGGGACCACTTTGTACAAGAAAGCTGGGTC AGTCGGAACAAGATGAGGAGGC	56	
SINE2-NR (N-terminal fusion)	GGGGACCACTTTGTACAAGAAAGCTGGGTCT TAAGTCGGAACAAGATGAGGAGG	56	

1.2. Primers used to Amplify Full Length KLCR1 with its promoter region

Primer name	Sequence	Tm (°C)	Target gene
KLCR1-F	GGGGACAAGTTTGTACAAAAAAGCAGGCTTCC CGCCA CAGAGATATCAATCTTACGGATGGAC	56	*KLCR1* (AT4G10840)
KLCR1-R	GGGGACCACTTTGTACAAGAAAGCTGGGTC GAACTTGAAACCGAGGCTGGG	55	

1.3. Primers used to Amplify truncations of KLCR1

Primer name	Sequence	Tm (°C)	Target gene
KLCR1ΔC-F	GGGGACAAGTTTGTACAAAAAAGCAGGCTTCC CGCCAATGCCAGCAATGCCAGGTCTCG	59	*KLCR1* (0-807 bp)
KLCR1ΔC-R	GGGGACCACTTTGTACAAGAAAGCTGGGTC ATCAGCTGCTTCCTCCAGTGAAGC	59	
KLCR1ΔN-F	GGGGACAAGTTTGTACAAAAAAGCAGGCTTCC CGCCAATGAGGAGATTGATGGCAATTATCTGC	57	*KLCR1* (808-1830 bp)
KLCR1ΔN-R	GGGGACCACTTTGTACAAGAAAGCTGGGTC GAACTTGAAACCGAGGCTGGG	56	

1.4. Genotyping Primers

Primer name	Sequence	Tm (°C)	Target gene
KLCR1-SF	GCTTGTTATGAAGAAGGTCTTAAGATC	55	*KLCR1*
KLCR1-SR	AGATAGTTTTCTTTAGGACTTTACCTTCC	56	*KLCR1*
KLCR2-SF	TATTTAAAGAGAGAGTGCAAGTAGGG	55	*KLCR2*
KLCR2-SR	CACCAAATTCAACCCAAGTTGTTTCT	55	*KLCR2*
KLCR2-S6F	ATGGACGTAGGAGAGAGCAATG	55	*KLCR2*
KLCR2-S6R	TGACATTGCCATGCTCGCTA	52	*KLCR2*
KLCR2-GF	TCTCAGAACCATAGAGAAGATGTTG	54	*KLCR2*
KLCR2-GR	TCAATAAACCGGTCTCTGTCCATTT	54	*KLCR2*
AtBRO1-8F	GCTATCGGAAGTTGTCTCTTAACTTC	56	*AtBRO1*
AtBRO1-8R	AGTACTTTGATCCATCATGCAAGACA	55	*AtBRO1*
AtBRO1-7R	TCATTGCCTGTAGTATCCTCCACC	57	*AtBRO1*
LB1	GCCTTTTCAGAAATGGATAAATAGCCTTGCTTCC	62	SAIL T-DNA left border
LBb1.3	ATTTTGCCGATTTCGGAAC	50	SALK T-DNA left border
o8409	ATATTGACCATCATACTCATTGC	50	GABI KAT T-DNA left border

1.5. Primers used for RT-PCR

Primer name	Sequence	Tm (°C)	Target gene
KLCR1-BF	ATGCCAGCAATGCCAGGTCT	54	*KLCR1*
KLCR1-BR	CTTCTGCTAAGTACCTGCAAGTTT	54	*KLCR1*
KLCR1-AF	GCTATGGGAAGGATAGAGGATGC	57	*KLCR2*
KLCR1-AR	TCAGAACTTGAAACCGAGGCTG	55	*KLCR2*
KLCR2-BF	ATGGACGTAGGAGAGAGCAATG	55	*KLCR2*
KLCR2-BR	CTGACTCAAGCTACCTTCTCCA	55	*KLCR2*
KLCR2-AF	TGTTGCTGCTGTAGATTGCAG	52	*KLCR2*
KLCR2-AR	GCATCATCTAACCTTCCCATTGC	55	*KLCR2*
KLCR2-RR	TCAATAAACCGGTCTCTGTCCATTT	54	*KLCR2*

References

Abe, T. & Hashimoto, T. (2005). Altered microtubule dynamics by expression of modified alpha-tubulin protein causes right-handed helical growth in transgenic Arabidopsis plants. *Plant J* **43**, 191-204.

Abel, S., Burstenbinder, K. & Muller, J. (2013). The emerging function of IQD proteins as scaffolds in cellular signaling and trafficking. *Plant Signal Behav* **8**, e24369.

Alonso, J. M., Stepanova, A. N., Leisse, T. J., Kim, C. J., Chen, H., Shinn, P., Stevenson, D. K., Zimmerman, J., Barajas, P., Cheuk, R., Gadrinab, C., Heller, C., Jeske, A., Koesema, E., Meyers, C. C., Parker, H., Prednis, L., Ansari, Y., Choy, N., Deen, H., Geralt, M., Hazari, N., Hom, E., Karnes, M., Mulholland, C., Ndubaku, R., Schmidt, I., Guzman, P., Aguilar-Henonin, L., Schmid, M., Weigel, D., Carter, D. E., Marchand, T., Risseeuw, E., Brogden, D., Zeko, A., Crosby, W. L., Berry, C. C. & Ecker, J. R. (2003). Genome-wide insertional mutagenesis of Arabidopsis thaliana. *Science* **301**, 653-7.

Amarilio, R., Ramachandran, S., Sabanay, H. & Lev, S. (2005). Differential regulation of endoplasmic reticulum structure through VAP-Nir protein interaction. *J Biol Chem* **280**, 5934-44.

Ambrose, J. C., Li, W., Marcus, A., Ma, H. & Cyr, R. (2005). A minus-end-directed kinesin with plus-end tracking protein activity is involved in spindle morphogenesis. *Mol Biol Cell* **16**, 1584-92.

Amendola, M. & van Steensel, B. (2014). Mechanisms and dynamics of nuclear lamina-genome interactions. *Curr Opin Cell Biol* **28**, 61-8.

Anderson, D. J. & Hetzer, M. W. (2008a). Reshaping of the endoplasmic reticulum limits the rate for nuclear envelope formation. *J Cell Biol* **182**, 911-24.

Anderson, D. J. & Hetzer, M. W. (2008b). Shaping the endoplasmic reticulum into the nuclear envelope. *J Cell Sci* **121**, 137-42.

Andreeva, Z., Ho, A. Y. Y., Barthet, M. M., Potocky, M., Bezvoda, R., Zarsky, V. & Marc, J. (2009). Phospholipase D family interactions with the cytoskeleton: isoform delta promotes plasma membrane anchoring of cortical microtubules. *Functional Plant Biology* **36**, 600-612.

Azimzadeh, J., Nacry, P., Christodoulidou, A., Drevensek, S., Camilleri, C., Amiour, N., Parcy, F., Pastuglia, M. & Bouchez, D. (2008). Arabidopsis TONNEAU1 proteins are essential for preprophase band formation and interact with centrin. *Plant Cell* **20**, 2146-59.

Bahmanyar, S., Biggs, R., Schuh, A. L., Desai, A., Muller-Reichert, T., Audhya, A., Dixon, J. E. & Oegema, K. (2014). Spatial control of phospholipid flux restricts endoplasmic reticulum sheet formation to allow nuclear envelope breakdown. *Genes Dev* **28**, 121-6.

Barlowe, C. K. & Miller, E. A. (2013). Secretory protein biogenesis and traffic in the early secretory pathway. *Genetics* **193**, 383-410.

Bashline, L., Li, S., Zhu, X. & Gu, Y. (2015). The TWD40-2 protein and the AP2 complex cooperate in the clathrin-mediated endocytosis of cellulose synthase to regulate cellulose biosynthesis. *Proc Natl Acad Sci U S A* **112**, 12870-5.

Bayer, E. M., Sparkes, I., Vanneste, S. & Rosado, A. (2017). From shaping organelles to signalling platforms: the emerging functions of plant ER-PM contact sites. *Curr Opin Plant Biol* **40**, 89-96.

Beaudouin, J., Gerlich, D., Daigle, N., Eils, R. & Ellenberg, J. (2002). Nuclear envelope breakdown proceeds by microtubule-induced tearing of the lamina. *Cell* **108**, 83-96.

Behnia, R. & Munro, S. (2005). Organelle identity and the signposts for membrane traffic. *Nature* **438**, 597.

Bisgrove, S. R., Lee, Y. R., Liu, B., Peters, N. T. & Kropf, D. L. (2008). The microtubule plus-end binding protein EB1 functions in root responses to touch and gravity signals in Arabidopsis. *Plant Cell* **20**, 396-410.

Blanchoin, L. & Staiger, C. J. (2010). Plant formins: diverse isoforms and unique molecular mechanism. *Biochim Biophys Acta* **1803**, 201-6.

Blatch, G. L. & Lassle, M. (1999). The tetratricopeptide repeat: a structural motif mediating protein-protein interactions. *Bioessays* **21**, 932-9.

Boevink, P., Oparka, K., Santa Cruz, S., Martin, B., Betteridge, A. & Hawes, C. (1998). Stacks on tracks: the plant Golgi apparatus traffics on an actin/ER network. *Plant J* **15**, 441-7.

Boruc, J., Zhou, X. & Meier, I. (2012). Dynamics of the plant nuclear envelope and nuclear pore. *Plant Physiol* **158**, 78-86.

Boudaoud, A., Burian, A., Borowska-Wykret, D., Uyttewaal, M., Wrzalik, R., Kwiatkowska, D. & Hamant, O. (2014). FibrilTool, an ImageJ plug-in to quantify fibrillar structures in raw microscopy images. *Nat Protoc* **9**, 457-63.

Brady, S. T. (1985). A novel brain ATPase with properties expected for the fast axonal transport motor. *Nature* **317**, 73-5.

Breeze, E., Dzimitrowicz, N., Kriechbaumer, V., Brooks, R., Botchway, S. W., Brady, J. P., Hawes, C., Dixon, A. M., Schnell, J. R. & Fricker, M. D. (2016). A C-terminal amphipathic helix is necessary for the in vivo tubule-shaping function of a plant reticulon. *Proceedings of the National Academy of Sciences* **113**, 10902-10907.

Bringmann, M., Li, E., Sampathkumar, A., Kocabek, T., Hauser, M. T. & Persson, S. (2012). POM-POM2/cellulose synthase interacting1 is essential for the functional association of cellulose synthase and microtubules in Arabidopsis. *Plant Cell* **24**, 163-77.

Broussard, J. A., Rappaz, B., Webb, D. J. & Brown, C. M. (2013). Fluorescence resonance energy transfer microscopy as demonstrated by measuring the activation of the serine/threonine kinase Akt. *Nature protocols* **8**, 265.

Burstenbinder, K., Moller, B., Plotner, R., Stamm, G., Hause, G., Mitra, D. & Abel, S. (2017). The IQD Family of Calmodulin-Binding Proteins Links Calcium Signaling to Microtubules, Membrane Subdomains, and the Nucleus. *Plant Physiol* **173**, 1692-1708.

Burstenbinder, K., Savchenko, T., Muller, J., Adamson, A. W., Stamm, G., Kwong, R., Zipp, B. J., Dinesh, D. C. & Abel, S. (2013). Arabidopsis calmodulin-binding protein IQ67-domain 1 localizes to microtubules and interacts with kinesin light chain-related protein-1. *J Biol Chem* **288**, 1871-82.

Cabezas, A., Bache, K. G., Brech, A. & Stenmark, H. (2005). Alix regulates cortical actin and the spatial distribution of endosomes. *Journal of cell science* **118**, 2625-2635.

Cao, P., Renna, L., Stefano, G. & Brandizzi, F. (2016). SYP73 anchors the ER to the actin cytoskeleton for maintenance of ER integrity and streaming in Arabidopsis. *Current Biology* **26**, 3245-3254.

Capasso, J. M., Keenan, T. W., Abeijon, C. & Hirschberg, C. B. (1989). Mechanism of phosphorylation in the lumen of the Golgi apparatus. Translocation of adenosine 5'-triphosphate into Golgi vesicles from rat liver and mammary gland. *J Biol Chem* **264**, 5233-40.

Cardona-Lopez, X., Cuyas, L., Marin, E., Rajulu, C., Irigoyen, M. L., Gil, E., Puga, M. I., Bligny, R., Nussaume, L., Geldner, N., Paz-Ares, J. & Rubio, V. (2015). ESCRT-III-Associated Protein ALIX Mediates High-Affinity Phosphate Transporter Trafficking to Maintain Phosphate Homeostasis in Arabidopsis. *Plant Cell* **27**, 2560-81.

Carrasco, S. & Meyer, T. (2011). STIM proteins and the endoplasmic reticulum-plasma membrane junctions. *Annu Rev Biochem* **80**, 973-1000.

Chang-Jie, J. & Sonobe, S. (1993). Identification and preliminary characterization of

a 65 kDa higher-plant microtubule-associated protein. *J Cell Sci* **105 (Pt 4)**, 891-901.

Chen, J., Stefano, G., Brandizzi, F. & Zheng, H. (2011). Arabidopsis RHD3 mediates the generation of the tubular ER network and is required for Golgi distribution and motility in plant cells. *Journal of cell science*, jcs. 084624.

Chen, Y.-F., Randlett, M. D., Findell, J. L. & Schaller, G. E. (2002). Localization of the ethylene receptor ETR1 to the endoplasmic reticulum of Arabidopsis. *Journal of Biological Chemistry* **277**, 19861-19866.

Chen, Y., Chen, T., Shen, S., Zheng, M., Guo, Y., Lin, J., Baluška, F. & Šamaj, J. (2006). Differential display proteomic analysis of Picea meyeri pollen germination and pollen-tube growth after inhibition of actin polymerization by latrunculin B. *The Plant Journal* **47**, 174-195.

Chung, K. P., Zeng, Y. & Jiang, L. (2016). COPII Paralogs in Plants: Functional Redundancy or Diversity? *Trends Plant Sci* **21**, 758-769.

Ciska, M. & Moreno Diaz de la Espina, S. (2014). The intriguing plant nuclear lamina. *Front Plant Sci* **5**, 166.

Clontech. (2013). Matchmaker® Gold Yeast Two-Hybrid System User Manual. Available at http://www.clontech.com. (Accessed July 2015).

Collings, D. A. (2008). Crossed-Wires: Interactions and Cross-Talk Between the Microtubule and MicrofilamentNetworks in Plants. In *Plant Microtubules: Development and Flexibility* (ed. P. Nick), pp. 47-79. Springer Berlin Heidelberg: Berlin, Heidelberg.

Crisp, M., Liu, Q., Roux, K., Rattner, J. B., Shanahan, C., Burke, B., Stahl, P. D. & Hodzic, D. (2006). Coupling of the nucleus and cytoplasm: role of the LINC complex. *J Cell Biol* **172**, 41-53.

Day, R. N. & Davidson, M. W. (2012). Fluorescent proteins for FRET microscopy: monitoring protein interactions in living cells. *Bioessays* **34**, 341-350.

De Craene, J. O., Courte, F., Rinaldi, B., Fitterer, C., Herranz, M. C., Schmitt-Keichinger, C., Ritzenthaler, C. & Friant, S. (2014). Study of the plant COPII vesicle coat subunits by functional complementation of yeast Saccharomyces cerevisiae mutants. *PLoS One* **9**, e90072.

De Magistris, P. & Antonin, W. (2018). The Dynamic Nature of the Nuclear Envelope. *Curr Biol* **28**, R487-R497.

Deeks, M. J., Calcutt, J. R., Ingle, E. K., Hawkins, T. J., Chapman, S., Richardson, A. C., Mentlak, D. A., Dixon, M. R., Cartwright, F., Smertenko, A. P., Oparka, K. & Hussey, P. J. (2012). A superfamily of actin-binding proteins at the

actin-membrane nexus of higher plants. *Curr Biol* **22**, 1595-600.

Deeks, M. J., Fendrych, M., Smertenko, A., Bell, K. S., Oparka, K., Cvrčková, F., Žárský, V. & Hussey, P. J. (2010). The plant formin AtFH4 interacts with both actin and microtubules, and contains a newly identified microtubule-binding domain. *J Cell Sci* **123**, 1209-1215.

Desai, A. & Mitchison, T. J. (1997). Microtubule polymerization dynamics. *Annu Rev Cell Dev Biol* **13**, 83-117.

Devos, D. P., Graf, R. & Field, M. C. (2014). Evolution of the nucleus. *Curr Opin Cell Biol* **28**, 8-15.

Dhonukshe, P. & Gadella, T. W., Jr. (2003). Alteration of microtubule dynamic instability during preprophase band formation revealed by yellow fluorescent protein-CLIP170 microtubule plus-end labeling. *Plant Cell* **15**, 597-611.

Dittmer, T. A., Stacey, N. J., Sugimoto-Shirasu, K. & Richards, E. J. (2007). LITTLE NUCLEI genes affecting nuclear morphology in Arabidopsis thaliana. *Plant Cell* **19**, 2793-803.

Drevensek, S., Goussot, M., Duroc, Y., Christodoulidou, A., Steyaert, S., Schaefer, E., Duvernois, E., Grandjean, O., Vantard, M., Bouchez, D. & Pastuglia, M. (2012). The Arabidopsis TRM1-TON1 interaction reveals a recruitment network common to plant cortical microtubule arrays and eukaryotic centrosomes. *Plant Cell* **24**, 178-91.

Duckney, P., Deeks, M. J., Dixon, M. R., Kroon, J., Hawkins, T. J. & Hussey, P. J. (2017). Actin-membrane interactions mediated by NETWORKED2 in Arabidopsis pollen tubes through associations with Pollen Receptor-Like Kinase 4 and 5. *New Phytol* **216**, 1170-1180.

Edwards, K., Johnstone, C. & Thompson, C. (1991). A simple and rapid method for the preparation of plant genomic DNA for PCR analysis. *Nucleic Acids Res* **19**, 1349.

Ehrhardt, D. W. & Shaw, S. L. (2006). Microtubule dynamics and organization in the plant cortical array. *Annu Rev Plant Biol* **57**, 859-75.

Ellgaard, L., Molinari, M. & Helenius, A. (1999). Setting the standards: quality control in the secretory pathway. *Science* **286**, 1882-1888.

Elliott, A. & Shaw, S. L. (2018). Update: Plant Cortical Microtubule Arrays. *Plant Physiol* **176**, 94-105.

Enrique, M., Mandinova, A., Steinmetz, M. O., Stoffler, D., Aebi, U. & Pollard, T. D. (2000). Polymerization and structure of nucleotide-free actin filaments. *Journal of*

molecular biology **295**, 517-526.

Erhardt, M., Stoppin-Mellet, V., Campagne, S., Canaday, J., Mutterer, J., Fabian, T., Sauter, M., Muller, T., Peter, C., Lambert, A. M. & Schmit, A. C. (2002). The plant Spc98p homologue colocalizes with gamma-tubulin at microtubule nucleation sites and is required for microtubule nucleation. *J Cell Sci* **115**, 2423-31.

Etienne-Manneville, S. & Hall, A. (2002). Rho GTPases in cell biology. *Nature* **420**, 629-35.

Evans, D. E., Pawar, V., Smith, S. J. & Graumann, K. (2014). Protein interactions at the higher plant nuclear envelope: evidence for a linker of nucleoskeleton and cytoskeleton complex. *Front Plant Sci* **5**, 183.

Faso, C., Chen, Y. N., Tamura, K., Held, M., Zemelis, S., Marti, L., Saravanan, R., Hummel, E., Kung, L., Miller, E., Hawes, C. & Brandizzi, F. (2009). A missense mutation in the Arabidopsis COPII coat protein Sec24A induces the formation of clusters of the endoplasmic reticulum and Golgi apparatus. *Plant Cell* **21**, 3655-71.

Fields, S. & Song, O.-k. (1989). A novel genetic system to detect protein–protein interactions. *Nature* **340**, 245.

Finn, R. D., Bateman, A., Clements, J., Coggill, P., Eberhardt, R. Y., Eddy, S. R., Heger, A., Hetherington, K., Holm, L., Mistry, J., Sonnhammer, E. L., Tate, J. & Punta, M. (2014). Pfam: the protein families database. *Nucleic Acids Res* **42**, D222-30.

Frank, M. J. & Smith, L. G. (2002). A small, novel protein highly conserved in plants and animals promotes the polarized growth and division of maize leaf epidermal cells. *Curr Biol* **12**, 849-53.

Frey, N., Klotz, J. & Nick, P. (2009). Dynamic bridges--a calponin-domain kinesin from rice links actin filaments and microtubules in both cycling and non-cycling cells. *Plant Cell Physiol* **50**, 1493-506.

Friml, J. & Jones, A. R. (2010). Endoplasmic reticulum: the rising compartment in auxin biology. *Plant Physiology* **154**, 458-462.

Fu, Y., Gu, Y., Zheng, Z., Wasteneys, G. & Yang, Z. (2005). Arabidopsis interdigitating cell growth requires two antagonistic pathways with opposing action on cell morphogenesis. *Cell* **120**, 687-700.

Fu, Y., Li, H. & Yang, Z. (2002). The ROP2 GTPase controls the formation of cortical fine F-actin and the early phase of directional cell expansion during Arabidopsis organogenesis. *Plant Cell* **14**, 777-94.

Fu, Y., Xu, T., Zhu, L., Wen, M. & Yang, Z. (2009). A ROP GTPase signaling pathway controls cortical microtubule ordering and cell expansion in Arabidopsis. *Curr Biol* **19**, 1827-32.

Furutani, I., Watanabe, Y., Prieto, R., Masukawa, M., Suzuki, K., Naoi, K., Thitamadee, S., Shikanai, T. & Hashimoto, T. (2000). The SPIRAL genes are required for directional control of cell elongation in Aarabidopsis thaliana. *Development* **127**, 4443-53.

Gaillard, J., Neumann, E., Van Damme, D., Stoppin-Mellet, V., Ebel, C., Barbier, E., Geelen, D. & Vantard, M. (2008). Two microtubule-associated proteins of Arabidopsis MAP65s promote antiparallel microtubule bundling. *Mol Biol Cell* **19**, 4534-44.

Galva, C., Kirik, V., Lindeboom, J. J., Kaloriti, D., Rancour, D. M., Hussey, P. J., Bednarek, S. Y., Ehrhardt, D. W. & Sedbrook, J. C. (2014). The microtubule plus-end tracking proteins SPR1 and EB1b interact to maintain polar cell elongation and directional organ growth in Arabidopsis. *Plant Cell* **26**, 4409-25.

Gao, C., Luo, M., Zhao, Q., Yang, R., Cui, Y., Zeng, Y., Xia, J. & Jiang, L. (2014). A unique plant ESCRT component, FREE1, regulates multivesicular body protein sorting and plant growth. *Curr Biol* **24**, 2556-63.

Gao, C., Zhuang, X., Shen, J. & Jiang, L. (2017). Plant ESCRT Complexes: Moving Beyond Endosomal Sorting. *Trends Plant Sci* **22**, 986-998.

Gardiner, J. C., Harper, J. D., Weerakoon, N. D., Collings, D. A., Ritchie, S., Gilroy, S., Cyr, R. J. & Marc, J. (2001). A 90-kD phospholipase D from tobacco binds to microtubules and the plasma membrane. *Plant Cell* **13**, 2143-58.

Gendre, D., Jonsson, K., Boutté, Y. & Bhalerao, R. P. (2015). Journey to the cell surface—the central role of the trans-Golgi network in plants. *Protoplasma* **252**, 385-398.

Gething, M.-J. (1999). Role and regulation of the ER chaperone BiP. In *Seminars in cell & developmental biology*, pp. 465-472. Elsevier.

Goddard, R. H., Wick, S. M., Silflow, C. D. & Snustad, D. P. (1994). Microtubule Components of the Plant Cell Cytoskeleton. *Plant Physiol* **104**, 1-6.

Gomez-Navarro, N. & Miller, E. (2016). Protein sorting at the ER-Golgi interface. *J Cell Biol* **215**, 769-778.

Gomord, V., Denmat, L. A., Fitchette-Lainé, A. C., Satiat-Jeunemaitre, B., Hawes, C. & Faye, L. (1997). The C-terminal HDEL sequence is sufficient for retention of secretory proteins in the endoplasmic reticulum (ER) but promotes vacuolar targeting of proteins that escape the ER. *The Plant Journal* **11**, 313-325.

Goto, C., Tamura, K., Fukao, Y., Shimada, T. & Hara-Nishimura, I. (2014). The Novel Nuclear Envelope Protein KAKU4 Modulates Nuclear Morphology in Arabidopsis. *Plant Cell* **26**, 2143-2155.

Gould, S. B., Garg, S. G. & Martin, W. F. (2016). Bacterial Vesicle Secretion and the Evolutionary Origin of the Eukaryotic Endomembrane System. *Trends Microbiol* **24**, 525-534.

Graumann, K., Vanrobays, E., Tutois, S., Probst, A. V., Evans, D. E. & Tatout, C. (2014). Characterization of two distinct subfamilies of SUN-domain proteins in Arabidopsis and their interactions with the novel KASH-domain protein AtTIK. *J Exp Bot* **65**, 6499-512.

Griffing, L. R. (2010). Networking in the endoplasmic reticulum. Portland Press Limited.

Griffing, L. R., Gao, H. T. & Sparkes, I. (2014). ER network dynamics are differentially controlled by myosins XI-K, XI-C, XI-E, XI-I, XI-1, and XI-2. *Frontiers in plant science* **5**, 218.

Gu, F., Crump, C. & Thomas, G. (2001). Trans-Golgi network sorting. *Cellular and Molecular Life Sciences CMLS* **58**, 1067-1084.

Gu, Y., Kaplinsky, N., Bringmann, M., Cobb, A., Carroll, A., Sampathkumar, A., Baskin, T. I., Persson, S. & Somerville, C. R. (2010). Identification of a cellulose synthase-associated protein required for cellulose biosynthesis. *Proc Natl Acad Sci U S A* **107**, 12866-71.

Gundersen, G. G. & Worman, H. J. (2013). Nuclear positioning. *Cell* **152**, 1376-89.

Gusarova, V., Seo, J., Sullivan, M. L., Watkins, S. C., Brodsky, J. L. & Fisher, E. A. (2007). Golgi-associated maturation of very low density lipoproteins involves conformational changes in apolipoprotein B, but is not dependent on apolipoprotein E. *J Biol Chem* **282**, 19453-62.

Haglund, K., Di Fiore, P. P. & Dikic, I. (2003). Distinct monoubiquitin signals in receptor endocytosis. *Trends in biochemical sciences* **28**, 598-604.

Hamada, T., Ueda, H., Kawase, T. & Hara-Nishimura, I. (2014). Microtubules contribute to tubule elongation and anchoring of endoplasmic reticulum, resulting in high network complexity in Arabidopsis thaliana. *Plant physiology*, pp. 114.252320.

Hamamoto, I., Nishimura, Y., Okamoto, T., Aizaki, H., Liu, M., Mori, Y., Abe, T., Suzuki, T., Lai, M. M., Miyamura, T., Moriishi, K. & Matsuura, Y. (2005). Human VAP-B is involved in hepatitis C virus replication through interaction with NS5A and NS5B. *J Virol* **79**, 13473-82.

Han, B., Chen, L., Wang, J., Wu, Z., Yan, L. & Hou, S. (2015). Constitutive Expresser of Pathogenesis Related Genes 1 Is Required for Pavement Cell Morphogenesis in Arabidopsis. *PLoS One* **10**, e0133249.

Harris, N. (1986). Organization of the endomembrane system. *Annual Review of Plant Physiology* **37**, 73-92.

Havelkova, L., Nanda, G., Martinek, J., Bellinvia, E., Sikorova, L., Slajcherova, K., Seifertova, D., Fischer, L., Fiserova, J., Petrasek, J. & Schwarzerova, K. (2015). Arp2/3 complex subunit ARPC2 binds to microtubules. *Plant Sci* **241**, 96-108.

Hawes, C., Schoberer, J., Hummel, E. & Osterrieder, A. (2010). Biogenesis of the plant Golgi apparatus. Portland Press Limited.

Hebert, D. N. & Molinari, M. (2007). In and out of the ER: protein folding, quality control, degradation, and related human diseases. *Physiological reviews* **87**, 1377-1408.

Henne, W. M., Buchkovich, N. J. & Emr, S. D. (2011). The ESCRT pathway. *Dev Cell* **21**, 77-91.

Hervé, J. C. & Bourmeyster, N. (2018). Rab GTPases, master controllers of eukaryotic trafficking. Taylor & Francis.

Hetzer, M. W., Walther, T. C. & Mattaj, I. W. (2005). Pushing the envelope: structure, function, and dynamics of the nuclear periphery. *Annu Rev Cell Dev Biol* **21**, 347-80.

Higaki, T., Kutsuna, N., Okubo, E., Sano, T. & Hasezawa, S. (2006). Actin microfilaments regulate vacuolar structures and dynamics: dual observation of actin microfilaments and vacuolar membrane in living tobacco BY-2 Cells. *Plant Cell Physiol* **47**, 839-52.

Higaki, T., Kutsuna, N., Sano, T., Kondo, N. & Hasezawa, S. (2010). Quantification and cluster analysis of actin cytoskeletal structures in plant cells: role of actin bundling in stomatal movement during diurnal cycles in Arabidopsis guard cells. *Plant J* **61**, 156-65.

Hirokawa, N. (1998). Kinesin and dynein superfamily proteins and the mechanism of organelle transport. *Science* **279**, 519-26.

Hirokawa, N., Niwa, S. & Tanaka, Y. (2010). Molecular motors in neurons: transport mechanisms and roles in brain function, development, and disease. *Neuron* **68**, 610-38.

Hogan, P. G., Lewis, R. S. & Rao, A. (2010). Molecular basis of calcium signaling in lymphocytes: STIM and ORAI. *Annu Rev Immunol* **28**, 491-533.

Hong, W. & Lev, S. (2014). Tethering the assembly of SNARE complexes. *Trends in cell biology* **24**, 35-43.

Howe, E. S., Clemente, T. E. & Bass, H. W. (2012). Maize histone H2B-mCherry: a new fluorescent chromatin marker for somatic and meiotic chromosome research. *DNA and cell biology* **31**, 925-938.

Hruz, T., Laule, O., Szabo, G., Wessendorp, F., Bleuler, S., Oertle, L., Widmayer, P., Gruissem, W. & Zimmermann, P. (2008). Genevestigator v3: a reference expression database for the meta-analysis of transcriptomes. *Adv Bioinformatics* **2008**, 420747.

Hua, R., Cheng, D., Coyaud, E., Freeman, S., Di Pietro, E., Wang, Y., Vissa, A., Yip, C. M., Fairn, G. D., Braverman, N., Brumell, J. H., Trimble, W. S., Raught, B. & Kim, P. K. (2017). VAPs and ACBD5 tether peroxisomes to the ER for peroxisome maintenance and lipid homeostasis. *J Cell Biol* **216**, 367-377.

Hussey, P. J., Ketelaar, T. & Deeks, M. J. (2006). Control of the actin cytoskeleton in plant cell growth. *Annu Rev Plant Biol* **57**, 109-25.

Isermann, P. & Lammerding, J. (2013). Nuclear mechanics and mechanotransduction in health and disease. *Curr Biol* **23**, R1113-21.

Ishida, T., Thitamadee, S. & Hashimoto, T. (2007). Twisted growth and organization of cortical microtubules. *J Plant Res* **120**, 61-70.

Ito, Y., Uemura, T. & Nakano, A. (2018). The Golgi entry core compartment functions as a COPII-independent scaffold for ER-to-Golgi transport in plant cells. *J Cell Sci* **131**.

Jürgens, G. (2004). Membrane trafficking in plants. *Annu. Rev. Cell Dev. Biol.* **20**, 481-504.

Jackson, C. L. (2009). Mechanisms of transport through the Golgi complex. *Journal of cell science* **122**, 443-452.

Jahn, R., Lang, T. & Sudhof, T. C. (2003). Membrane fusion. *Cell* **112**, 519-33.

Jevtic, P., Edens, L. J., Vukovic, L. D. & Levy, D. L. (2014). Sizing and shaping the nucleus: mechanisms and significance. *Curr Opin Cell Biol* **28**, 16-27.

Johnson, N., Powis, K. & High, S. (2013). Post-translational translocation into the endoplasmic reticulum. *Biochimica et Biophysica Acta (BBA)-Molecular Cell Research* **1833**, 2403-2409.

Kabsch, W., Mannherz, H. G., Suck, D., Pai, E. F. & Holmes, K. C. (1990). Atomic structure of the actin: DNase I complex. *Nature* **347**, 37.

Kagiwada, S. & Zen, R. (2003). Role of the yeast VAP homolog, Scs2p, in INO1 expression and phospholipid metabolism. *J Biochem* **133**, 515-22.

Kalinowska, K., Nagel, M. K., Goodman, K., Cuyas, L., Anzenberger, F., Alkofer, A., Paz-Ares, J., Braun, P., Rubio, V., Otegui, M. S. & Isono, E. (2015). Arabidopsis ALIX is required for the endosomal localization of the deubiquitinating enzyme AMSH3. *Proc Natl Acad Sci U S A* **112**, E5543-51.

Kanekura, K., Nishimoto, I., Aiso, S. & Matsuoka, M. (2006). Characterization of amyotrophic lateral sclerosis-linked P56S mutation of vesicle-associated membrane protein-associated protein B (VAPB/ALS8). *J Biol Chem* **281**, 30223-33.

Kang, B. H., Nielsen, E., Preuss, M. L., Mastronarde, D. & Staehelin, L. A. (2011). Electron tomography of RabA4b-and PI-4Kβ1-labeled trans Golgi network compartments in Arabidopsis. *Traffic* **12**, 313-329.

Kapila, J., DeRycke, R., VanMontagu, M. & Angenon, G. (1997). An Agrobacterium-mediated transient gene expression system for intact leaves (vol 122, pg 101, 1997). *Plant Science* **124**, 227-227.

Kawamura, E., Himmelspach, R., Rashbrooke, M. C., Whittington, A. T., Gale, K. R., Collings, D. A. & Wasteneys, G. O. (2006). MICROTUBULE ORGANIZATION 1 regulates structure and function of microtubule arrays during mitosis and cytokinesis in the Arabidopsis root. *Plant Physiol* **140**, 102-14.

Kawano, M., Kumagai, K., Nishijima, M. & Hanada, K. (2006). Efficient trafficking of ceramide from the endoplasmic reticulum to the Golgi apparatus requires a VAMP-associated protein-interacting FFAT motif of CERT. *J Biol Chem* **281**, 30279-88.

Kienzle, C. & von Blume, J. (2014). Secretory cargo sorting at the trans-Golgi network. *Trends in cell biology* **24**, 584-593.

Kim, J., Sitaraman, S., Hierro, A., Beach, B. M., Odorizzi, G. & Hurley, J. H. (2005). Structural basis for endosomal targeting by the Bro1 domain. *Dev Cell* **8**, 937-47.

Kopczak, S. D., Haas, N. A., Hussey, P. J., Silflow, C. D. & Snustad, D. P. (1992). The small genome of Arabidopsis contains at least six expressed alpha-tubulin genes. *Plant Cell* **4**, 539-47.

Kost, B. & Chua, N. H. (2002). The plant cytoskeleton: vacuoles and cell walls make the difference. *Cell* **108**, 9-12.

Krysan, P. J., Young, J. C. & Sussman, M. R. (1999). T-DNA as an insertional mutagen in Arabidopsis. *Plant Cell* **11**, 2283-90.

Ladinsky, M. S., Mastronarde, D. N., McIntosh, J. R., Howell, K. E. & Staehelin, L. A. (1999). Golgi structure in three dimensions: functional insights from the normal rat kidney cell. *J Cell Biol* **144**, 1135-49.

Larkin, M. A., Blackshields, G., Brown, N. P., Chenna, R., McGettigan, P. A., McWilliam, H., Valentin, F., Wallace, I. M., Wilm, A., Lopez, R., Thompson, J. D., Gibson, T. J. & Higgins, D. G. (2007). Clustal W and Clustal X version 2.0. *Bioinformatics* **23**, 2947-8.

Laurent, F., Labesse, G. & de Wit, P. (2000). Molecular cloning and partial characterization of a plant VAP33 homologue with a major sperm protein domain. *Biochem Biophys Res Commun* **270**, 286-92.

Lawrence, C. J., Dawe, R. K., Christie, K. R., Cleveland, D. W., Dawson, S. C., Endow, S. A., Goldstein, L. S., Goodson, H. V., Hirokawa, N., Howard, J., Malmberg, R. L., McIntosh, J. R., Miki, H., Mitchison, T. J., Okada, Y., Reddy, A. S., Saxton, W. M., Schliwa, M., Scholey, J. M., Vale, R. D., Walczak, C. E. & Wordeman, L. (2004). A standardized kinesin nomenclature. *J Cell Biol* **167**, 19-22.

Le, J., Mallery, E. L., Zhang, C., Brankle, S. & Szymanski, D. B. (2006). Arabidopsis BRICK1/HSPC300 is an essential WAVE-complex subunit that selectively stabilizes the Arp2/3 activator SCAR2. *Curr Biol* **16**, 895-901.

Lee, H., Sparkes, I., Gattolin, S., Dzimitrowicz, N., Roberts, L. M., Hawes, C. & Frigerio, L. (2013). An A rabidopsis reticulon and the atlastin homologue RHD3-like2 act together in shaping the tubular endoplasmic reticulum. *New Phytologist* **197**, 481-489.

Lev, S., Ben Halevy, D., Peretti, D. & Dahan, N. (2008). The VAP protein family: from cellular functions to motor neuron disease. *Trends Cell Biol* **18**, 282-90.

Levy, A., Zheng, J. Y. & Lazarowitz, S. G. (2015). Synaptotagmin SYTA forms ER-plasma membrane junctions that are recruited to plasmodesmata for plant virus movement. *Curr Biol* **25**, 2018-25.

Li, H., Xu, T., Lin, D., Wen, M., Xie, M., Duclercq, J., Bielach, A., Kim, J., Reddy, G. V., Zuo, J., Benkova, E., Friml, J., Guo, H. & Yang, Z. (2013). Cytokinin signaling regulates pavement cell morphogenesis in Arabidopsis. *Cell Res* **23**, 290-9.

Li, S., Blanchoin, L., Yang, Z. & Lord, E. M. (2003). The putative Arabidopsis arp2/3 complex controls leaf cell morphogenesis. *Plant Physiol* **132**, 2034-44.

Li, S., Lei, L., Somerville, C. R. & Gu, Y. (2012). Cellulose synthase interactive protein 1 (CSI1) links microtubules and cellulose synthase complexes. *Proc Natl Acad Sci U S A* **109**, 185-90.

Liang, H., Zhang, Y., Martinez, P., Rasmussen, C. G., Xu, T. & Yang, Z. (2018).

The Microtubule-Associated Protein IQ67 DOMAIN5 Modulates Microtubule Dynamics and Pavement Cell Shape. *Plant Physiol* **177**, 1555-1568.

Lin, D., Cao, L., Zhou, Z., Zhu, L., Ehrhardt, D., Yang, Z. & Fu, Y. (2013). Rho GTPase signaling activates microtubule severing to promote microtubule ordering in Arabidopsis. *Curr Biol* **23**, 290-7.

Lin, D., Ren, H. & Fu, Y. (2015). ROP GTPase-mediated auxin signaling regulates pavement cell interdigitation in Arabidopsis thaliana. *J Integr Plant Biol* **57**, 31-9.

Lippincott-Schwartz, J. & Phair, R. D. (2010). Lipids and cholesterol as regulators of traffic in the endomembrane system. *Annu Rev Biophys* **39**, 559-78.

Liu, Z., Schneider, R., Kesten, C., Zhang, Y., Somssich, M., Zhang, Y., Fernie, A. R. & Persson, S. (2016). Cellulose-Microtubule Uncoupling Proteins Prevent Lateral Displacement of Microtubules during Cellulose Synthesis in Arabidopsis. *Dev Cell* **38**, 305-15.

Loewen, C. J., Roy, A. & Levine, T. P. (2003). A conserved ER targeting motif in three families of lipid binding proteins and in Opi1p binds VAP. *EMBO J* **22**, 2025-35.

Lord, C., Ferro-Novick, S. & Miller, E. A. (2013). The highly conserved COPII coat complex sorts cargo from the endoplasmic reticulum and targets it to the golgi. *Cold Spring Harb Perspect Biol* **5**.

Lu, L., Ladinsky, M. S. & Kirchhausen, T. (2009). Cisternal organization of the endoplasmic reticulum during mitosis. *Mol Biol Cell* **20**, 3471-80.

Lucas, J. R., Courtney, S., Hassfurder, M., Dhingra, S., Bryant, A. & Shaw, S. L. (2011). Microtubule-associated proteins MAP65-1 and MAP65-2 positively regulate axial cell growth in etiolated Arabidopsis hypocotyls. *Plant Cell* **23**, 1889-903.

Müller, M. P. & Goody, R. S. (2018). Molecular control of Rab activity by GEFs, GAPs and GDI. *Small GTPases* **9**, 5-21.

MacGurn, J. A., Hsu, P. C. & Emr, S. D. (2012). Ubiquitin and membrane protein turnover: from cradle to grave. *Annu Rev Biochem* **81**, 231-59.

Madison, S. L., Buchanan, M. L., Glass, J. D., McClain, T. F., Park, E. & Nebenführ, A. (2015). Class XI myosins move specific organelles in pollen tubes and are required for normal fertility and pollen tube growth in Arabidopsis. *Plant physiology*, pp. 01161.2015.

Manford, A. G., Stefan, C. J., Yuan, H. L., MacGurn, J. A. & Emr, S. D. (2012). ER-to-plasma membrane tethering proteins regulate cell signaling and ER morphology. *Developmental cell* **23**, 1129-1140.

Mao, T., Jin, L., Li, H., Liu, B. & Yuan, M. (2005). Two microtubule-associated proteins of the Arabidopsis MAP65 family function differently on microtubules. *Plant Physiol* **138**, 654-62.

Marti, L., Fornaciari, S., Renna, L., Stefano, G. & Brandizzi, F. (2010). COPII-mediated traffic in plants. *Trends Plant Sci* **15**, 522-8.

Martoglio, B. & Dobberstein, B. (1998). Signal sequences: more than just greasy peptides. *Trends in cell biology* **8**, 410-415.

Mathur, J. (2004). Cell shape development in plants. *Trends Plant Sci* **9**, 583-90.

Mathur, J. (2006). Local interactions shape plant cells. *Curr Opin Cell Biol* **18**, 40-6.

Mathur, J., Mathur, N., Kernebeck, B. & Hulskamp, M. (2003). Mutations in actin-related proteins 2 and 3 affect cell shape development in Arabidopsis. *Plant Cell* **15**, 1632-45.

McFarlane, H. E., Lee, E. K., van Bezouwen, L. S., Ross, B., Rosado, A. & Samuels, A. L. (2017). Multiscale Structural Analysis of Plant ER-PM Contact Sites. *Plant Cell Physiol* **58**, 478-484.

Mehrshahi, P., Johnny, C. & DellaPenna, D. (2014). Redefining the metabolic continuity of chloroplasts and ER. *Trends Plant Sci* **19**, 501-7.

Meier, I., Griffis, A. H., Groves, N. R. & Wagner, A. (2016). Regulation of nuclear shape and size in plants. *Curr Opin Cell Biol* **40**, 114-123.

Meinke, D. (1994). Seed development in *Arabidopsis thaliana. In* CR Somerville, EM Meyerowitz, eds, *Arabidopsis*. Cold Spring Harbor Laboratory Press, Cold Spring Harbor, NY.

Mineyuki, Y. (1999). The preprophase band of microtubules: Its function as a cytokinetic apparatus in higher plants. In *International Review of Cytology - a Survey of Cell Biology, Vol 187* (ed. K. W. Jeon), pp. 1-49. Elsevier Academic Press Inc: San Diego.

Mineyuki, Y. (2007). Plant microtubule studies: past and present. *J Plant Res* **120**, 45-51.

Mironov, A. A. (2014). ER-Golgi transport could occur in the absence of COPII vesicles. *Nat Rev Mol Cell Biol* **15**, 1.

Mitchison, T. & Kirschner, M. (1984). Dynamic instability of microtubule growth. *Nature* **312**, 237-42.

Muhlhausser, P. & Kutay, U. (2007). An in vitro nuclear disassembly system reveals

a role for the RanGTPase system and microtubule-dependent steps in nuclear envelope breakdown. *J Cell Biol* **178**, 595-610.

Muller, S., Smertenko, A., Wagner, V., Heinrich, M., Hussey, P. J. & Hauser, M. T. (2004). The plant microtubule-associated protein AtMAP65-3/PLE is essential for cytokinetic phragmoplast function. *Curr Biol* **14**, 412-7.

Murata, T. & Hasebe, M. (2007). Microtubule-dependent microtubule nucleation in plant cells. *J Plant Res* **120**, 73-8.

Murphy, S. P., Simmons, C. R. & Bass, H. W. (2010). Structure and expression of the maize (Zea mays L.) SUN-domain protein gene family: evidence for the existence of two divergent classes of SUN proteins in plants. *BMC Plant Biol* **10**, 269.

Nakajima, K., Furutani, I., Tachimoto, H., Matsubara, H. & Hashimoto, T. (2004). SPIRAL1 encodes a plant-specific microtubule-localized protein required for directional control of rapidly expanding Arabidopsis cells. *Plant Cell* **16**, 1178-90.

Nakamura, M., Ehrhardt, D. W. & Hashimoto, T. (2010). Microtubule and katanin-dependent dynamics of microtubule nucleation complexes in the acentrosomal Arabidopsis cortical array. *Nat Cell Biol* **12**, 1064-70.

Naoi, K. & Hashimoto, T. (2004). A semidominant mutation in an Arabidopsis mitogen-activated protein kinase phosphatase-like gene compromises cortical microtubule organization. *Plant Cell* **16**, 1841-53.

Napier, R. M., Fowke, L. C., Hawes, C., Lewis, M. & Pelham, H. (1992). Immunological evidence that plants use both HDEL and KDEL for targeting proteins to the endoplasmic reticulum. *Journal of Cell Science* **102**, 261-271.

Nebenführ, A. & Dixit, R. (2018). Kinesins and myosins: molecular motors that coordinate cellular functions in plants. *Annual review of plant biology* **69**, 329-361.

Nyathi, Y., Wilkinson, B. M. & Pool, M. R. (2013). Co-translational targeting and translocation of proteins to the endoplasmic reticulum. *Biochimica et Biophysica Acta (BBA)-Molecular Cell Research* **1833**, 2392-2402.

Oda, Y. (2018). Emerging roles of cortical microtubule-membrane interactions. *J Plant Res* **131**, 5-14.

Oda, Y. & Fukuda, H. (2011). Dynamics of Arabidopsis SUN proteins during mitosis and their involvement in nuclear shaping. *Plant J* **66**, 629-41.

Oda, Y. & Fukuda, H. (2012). Initiation of cell wall pattern by a Rho- and microtubule-driven symmetry breaking. *Science* **337**, 1333-6.

Oda, Y., Iida, Y., Kondo, Y. & Fukuda, H. (2010). Wood cell-wall structure requires

local 2D-microtubule disassembly by a novel plasma membrane-anchored protein. *Curr Biol* **20**, 1197-202.

Odorizzi, G. (2006). The multiple personalities of Alix. *J Cell Sci* **119**, 3025-32.

Orlova, A. & Egelman, E. H. (1992). Structural basis for the destabilization of F-actin by phosphate release following ATP hydrolysis. *Journal of molecular biology* **227**, 1043-1053.

Ovecka, M., Vaskebova, L., Komis, G., Luptovciak, I., Smertenko, A. & Samaj, J. (2015). Preparation of plants for developmental and cellular imaging by light-sheet microscopy. *Nat Protoc* **10**, 1234-47.

Pan, S., Wang, R., Zhou, X., He, G., Koomen, J., Kobayashi, R., Sun, L., Corvera, J., Gallick, G. E. & Kuang, J. (2006). Involvement of the conserved adaptor protein Alix in actin cytoskeleton assembly. *Journal of Biological Chemistry* **281**, 34640-34650.

Paredez, A. R., Somerville, C. R. & Ehrhardt, D. W. (2006a). Visualization of cellulose synthase demonstrates functional association with microtubules. *Science* **312**, 1491-5.

Paredez, A. R., Somerville, C. R. & Ehrhardt, D. W. (2006b). Visualization of cellulose synthase demonstrates functional association with microtubules. *Science* **312**, 1491-1495.

Park, E. & Nebenführ, A. (2013). Myosin XIK of Arabidopsis thaliana accumulates at the root hair tip and is required for fast root hair growth. *PloS one* **8**, e76745.

Parrotta, L., Cresti, M. & Cai, G. (2014). Accumulation and post-translational modifications of plant tubulins. *Plant Biol (Stuttg)* **16**, 521-7.

Pauly, M. & Keegstra, K. (2016). Biosynthesis of the Plant Cell Wall Matrix Polysaccharide Xyloglucan. *Annu Rev Plant Biol* **67**, 235-59.

Pawar, V., Poulet, A., Detourne, G., Tatout, C., Vanrobays, E., Evans, D. E. & Graumann, K. (2016). A novel family of plant nuclear envelope-associated proteins. *J Exp Bot* **67**, 5699-5710.

Pennetta, G., Hiesinger, P. R., Fabian-Fine, R., Meinertzhagen, I. A. & Bellen, H. J. (2002). Drosophila VAP-33A directs bouton formation at neuromuscular junctions in a dosage-dependent manner. *Neuron* **35**, 291-306.

Perrin, B. J. & Ervasti, J. M. (2010). The actin gene family: function follows isoform. *Cytoskeleton (Hoboken)* **67**, 630-4.

Petrasek, J. & Schwarzerova, K. (2009). Actin and microtubule cytoskeleton

interactions. *Curr Opin Plant Biol* **12**, 728-34.

Piper, R. C. & Luzio, J. P. (2007). Ubiquitin-dependent sorting of integral membrane proteins for degradation in lysosomes. *Current Opinion in Cell Biology* **19**, 459-465.

Pollard, T. D. & Borisy, G. G. (2003). Cellular motility driven by assembly and disassembly of actin filaments. *Cell* **112**, 453-65.

Preuss, M. L., Kovar, D. R., Lee, Y. R., Staiger, C. J., Delmer, D. P. & Liu, B. (2004a). A plant-specific kinesin binds to actin microfilaments and interacts with cortical microtubules in cotton fibers. *Plant Physiol* **136**, 3945-55.

Preuss, M. L., Serna, J., Falbel, T. G., Bednarek, S. Y. & Nielsen, E. (2004b). The Arabidopsis Rab GTPase RabA4b localizes to the tips of growing root hair cells. *The Plant Cell* **16**, 1589-1603.

Qian, P., Hou, S. & Guo, G. (2009). Molecular mechanisms controlling pavement cell shape in Arabidopsis leaves. *Plant Cell Rep* **28**, 1147-57.

Rahman, A., Friedman, D. S. & Goldstein, L. S. (1998). Two kinesin light chain genes in mice. Identification and characterization of the encoded proteins. *J Biol Chem* **273**, 15395-403.

Reddy, A. S. & Day, I. S. (2001). Kinesins in the Arabidopsis genome: a comparative analysis among eukaryotes. *BMC Genomics* **2**, 2.

Rice, P., Longden, I. & Bleasby, A. (2000). EMBOSS: the European Molecular Biology Open Software Suite. *Trends Genet* **16**, 276-7.

Richardson, L. G., Howard, A. S., Khuu, N., Gidda, S. K., McCartney, A., Morphy, B. J. & Mullen, R. T. (2011). Protein-Protein Interaction Network and Subcellular Localization of the Arabidopsis Thaliana ESCRT Machinery. *Front Plant Sci* **2**, 20.

Riedl, J., Crevenna, A. H., Kessenbrock, K., Yu, J. H., Neukirchen, D., Bista, M., Bradke, F., Jenne, D., Holak, T. A. & Werb, Z. (2008). Lifeact: a versatile marker to visualize F-actin. *Nature methods* **5**, 605.

Ringli, C., Bigler, L., Kuhn, B. M., Leiber, R. M., Diet, A., Santelia, D., Frey, B., Pollmann, S. & Klein, M. (2008). The modified flavonol glycosylation profile in the Arabidopsis rol1 mutants results in alterations in plant growth and cell shape formation. *Plant Cell* **20**, 1470-81.

Robinson, D. G., Brandizzi, F., Hawes, C. & Nakano, A. (2015). Vesicles versus Tubes: Is Endoplasmic Reticulum-Golgi Transport in Plants Fundamentally Different from Other Eukaryotes? *Plant Physiol* **168**, 393-406.

Rocchetti, A., Hawes, C. & Kriechbaumer, V. (2014). Fluorescent labelling of the actin cytoskeleton in plants using a cameloid antibody. *Plant methods* **10**, 12.

Rosero, A., Oulehlova, D., Stillerova, L., Schiebertova, P., Grunt, M., Zarsky, V. & Cvrckova, F. (2016). Arabidopsis FH1 Formin Affects Cotyledon Pavement Cell Shape by Modulating Cytoskeleton Dynamics. *Plant Cell Physiol* **57**, 488-504.

Rosero, A., Zarsky, V. & Cvrckova, F. (2013). AtFH1 formin mutation affects actin filament and microtubule dynamics in Arabidopsis thaliana. *J Exp Bot* **64**, 585-97.

Saedler, R., Mathur, N., Srinivas, B. P., Kernebeck, B., Hulskamp, M. & Mathur, J. (2004). Actin control over microtubules suggested by DISTORTED2 encoding the Arabidopsis ARPC2 subunit homolog. *Plant Cell Physiol* **45**, 813-22.

Sakai, T., Honing, H., Nishioka, M., Uehara, Y., Takahashi, M., Fujisawa, N., Saji, K., Seki, M., Shinozaki, K., Jones, M. A., Smirnoff, N., Okada, K. & Wasteneys, G. O. (2008). Armadillo repeat-containing kinesins and a NIMA-related kinase are required for epidermal-cell morphogenesis in Arabidopsis. *Plant J* **53**, 157-71.

Sakamoto, Y. & Takagi, S. (2013). LITTLE NUCLEI 1 and 4 regulate nuclear morphology in Arabidopsis thaliana. *Plant Cell Physiol* **54**, 622-33.

Salina, D., Bodoor, K., Eckley, D. M., Schroer, T. A., Rattner, J. B. & Burke, B. (2002). Cytoplasmic dynein as a facilitator of nuclear envelope breakdown. *Cell* **108**, 97-107.

Salvador-Gallego, R., Hoyer, M. J. & Voeltz, G. K. (2017). SnapShot: Functions of Endoplasmic Reticulum Membrane Contact Sites. *Cell* **171**, 1224-1224 e1.

Sampathkumar, A., Gutierrez, R., McFarlane, H., Bringmann, M., Lindeboom, J., Emons, A.-M., Samuels, L., Ketelaar, T., Ehrhardt, D. & Persson, S. (2013). Patterning and life-time of plasma membrane localized cellulose synthase is dependent on actin organization in Arabidopsis interphase cells. *Plant physiology*, pp. 113.215277.

Sampathkumar, A., Lindeboom, J. J., Debolt, S., Gutierrez, R., Ehrhardt, D. W., Ketelaar, T. & Persson, S. (2011). Live cell imaging reveals structural associations between the actin and microtubule cytoskeleton in Arabidopsis. *Plant Cell* **23**, 2302-13.

Sandoz, P. A. & Van der Goot, F. G. (2015). How many lives does CLIMP-63 have? Portland Press Limited.

Saraogi, I. & Shan, S. o. (2011). Molecular Mechanism of Co-translational Protein Targeting by the Signal Recognition Particle. *Traffic* **12**, 535-542.

Schmidt, O. & Teis, D. (2012). The ESCRT machinery. *Curr Biol* **22**, R116-20.

Schottkowski, M., Ratke, J., Oster, U., Nowaczyk, M. & Nickelsen, J. (2009). Pitt, a novel tetratricopeptide repeat protein involved in light-dependent chlorophyll biosynthesis and thylakoid membrane biogenesis in Synechocystis sp. PCC 6803. *Mol Plant* **2**, 1289-97.

Sedbrook, J. C., Ehrhardt, D. W., Fisher, S. E., Scheible, W. R. & Somerville, C. R. (2004). The Arabidopsis sku6/spiral1 gene encodes a plus end-localized microtubule-interacting protein involved in directional cell expansion. *Plant Cell* **16**, 1506-20.

Seltzer, V., Janski, N., Canaday, J., Herzog, E., Erhardt, M., Evrard, J. L. & Schmit, A. C. (2007). Arabidopsis GCP2 and GCP3 are part of a soluble gamma-tubulin complex and have nuclear envelope targeting domains. *Plant J* **52**, 322-31.

Shen, J., Gao, C., Zhao, Q., Lin, Y., Wang, X., Zhuang, X. & Jiang, L. (2016). AtBRO1 Functions in ESCRT-I Complex to Regulate Multivesicular Body Protein Sorting. *Mol Plant* **9**, 760-763.

Shibata, Y., Voeltz, G. K. & Rapoport, T. A. (2006). Rough sheets and smooth tubules. *Cell* **126**, 435-439.

Siao, W., Wang, P., Voigt, B., Hussey, P. J. & Baluska, F. (2016). Arabidopsis SYT1 maintains stability of cortical endoplasmic reticulum networks and VAP27-1-enriched endoplasmic reticulum-plasma membrane contact sites. *J Exp Bot* **67**, 6161-6171.

Skehel, P. A., Martin, K. C., Kandel, E. R. & Bartsch, D. (1995). A VAMP-binding protein from Aplysia required for neurotransmitter release. *Science* **269**, 1580-3.

Smertenko, A. P., Kaloriti, D., Chang, H. Y., Fiserova, J., Opatrny, Z. & Hussey, P. J. (2008). The C-terminal variable region specifies the dynamic properties of Arabidopsis microtubule-associated protein MAP65 isotypes. *Plant Cell* **20**, 3346-58.

Smith, L. G. (2003). Cytoskeletal control of plant cell shape: getting the fine points. *Curr Opin Plant Biol* **6**, 63-73.

Smith, L. G. & Oppenheimer, D. G. (2005). Spatial control of cell expansion by the plant cytoskeleton. *Annu Rev Cell Dev Biol* **21**, 271-95.

Snustad, D. P., Haas, N. A., Kopczak, S. D. & Silflow, C. D. (1992). The small genome of Arabidopsis contains at least nine expressed beta-tubulin genes. *Plant Cell* **4**, 549-56.

Sohn, M., Korzeniowski, M., Zewe, J. P., Wills, R. C., Hammond, G. R. V., Humpolickova, J., Vrzal, L., Chalupska, D., Veverka, V., Fairn, G. D., Boura, E. & Balla, T. (2018). PI(4,5)P2 controls plasma membrane PI4P and PS levels via ORP5/8 recruitment to ER-PM contact sites. *J Cell Biol* **217**, 1797-1813.

Sollner, T., Whiteheart, S. W., Brunner, M., Erdjument-Bromage, H., Geromanos, S., Tempst, P. & Rothman, J. E. (1993). SNAP receptors implicated in vesicle targeting and fusion. *Nature* **362**, 318-24.

Soussan, L., Burakov, D., Daniels, M. P., Toister-Achituv, M., Porat, A., Yarden, Y. & Elazar, Z. (1999). ERG30, a VAP-33-related protein, functions in protein transport mediated by COPI vesicles. *J Cell Biol* **146**, 301-11.

Sparkes, I., Hawes, C. & Frigerio, L. (2011). FrontiERs: movers and shapers of the higher plant cortical endoplasmic reticulum. *Current opinion in plant biology* **14**, 658-665.

Sparkes, I., Runions, J., Hawes, C. & Griffing, L. (2009). Movement and remodeling of the endoplasmic reticulum in nondividing cells of tobacco leaves. *The Plant Cell* **21**, 3937-3949.

Staehelin, L. A. & Moore, I. (1995). The plant Golgi apparatus: structure, functional organization and trafficking mechanisms. *Annual review of plant biology* **46**, 261-288.

Stefan, C. J., Manford, A. G., Baird, D., Yamada-Hanff, J., Mao, Y. & Emr, S. D. (2011). Osh proteins regulate phosphoinositide metabolism at ER-plasma membrane contact sites. *Cell* **144**, 389-401.

Stefano, G., Renna, L., Wormsbaecher, C., Gamble, J., Zienkiewicz, K. & Brandizzi, F. (2018). Plant Endocytosis Requires the ER Membrane-Anchored Proteins VAP27-1 and VAP27-3. *Cell Rep* **23**, 2299-2307.

Struk, S. & Dhonukshe, P. (2014). MAPs: cellular navigators for microtubule array orientations in Arabidopsis. *Plant Cell Rep* **33**, 1-21.

Suda, Y. & Nakano, A. (2012). The Yeast G olgi Apparatus. *Traffic* **13**, 505-510.

Sugiyama, Y., Wakazaki, M., Toyooka, K., Fukuda, H. & Oda, Y. (2017). A Novel Plasma Membrane-Anchored Protein Regulates Xylem Cell-Wall Deposition through Microtubule-Dependent Lateral Inhibition of Rho GTPase Domains. *Curr Biol* **27**, 2522-2528 e4.

Suwastika, I. N., Uemura, T., Shiina, T., Sato, M. H. & Takeyasu, K. (2008). SYP71, a plant-specific Qc-SNARE protein, reveals dual localization to the plasma membrane and the endoplasmic reticulum in Arabidopsis. *Cell structure and function* **33**, 185-192.

Szul, T. & Sztul, E. (2011). COPII and COPI traffic at the ER-Golgi interface. *Physiology (Bethesda)* **26**, 348-64.

Takagi, J., Renna, L., Takahashi, H., Koumoto, Y., Tamura, K., Stefano, G., Fukao, Y., Kondo, M., Nishimura, M., Shimada, T., Brandizzi, F. &

Hara-Nishimura, I. (2013). MAIGO5 functions in protein export from Golgi-associated endoplasmic reticulum exit sites in Arabidopsis. *Plant Cell* **25**, 4658-75.

Tamura, K., Goto, C. & Hara-Nishimura, I. (2015). Recent advances in understanding plant nuclear envelope proteins involved in nuclear morphology. *J Exp Bot* **66**, 1641-7.

Tamura, K., Iwabuchi, K., Fukao, Y., Kondo, M., Okamoto, K., Ueda, H., Nishimura, M. & Hara-Nishimura, I. (2013). Myosin XI-i links the nuclear membrane to the cytoskeleton to control nuclear movement and shape in Arabidopsis. *Curr Biol* **23**, 1776-81.

Tavassoli, S., Chao, J. T., Young, B. P., Cox, R. C., Prinz, W. A., de Kroon, A. I. & Loewen, C. J. (2013). Plasma membrane--endoplasmic reticulum contact sites regulate phosphatidylcholine synthesis. *EMBO Rep* **14**, 434-40.

Thitamadee, S., Tuchihara, K. & Hashimoto, T. (2002). Microtubule basis for left-handed helical growth in Arabidopsis. *Nature* **417**, 193-6.

Tolley, N., Sparkes, I., Craddock, C. P., Eastmond, P. J., Runions, J., Hawes, C. & Frigerio, L. (2010). Transmembrane domain length is responsible for the ability of a plant reticulon to shape endoplasmic reticulum tubules in vivo. *The Plant Journal* **64**, 411-418.

Tolley, N., Sparkes, I. A., Hunter, P. R., Craddock, C. P., Nuttall, J., Roberts, L. M., Hawes, C., Pedrazzini, E. & Frigerio, L. (2008). Overexpression of a plant reticulon remodels the lumen of the cortical endoplasmic reticulum but does not perturb protein transport. *Traffic* **9**, 94-102.

Torruella, G., Derelle, R., Paps, J., Lang, B. F., Roger, A. J., Shalchian-Tabrizi, K. & Ruiz-Trillo, I. (2011). Phylogenetic relationships within the Opisthokonta based on phylogenomic analyses of conserved single-copy protein domains. *Molecular biology and evolution* **29**, 531-544.

Turgay, Y., Champion, L., Balazs, C., Held, M., Toso, A., Gerlich, D. W., Meraldi, P. & Kutay, U. (2014). SUN proteins facilitate the removal of membranes from chromatin during nuclear envelope breakdown. *J Cell Biol* **204**, 1099-109.

Twell, D., Park, S. K., Hawkins, T. J., Schubert, D., Schmidt, R., Smertenko, A. & Hussey, P. J. (2002). MOR1/GEM1 has an essential role in the plant-specific cytokinetic phragmoplast. *Nat Cell Biol* **4**, 711-4.

Ueda, H., Yokota, E., Kuwata, K., Kutsuna, N., Mano, S., Shimada, T., Tamura, K., Stefano, G., Fukao, Y., Brandizzi, F., Shimmen, T., Nishimura, M. & Hara-Nishimura, I. (2016). Phosphorylation of the C Terminus of RHD3 Has a Critical Role in Homotypic ER Membrane Fusion in Arabidopsis. *Plant Physiol* **170**,

867-80.

Uemura, T., Suda, Y., Ueda, T. & Nakano, A. (2014). Dynamic behavior of the trans-Golgi network in root tissues of Arabidopsis revealed by super-resolution live imaging. *Plant and Cell Physiology* **55**, 694-703.

Ungricht, R. & Kutay, U. (2017). Mechanisms and functions of nuclear envelope remodelling. *Nat Rev Mol Cell Biol* **18**, 229-245.

Vale, R. D., Reese, T. S. & Sheetz, M. P. (1985). Identification of a novel force-generating protein, kinesin, involved in microtubule-based motility. *Cell* **42**, 39-50.

Van Leene, J., Eeckhout, D., Cannoot, B., De Winne, N., Persiau, G., Van De Slijke, E., Vercruysse, L., Dedecker, M., Verkest, A. & Vandepoele, K. (2015). An improved toolbox to unravel the plant cellular machinery by tandem affinity purification of Arabidopsis protein complexes. *Nature protocols* **10**, 169.

Vedrenne, C. & Hauri, H. P. (2006). Morphogenesis of the endoplasmic reticulum: beyond active membrane expansion. *Traffic* **7**, 639-46.

Verhey, K. J. & Hammond, J. W. (2009). Traffic control: regulation of kinesin motors. *Nat Rev Mol Cell Biol* **10**, 765-77.

Verhey, K. J., Kaul, N. & Soppina, V. (2011). Kinesin assembly and movement in cells. *Annu Rev Biophys* **40**, 267-88.

Viotti, C., Bubeck, J., Stierhof, Y.-D., Krebs, M., Langhans, M., van den Berg, W., van Dongen, W., Richter, S., Geldner, N. & Takano, J. (2010). Endocytic and secretory traffic in Arabidopsis merge in the trans-Golgi network/early endosome, an independent and highly dynamic organelle. *The Plant Cell*, tpc. 109.072637.

Viotti, C., Krüger, F., Krebs, M., Neubert, C., Fink, F., Lupanga, U., Scheuring, D., Boutté, Y., Frescatada-Rosa, M. & Wolfenstetter, S. (2013). The endoplasmic reticulum is the main membrane source for biogenesis of the lytic vacuole in Arabidopsis. *The Plant Cell*, tpc. 113.114827.

Voeltz, G. K., Rolls, M. M. & Rapoport, T. A. (2002). Structural organization of the endoplasmic reticulum. *EMBO Rep* **3**, 944-50.

Voinnet, O., Rivas, S., Mestre, P. & Baulcombe, D. (2003). Retracted: an enhanced transient expression system in plants based on suppression of gene silencing by the p19 protein of tomato bushy stunt virus. *The Plant Journal* **33**, 949-956.

von Blume, J., Alleaume, A.-M., Kienzle, C., Carreras-Sureda, A., Valverde, M. & Malhotra, V. (2012). Cab45 is required for Ca2+-dependent secretory cargo sorting at the trans-Golgi network. *J Cell Biol* **199**, 1057-1066.

Wada, H. (2012). Hierarchical helical order in the twisted growth of plant organs. *Phys Rev Lett* **109**, 128104.

Walia, A., Lee, J. S., Wasteneys, G. & Ellis, B. (2009). Arabidopsis mitogen-activated protein kinase MPK18 mediates cortical microtubule functions in plant cells. *Plant J* **59**, 565-75.

Walter, P. & Johnson, A. E. (1994). Signal sequence recognition and protein targeting to the endoplasmic reticulum membrane. *Annual review of cell biology* **10**, 87-119.

Wang, C., Li, J. & Yuan, M. (2007). Salt tolerance requires cortical microtubule reorganization in Arabidopsis. *Plant Cell Physiol* **48**, 1534-47.

Wang, C. & Wang, X. (2001). A novel phospholipase D of Arabidopsis that is activated by oleic acid and associated with the plasma membrane. *Plant Physiol* **127**, 1102-12.

Wang, C., Zhang, L. J. & Huang, R. D. (2011). Cytoskeleton and plant salt stress tolerance. *Plant Signal Behav* **6**, 29-31.

Wang, H., Dittmer, T. A. & Richards, E. J. (2013). Arabidopsis CROWDED NUCLEI (CRWN) proteins are required for nuclear size control and heterochromatin organization. *BMC Plant Biol* **13**, 200.

Wang, P., Hawkins, T. J., Richardson, C., Cummins, I., Deeks, M. J., Sparkes, I., Hawes, C. & Hussey, P. J. (2014). The plant cytoskeleton, NET3C, and VAP27 mediate the link between the plasma membrane and endoplasmic reticulum. *Curr Biol* **24**, 1397-1405.

Wang, P. & Hussey, P. J. (2017). NETWORKED 3B: a novel protein in the actin cytoskeleton-endoplasmic reticulum interaction. *Journal of experimental botany* **68**, 1441-1450.

Wang, P., Richardson, C., Hawkins, T. J., Sparkes, I., Hawes, C. & Hussey, P. J. (2016). Plant VAP27 proteins: domain characterization, intracellular localization and role in plant development. *New Phytol* **210**, 1311-26.

Wang, Y. H. (2008). How effective is T-DNA insertional mutagenesis in Arabidopsis? *Journal of Biochemical Technology* **1**, 11-20.

Wasteneys, G. O. & Galway, M. E. (2003). Remodeling the cytoskeleton for growth and form: an overview with some new views. *Annu Rev Plant Biol* **54**, 691-722.

Wasteneys, G. O. & Yang, Z. (2004). New views on the plant cytoskeleton. *Plant Physiol* **136**, 3884-91.

Waterhouse, A. M., Procter, J. B., Martin, D. M., Clamp, M. & Barton, G. J. (2009). Jalview Version 2--a multiple sequence alignment editor and analysis workbench. *Bioinformatics* **25**, 1189-91.

Wei, L., Zhang, W., Liu, Z. & Li, Y. (2009). AtKinesin-13A is located on Golgi-associated vesicle and involved in vesicle formation/budding in Arabidopsis root-cap peripheral cells. *BMC plant biology* **9**, 138.

Weir, M. L., Xie, H., Klip, A. & Trimble, W. S. (2001). VAP-A binds promiscuously to both v- and tSNAREs. *Biochem Biophys Res Commun* **286**, 616-21.

Welch, M. D., Mallavarapu, A., Rosenblatt, J. & Mitchison, T. J. (1997). Actin dynamics in vivo. *Curr Opin Cell Biol* **9**, 54-61.

Wemmer, M., Azmi, I., West, M., Davies, B., Katzmann, D. & Odorizzi, G. (2011). Bro1 binding to Snf7 regulates ESCRT-III membrane scission activity in yeast. *J Cell Biol* **192**, 295-306.

Wendrich, J., Yang, B.-J., Mijnhout, P., Xue, H.-W., De Rybel, B. & Weijers, D. (2018). IQD proteins integrate auxin and calcium signaling to regulate microtubule dynamics during Arabidopsis development. *bioRxiv*, 275560.

Whittington, A. T., Vugrek, O., Wei, K. J., Hasenbein, N. G., Sugimoto, K., Rashbrooke, M. C. & Wasteneys, G. O. (2001). MOR1 is essential for organizing cortical microtubules in plants. *Nature* **411**, 610-3.

Wilson, K. L. & Dawson, S. C. (2011). Evolution: functional evolution of nuclear structure. *J Cell Biol* **195**, 171-81.

Winter, D., Vinegar, B., Nahal, H., Ammar, R., Wilson, G. V. & Provart, N. J. (2007). An "Electronic Fluorescent Pictograph" browser for exploring and analyzing large-scale biological data sets. *PLoS One* **2**, e718.

Wong, X., Luperchio, T. R. & Reddy, K. L. (2014). NET gains and losses: the role of changing nuclear envelope proteomes in genome regulation. *Curr Opin Cell Biol* **28**, 105-20.

Wootton, J. C. & Federhen, S. (1996). Analysis of compositionally biased regions in sequence databases. *Methods Enzymol* **266**, 554-71.

Wyles, J. P. & Ridgway, N. D. (2004). VAMP-associated protein-A regulates partitioning of oxysterol-binding protein-related protein-9 between the endoplasmic reticulum and Golgi apparatus. *Exp Cell Res* **297**, 533-47.

Xu, T., Dai, N., Chen, J., Nagawa, S., Cao, M., Li, H., Zhou, Z., Chen, X., De Rycke, R., Rakusova, H., Wang, W., Jones, A. M., Friml, J., Patterson, S. E., Bleecker, A. B. & Yang, Z. (2014). Cell surface ABP1-TMK auxin-sensing complex

activates ROP GTPase signaling. *Science* **343**, 1025-8.

Xu, T., Qu, Z., Yang, X., Qin, X., Xiong, J., Wang, Y., Ren, D. & Liu, G. (2009). A cotton kinesin GhKCH2 interacts with both microtubules and microfilaments. *Biochem J* **421**, 171-80.

Xu, T., Wen, M., Nagawa, S., Fu, Y., Chen, J. G., Wu, M. J., Perrot-Rechenmann, C., Friml, J., Jones, A. M. & Yang, Z. (2010). Cell surface- and rho GTPase-based auxin signaling controls cellular interdigitation in Arabidopsis. *Cell* **143**, 99-110.

Yalovsky, S., Bloch, D., Sorek, N. & Kost, B. (2008). Regulation of membrane trafficking, cytoskeleton dynamics, and cell polarity by ROP/RAC GTPases. *Plant Physiol* **147**, 1527-43.

Yang, L., Guan, T. & Gerace, L. (1997). Integral membrane proteins of the nuclear envelope are dispersed throughout the endoplasmic reticulum during mitosis. *J Cell Biol* **137**, 1199-210.

Yang, Z. (2008). Cell polarity signaling in Arabidopsis. *Annu Rev Cell Dev Biol* **24**, 551-75.

Yu, L., Nie, J., Cao, C., Jin, Y., Yan, M., Wang, F., Liu, J., Xiao, Y., Liang, Y. & Zhang, W. (2010). Phosphatidic acid mediates salt stress response by regulation of MPK6 in Arabidopsis thaliana. *New Phytol* **188**, 762-73.

Yuen, C. Y., Pearlman, R. S., Silo-Suh, L., Hilson, P., Carroll, K. L. & Masson, P. H. (2003). WVD2 and WDL1 modulate helical organ growth and anisotropic cell expansion in Arabidopsis. *Plant Physiol* **131**, 493-506.

Zeng, Y., Chung, K. P., Li, B., Lai, C. M., Lam, S. K., Wang, X., Cui, Y., Gao, C., Luo, M., Wong, K. B., Schekman, R. & Jiang, L. (2015). Unique COPII component AtSar1a/AtSec23a pair is required for the distinct function of protein ER export in Arabidopsis thaliana. *Proc Natl Acad Sci U S A* **112**, 14360-5.

Zhang, C., Halsey, L. E. & Szymanski, D. B. (2011). The development and geometry of shape change in Arabidopsis thaliana cotyledon pavement cells. *BMC Plant Biol* **11**, 27.

Zhang, C., Mallery, E. L., Schlueter, J., Huang, S., Fan, Y., Brankle, S., Staiger, C. J. & Szymanski, D. B. (2008). Arabidopsis SCARs function interchangeably to meet actin-related protein 2/3 activation thresholds during morphogenesis. *Plant Cell* **20**, 995-1011.

Zhang, M., Wu, F., Shi, J., Zhu, Y., Zhu, Z., Gong, Q. & Hu, J. (2013). ROOT HAIR DEFECTIVE3 family of dynamin-like GTPases mediates homotypic endoplasmic reticulum fusion and is essential for Arabidopsis development. *Plant Physiol* **163**, 713-20.

Zhang, Q., Lin, F., Mao, T., Nie, J., Yan, M., Yuan, M. & Zhang, W. (2012). Phosphatidic acid regulates microtubule organization by interacting with MAP65-1 in response to salt stress in Arabidopsis. *Plant Cell* **24**, 4555-76.

Zhang, Q., Song, P., Qu, Y., Wang, P., Jia, Q., Guo, L., Zhang, C., Mao, T., Yuan, M., Wang, X. & Zhang, W. (2017). Phospholipase Ddelta negatively regulates plant thermotolerance by destabilizing cortical microtubules in Arabidopsis. *Plant Cell Environ* **40**, 2220-2235.

Zhang, X. & Wang, Y. (2016). Glycosylation Quality Control by the Golgi Structure. *J Mol Biol* **428**, 3183-3193.

Zhao, Q., Brkljacic, J. & Meier, I. (2008). Two distinct interacting classes of nuclear envelope-associated coiled-coil proteins are required for the tissue-specific nuclear envelope targeting of Arabidopsis RanGAP. *Plant Cell* **20**, 1639-51.

Zheng, Y., Wong, M. L., Alberts, B. & Mitchison, T. (1995). Nucleation of microtubule assembly by a gamma-tubulin-containing ring complex. *Nature* **378**, 578-83.

Zhou, X., Graumann, K., Evans, D. E. & Meier, I. (2012). Novel plant SUN-KASH bridges are involved in RanGAP anchoring and nuclear shape determination. *J Cell Biol* **196**, 203-11.

Zhou, X., Graumann, K. & Meier, I. (2015a). The plant nuclear envelope as a multifunctional platform LINCed by SUN and KASH. *J Exp Bot* **66**, 1649-59.

Zhou, X., Graumann, K., Wirthmueller, L., Jones, J. D. & Meier, I. (2014). Identification of unique SUN-interacting nuclear envelope proteins with diverse functions in plants. *J Cell Biol* **205**, 677-92.

Zhou, X., Groves, N. R. & Meier, I. (2015b). Plant nuclear shape is independently determined by the SUN-WIP-WIT2-myosin XI-i complex and CRWN1. *Nucleus* **6**, 144-53.

Zhou, X., Groves, N. R. & Meier, I. (2015c). SUN anchors pollen WIP-WIT complexes at the vegetative nuclear envelope and is necessary for pollen tube targeting and fertility. *J Exp Bot* **66**, 7299-307.

Zhou, X. & Meier, I. (2013). How plants LINC the SUN to KASH. *Nucleus* **4**, 206-15.

Zhu, C. & Dixit, R. (2012). Functions of the Arabidopsis kinesin superfamily of microtubule-based motor proteins. *Protoplasma* **249**, 887-99.

Zhu, C., Ganguly, A., Baskin, T. I., McClosky, D. D., Anderson, C. T., Foster, C., Meunier, K. A., Okamoto, R., Berg, H. & Dixit, R. (2015). The FRA1 kinesin

contributes to cortical microtubule-mediated trafficking of cell wall components. *Plant physiology*, pp. 114.251462.

Zuleger, N., Robson, M. I. & Schirmer, E. C. (2011). The nuclear envelope as a chromatin organizer. *Nucleus* **2**, 339-49.

Zupan, J. R. & Zambryski, P. (1995). Transfer of T-DNA from Agrobacterium to the plant cell. *Plant Physiol* **107**, 1041-7.